Development and applications of tracking of pellet streams

ANDRZEJ PYSZNIAK

A doctoral dissertation
prepared at the Institute of Physics of the Jagiellonian University
and at the Institute of Physics and Astronomy of the Uppsala University,
conferred by prof. Zbigniew Rudy and prof. Tord Johansson.
Kraków, October 2014

Abstract

The development of a system for optical tracking of frozen hydrogen microsphere targets (pellets) was done. It is intended for the upcoming hadron physics experiment PANDA at FAIR, Darmstadt, Germany. Knowledge of the interaction position, obtained with this system, will improve background rejection, precision of particle track reconstruction and will also help distinguish between primary and secondary vertices.

Investigations of pellet detection conditions and pellet stream parameters were performed at Uppsala Pellet Test Station located at The Svedberg Laboratory. Various illumination and detection conditions were checked and optimized. The gained knowledge has been used to develop Monte Carlo procedures simulating experiments with pellets. Then simulations of pellet tracking were carried out including the constraints from the PANDA setup. The performance of the tracking was checked for various pellet stream and pellet detection conditions. Two procedures of pellet track reconstruction were developed – a fast procedure and a high efficiency procedure. The studies were done for one tracking section (just below pellet generator) and for two sections (the second just above pellet dump) and showed that the resolution of the tracking system can be better than 100 μm (sigma) in each direction and that the interaction point will be reconstructed for 70-95% of hadronic events, for suitable pellet stream and detection conditions.

Usage of pellet tracking information in the hadronic data analysis was discussed, concerning the data taking, particle track reconstruction together with the PANDA micro vertex detector, hadronic event classification and treatment of the various classes. Test measurements with the WASA setup at FZJ, Jülich, Germany were done to check how the information about the number of pellets in the accelerator beam region can be used in the hadronic data analysis. Instantaneous rates of WASA "elastic" triggers were used for classification of hadronic events as coming from pellets or from a background. The study clearly showed that one can distinguish between the two event classes. The study gave experience in using two different systems synchronized with each other – the experiment's DAQ and another system that works with a much longer time scale – similar to the pellet tracking system.

Keywords: PANDA, cryogenic target, pellet, pellet target, pellet tracking

Contents

Chapter 1

Introduction

The subject of the thesis is the development of a target device allowing an increase of the quality of the data in accelerator based hadron physics experiments studying fundamental properties of matter.

1.1. The physics of strong interaction

The elementary particles from which all visible matter is built are *leptons* and *quarks*. The most known lepton is the *electron*. It is also the lightest of the charged leptons, which also includes the *muon* and the *tauon*. Only the electron is stable. The other two decay within a small fraction of a second after their creation in high energy interactions. Each of the charged leptons has its neutral lepton partner, a *neutrino* – there exist the electron neutrino, the muon neutrino and the tauon neutrino. The quarks are another group of charged elementary particles. The two lightest of them are called *up* and *down*. The nucleons – protons and neutrons – forming atomic nuclei, are composed of these quarks. The other four quarks are called *charm*, *strange*, *top* and *bottom*. Particles composed of these quarks can be created in collisions of highly energetic particles. Each of the mentioned leptons and quarks exist as "normal" particles and as anti-particles.

Quarks do not exist separately but only bound into *hadrons*. *Baryons* are hadrons consisting of three constituent quarks. The most commonly known baryons are protons and neutrons. Hadrons consisting of a quark and an antiquark are called *mesons*. Examples of them are *pions* and *eta* mesons. Many different baryons and mesons exist. Studying them is a subject of nuclear and high energy physics. The proton is the only stable hadron. Neutrons are stable only inside of atomic nuclei.

All interactions taking place in nature can be reduced to four fundamental interactions: *gravitational*, *electromagnetic*, *strong* and *weak*. The interactions are mediated by force carriers. Exchange of these force car-

rier particles is observed on macroscopic scale as interactions between elements of a system. The force carriers, or *gauge bosons*, are the third group of elementary particles. The electromagnetic interaction is mediated by *photons* and the weak interaction is mediated by three bosons: W^+, W^- and Z^0. The strong force is carried by *gluons*. The existence of a force carrier for gravity (*graviton*) is still a subject for searches. While the gravitational and electromagnetic interactions act over potentially infinite distance, the strong and weak nuclear interactions act only on the subatomic scale.

The strong force keeps the quarks bound into hadrons. By analogy to charge in the electromagnetic interaction, the strong interaction is also said to involve a certain charge. In this case, there are three different variants of charge. By analogy to optics these charge variants are called with the names of the primary colors: red, green and blue. Similarly to normal charge being positive or negative, also in addition to positive red, green and blue charges, there exist negative anti-charges (anti-colors): anti-red, anti-green and anti-blue. Only color neutral objects can be observed which means that the colors of quarks in a hadron have to add up to what in the optics analogy would give a white color (*e.g.* red-green-blue or color-anticolor). It should be also noted, that a given color is not an intrinsic property of quarks. The colors are constantly changing by emission and absorption of gluons. In this way the strong interaction is mediated.

The strong interaction displays two peculiar properties: *color confinement* and *asymptotic freedom*. The asymptotic freedom means, that for small distances between quarks, smaller than the size of a nucleon, the interaction becomes very weak and quarks and gluons behave like non-interacting. To put it in other words, the *coupling constant* of the interactions becomes very weak. The color confinement means, that for bigger distances between quarks, the interaction between them becomes stronger (the coupling constant increases) which in turn leads to that isolated quarks cannot be observed. This is very different from the case of the electromagnetic interaction, where the force between the charges diminishes while taking the charges apart, allowing *e.g.* for the negatively charged electrons in the atom to be unbound from the positively charged nucleus. In the case of the strong force, the separation of quarks to bigger distances requires more and more energy. At some point this energy is big enough to create quark-antiquark pairs that form new hadrons with the quarks originally being separated.

The essence of basic research is to gain deeper understanding of the nature by discovering new phenomena and developing models capable of explaining them. Nuclear and particle physics deals with the very fundamental questions concerning the matter constituting our universe and the interactions present in nature. One area of interest of this

branch of physics is the subject of hadrons and the strong interaction. Many properties of this interaction are still to be understood. Many predictions of the current theories have to be checked. The theories have to be made more complete. To achieve all this, new experimental results are needed.

A theory called *Quantum Chromodynamics* (QCD) has been developed to describe all the properties of strong interaction. It is a part of a set of theories called the *Standard Model* of particle physics, summarizing our current knowledge about the particles and interactions present in the universe. Foundations for QCD have been laid 50 or so years ago and the application of theory is being constantly developed and improved ever since.

In the high energy regime, which corresponds to small distances between quarks and thus a weak coupling constant, the description of the strong force is easier because it is possible to use a *perturbative approach*. In this approach, the complicated system is described in terms of a simpler system with an addition of a small disturbance (perturbation). More problematic is the QCD in the low energy regime implying a strong coupling constant. In these conditions it is not possible to use the perturbative approach. This region is still the least known and new measurements are especially needed. The situation will be improved with the new PANDA experiment.

1.2. The PANDA experiment

The PANDA experiment ($\bar{P}ANDA$ – antiProton ANnihilation at DArmstadt) [1] is a new experiment being developed for FAIR facility (Facility for Antiproton and Ion Research) located at the GSI research center in Darmstadt, Germany. PANDA will be operated at the HESR accelerator (High Energy Storage Ring) providing anti-proton beams with momenta of 1.5 – 15 GeV/c. The target material will be mainly hydrogen (protons) but it will be also possible to use heavier gases. The planned luminosity is $2 \times 10^{32} cm^{-2} s^{-1}$. HESR is equipped with electron and stochastic cooling of the beam, which gives very well defined beam energy and allows to measure the masses and widths of hadronic resonances with accuracies of 50 – 100 keV. One of the advantages of colliding antiprotons with protons is that it makes possible formation of states of all quantum numbers. $\bar{p}p$ collisions will allow for hadron spectroscopy of charmonium, D mesons and strange and charmed baryons. Also, it will be possible to search for glueballs (particles consisting solely of gluons) and hybrids (consisting of quark, antiquark and excited glue). These states are allowed by QCD, but their existence has not been confirmed experimentally. At PANDA it will be possible to search

for gluonic hadrons with masses above 2.5 GeV/c^2, where the density of conventional quark-antiquark states becomes smaller. Also a study of non-perturbative QCD dynamics will be possible in baryon-antibaryon interactions. Collisions of antiprotons with heavier nuclei will allow for study of $\Lambda\Lambda$ hypernuclei and hadrons in the nuclear medium. The range of operation of the PANDA experiment is shown in Figure 1.2.1.

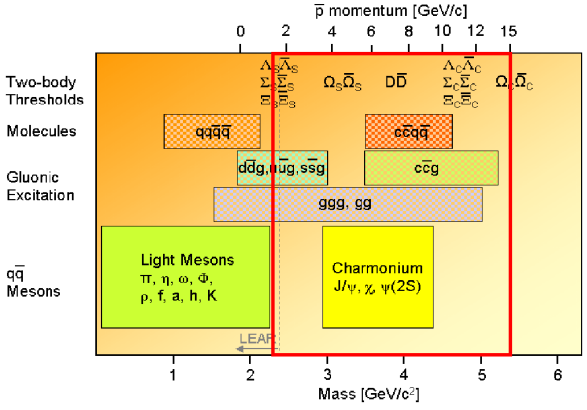

Figure 1.2.1: Range of operation of the PANDA experiment (as indicated by the red frame)

The measurements in which the PANDA detector will be used set requirements for its properties [1,2]. Full acceptance is needed for proper partial wave analysis of charmonium states and exotic hadrons in the charmonium region. The electromagnetic calorimeters have to have a low photon threshold to properly detect events with many photons in the final state. A vertex detector and kaon identification is needed to reconstruct charmed mesons. Effective muon detection is necessary as they occur as results of J/ψ decays, semi-leptonic charm meson decays and the Drell-Yan process. High energy protons from wide angle Compton scattering also need to be detected. Hyperon cascades need to be detected to investigate hypernuclei. Efficient detection of electrons and protons and separating them from pions is important for the measurement of proton form factors. Good momentum resolution (of the order of 1%) is desirable for precise reconstruction of invariant masses. All elements of the setup should make possible operation with high rate of interactions, up to 20 million per second, to enable precision measurements and measuring of low cross-section processes. Efficient event selection is needed to perform measurements of several reaction channels in parallel.

PANDA is a 4π detector setup (Figure 1.2.2) and consists of two main parts: a target spectrometer and a forward spectrometer [1, 2].

Both parts contain tracking detectors, particle identification detectors, calorimeters and muon detectors. The target spectrometer is equipped with a superconducting coil providing a 2 T magnetic field. The forward spectrometer is equipped with an ordinary dipole magnet. The target spectrometer is a barrel shaped set of detectors surrounding the interaction point. The central part of the barrel covers the angles from 22 to 140 degrees and the forward end cap covers the angles from 5 to 22 degrees in vertical direction and from 10 to 22 degrees in horizontal direction. Particles with polar angles above 140 degrees are detected by the backward end cap of the target spectrometer. The forward spectrometer is built to record forward going particles that are abundant in fixed target experiments.

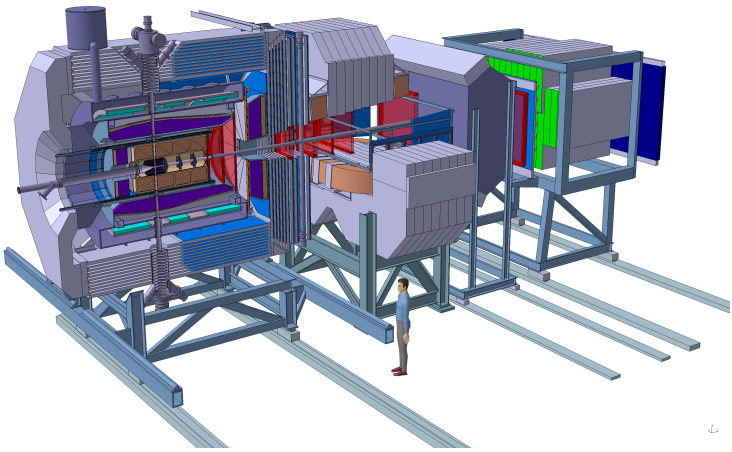

Figure 1.2.2: The PANDA detector setup [1]

The PANDA setup readout works in a self-triggering scheme. Data from the detectors are continuously digitized and valid hits are searched for. Patterns in the separate detectors, such as hit clusters, fragments of particle tracks, fragments of light rings in Cherenkov detectors, are found in real time. Also the first selection of interesting time intervals is done. The data are saved after the online reconstruction process, which enables flexibility in applying event selection algorithms.

The innermost detector in the target spectrometer is a micro-vertex detector consisting of two layers of silicon pixel detectors and two layers of silicon strip detectors. The detector offers a resolution (sigma) in the order of 60–90 μm in all directions for events which occurred in the range -/+ 3 mm from the nominal interaction point (along the accelerator beam) and tracks with polar angles above 20°. Tracks of the particles curved in the solenoid field will be measured with a Straw

Tube Tracker (STT). For small polar angles, large planar Gas Electron Multiplier (GEM) detectors will be installed in the forward end cap. Tracking in the forward spectrometer will be done with straw tube chambers.

Particle identification will be based on various physical processes, since it is required to identify particles with momenta ranging from 200 MeV/c up to 10 GeV/c. The main method of charged particle identification will be based on the Cherenkov effect. Two detectors measuring internally reflected Cherenkov light (DIRC) will be used in the target spectrometer. The forward spectrometer will contain a ring imaging Cherenkov detector (RICH). The time of flight method will be also employed in particle identification, making use of fast plastic scintillators covering the interaction point, providing event timing with 100 ps resolution. They will work together with hodoscopes installed in the central part of the barrel and in both end caps as well as a wall of scintillating panels mounted behind the dipole magnet. The hodoscopes will also provide discrimination between charged and neutral particles. Energy loss in single elements will be also used to identify particles below 1 GeV/c. Muons will be detected with layers of drift tubes interleaving with layers of absorbing material, located in the magnet yoke, in the space between two spectrometers and at the end of the forward spectrometer.

High precision electromagnetic calorimetry is required in the energy range from a few MeV up to several GeV. The material of the calorimeter crystals has to provide high energy resolution, fast response and low energy threshold. Also a high light yield is required along with high density and radiation hardness. To meet these requirements, the calorimeter is made of approx. 16 000 lead-tungstate ($PbWO_4$) crystals, distributed over three parts of the target spectrometer, forward, barrel and backward. The forward spectrometer contains a Shashlik type sampling calorimeter.

1.3. Particle tracking

Particle tracking in PANDA will be done with a micro vertex detector (MVD), STT (central tracker) and GEMs in the Target Spectrometer and drift detectors in the Forward Spectrometer. These elements are visible in Figure 1.3.1. The detector the closest to the interaction point is the MVD [3]. The inner radius of the detector is 25 mm and the outer radius is 130 mm. It is designed mainly to reconstruct the point of origin of detected particles. It will also be the only detector able to detect charged particles with low momenta, having small bending radii in the magnetic field.

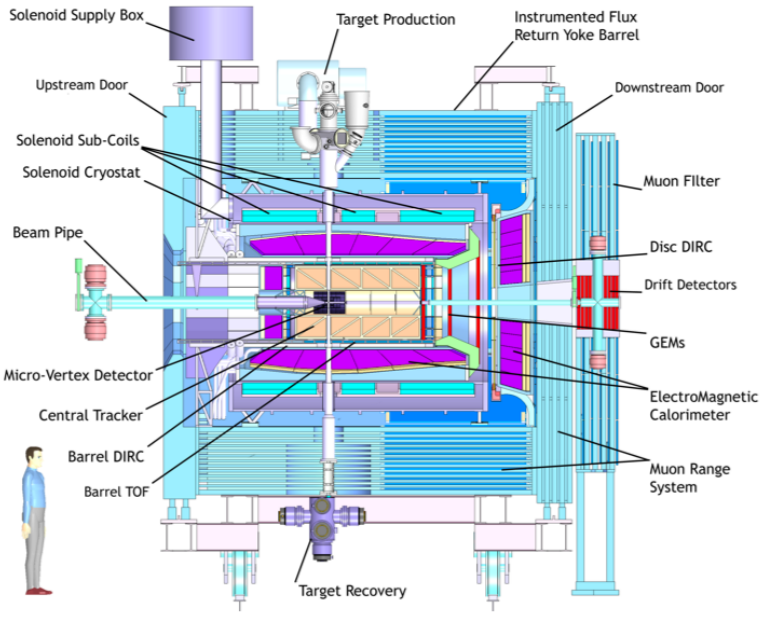

Figure 1.3.1: Side of the Target Spectrometer of PANDA [3]

The structure of the MVD is shown in Figure 1.3.2. It consists of four barrel layers and six layers in the forward part. Two inner barrel layers and all six forward wheels are made of silicon pixel detectors. Silicon strip detectors are used for two outer barrel layers and for outer rings added to two last forward wheels for increased angular coverage.

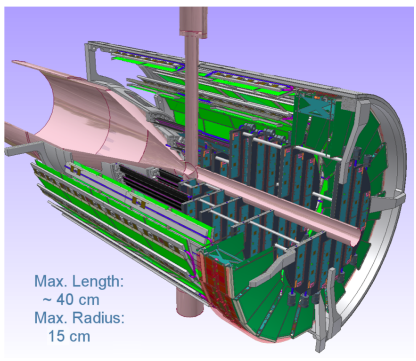

Figure 1.3.2: The Micro Vertex Detector [3]

The track reconstruction procedure in PandaRoot analysis framework has three stages. In the first step, the algorithms operate locally to find tracklets in each subdetector. Then, the tracklets from different

subdetectors are merged and global track finding is performed. In the last step the resulting tracks are globally fitted. Vertexing procedures are later applied to find event vertices based on the found tracks.

The resulting vertex finding resolution for different polar angles and different positions along accelerator beam axis is shown in Figure 1.3.3. The resolution deteriorates drastically for polar angles below 20°. At least four hits in MVD are required for effective track reconstruction in this subdetector and this is most often not the case for low polar angles, below 10°. Also, for polar angles below 20°the distance of the first hit from the nominal interaction region is high (approx. 100 mm), which further deteriorates the resolution. The resolution deteriorates also for positions along the accelerator beam further away than 3 mm from the nominal interaction region – outside this region the pattern recognition procedures work less efficiently.

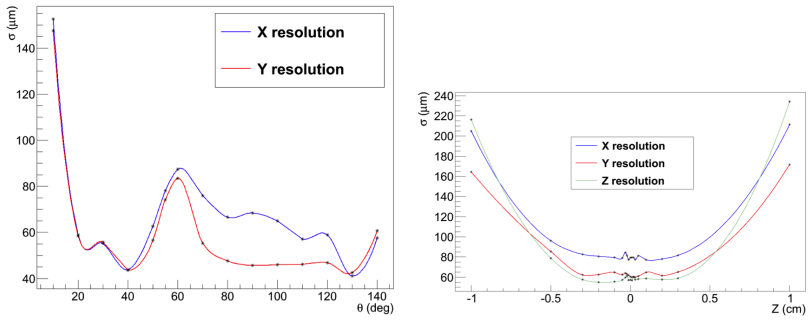

Figure 1.3.3: MVD vertex finding resolution for different polar angles (left plot) and for different position along accelerator beam axis (right plot). A study with 1 GeV/c pions; all tracking detectors are used in the track reconstruction [3]

Vertices are normally located in the target material. Having a discrete target of small size and knowing its position would give information about the interaction point. Knowing the position of the interaction point from this source, independent of MVD information, would provide an additional point for the track fitting, making it more precise. Also, by knowing this position with a resolution similar to the resolution given by MVD and STT, one may distinguish if the found vertex was primary or secondary. This would also provide valuable information about the vertex position for neutral particles, not detected by the MVD and STT. Since the interactions may occur also in various kinds of other material, the knowledge if the target material could possibly be the source of a given interaction will also help to reject background events.

1.4. Usage of cluster and pellet targets

To have hydrogen as target material in hadron physics experiment requires normally a cryogenic installation. Frozen hydrogen is the only solution that provides high density of the target material, good vacuum conditions and minimum of structural material in the interaction region [4].

One kind of targets is pellets [5–7]. Pellets are small spheres of frozen hydrogen. They are produced at some distance from the interaction region, above the particle detector system, and can travel inside thin pipes. Another type of target is a cluster jet, containing clusters of various number of gas molecules [8]. Among these two solutions pellets provide better luminosity – the rate of interactions is higher because the density of matter in a pellet stream is much bigger than in a cluster jet, which implies a higher probability of interaction. Also, pellet targets provide better sustained vacuum conditions.

Last, but not least, the pellet target provides a possibility of knowing the position of single pellets at any moment. In the cluster jet target the interaction region is given by the overlap of the jet and accelerator beam. The pellet stream also has a certain extension, but in this case it is possible to determine the position of single pellets. The work described in this thesis will be concentrated on developing and utilizing this possibility given by the pellet target.

Pellet targets, as well as cluster jet targets, allow the experiments to be operated as internal target experiments, which means that the target and detector system are located at the storage ring. This is possible because pellets and clusters interact only with a very small fraction of particles in the beam and the beam may operate for many seconds or minutes before the need of next injection.

Both of the mentioned target types are planned to be used in the PANDA setup. A pellet target is currently used in the WASA-at-COSY experiment [9, 10], located in Forschungszentrum Jülich (FZJ) in Germany. The WASA (Wide Angle Shower Apparatus) detector setup was originally built at the The Svedberg Laboratory (TSL) and operated in the CELSIUS storage ring. In 2005 WASA was moved and installed at the COSY accelerator (COoler SYnchrotron) in FZJ. WASA is a 4π detector system (Figure 1.4.1), consisting of two main parts - a forward part, designed to measure recoil particles and scattered projectiles, and a central part, designed mainly to record decay products of produced short lived particles. COSY operates in momentum range 0.3 - 3.7 GeV/c. Experiments performed at this setup allowed to study reactions involving of *e.g.* π, η and ω particles – see *e.g.* published articles [11–20].

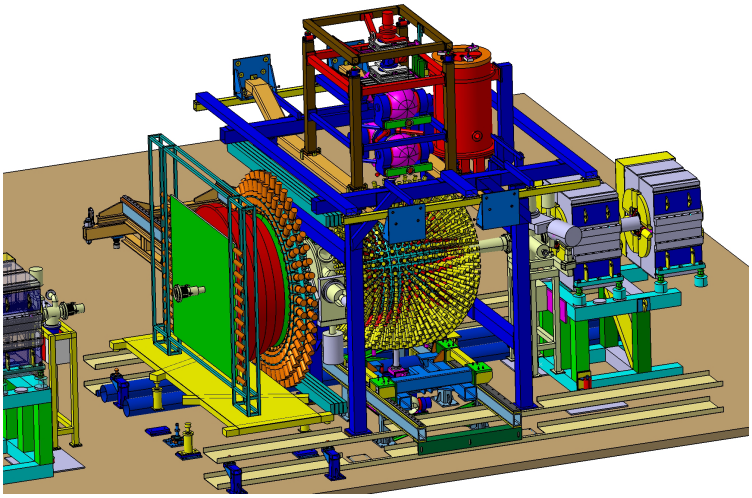

Figure 1.4.1: The WASA detector setup

1.5. Background events

Not all collected hadronic events are results of interaction of the accelerator beam particles with the target material – pellets or clusters. Some of the recorded events come from various kinds of background such as a gas present in the scattering chamber or interactions of accelerator beam halo with the structural material. Such events may be a substantial fraction of all events. Experiments at WASA have shown that even 25 – 50% of all events do not originate from pellets in the nominal interaction region. This is possible because the volume where the background events may be produced and still be accepted is very big comparing to the size of the normal interaction region. Because of this, even for a low background level, the total number of background events may be high.

The background level in WASA is estimated based on analysis of the hadronic data to be of the order of a few per mille. This is in agreement with studies based on checking the pressures in scattering chamber and the rate of beam decay in different conditions: with pellet target running and pellets present in the accelerator beam region, with pellet target running but with pellets missing the accelerator beam and without pellets. Similar studies for the cluster target at the ANKE detector in COSY indicate a significantly higher background level with this kind of target compared to pellet target.

1.6. Interaction vertex determination and pellet tracking

Position of the interaction vertex is normally determined by the overlap of the target stream and accelerator beam. For pellet targets this region has a size of a few mm in each direction. More precise knowledge of the interaction region would provide an additional point in determination of particle tracks (trajectories), which would provide more precise determination of particle four vectors and thus a better accuracy of analysis results. As mentioned, the PANDA setup is equipped with an MVD and STT for charged particle tracking. Pellet tracking would deliver an additional measurement point of the same accuracy as the MVD and STT. Besides improving the track fit quality, it will also provide independent help in resolving ambiguities occurring during the reconstruction. Moreover, the position of the pellet during the interaction is the only way of knowing the primary interaction vertex in case when the particle produced in the collision decays at some distance from the production point [21]. Examples of such particles are listed in Table 1.6.1.

Table 1.6.1: Examples of particles with decay length ($c\tau$) between 0.1 and 100 mm [22]

Particle	Distance
$D^0(1865)$	0.12 mm
$D^{+/-}(1869)$	0.3 mm
$\Lambda(1116)$	79 mm
$\Sigma^+(1189)$, $\Sigma^-(1197)$	24, 44 mm
$\Xi^0(1315)$, $\Xi^-(1321)$	87, 49 mm
$\Omega^-(1672)$	25 mm

A slightly modernized version of the WASA pellet target generator is operated at The Svedberg Laboratory (TSL) in Uppsala. This device operates standalone *i.e.* is not a part of a hadron physics experiment and is called the Uppsala Pellet Test Station (UPTS). It is used for developments of pellet target techniques as well as delivers pellets for tests connected to the pellet tracking system development.

The pellet tracking system is the solution to the task of determination of pellets position in the interaction region. The tracking will be realized by placing a number of fast CCD cameras at different levels along the pellet stream. The synchronized cameras will provide time and position information for pellets passing in front of them. The data obtained at single levels will then be used in the process of track reconstruction.

Knowing the tracks of the pellets, so their three dimensional position at any moment, one can check if any pellets were in the interaction region at the time of a hadronic interaction. If so, one is able to precisely

know their position. A situation with exactly one pellet in the interaction region is preferred because it prevents ambiguities. However even with more than one pellet it is possible to use their positions as hypotheses in the fit and together with other information disentangle the ambiguity.

The pellet tracking can be also used in online analysis to determine various properties of the pellet stream and its quality, such as pellet rate and stream divergence.

1.7. Description of the pellet target

In this section the pellet target design and operation are presented taking as an example the pellet target system installed at the WASA detector. As mentioned, UPTS and WASA pellet targets are very similar and differ only in some non-crucial mechanical aspects (see Section 2.1).

The elements of the WASA pellet target are shown in Figure 1.7.1. Since the space between the pellet generator and the interaction point is occupied by the particle detector system, pellets travel this approx. 2.7 meters distance inside a thin pipe. Then, after a similar distance, the pellets are collected in the dump.

The necessary high-vacuum conditions are provided by a set of turbo pumps. After passing the interaction region, pellets travel inside a pipe to the pellet dump. The construction of the dump prevents pellets from scattering back to the interaction region; they evaporate and the gas is removed by vacuum pumps.

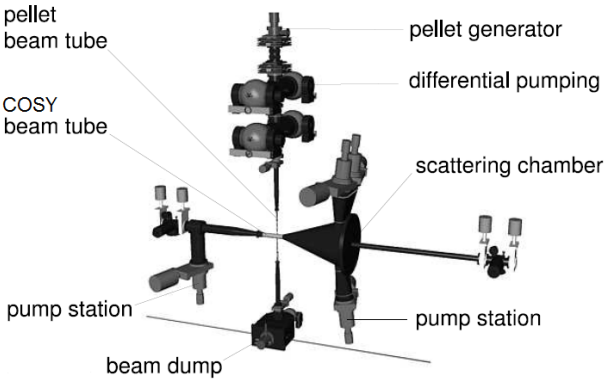

Figure 1.7.1: Pellet target [10]

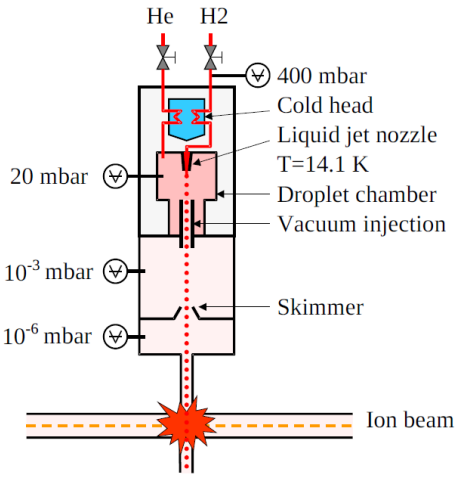

Figure 1.7.2: Scheme of the pellet generator

The idea of the pellet generator is shown in Figure 1.7.2. Pellets are made from hydrogen gas, which is first purified in order for the device to operate with high reliability. The purity of the gas is better than 99.9999%. Then, the hydrogen is cooled down to a temperature ≈ 14.1 K by a so-called cold head. The cold head is a cryogenic refrigerator based on helium in a closed cycle. The desired temperature is maintained by a precise electronically-controlled electric heating system.

The hydrogen liquefies and is injected by a nozzle into the so-called droplet chamber. The nozzle has an opening diameter ≈ 11 μm. The hydrogen pressure before the nozzle (driving pressure) is typically 400 – 600 mbar, and the pressure inside the droplet chamber is usually 18 – 23 mbar. Besides evaporated hydrogen gas, the droplet chamber is also filled with helium.

Inside the droplet chamber the liquid stream breaks up into droplets. The nozzle vibrates with a fixed frequency in the range 40 – 90 kHz, which stimulates the break up process. The droplets then enter the Vacuum Injection Capillary (VIC). The distance between the nozzle and VIC is ≈ 7 mm. The droplet chamber is shown in upper picture in Figure 1.7.3.

The length of the VIC is ≈ 70 mm and the inner diameter is ≈ 1 mm. The pressure after the VIC is of the order of 10^{-4} mbar. Because of the high pressure gradient in VIC, droplets freeze and are also accelerated. After the exit of VIC they are solid and are called pellets (lower picture in Figure 1.7.3). They have a diameter of 20 – 30 μm and travel with a velocity of 70 – 80 m/s. The distance between pellets is a few millimeters.

After leaving the VIC, pellets travel inside vacuum pipes. Because of slight divergence of the pellet stream, its diameter increases with

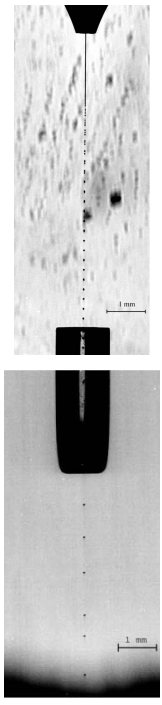

Figure 1.7.3: Droplets (upper picture) and pellets (lower picture). The nozzle is visible in the upper part of the upper picture. The VIC is visible in the lower part of the upper picture and in the upper part of the lower picture

increasing distance from VIC. To collimate the stream, a skimmer is installed at a distance approx. 0.7 m from the pellet generator. The skimmer is a cone with a hole of about 1 mm diameter at its axis. Only pellets of small divergence pass through the skimmer.

After passing skimmer the vacuum improves and is in the order of 10^{-5} mbar. The size of the pellet pipe decreases when approaching the accelerator beam pipe, where the inner diameter is 5 mm. The pellet stream at this position has a diameter of 3.8 mm.

The pressure in the scattering chamber is in the order of 10^{-6} mbar with pellets and in the order of 10^{-8} mbar when the pellet stream is off.

1.8. Layout of the studies

The studies described in this thesis are based on experiments carried out at Uppsala Pellet Test Station (UPTS) and at the WASA-at-COSY experimental site.

The prerequisite for development of pellet tracking system is a study of pellet detection conditions. This is the content of the Chapter 2.

Various illumination conditions were checked, with different models of lasers, different optics, different illumination angles and number of lasers. Also different models of cameras were checked, with different optics and operated with different cycle structure. Means of processing the image from the cameras to obtain information about detected pellets were investigated. The chapter contains a description of the Uppsala Pellet Test Station and the means of pellet detection. The results of the studies and the best found settings obtained are presented. Also, a description of the simulation procedures developed to simulate pellet detection process is presented.

Chapter 3 describes the studies of the pellet stream. Parameters of the stream were measured at fixed levels and also in correlation between different measurement levels. Distributions of pellet stream density, pellet stream shape and divergence were measured. Also, measurements of pellet velocity, velocity spread and a source of the velocity spread were carried out. A description of simulation procedures developed to simulate pellet stream behavior is also presented.

Chapter 4 contains a description of design simulations of the tracking system for PANDA. Based on realistic pellet stream and detection parameters from UPTS measurements and constraints from the PANDA setup, simulations of pellet tracking performance were carried out. Various parameters of pellet stream and pellet detection were checked. A procedure of pellet track reconstruction was developed for the purpose of the study. It also will be possible to be used in the data analysis when full scale pellet tracking is operated at a particle detector system.

Chapter 5 contains a discussion of usage of the information from pellet tracking in hadron data analysis. Also, an advanced algorithm of pellet track reconstruction is described. This algorithm is very robust, flexible and provides very high reconstruction efficiency even in case of substantial detection inefficiencies.

The most important parts of the work on the pellet tracking system are tests of the system when operated at a real hadron physics experiment. Before such opportunity is at PANDA site, some initial test measurements have now been done at WASA , as described in Chapter 6, providing valuable input to the design studies. One of the information given by the pellet tracking is the number of pellets present in the interaction region. The possibility of obtaining and making use of such information was checked in a different way - by using a Long Range TDC (Time-to-Digital Converter), recording times of elastic scattering events. Based on the instantaneous event rate and the knowledge that presence of pellet in the beam region increases this rate, an event classification method was developed and the hadronic data were analyzed separately for “pellet” and “non-pellet” case. The study has clearly shown that one can distinguish between the two event classes.

Moreover, the method gave experience on using two different systems synchronized with each other - normal experiment DAQ and another system, which works with a much longer time scale - similar to the pellet tracking system.

Acronyms used in the thesis are listed in Appendix A. Terms defined for the purpose of the described studies, as well as definition of the coordinate system of WASA and PANDA, can be found in Appendix B.

The following activities described in the thesis were done by the author:

a) participation in hadron physics experiments using pellet target at the WASA-at-COSY detector setup;

b) participation in experimental tests of pellet detection conditions and pellet stream parameters at UPTS;

c) analysis of the UPTS experimental data obtained in velocity measurement configuration;

d) preparation of detailed procedures simulating the behavior of pellets in the stream and of pellet detection;

e) preparation of pellet track reconstruction procedures and performing detailed design simulations of resolution and performance of the tracking system for PANDA;

f) analysis of the data from Long Range TDC and preparing procedures simulating the spectra;

g) analysis of data from the WASA-at-COSY detector setup with usage of Long Range TDC information.

Some results connected to a) are published in References [11–20]. Results from b) and c) are published in References [23, 24] and a brief account of d) and e) is given in References [24, 25] and were presented at the INPC2013 [26] and LEAP2013 [27] conferences. The results from f) and g) are published in Reference [28] and were presented at the MESON2014 conference [29].

Chapter 2

Investigation of pellet detection conditions

The pellet detection conditions have been investigated at the Uppsala Pellet Test Station. After a description of the possibilities offered at the station, various aspects of pellet illumination and detection equipment are discussed. The experimental results are followed by a description of the Monte Carlo procedures developed to simulate and understand the pellet detection process.

2.1. UPTS, the Uppsala Pellet Test Station

The UPTS at TSL in Uppsala is a pellet target test and development device which operates standalone. This allows for measurements and improvements of pellet generation conditions and pellet stream properties. UPTS is also where a pellet tracking system for PANDA is being developed.

The construction of UPTS is very much similar to the construction of the WASA pellet target. The main differences are the position and construction of the observation windows and the position of the big turbo pumps and the skimmer. Pictures of UPTS are shown in Figure 2.1.1. Positions of the observation windows are indicated.

Table 2.1.1 summarizes an example of pellet generation conditions at UPTS and Table 2.1.2 summarizes an example of pellet stream conditions.

UPTS contains 6 levels, where pellets (and droplets) may be observed. They are named and defined as follows:

- DC – located at the droplet chamber. Four observation windows in one plane every 90°are located there.
- VIC – located directly below the VIC exit. Four observation windows in one plane every 90°are located there.

- PTR gen – located ≈27 cm below VIC exit. Six windows are located there – four observation windows every 90°, and two small windows for illumination, located between the observation windows, opposite do each other.
- Skimmer – located directly above the skimmer, ≈1.5 m below the generation point. The level contains eight windows in total – four observation windows every 90°and four small windows for illumination, located between them.
- PTR up – upper level of the specially designed tracking section located ≈35 cm below the skimmer. The level also contains eight windows – four observation windows and four small windows for illumination.
- PTR low – the second level of the tracking section, with the same window arrangement as PTR up. Located ≈8 cm below PTR up.

The inner diameter of the observation windows is 32 mm, and the diameter of the illumination windows is 16 mm.

Table 2.1.1: Example of pellet generation conditions at UPTS

Nozzle diameter	12.9 μm
Nozzle temperature	14.1 K
Droplets frequency	≈63 kHz
Hydrogen driving pressure	≈400 mbar
Pressure in the droplet chamber	≈21 mbar
Droplets velocity	≈22 m/s
Distance between droplets	0.34 mm
Pellet diameter	25-30 μm (guess)
Pellet velocity	77.9 m/s
Pellet velocity spread (σ_v/v)	0.42 %

Table 2.1.2: Example of pellet stream conditions at UPTS (FW stands for full width of the distribution, FWHM means full width at half maximum)

Above skimmer	
Pellet rate	≈57 k/s
FWHM	2.1 mm
FW	≈3.7 mm

At PTR chambers	
Pellet rate	≈22.5 k/s
FW	≈2.5 mm

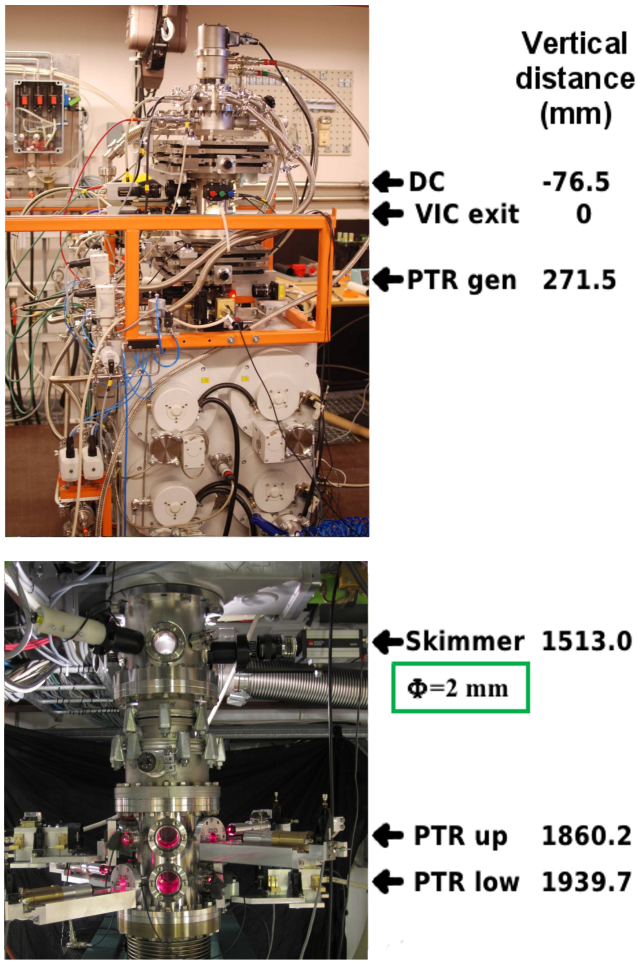

Figure 2.1.1: Uppsala Pellet Test Station. Upper and lower part of the station is shown with installed equipment for pellet observations. Positions of observation windows are indicated

2.2. Pellet detection

Pellets are illuminated with lasers installed at the windows of the measurement sections. For tuning purposes pellets may be observed with standard CCD cameras. For measurements, line-scan cameras are installed.

2.2.1. Illumination

Pellets are illuminated with lasers. Most are of type 50 mW Lasiris SNF and give a narrow-beam width line profile. The working distance is 185

mm. The lasers provide 1°or 5°illumination angle, which corresponds to a width of 3 or 16 mm at the working distance. The angle depends on the kind of optics used. Thus, for the 5°option, the light intensity is approx. 5 times lower than for the 1°option. The height of the illuminated area is about 50 μm in both cases.

The lasers are mounted at the windows in specially designed holders. The holders allow for adjustment of the vertical and horizontal position of the lasers and their tilt angles. It is also possible to rotate the lasers and to set them at the optimal working distance.

Additional illumination windows located between the standard observation windows allowed for investigation of different illumination setups. 90°, as well as 45°and 135°angle between camera and laser were checked. The 135°setup proved to provide the best illumination conditions (with one laser). The refraction of light in pellets (135°) is about three times stronger than the reflection (45°).

Figure 2.2.1: Lasers used for illumination of pellets

2.2.2. Cameras

The devices used to observe pellets and measure pellet stream properties are, so called, Line Scan (LS) CCD cameras. They operate similarly to standard CCD cameras, but have only one line of pixels. In the measurements of pellet stream properties there is no need for two dimensional pictures and the presence of only one line of pixels gives an advantage in speed.

The camera type used (AViiVA SM2) can operate with frequencies up to almost 100 kHz. This means that every picture takes 10 μs. The camera sensor line consists of 512 pixels. Each pixel has a size 14 μm squared. Odd and even pixels are read out separately. The camera has a ≈2 μs dead time, resulting from the time needed for the transfer of

collected charge. At this time the camera does not collect light, which is a source of inefficiency.

Figure 2.2.2: Line-scan camera used in the measurements

2.2.3. Optics

The cameras can be equipped with 50 mm or 25 mm lenses. There are also additional extension rings mounted between the camera and the lens. The working distance (focus) is at the distance ≈250 mm. With a physical pixel size of 14 μm squared, the effective pixel size is 37 μm squared for the 50 mm lenses and 75 μm for the 25 mm lenses. This leads to a detection resolution equal to σ = 20 μm and σ = 40 μm, respectively.

The depth of field (DOF) is approx. ± 2.5 mm for the 50 mm lenses and approx. ± 5 mm for the 25 mm lenses. An image of pellets which travel further from the stream axis is deteriorated, which consequently leads to a drop in the resolution.

2.2.4. Laser–camera arrangement and alignment

An efficient pellet detection requires big aperture of the optics, to collect as much light as possible, which in turn requires sufficient diameter of the observation windows. This requires an adequate size of the vacuum chambers, to make installation of such windows possible (≈130 mm diameter pipes are used). These dimensions, together with mechanical requirements such as size of the holders, lead to choosing a working distance of about 200 mm.

The intense illumination of the pellets, needed for effective detection, requires a focused laser beam. On the other hand, the laser beam has to be high enough to illuminate whole pellet which has a 20 – 35 μm

diameter (and wide enough to illuminate the whole pellet stream). This leads to a laser beam height of 50 – 100 μm (and an illumination angle 1 or 5 degrees, as mentioned earlier).

Also, the height of the camera field of view has to be big enough to collect as much light from a pellet as possible and to see the whole pellet. It is necessary to provide a good time resolution, on the other hand, so the pellet has to be visible to the camera by a time shorter than the exposure time. These requirements also lead to a camera field of view height of 50 – 100 μm.

To detect pellets efficiently it is crucial to ensure good alignment between lasers and cameras, since the area illuminated by the laser is very narrow, and also the camera field of view is very narrow. This requires a precise alignment to ensure that the two areas overlap fully over the whole observed area.

The first step of the alignment is ensuring, that the camera and lasers axes are horizontal and that the camera field of view and the area illuminated by laser are horizontal. Then, further alignment is done mainly by changing the vertical position of lasers, relative to the cameras. The correctness of the alignment is evaluated based on the rate and brightness of observed pellets. As the correct alignment is assumed the situation when the pellet rate is the highest and pellets are the brightest.

The test with various arrangements of lasers and cameras lead to a conclusion, that during normal operation conditions it will be possible to detect at least 90% of pellets coming during camera exposure time.

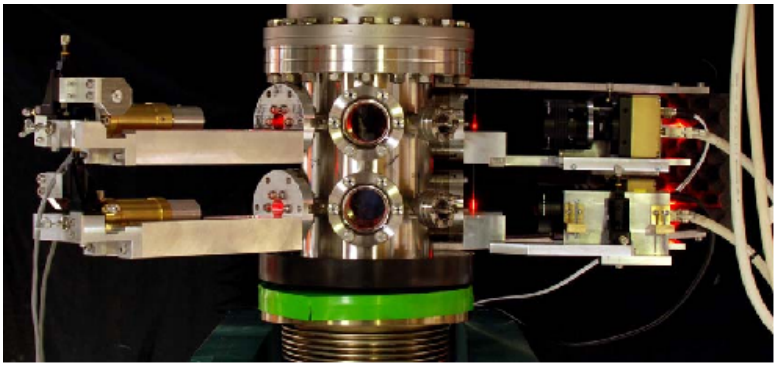

Figure 2.2.3: Line-scan cameras and lasers installed at the observation windows with holders allowing for their alignment

2.2.5. Data processing

Figure 2.2.4 shows a preview of a picture from a LS camera. The horizontal lines of the picture are measurements from subsequent moments

of time (camera cycles). In the picture one can see the pellets visible as darker spots. (Also synchronization lines are visible on the right edge of the picture; they are used for monitoring the synchronization between two cameras. The vertical lines appearing in the picture result from different background levels for even and odd pixels).

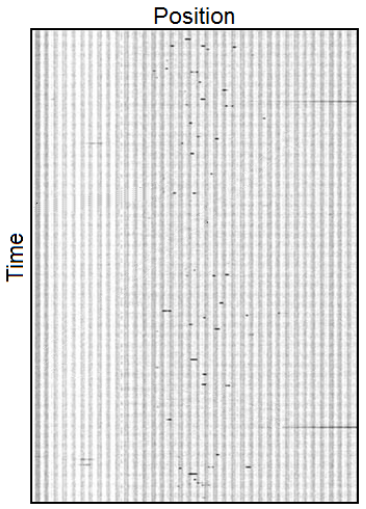

Figure 2.2.4: Preview of a picture from the line scan camera presented as a negative. Pellets are visible as dark spots close to the vertical axis of the picture. The horizontal lines at the right edge of the picture come from the synchronization diode. The vertical lines are a result of different background level for even and odd pixels

These raw images from cameras have to be processed in order to use them in pellet measurements. Currently an FPGA based electronics has been developed to enable fast processing of images from many cameras. However, the described measurements have been conducted with the previous version of the system, where the image processing was being done with a standard PC.

In such a setup, the cameras are connected to the computer via a device called frame grabber. This device collects the image lines from the cameras and when a certain number of lines is collected, they are combined into a so called frame. The frame is then sent to the analysis program. (Figure 2.2.4 shows a fragment of such frame). The frames are separated by gaps, much longer than the frame duration, when no data is collected. This is caused by the limited capacity of the PC to transfer data. The frames from the two cameras are synchronized by an external trigger signal. The speed limitation is resolved by the new FPGA based read-out system

The analysis program subtracts a pedestal from each pixel of the image. The pedestal is calculated by collecting an image sample with-

out pellets. The average value of light collected in each pixel is later being subtracted from the images. (The newer cameras also have a very efficient automatic pedestal subtraction).

Consecutive pixels in a single line (single exposure) with a light integral above a certain threshold are selected as one cluster. A weighted mean position of pixels in the cluster is taken as the measured pellet position. The amount of light collected in the pixels is used as a weight.

2.2.6. Cameras with shifted cycle

Presence of the dead time in the LS camera cycle introduces a considerable detection inefficiency of ≈20%. A solution to this problem would be to use two cameras mounted at the same level, looking at pellets from opposite directions. Cycles of the cameras will be shifted relative to each other by half a cycle. In the result, at any moment at least one camera will be in the exposure time, detecting pellets. Moreover, by comparing the information from two cameras and checking which one detected the pellet and in which cycle, it is possible to improve the time resolution 3 – 4 times. The idea of operation with shifted cycle is shown in Figure 2.2.5.

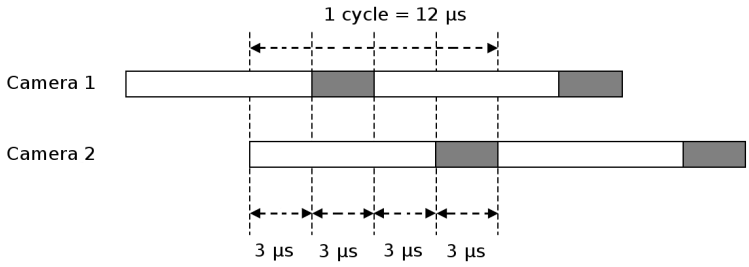

Figure 2.2.5: Visualization of an idea of two synchronized cameras with shifted cycle

2.3. Simulations of pellet detection

A procedure of simulating the pellet detection process was developed to enable accurate reproduction of experiments with pellets.

In the simulations the true position and time of each pellet at the measurement levels are calculated. This information is then used as a base for the process of simulating the measurements of the pellet position and time. This simulation takes into account various aspects of the measurement, as illumination, optical imperfections and electronic noise. The example plots visualizing the described properties are based on an example set of parameters listed in Table 2.3.1.

Pellet and camera physical properties

Pellet shape and size The simulated pellet is assumed to be a cube with its faces directed towards the cameras (*i.e.* it is visible as a square). The size is a constant value, the same for all pellets. (At the current stage of understanding the pellet detection process this simplification of the pellet shape is acceptable).

Camera field of view and cycle structure The camera is assumed to be a line of square pixels of a chosen size. It operates with a cycle of certain length, consisting of exposure time, when pellets may be detected, and dead time, when pellets are not detected.

Illumination

Pellet brightness (the amount of light reflected/refracted by the pellet in a unit of time) The pellet brightness is a property of illumination. The brightness is different for different pellets due to various effects. The value is generated randomly from a user-chosen distribution. Example of simulated pellet brightness is shown in Figure 2.3.1.

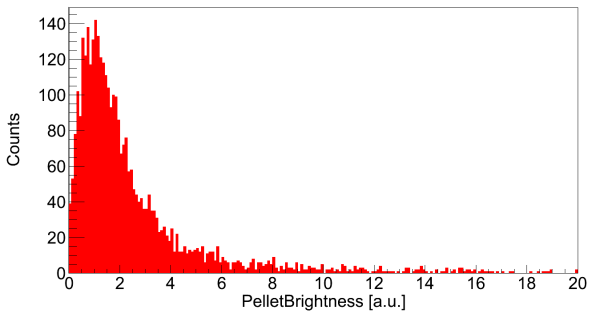

Figure 2.3.1: Pellet brightness (amount of light reflected/refracted in a unit of time). It is generated randomly from a distribution (see Table 2.3.1)

Camera optics

Pellet visible size Due to various optical effects, like the effect of the depth of field or optical aberrations, pellets may appear bigger than they are in reality. This is simulated by multiplying the physical pellet size (length in a certain direction), by a value taken randomly from a user-chosen distribution. This is done independently for each of XZY directions. Example of the simulated pellet visible size is shown in Figure 2.3.2.

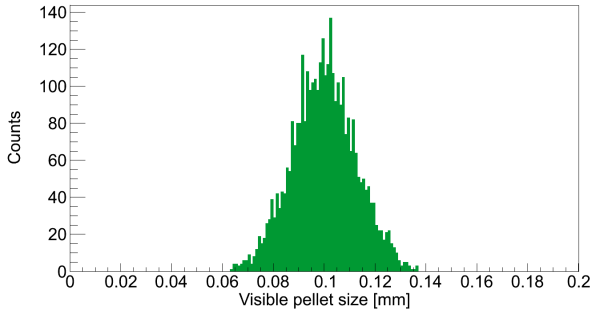

Figure 2.3.2: Visible pellet size. This number is taken by multiplying the simulated real pellet size (constant), by a number generated randomly from a distribution (see Table 2.3.1)

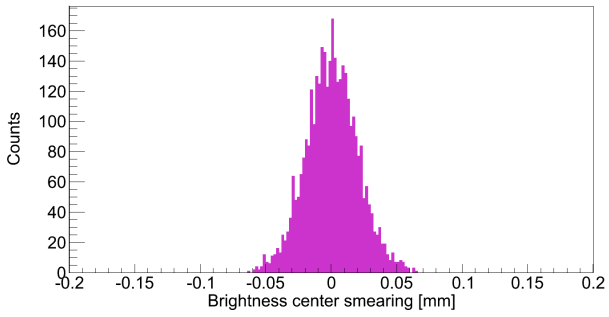

(a) X direction

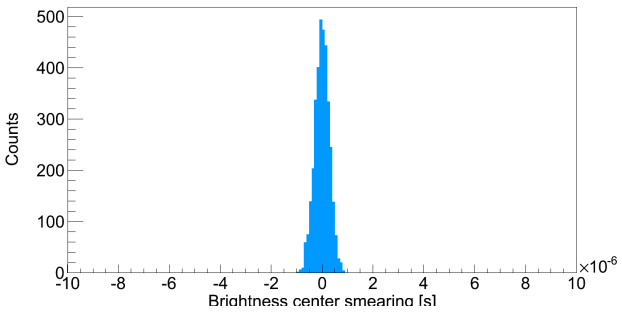

(b) Time

Figure 2.3.3: Brightness center smearing in X direction and in time. The brightness center smearing in X is calculated by adding a certain value to the true pellet position (center of mass position). This value is calculated by multiplying the visible pellet size by a random number generated from a distribution (see Table 2.3.1). The brightness center smearing in time is calculated similarly to the brightness center in position, but the Y position is converted to corresponding time, using the pellet velocity at this point

Position of the center of brightness with respect to the center of mass The calculated true pellet position is the position of its center of mass. What is measured by the camera is, however, the center of brightness. Even if one assumes perfect quality of the electronics and infinite resolution of the camera sensor, the calculated center of brightness is not necessarily the center of mass, due to various optical effects. Thus, the second step in simulating effects of optics in pellet detection, is simulating its center of brightness. A random value is picked from a user-chosen distribution. This value is multiplied by the visible pellet size and added to the position of the pellet center of mass. This is done independently for each of XZY directions. Example of the simulated pellet brightness center distribution is shown in Figure 2.3.3.

Detection process

Maximum possible amount of light collected (theoretical light integral) The amount of collected light (light integral, Figure 2.3.4) depends on the overlap between pellet and sensor line. Figure 2.3.5 shows schematically this overlap during the pellet passage in front of the camera. The integral of the overlap function (transformed from position to time coordinate - passage time instead of position at horizontal axis) multiplied by the pellet brightness (amount of light per time) gives the light integral.

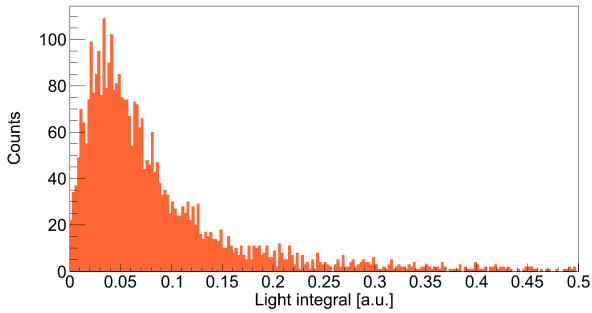

Figure 2.3.4: Theoretical light integral. The theoretical light integral shows the amount of light that would be collected by the sensor line (all possible pixels) without presence of dead time and noise in pixels

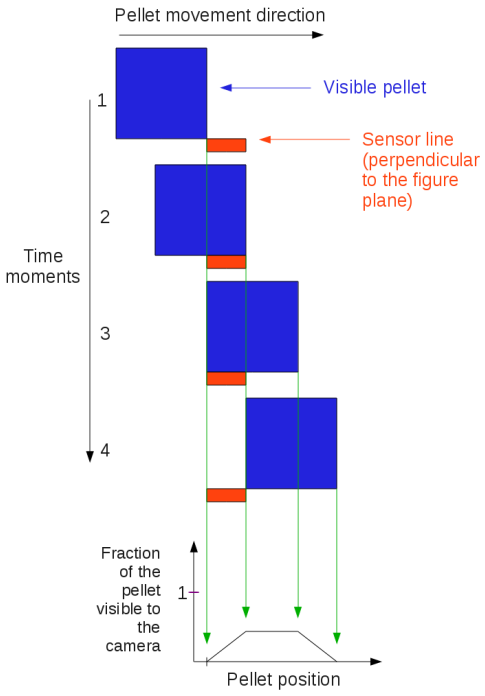

Figure 2.3.5: Pellet and pixels overlap during pellet passage in front of the sensor line. The total distance when the pellet is visible to the camera is a sum of visible pellet size and pixel size. The function has a different shape in three ranges, visible at the bottom of the figure. The transition between first and second range takes place at the position corresponding to the shorter of the visible pellet size and pixel size. The transition between the second and third range takes place in the position corresponding to the longer of the two sizes mentioned before. The function maximum value would be equal to one, if the visible pellet size was smaller or equal to the pixel size

Light collected taking into account the camera cycle (corrected light integral) Because the camera has a certain dead time, it often happens that the pellet appears in front of the camera when it is in dead time, and continues its passage when the camera is in exposure time. Or, inversely, the pellet can start its passage in exposure time, but before it has left the range of the camera, the camera switches to dead time. In this case the overlap function should be integrated in a limited range, depending on the pellet position in the moment when the camera switched between the exposure and dead time. A corrected light integral is calculated in this manner. It is used in the further detection stages. Example of a corrected light integral is shown in Figure 2.3.6.

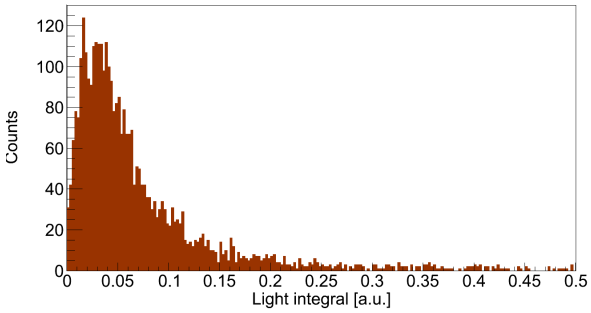

Figure 2.3.6: Corrected light integral. The corrected light integral takes the camera dead time into account

Light collected in single pixels along the sensor line The amount of light collected by the sensor line (corrected light integral) is divided between single pixels, proportionally to the overlap between pellet and pixel.

Signal noise for pixels The amount of light collected by a pixel is multiplied by a random number from a user-chosen distribution. This is done independently for each pixel and simulates noise in the electronics.

Measured light integral The amount of light collected by all pixels in the cluster (detected pellet) is the measured light integral. It is the final value of the simulated light integral. A distribution of it is shown in Figure 2.3.7.

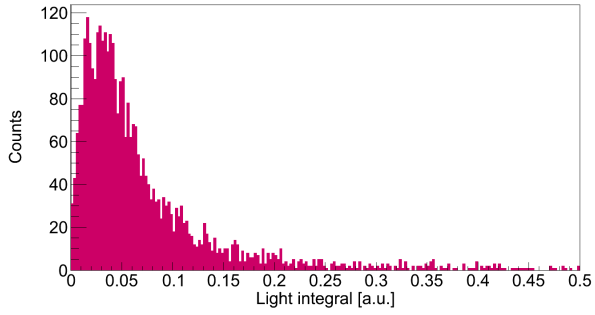

Figure 2.3.7: Measured light integral. The measured light integral takes into account also the noise in pixels

Detection threshold

Threshold on light collected in a single pixel During the detection one may accept only pixels which collected an amount of light greater than a certain threshold. Only these pixels are used to build the cluster.

Threshold on light collected in a cluster of pixels (detected pellet) During the detection one may accept only clusters with a total amount of collected light (measured light integral) greater than a certain threshold. Only these pellets are considered to be detected.

Determination of pellet position and time

Transverse (X or Z) position When a pellet passing in front of the camera gives signal within only one pixel, the position of the pixel center is taken as the measured pellet position. If the pellet passes in front of more than one pixel, its position is calculated as the weighted mean position of the pixels centers with the amount of light collected in each pixel taken as a weight. An example distribution of simulated measured pellet position is shown in Figure 2.3.8. The resolution, based on the difference between measured and true values, is shown in Figure 2.3.9a.

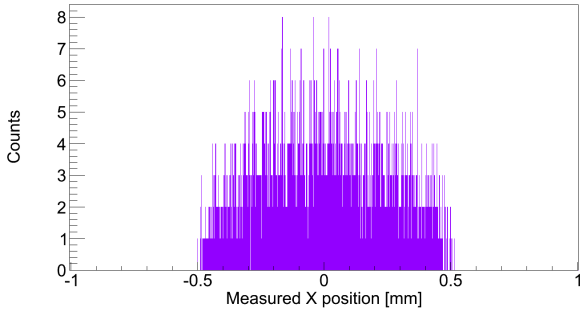

Figure 2.3.8: Measured pellet X position

Time Measured pellet time is recorded as the center of the exposure time, during which the pellet passed in front of the camera. When a pellet was detected in two exposure times, the one is taken, when the pellet was detected for the longer time. Example resolution of the time measurement is shown in Figure 2.3.9b.

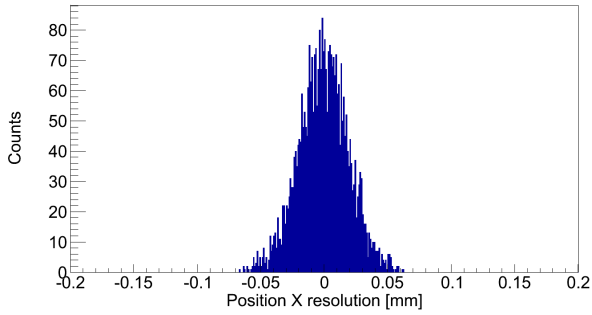

(a) X position

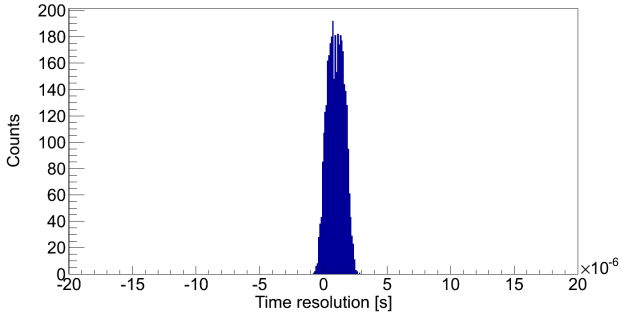

(b) Time

Figure 2.3.9: Resolution of X position measurement and time measurement. The value is the measured position/time minus the true position/time. The resolution is mainly an effect of the brightness center smearing

Table 2.3.1: Parameters of the example pellet detection simulations

Real pellet size		25 μm
Effective pixel size		37 μm
(Effective pixel size[1]		75 μm)
Camera cycle	period	2.0 μs
	exposure	2.0 μs
Brightness center position smearing	distribution	Gaussian
	center	0.0
	sigma	0.2
	range	from -3 to +3 sigmas
Pellet brightness smearing	distribution	Landau[2]
	location parameter	1.0
	width	0.5
	range	from 0.0 to 20.0
Pellet visible size smearing	distribution	Gaussian
	center	4.0
	sigma	0.5
	range	from -3 to +3 sigmas
Noise in pixels	distribution	Gaussian
	center	1.0
	sigma	0.02
	range	from -3 to +3 sigmas
Threshold on light integral from pellet		0.01 arb. unit
Threshold on light integral from pixel		0. (*i.e.* not used)

2.4. Summary – pellet detection

Pellet detection using line-scan CCD cameras and line-focusing diode-lasers has been investigated.

- Illumination conditions were optimized.
- Detection efficiency greater than 90% is obtained (the camera dead time not taken into account).
- A reliable procedure of simulating the pellet detection process was prepared.

[1] Alternative value of the pixel size, obtained for 25 mm lens

[2] Probability density function of the Landau distribution:

$$p(x) = \frac{1}{\xi}\phi(\lambda)$$

with

$$\phi(\lambda) = \frac{1}{2\pi i}\int_{c-i\infty}^{c+i\infty} e^{\lambda s + s\log s}\, ds,$$

where $\lambda = (x - x_0)/\xi$ and x being the argument, ξ being the width parameter and x_0 being the location parameter.

Chapter 3

Experimental study of pellet stream properties

Various parameters of the pellet stream have been investigated at the UPTS (Uppsala Pellet Test Station). The studies concern the shape of the stream at different measurement levels, divergence of the stream as well as pellets' velocity and velocity spread. Possible sources of the velocity spread have been investigated. Also, the probability to identify measured information belonging to a certain pellet was studied. A first experimental study of the pellet tracking principle has been made, resulting in an accurate reconstruction of the pellet generation point. The experimental results are followed by a detailed description of MC simulation procedures, developed to reproduce the measurement results.

3.1. Pellet position distribution in the stream

A straightforward measurement of the pellet stream properties is that of the density distribution. Figure 3.1.1 shows example distributions at different measurement levels.

The stream is initially very narrow (σ = 0.77 pxl = 0.02 mm a few mm below VIC exit) and is Gaussian shaped. After ≈270 mm (at PTRgen) the width (sigma) has increased to 0.3 mm (8.3 pxl), and a small tails around the peak may appear. At the distance ≈1500 mm below VIC, directly above the skimmer, the stream is wide as expected ($\sigma \approx$ 1.8 mm = 50 pxl). The visible asymmetry of the distribution in the example plot is a result of alignment, when the stream axis (*i.e.* the most dense region of the stream) did not coincide with the skimmer axis. The skimmer with its 2 mm opening diameter removes pellets with the biggest divergence and ≈370 mm lower, at PTRup, the full width of the distribution is ≈2.6 mm (70 pxl). 80 mm lower, at PTRlow, the full width is ≈3.0 mm (80 pxl).

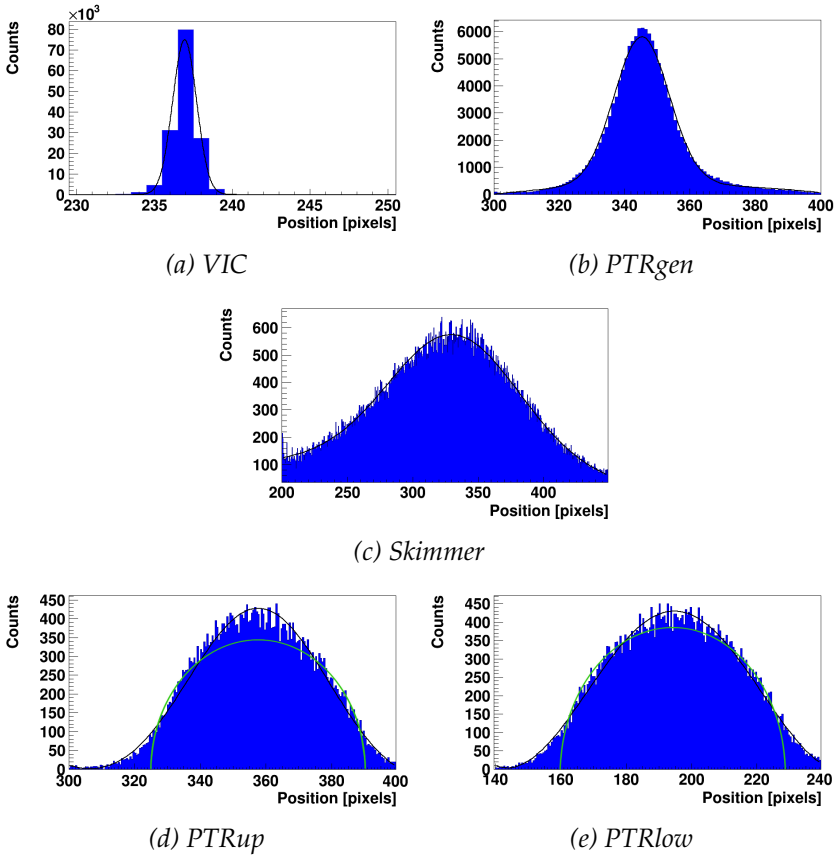

Figure 3.1.1: Example pellet position distributions at different measurement levels. One pixel corresponds to 26 μm at VIC and to 37 μm at other measurement levels. The solid line is an effect of fitting a sum of a Gaussian function and a parabola to the data. The plots for PTRup and PTRlow additionally contain a schematically marked shape of the distribution (green line) which one would expect assuming only linear (geometrical) pellet divergence and uniform pellet density in the stream after the skimmer.

The shape of distributions at these two last levels reflects the result of the skimmer which truncates the distribution edges.

From the width of the distributions at VIC, PTRgen and Skimmer and distance between these sections, one can deduce that the angular divergence of the stream is 0.7 – 1 mrad. The value varies because of different experimental conditions. Moreover, it is hard to determine it precisely even in a single measurement because of the irregular shape of the distributions, which makes the determination of stream width somewhat arbitrary.

The main source of pellet stream divergence may be found in the properties of vacuum injection where the pellets are propelled by a gas

stream and diverge after leaving the VIC, maintaining their initial direction in their further travel. The width of the pellet stream distribution at different distances from the VIC (different measurement levels) is consistent with such a linear divergence. This is also consistent with studies in Section 3.4, aiming to reconstruct pellet tracks.

Another source of stream divergence is collisions between pellets and interaction of pellets with the surrounding gas. This kind of interactions would result in more random behavior of pellets forming *e.g.* the tails of the distributions visible in the cases of PTRgen and Skimmer (see Figure 3.1.1b and 3.1.1c). The collisions between pellets take place almost only in the first few decimeters after the VIC, where the pellet stream is still dense – with small diameter and high pellet rate (see [30]). This is consistent with the fact that the tails are practically gone after passing the skimmer, in case of PTRlow and PTRup (see Figure 3.1.1d and 3.1.1e). Influence of gas present in the vacuum chambers on the pellet stream shape has been checked for the pellet position distribution at Skimmer, where the width of the distribution doubled after increasing the pressure in the chambers above the skimmer from 10^{-4} to 10^{-2} mbar. From this one can deduce that the widening of the pellet stream caused by this effect is in normal working conditions below a single percent level. Gravity is expected to have even smaller influence on the pellet stream width, influencing transverse pellet position in a scale comparable to the pellet size.

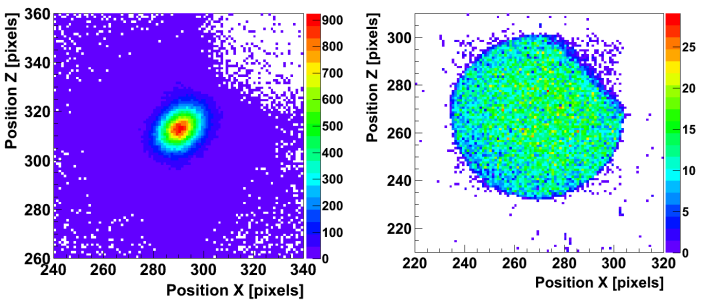

(a) PTRgen *(b) PTRlow*

Figure 3.1.2: Example of two-dimensional pellet position distributions

It is possible to make two-dimensional profiles of the stream by sing two synchronized cameras installed at the same level at an angle of 90°relative to each other. In this case the measurements recorded at the same time by both cameras are taken as x and z coordinates of a pellet. Figure 3.1.2 shows examples of such distributions. The circular shape of the stream is clearly visible. It has smooth edges at the PTRgen position

and is a very clearly cut circle at the PTRlow, so after collimation by the skimmer. Also, a possible illumination inefficiency can be observed, as it is visible in the example for PTRlow (Figure 3.1.2b, upper right corner), where the laser beam did not illuminate the whole stream.

3.2. Pellet velocity and velocity spread

The pellet velocity can be determined by measuring the time of flight between two observation levels. At least two synchronized cameras are required to make such a measurement. After collecting the sample, the data are analyzed offline.

The idea of measuring velocity by measurement of the time of flight seems straightforward. However, a problem arises when one takes into account the fact that at any given moment there are usually many pellets between the cameras. After a pellet is measured by the upper camera, the lower camera will measure many other pellets, before this particular pellet is recorded there. This implies that the procedure of measuring pellet time of flight is at the same time a procedure of pellet identification.

The idea of the analysis is to compare the time of a pellet detected by the lower camera with times of a certain number of pellets detected by the upper camera before this moment. This list of measurements from the upper camera used in the comparison is called a *queue*. The length of the queue (the number of pellets to compare) is chosen during the analysis based on the pellet rate and distance between the cameras (thus the number of pellets present in the same moment between the cameras), to assure that the correct pellet will be among the compared pellets.

The comparison of the measurements from both cameras is straightforward since the cameras are synchronized and the measurements from both cameras are stored in one chronologically ordered stream. One must note, however, that the data are collected in frames of a certain duration (see Section 2.2.5). The frames are separated and the time between them, when no data is collected, is longer than the frame duration. Because of that, measurements from the beginning of a frame are compared to a smaller number of pellets than the nominal queue size. This also means that in total there are more comparisons with small time difference than comparisons with larger time difference. Also, at the beginning of the frame the correct pellet will not be present in the queue.

The idea of how the comparison procedure works is presented in Figure 3.2.1.

The time differences obtained from the comparison are put into a histogram (time-difference spectrum, dT spectrum). Example spectra

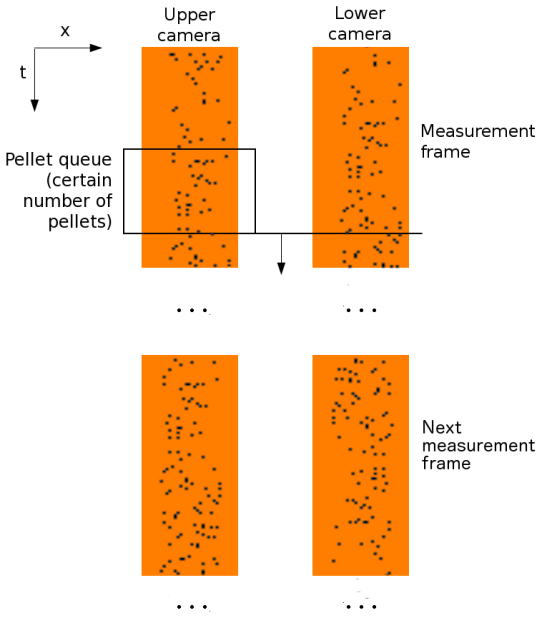

Figure 3.2.1: Pellet queue (see text)

obtained between different measurement levels are presented in Figures 3.2.2 - 3.2.4. Experimental results are compared to MC simulations, described in detail in Section 3.6. Two features in the time-difference spectrum are clearly visible: a smooth background and one distinct peak. The background is a result of incorrect comparisons *i.e.* comparing the times of different pellets. The peak is a result of comparing the times of the same pellet recorded by both cameras.

The position of the peak is then the measured time of flight. In the presented plots the time is expressed as a number of camera cycles (lines, since one line of picture is produced in each cycle). The other property of the pellet stream, which can be determined from the peak width, is the velocity spread. It turns out that the velocity of the pellets in the stream is not uniform, but forms a Gaussian shaped distribution with a sigma of approx. 0.5% - 1% (relative velocity spread, $\delta v/v$).

The background in the spectrum is bigger when the distance between measurement levels is bigger and the pellet rate is higher, since this is a situation when comparison of two different pellets is more probable.

The slope of the background visible in the dT histogram is a result of the frames which cause more comparisons between pellets with small time difference (when the queue is filled with less events) than between

pellets with bigger time difference (when the queue is filled with more events).

The truncation of the background on the right hand side is a result of limited size of the queue. Because of this the maximum time between pellets is limited. The smooth shape of this edge is a result of pellet loss and velocity spread, which make the effect stochastic.

The features of the spectrum were studied in detail with the help of Monte Carlo simulations, which allowed understanding the influence of different detection and pellet stream parameters on the shape of the spectrum. This is described in detail in Section 3.6.

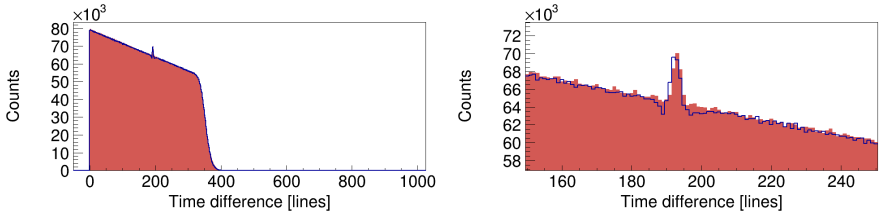

Figure 3.2.2: Time difference between pellets recorded at VIC exit and PTR gen (distance 270 mm) with magnification of the correlation peak region. Camera period: 20 µs. Experiment - blue line, MC - red area

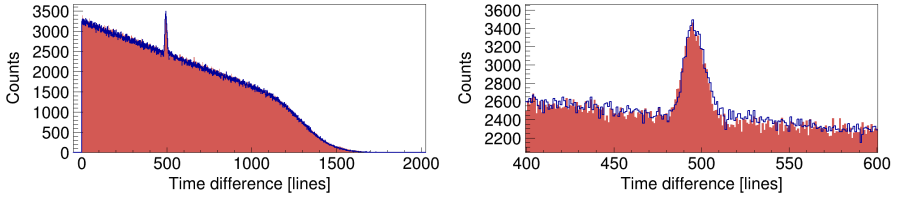

Figure 3.2.3: Time difference between pellets recorded directly above the skimmer and at PTR lower (distance 420 mm) with magnification of the correlation peak region. Camera period: 12.5 µs. Experiment - blue line, MC - red area

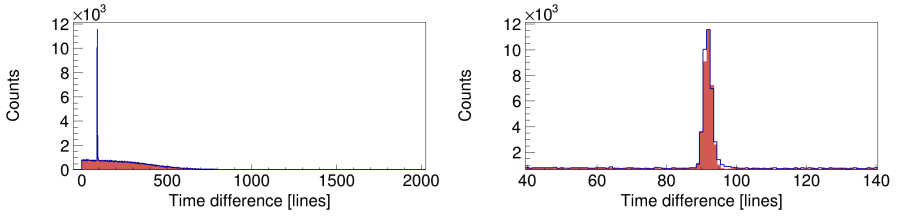

Figure 3.2.4: Time difference between pellets recorded at PTR lower and PTR upper (distance 80 mm) with magnification of the correlation peak region. Camera period: 12.5 µs. Experiment - blue line, MC - red area

3.3. Pellet identification

The time difference spectra provide a possibility of pellet identification. Since all correct measurement combinations (*i.e.* measurements of the same pellet at two cameras) are present in the coincidence peak, one can make a cut in the spectrum selecting only events from the time difference range corresponding to the peak.

It is, however, not possible to completely separate the correct combinations from the incorrect ones, because of the background, present in the selected time difference range. The level of the background depends on the probability of incorrect pellet identification. For a given measurement conditions it is higher for bigger distance between the measurement levels and for higher pellet rate at these levels. Earlier simulation studies [30] analyzed this question quantitatively for different conditions. For typical experimental conditions the probability of correct identification of a pellet between levels separated by 300 mm for a pellet rate of 20 k/s is of the order of 50%, while the same probability for a 100 mm distance between levels with 5 k/s pellet rate is of the order of 95%. Taking this into account, the best pellet identification possibility is offered by the PTRup and PTRlow as seen in Figure 3.2.4.

3.4. Reconstruction of the pellet generation point

Identifying measurements of the same pellet and having its position measured at two levels, it is possible to reconstruct a pellet track. In this case a bigger distance between the levels proves an advantage by offering a bigger lever arm for the track extrapolation. For this reason, the pair Skimmer – PTRlow has been used in tests of pellet track reconstruction, offering the best combination of reconstruction resolution and pellet identification possibility (see Figure 3.2.3). For all measurement pairs accepted in the cut, pellet tracks were calculated as straight lines, based on transverse pellet position measured by the cameras. The vertical positions of the cameras were also known.

The most straightforward way of checking pellet reconstruction is extrapolating the pellet tracks to the VIC exit, where all pellets originate from. All pellet tracks should meet at this position. This can be seen in the left plot in Figure 3.4.1, where all reconstructed tracks are drawn. The point where the tracks focus agrees with the distance to the VIC. Figure 3.4.2 shows a MC simulation of the described reconstruction.

The divergent tracks also visible in the two-dimensional plot for the experimental data are a result of incorrect combinations and of scattered pellets which current direction does not extrapolate back to the VIC. This presence of pellets moving in straight lines from the VIC together

with a presence of tracks which cannot come from pellets traveling from the direction of the VIC agree with the information in Section 3.1, where the shape of the stream distribution and its divergence is discussed. This also agrees with the MC simulations, where only free pellet movement with no interactions is modeled.

By making a slice in the two-dimensional plot at the position of the VIC exit (right plot in Figure 3.4.1), one obtains the resolution of the reconstruction $\sigma \approx 100$ μm. From this resolution and taking into account the distance to the measurement levels and the distance between them, it is possible, using simple uncertainty propagation formulas, to calculate the detection resolution, which is estimated to be ≈20 μm in the transverse direction.

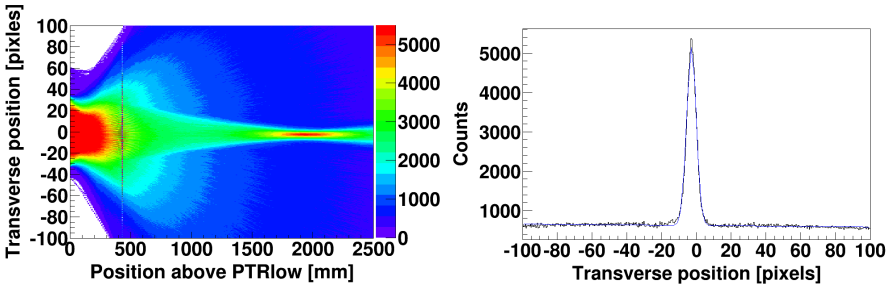

Figure 3.4.1: Extrapolation of a pellet track from experimental data (left plot), and a slice taken at the nominal position of the VIC (right plot). In the left plot, PTRlow corresponds to position 0 mm at the horizontal axis, Skimmer is located at position 420 mm and the position 1940 mm corresponds to the VIC exit

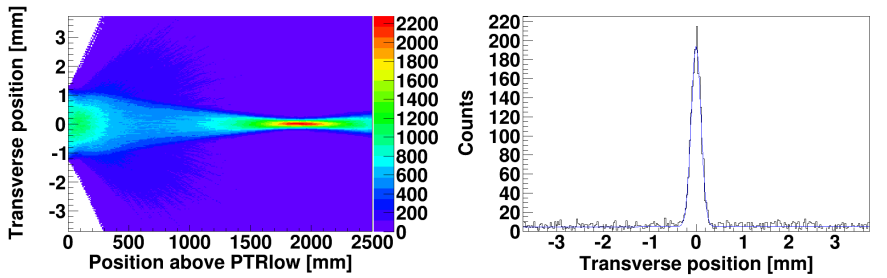

Figure 3.4.2: Simulation of pellet track extrapolation (see Figure 3.4.1). The scales of the plots correspond to the scales of the experimental plots (1 pixel = 37 μm)

3.5. Source of the velocity spread

The width of the coincidence peak in the time-difference spectrum is a result of the velocity spread in the stream - the fact that different

pellets travel with different velocity. The presence of the velocity spread raises the question about its source and properties. There are two main possibilities:

1. the velocity is angle dependent and at a certain angle the velocity spread may be very small, or
2. the velocity for all angles is the same and also the velocity spread is similar to the spread in the whole sample.

A study was done to find the source of the velocity spread by making separate time difference spectra for different pellet positions and angles.

For this study two line-scan cameras and two lasers were used in the configuration shown in Figure 3.5.1 and described in Table 3.5.1.

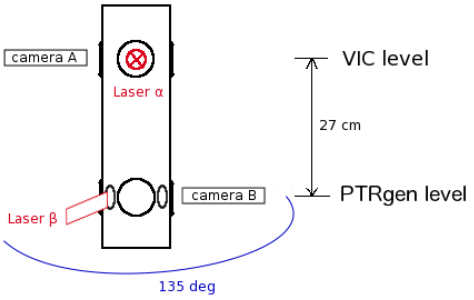

Figure 3.5.1: Experimental setup

Table 3.5.1: Experimental setup

	Camera location	Camera-laser angle	Effective pixel size
Upper camera (A)	directly below VIC	90°	26 μm
Lower camera (B)	≈27 cm below VIC (at PTR gen)	135°	37 μm

Distance between cameras: 27 cm

Cameras were sitting opposite to each other.

Cycle settings:	
Cycle length	20 μs
Exposure time	16 μs

A number of measurement runs were conducted. Several parameters were changed for different runs. The example results presented

in this section were obtained for hydrogen driving pressure 400 mbar, droplet chamber pressure 23 mbar and generator frequency 41 090 Hz. Example pellet distributions are shown in Figure 3.5.2.

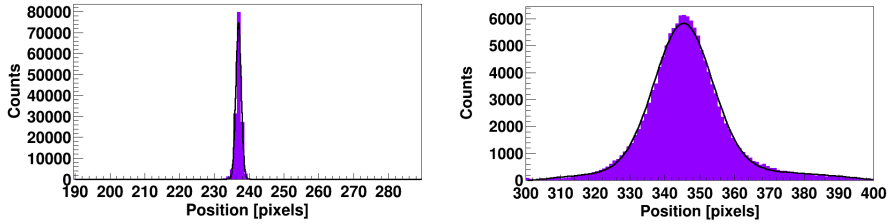

Figure 3.5.2: Distributions of the pellet stream measured by camera A (left plot) and camera B (right plot). Sums of a second degree polynomial and Gaussian function are fitted. Center of distribution for the upper camera is in position 237 pxl and the width (sigma) equals to 0.77 pxl, which corresponds to 20 μm. Center of the camera B distribution is in position 345.3 pxl and sigma is 8.34 pxl (309 μm)

The time of detection of each pellet by the lower camera (camera B) was compared to the time of detection of a number of preceding pellets (in these experiments: 200) detected by the upper camera (camera A). This time difference, expressed in number of camera lines (cycles), is plotted as a histogram in Figure 3.5.3, left plot. The peak seen over the combinatorial background corresponds to the time difference between two measurements of the same pellet. The width of this peak is a result of the velocity spread.

In the next step, a cut for only non-crossing pellets was made:

$$(x_A \geq center_A \; AND \; x_B \leq center_B) \; OR \; (x_A \leq center_A \; AND \; x_B \geq center_B)$$

(note that the cameras were aimed in opposite directions). The resulting histogram is shown in Figure 3.5.3, right plot. Only non-crossing pellets were taken into account in the further analysis.

A cut was made to determine the values of velocity and velocity spread for pellets recorded by the lower camera at different transverse positions. The range of the lower camera was divided into a few sub-ranges. For each sub-range a separate time difference histogram was made, by using only pellets from the sub-range of the lower camera pellet position and the whole range of the upper camera pellet positions. Example histograms for two different B-ranges are shown in Figure 3.5.4.

A cut for different pellet angles was also made. In this case, additionally, only pellets moving away from the center (spreading) were counted. Figure 3.5.5 shows the example results.

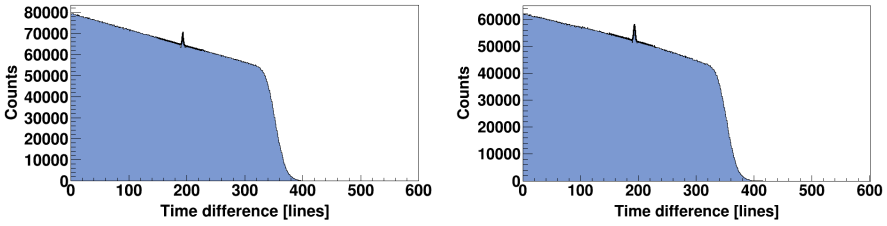

Figure 3.5.3: Time difference between pellets recorded by the cameras (see text). The left plot is a histogram for all pellets, and the right one is for non crossing pellets. A sum of linear and Gaussian functions is fitted. The mean time of flight between cameras is 193.1 lines (3.86 ms), which corresponds to 69.9 m/s. The width of the peak (sigma) is 1.13 for the left plot, and 1.22 for the right plot, which corresponds to a velocity spread equal to, 0.59% and 0.63%, respectively

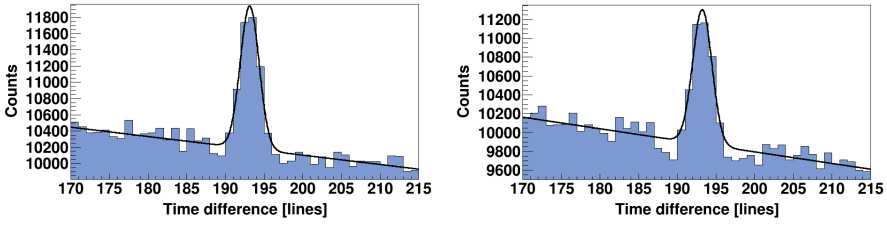

Figure 3.5.4: Time difference between pellets recorded by the cameras, for two different ranges of pellet position measured by the lower camera. Left plot: x_B in range 330–340 pxl, peak at 193.1 lines (69.9 m/s), σ = 0.64%. Right plot: x_B in range 340-345 pxl, peak at 193.2 lines (69.9 m/s), σ = 0.63%

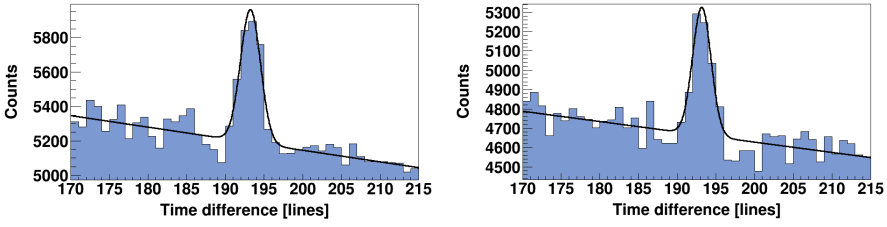

Figure 3.5.5: Time difference between pellets recorded by the cameras, for two different angles. Left plot: angle in range -0.04° – -0.02°, peak at 193.2 lines (69.9 m/s), σ = 0.67%. Right plot: angle in range -0.02° – 0.00°, peak at 193.2 lines (69.9 m/s), σ = 0.62%

Graphs summarizing these values were made based on the values of velocity and velocity spread for different positions and angles. Example plots for the discussed run are shown in Figure 3.5.6 and 3.5.7.

To visualize the magnitude of the velocity variation, the Y-axis of the velocity profiles is within the range [$v_{mean} - \sigma_{mean}$, $v_{mean} + \sigma_{mean}$]. The Y-range of the velocity spread profiles is from $0.8\sigma_{mean}$ to $1.2\sigma_{mean}$. The velocity and velocity spread corresponding to the edge values of angle and position might vary a lot from the mean value and are rather unreliable. On the other hand velocity and velocity spread for small angles and close to the distribution center, are close to the mean values and more uniform.

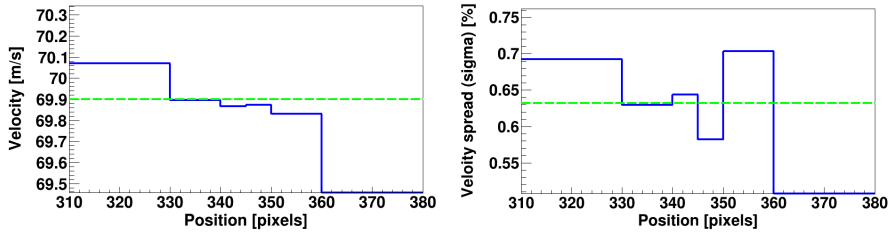

Figure 3.5.6: Velocity (left plot) and velocity spread (right plot) as a function of the transverse position of the pellet as recorded by the lower camera. The Y-axis range of the left plot is from $v_{mean} - \sigma_{mean}$ to $v_{mean} + \sigma_{mean}$. The Y-axis range of the right plot is from $0.8\sigma_{mean}$ to $1.2\sigma_{mean}$

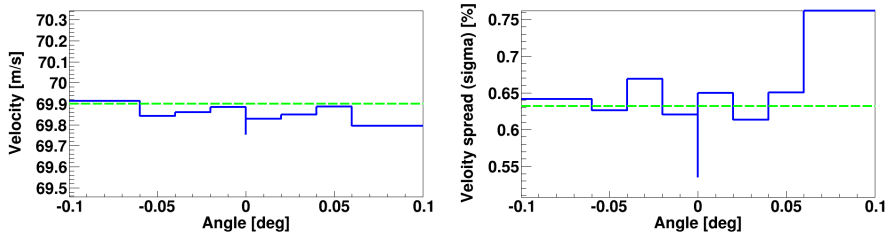

Figure 3.5.7: Velocity (left plot) and velocity spread (right plot) for different angles. The Y-axis range of the left plot is from $v_{mean} - \sigma_{mean}$ to $v_{mean} + \sigma_{mean}$. The Y-axis range of the right plot is from $0.8\sigma_{mean}$ to $1.2\sigma_{mean}$. The angle 0 means the mean angle of the stream

From the presented studies one can observe that the mean velocity and velocity spread of the pellets in different parts of the stream, independent of direction, is similar and is also similar to the mean velocity and velocity spread in the whole sample. Thus, the velocity spread present in the whole sample cannot be attributed to spatial non uniformity of the velocity in the stream. This leads to the conclusion that the velocity spread in the stream is independent on the pellet direction and is either random for all pellets or is the result of a micro time structure of the pellet velocity.

3.6. Simulations of pellet stream behavior and measurements

There are a few reasons for developing Monte Carlo simulations reproducing the measurements at UPTS:

- to make sure that the measured properties are well understood;
- to discover new properties and dependencies that can be measured and checked experimentally;
- to have reliable simulations which can be used in predictive studies.

This section describes the design and the usage of the pellet Monte Carlo simulation software and the results of the study of pellet stream properties with the help of such simulations. The previously existing version of the program [31] was modified and extended for the purpose of the studies described in this thesis.

3.6.1. Basic properties

Number of initially generated pellets It is possible to set the initial number of generated pellets. This number would correspond to the number of nozzle vibrations (generator periods) during a certain time, so in turn, the total number of produced droplets. The number of pellets in the next stages of the simulations would be generally (much) smaller due to pellet losses.

Generation frequency and generation time smearing A time of generation is assigned to each pellet based on the generation frequency. This time can be further smeared, because the pellets leaving the VIC may not exit in a constant pace (due to *e.g.* a non-uniform velocity in the VIC).

Vertical generation position It is possible to set a vertical (Y) position of the pellet generation point. This corresponds to the position of the VIC exit. This position is set relative to the assumed accelerator beam position (the coordinate system in the simulations is the same as for the WASA and PANDA detector systems).

Horizontal generation position and its smearing The horizontal generation position can be smeared according to a desired distribution. This reproduces the fact that after leaving the VIC the pellets do not travel perfectly one after another, but the stream has already a certain

(small) width. For each of the X and Z directions, the position is generated independently from the distribution.

Stream divergence Since the pellet stream has a certain divergence, it is also possible to set this parameter in the simulations. The pellet direction (angle) after the generation point (after leaving the VIC) is chosen from the desired distribution. For each of the X and Z directions the value is generated independently.

Velocity and velocity spread The initial velocity of each pellet is chosen randomly from a desired distribution, based on the mean velocity and velocity spread (width of the distribution) set by the user before the simulations. The velocity spread reflects *e.g.* non uniform pellet acceleration, resulting from the differences in pellets size, shape etc.

Gravity Since the pellets accelerate due to gravity, it is possible to apply this effect in simulations.

Skimmer The presence of a skimmer is implemented in simulations by removing from further processing all pellets which at a certain distance from the generation point (position of the skimmer entrance) pass further from the (vertical) beam axis than a certain distance (skimmer radius).

Position of measurement levels Measurements of the pellet stream properties are done in the simulations at certain positions (distances from the generation point), reflecting the positions of observation windows in the real device. The number of measurement levels can also be set.

Pellet loss at generation Pellets are lost during the generation, when they do not leave the VIC (because they disintegrated there). This effect is taken into account in simulations and it is possible to set a fraction of pellets surviving generation. If a given pellet survives is determined randomly according to that fraction (probability). Pellets which did not survive are not used in the further processing.

Pellet loss during the way Pellets are lost also during their way. The procedure here is similar to the loss at generation. The only difference is that the loss during pellet way occurs continuously along the stream. The practical implication of this is that the number of pellets that can be detected by the cameras at different levels is affected. So in the simulations the loss is realized before each measurement level and it reflects all the loss which took place since the previous level.

3.6.2. Structure of the time-difference spectrum

The structure of the time-difference spectrum was studied with help of the MC simulations to understand its origin and use it in more detailed studies of pellet stream parameters.

Behind the time-difference histogram

A time-difference histogram appears as one distinct coincidence peak on the top of a smooth background. In reality, the whole histogram is a sum of many Gaussian-shaped peaks.

The main peak, with a center at the point corresponding to the pellet time of flight between measurement levels, represents measurements of the same pellet by both cameras. This main peak is surrounded by many peaks resulting from combinations between different pellets. The distance between peaks corresponds to the time between generation of two subsequent pellets (*i.e.* the generator cycle). Separated peaks can be observed for low generation frequency (Figure 3.6.1). The peak neighboring to the right of the main peak comes from a comparison with a pellet generated in the previous cycle and the peak neighboring to the left, from a comparison with a pellet from the next cycle.

When the generation frequency is high (relative to the camera frequency), the peaks overlap resulting in a smooth solid background. The height of the background is also larger then, compared to the height of the separate peaks (Figure 3.6.2). The closer the peaks are to each other, the more height they gain from overlapping with their neighbors. However, the elevation of the main peak over the surrounding peaks does not change (Figure 3.6.3).

The changes of the properties of the single peaks result in a change of the shape of the plot. Figure 3.6.4 shows another example – decreasing number of events in the secondary peaks resulting in the slope in the background.

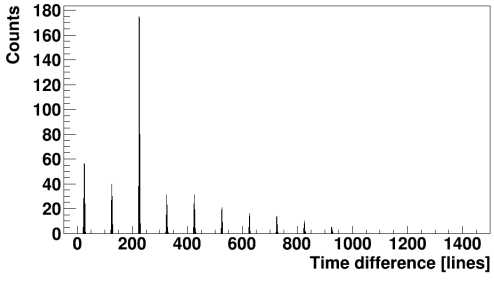

Figure 3.6.1: Separate peaks of background visible in the dT spectrum when the generation frequency is small relative to the camera frequency (MC)

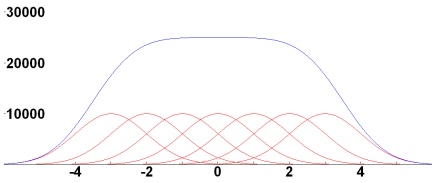

Figure 3.6.2: Visualization of a sum of Gaussian peaks

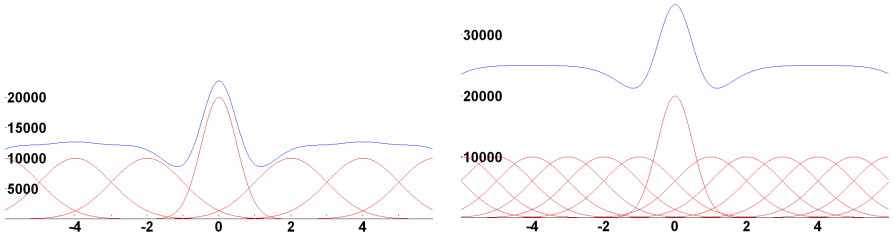

Figure 3.6.3: Formation of time difference spectra from separate peaks. The main peak has the same integral as the secondary peaks, but is two times higher. The distance between the peaks is 2 secondary peak sigmas (left plot) and 1 secondary peak sigma (right plot)

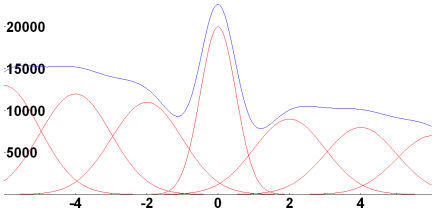

Figure 3.6.4: Illustration of how the changing number of events in the secondary peaks produces the slope in the background

Properties of the peaks

The height is what enables us to distinguish the main peak from the others. Since the height h of a Gaussian function is proportional to the number of events N and inversely proportional to the distribution width σ:

$$h = \frac{N}{\sigma\sqrt{2\pi}} \tag{3.6.1}$$

($\sqrt{2\pi} \approx 2.5$), then the width of the peaks or number of events in them are the parameters which should be different.

Width of the peaks

The width of the main peak is a direct result of the velocity spread. The width of the secondary peaks is a quadratic-sum of smearing resulting from the velocity spread and the generation time smearing according to the formula:

$$\begin{cases} \sigma^t_{main} &= \frac{d}{v}\sigma^{rel}_{vel} \\ \sigma^t_{add} &= \sqrt{\left(d_1^2 + d_2^2\right)\cdot\left(\frac{\sigma^{rel}_{vel}}{v}\right)^2 + 2\cdot\left(\sigma^t_{gen}\right)^2} \end{cases} \tag{3.6.2}$$

where: σ^t_{main} - width of the main peak measured in time units, σ^t_{add} - width of the additional peaks measured in time units, v - mean pellet velocity in the stream, σ^{rel}_{vel} - relative velocity spread in the stream, d_1 - distance of the first camera to the generation point, d_2 - distance of the second camera to the generation point, $d = d_2 - d_1$ - distance between cameras, σ^t_{gen} - generation time smearing measured in time units.

Number of events in the peaks Without pellet losses, detection inefficiency and data taking inefficiency, the number of pellets in each peak would be the same. The presence of them changes these numbers:

- Pellet loss before both cameras changes the number of events in the main peak by the same factor. The number of events in the secondary peaks decreases as a square of this factor, because the number of possible comparisons between different pellets decreases quadratically in this situation. The result is that for a bigger pellet loss the main peak is more pronounced.
- Detection inefficiency (the same for both cameras, taking into account the camera dead time and additional inefficiencies) decreases the number of events in both the main peak and the secondary peaks by the square of the inefficiency factor (since the number of possible correct and incorrect comparisons decreases quadratically in this situation).
- Pellet loss between measurement levels changes the number of events in the main peak and in the secondary peaks by the same factor (since the number of possible correct and incorrect comparisons decreases linearly in this situation).
- A change in the ratio of camera and generation frequencies changes the overlap between peaks and thus the height of the pedestal. However the elevation of the main peak stays the same (see Figure 3.6.3).

The different width of the peaks (and hence their height) is together with the pellet loss the reason why one is able to measure pellets velocity. **With no velocity spread and 100% survival fraction it would not be possible to distinguish the right combination measurement combination in the two cameras.**

The number of events in the correlation peak

The number of pellets in the coincidence peak N_{peak} can be described with the following formula:

$$N_{peak} = N_{lower} \cdot D_{totU} \cdot C, \tag{3.6.3}$$

where: N_{lower} - number of pellets detected by the lower camera, D_{totU} - total detection efficiency of the upper camera, C - comparison efficiency.

Total detection efficiency D_{tot} depends on random inefficiency I_{rndm}, camera exposure time E, camera period P and additional time t_{edge} resulting from the fact that the pellet may be detected also when it is seen partially at the edges of the camera exposure time:

$$D_{tot} = (1 - I_{rndm}) \cdot \left(\frac{E + t_{edge}}{P} \right). \tag{3.6.4}$$

The time t_{edge} depends on the detection threshold and various properties of the detection process and has the highest theoretically possible value when the detection threshold is set to 0:

$$t_{edge,max} = \frac{x_{pel} + x_{pix}}{v}, \tag{3.6.5}$$

where: x_{pel} - visible pellet size, x_{pix} - effective pixel size, v - pellet velocity.

The comparison efficiency parameter takes into account that pellets detected at the beginning of a frame in the lower camera were passing the upper camera before the frame started:

$$C = 1 - \frac{T_{TOF}}{N_{lns}}, \tag{3.6.6}$$

T_{TOF} - pellet time of flight between cameras, expressed in lines; N_{lns} - number of lines in one frame.

3.6.3. The simulation procedure of pellet target operation and exploratory knowledge gathered

The simulations do not operate on the lowest level and do not model various effects responsible for pellet acceleration in VIC, pellet collisions etc. The effect of the passage through the VIC is already set in

the beginning of the simulations as velocity, velocity smearing, loss at generation etc. Also further pellet loss is set to reproduce the results of the experiments.

To simulate an experiment one has to follow the procedure described below.

Parameters set directly

Some of the parameters are set in the simulations exactly as they are set in experiments, since they are a part of the experimental setup. These parameters are: **generation frequency**, **camera period and dead time** (described in detail in Section 2.3) and also the **number of pellets in the sample**.

The number of pellets, N, in the sample can be calculated knowing the number of frames in measurement n_{fr}, number of lines in a frame n_{lns}, exposure time T_{exp} and generation frequency f_{gen}:

$$N = n_{fr} n_{lns} T_{exp} f_{gen} \tag{3.6.7}$$

Parameters set indirectly

Most of the parameters of the simulation, such as **loss at generation**, **loss between measurement levels**, **detection inefficiency**, **stream divergence**, are estimated to reproduce the measurements. These parameters are set so that the properties such as width (and shape) of the pellet stream distribution and the number of pellets detected at the different measurement levels, as well as the shape of the time difference spectrum (position and width of the peak, height of the peak, height of the background, shape of the background, number of entries) agree with the experiment.

Obtaining a final set of parameters is an iterative (and often complicated) procedure, because often a change of one parameter results in a change of many measured properties, and one measured property can be affected by many simulation parameters. Because of this, however, the simulations make it possible to determine values of various parameters which cannot be measured directly.

Obtaining agreement between simulations and experiment

The horizontal generation point smearing is set based on the width of the distribution at VIC.

The pellet stream divergence is set based on the width of the stream at VIC and PTRgen. It also it has to be consistent with the width at Skimmer. This, however, is more difficult to be measured accurately because of the pronounced tails and often asymmetric shape of the distribution.

The number of pellets detected at VIC, compared to the total number of droplets produced during the measurement, gives information about the product *GenerationSurvivalRatio* × *DetectionEfficiency*. The number of pellets detected by the camera at PTRgen gives the pellet loss before VIC and PTRgen measurement levels (assuming the same detection efficiency).

The loss of pellets between Skimmer and PTRup is a result of two effects: "normal" pellet loss and pellet loss at the skimmer. In the first approach the loss at the skimmer results from the stream divergence, which is set based on the distribution width. Sometimes, however, this distribution has to be adjusted (again, because of its non-consistent shape) to make the simulated pellet loss from different sources reproduce the experiment.

The mean velocity and velocity spread is set, based on experimental results. The value for the velocity spread results in an initial value of the width, and consequently the height, of the correlation peak in the dT spectrum. If the measured width in simulations turns out to be different from the experimental one, the input value can be changed. This will result also in a change of the peak height. When the peak width equals the experimental value, the height is used to disentangle the pellet loss and detection inefficiency.

As it was said before, for a given number of pellets detected by the cameras, the correlation peak is lower when there was detection inefficiency and is higher when there was pellet loss before first of the two measurement levels. The highest peak is obtained in a situation with no detection inefficiency (for a certain dead time this means a lack of additional inefficiency). When the simulated peak is still too low, this suggests that the real efficiency is higher than the camera *Exposure/Period* ratio. This is explained by the fact that, because of the size of the pellet and sensor, the pellet is visible partially also at the edges of camera exposure time. The detection efficiency may be adjusted by setting the proper value for the detection threshold (corresponding to a minimum pellet-pixel overlap when the pellet is still detected).

The shape of the right-hand edge of the dT spectrum is a result of a certain distribution of the queue duration. It required additional measures to make the simulation reproduce this feature of the experimental results. The following section contains a discussion of this topic.

3.6.4. Fluctuations of the pellet rate

It was discovered that the distribution of the length in time of the queue was different in the data than in Monte Carlo (Figure 3.6.5). This distribution shows a time between the first and the last pellet in the queue, containing a certain (generally – fixed) number of pellets (see Section

3.2). The difference between the experimental and simulated distributions, occurring initially, shows that the experimental distribution is broader than it is expected from the Bernoulli distribution. Therefore, there must be some fluctuations of the pellet rate.

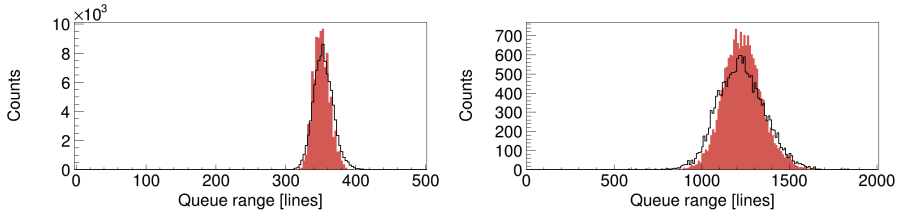

Figure 3.6.5: Distribution of the time-length of queues before correction, for VIC–PTRgen (left plot) and PTRgen–Skimmer (right plot). Black line - data, red area - MC

Due to small statistics, it was not possible to see any pattern of varying pellet rate during a measurement. Therefore, a procedure was developed to provide effective simulations of the effect. The pellet rate was modulated by periodic changes of the pellet survival probability at generation.

As the base function for the modulations, an inverse error function was used $InvErf(z)$, where the error function $Erf(w)$ has a form:

$$Erf(w) = \frac{2}{\sqrt{\pi}} \int_0^w e^{-t^2} dt$$

The function $InvErf(z)$ was then transformed to make a periodic function using the formula

$$z(x) = \begin{cases} -4x+1 & ,x \in [0,0.5) \\ 4x-3 & ,x \in [0.5,1) \end{cases}$$

where

$$x = \frac{t \bmod T}{T}$$

is a fraction of the modulation cycle, with t being the current time in the simulation, T being the period of modulation and mod meaning modulo.

The final simulated probability for the pellet survival $P_{surv,mod}$ is given by

$$P_{surv,mod} = P_{surv,mean} + A \cdot InvErfTrunc(z),$$

where $InvErfTrunc(z)$ is the truncated inverse of the error function, $P_{surv,mean}$ is the mean survival probability, set in the simulations, and A is the amplitude of modulation.

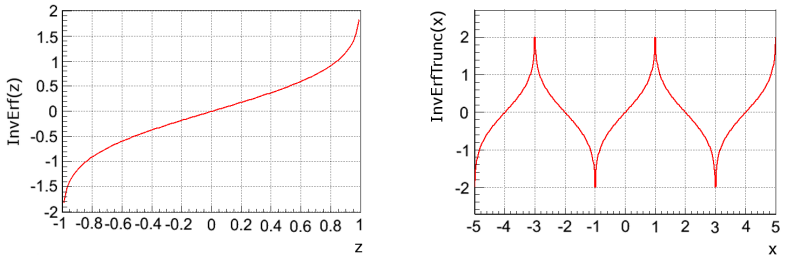

Figure 3.6.6: Inverse of the error function (InvErf(z), left plot) and a periodic function based on the truncated InvErf, used for modulation of the pellet survival fraction (right)

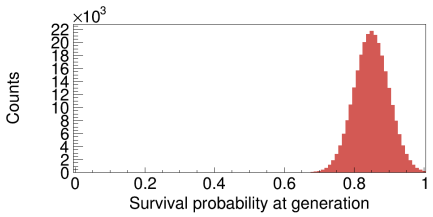

Figure 3.6.7: Distribution of the survival probability at generation after modulation

Among other functions tested (*e.g.* triangular and sinusoidal), this one proved to be the only one possible to be used in this application, since it is the only one for which the probability of being at a certain distance from the "equilibrium" is described by a Gaussian distribution. And this kind of distribution was required to broaden the initially simulated distribution to make it match the experimental one, without changing its main shape.

The studies showed that the optimal value for the period of the function is 0.05 s. The amplitude was set individually for each situation.

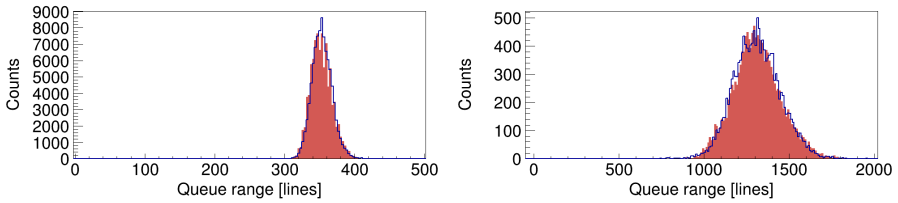

Figure 3.6.8: Distribution of the time-length of queues after correction, for VIC–PTRgen (left plot) and PTRgen–Skimmer (right plot). Black line - data, red solid - MC

Table 3.6.1: Parameters of demo simulations reproducing experiments at UPTS

	VIC – PTRgen	Skimmer – PTRlow	PTRup – PTRlow
		Experiment	
Settings			
Generation frequency	41 090 Hz	41 526 Hz	41 526 Hz
Camera cycle	20/16 μs	12.5/10 μs	12.5/10 μs
Frame size	1024 lns	2024 lns	2024 lns
Queue size	200 plts	100 plts	10 plts
Number of frames	256	1024	1024
Measured values			
Number of pellets at upper camera	147 434	152 026	39 440
Number of pellets at lower camera	140 663	43 975	41 023
Velocity	70.1 m/s	68.18 m/s	69.68 m/s
Main peak sigma	0.58%	1.15%	1.24%
Stream divergence		1.23 mrad	
		Simulations	
Settings			
Generation frequency	41 090 Hz	41 526 Hz	41 526 Hz
Number of generated events	215 400	1 075 800	1 075 800
Generation survival fraction	0.843	0.82	0.82
Loss fraction between VIC—PTRgen	0.0458	0.12	0.12
Loss fraction between PTRgen—Skmr	–	0.583	0.6
Initial mean velocity	69.89 m/s	67.88 m/s	69.42 m/s
Velocity spread	0.39 m/s (0.558%)	0.83 m/s (1.22%)	0.827 m/s (1.19%)
Gen. surv. frac. modulation function	InvErf	InvErf	InvErf
Gen. surv. frac. mod. period	0.05 s	0.05 s	0.05 s
Gen. surv. frac. mod. amplitude	0.03	0.08	0.08
Stream divergence	0.77 mrad	1.13 mrad	1.13 mrad
Exposure threshold	0.05	0.05	0.05
Additional det. ineff. at VIC	0.04	–	–
Additional det. ineff. at PTRgen	0.04	–	–
Additional det. ineff. at Skimmer	–	0.466	–
Additional det. ineff. at PTRup	–	–	0.04
Additional det. ineff. at PTRlow	–	0.	0.
Queue size	200 plts	100 plts	10 plts
Frame size	1024 lns	2024 lns	2024 lns
Number of frames	256	1024	1024
Measured values			
Number of pellets at upper camera	147 773	151 496	39 363
Number of pellets at lower camera	141 064	44 006	40 869
		Comments	
	without cut for multiplicity	cut for multiplicity was used – pellets detected in the same line were omitted	cut for multiplicity was used – pellets detected in the same line were omitted

3.7. Summary – pellet stream measurements

Pellet stream properties have been investigated at the UPTS.

- The number of pellets and position distributions in the stream, as well as time correlations between pellets detected at different levels were measured.
- The measurements gave information about various pellet stream parameters:
  - stream divergence (typically 0.7 – 1.2 mrad),
  - pellet velocity (typically 70 – 80 m/s),
  - velocity spread (typically 0.5 – 1 %) and
  - pellet rates at different measurement levels (approx. 30 – 80 k/s at VIC, 20 – 70 k/s at PTRgen, 20 – 60 k/s at Skimmer, 5 – 20 k/s at PTRup/low)
- The experimental results are well reproduced by the detailed simulations.
- The simulations are reliable enough to be used to predict pellet stream and pellet detection performance in the design of a full scale pellet tracking system.

Chapter 4

Tracking system design

The understanding of pellet detection conditions and pellet stream parameters, together with the developed pellet Monte Carlo simulation framework, have been used to prepare design studies of a pellet tracking system for PANDA. The aim was to check the resolution and performance of such system given different conditions of the pellet stream, detection configuration and data processing. The study shows that it is possible to construct a system meeting the required performance parameters.

4.1. Introduction

4.1.1. Motivation

The interaction region is given by the overlap of the pellet stream and the accelerator beam and has a size of a few millimeters. However, one would like to know the interaction point more precisely, to have better possibility to reconstruct the particle tracks coming from the interaction point. One would also like to suppress background events that do not come from a pellet, but *e.g.* may occur in rest gas present in the beam pipe.

A solution is provided by the pellet tracking system [23,32]. The goal of the system is to track single pellets in order to know their position accurately at the time of an interaction. The desired resolution is a few tenths of a millimeter.

The tracking will be accomplished using lasers and fast line-scan (*i.e.* one dimensional) CCD cameras. The cameras, placed at different levels along the pellet stream, will measure pellets' position and time of passage (Figure 4.1.1). Then, the information from many cameras will be put together to identify and reconstruct the track of each pellet. Information about the pellet position in the interaction region at the time of an interaction will be used in the analysis of the experimental data.

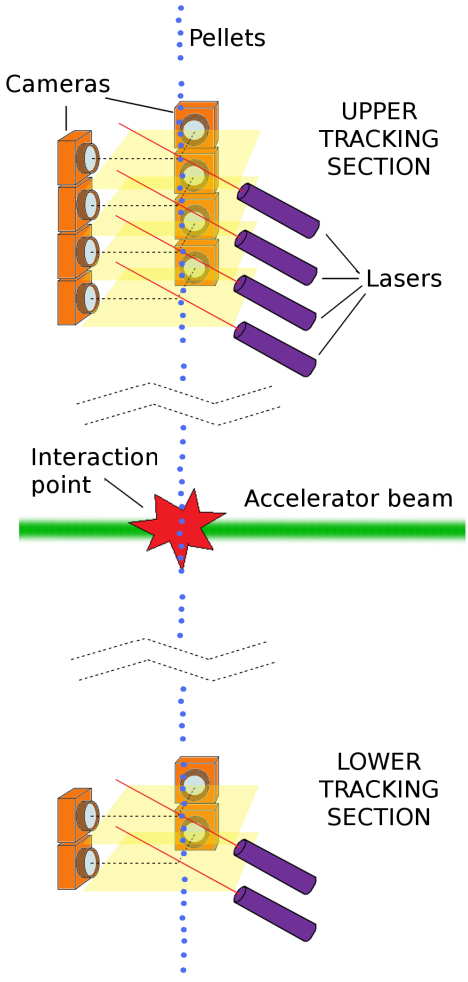

Figure 4.1.1: Principle of operation of a pellet tracking system

4.1.2. Goals

To be useful, the tracking system must be highly efficient and provide tracking information for essentially all pellets that pass the interaction region. The information to be provided includes:

- Positions of individual pellets at the time of an interaction and quality of the position information.
- Number of pellets in the interaction region at a given time and uncertainty of this number.
- General quality of the pellet stream and of the measurements during a longer time interval.

The position along the accelerator beam gives the most important coordinate (z – see the coordinate system definition in Appendix B) for the event reconstruction, both for the case of short lived reaction products and for reactions from possible background gas. In the vertical direction (y) along the pellet beam the resolution should be good enough to allow a good estimate of the number of pellets in the interaction region *i.e.* the resolution (sigma) should be small in comparison to the vertical extension of the accelerator beam. In practice this means that a $\sigma < 1$ mm is required for a 5-10 mm beam size. There must also be sufficient redundancy in the measurements so that consistence and quality of the tracks can be evaluated. This includes the possibility to check whether a track could originate from the pellet generation point or not.

The knowledge of the number of pellets in the interaction region at the time of a hadronic event is of course crucial for the possibility to use the position information. Exactly one pellet in the region is the desirable situation since in this case the reaction most probably occurred in that pellet. If there were more pellets one might get some help in event reconstruction by assuming the different positions as origins for the reaction. If there was no pellet, the reaction probably occurred in rest gas. It is interesting to know how well the tracking system can distinguish these different cases.

A measure of the general quality of the pellet stream and tracking system could be the fraction of tracking detector data that contributes to well behaving pellet tracks and the micro time structure of such tracks.

The overall goal is to have useful *i.e.* correct tracking information for as many hadronic events as possible. With this in mind one can define some kind of tracking efficiency. It is reasonable to aim for a value above 70%. One should also preferably know for each event if the information is useful or not.

4.1.3. Basis and layout of the studies

The aim of these simulation studies is to check how the expected position resolution and tracking performance for different design variants meets the goals and requirements discussed above and find out how they depend on various parameters describing the pellet and pellet stream properties and the detection process.

The geometrical conditions and tracking equipment configurations are based on a conceptual design for PANDA (Figures 4.1.2 and 4.1.3) where two 0.4 m long sections of the pellet beam pipe are reserved for the tracking system, one at the pellet generator and the other one at the dump. At each section four levels of measurements can be accommodated. Earlier simulation studies [30] with realistic pellet beam

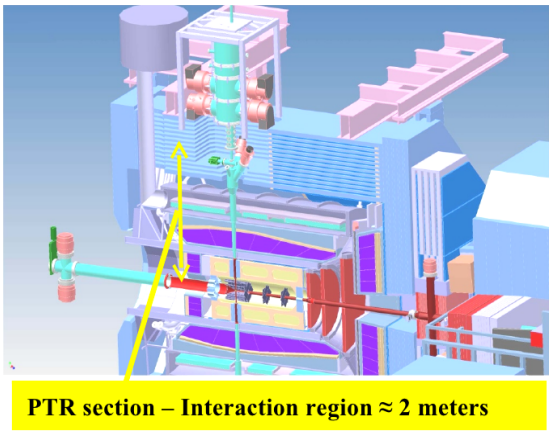

Figure 4.1.2: The PANDA setup with space reserved for pellet tracking seen at the top in a recess in the iron yoke.

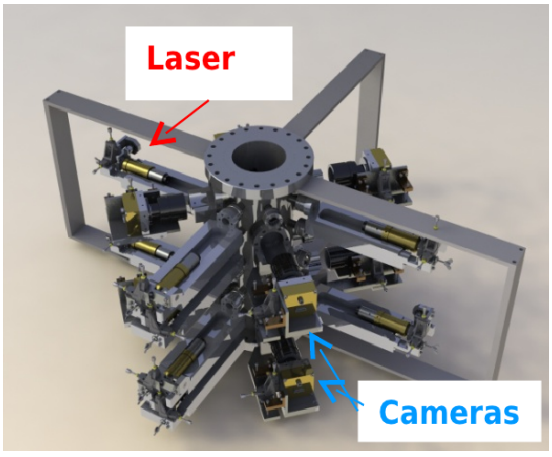

Figure 4.1.3: Conceptual design of the upper pellet tracking section for PANDA. There are four levels with cameras and lasers for pellet measurements.

parameters including a relative velocity spread of 1% and a pellet frequency around 15 k/s showed that the distance between measurement positions should not be more than 5 cm for high efficiency in velocity determination and around 20 cm for obtaining the required accuracy in the interaction position determination. The levels in each section are therefore separated by 50 - 100 mm. Two levels are for x position and two for z position determination. The velocity and direction determination can then be done over a path length of 50 - 225 mm. To have two tracking sections gives more redundancy with improved accuracy and extended possibilities for tuning and checking. Important checks concern efficiency and alignment.

The upper section provides better detection possibilities because of small diameter of the pellet stream (≈2 mm). This means that the stream fits well within the camera field of view, and since it is possible to use 50 mm optics in this case (see Section 2.2.3), the detection resolution is also better (σ = 20 μm compared to σ = 40 μm for the lower section). The light intensity can also be higher because it is enough to illuminate a smaller region.

Detailed studies of tracking performance, described in this work, are based on the upper tracking section only. However, to determine the gain in tracking performance resulting from the use of lower tracking section, example results for typical conditions are also presented. The resolution has been studied for both cases - with and without the lower tracking section. This section contains three measurement levels separated by 60 mm, two of them participating in the tracking in z direction and one for the x direction. Addition of the lower tracking section substantially increases the lever arm for pellet velocity determination (≈20 times). This is especially important given the limitations of time measurement resolution. The significant distance between the measurement sections influences also the direction determination. However, in this case the theoretical gain in the already high resolution may not be reached due to the limited precision of mechanical mounting and alignment.

It is necessary to have a careful tuning of the cameras and lasers positions and angles for the system to operate. One has to make sure that the plane of the camera field of view and the plane lit by the laser overlap fully. The tracking system will provide information about pellet position relative to the cameras. To use information from the system, it will be necessary to calibrate the devices. The positions of the cameras relative to each other and relative to the VIC and the interaction region have to be determined and monitored. Centers of the pellet stream density distributions can be used for the VIC and the camera calibration in X and Z directions. To do the alignment with the accelerator beam one will use event rates of *e.g.* elastic scattering reactions with pellets and accelerator beam. For alignment in the Y direction, the usage of a very low pellet rate will be needed.

Results from tests done with a tracking prototype system at the UPTS (Uppsala Pellet Test Station), provide both input data on the performance of different system components and give a possibility to tune and check the simulation procedure. The tests were described in Chapters 2 and 3. These chapters contain also descriptions of the simulation procedures developed to reproduce experimental results. The simulations include the pellet stream behavior and the pellet measurement process.

A tracking procedure is needed to be able to evaluate (via model-

ing) the tracking accuracy and efficiency. Two versions of a tracking algorithm have been developed for this purpose – a simpler and fast algorithm and a high efficiency more advanced algorithm. The design studies presented in this chapter are based on usage of the simplified algorithm. Results of the more advanced algorithm are discussed in Section 4.2.8, where the efficiency of track reconstruction and tracking performance are compared for the algorithms. A comprehensive description of the more advanced algorithm is found in Chapter 5.

The simulation of the complete system with pellet stream, pellet measurements and the tracking procedure is described in Section 4.2. In order to evaluate the results especially with respect to tracking performance, classification schemes both for level measurements and for reconstructed pellet tracks were developed. This scheme and a detailed investigation of the track reconstruction performance are presented in sections 4.2.2-4.2.5.

The simulated geometrical setup is restricted by the boundary conditions given in PANDA and the parameters connected to the pellets and the pellet measurements are based on the conditions at UPTS. Tracking performance and position resolution were studied for various parameter settings.

The position resolution at the interaction region is mainly influenced by the position measurement accuracy, the time resolution and the lever arm of the measurement levels (a ratio of the distance between the measurement levels to the distance between the measurement levels and the interaction region). Some different camera cycles, corresponding to the presently operating cameras at UPTS and faster ones, were used. The influence on the transverse position resolution of different measurement layer configurations and the inclusion of the pellet generation point (at the VIC exit) in the track fit was studied.

The tracking performance varies strongly with pellet rate and time structure of the pellets in the stream. The time structure depends mainly on losses along the stream and on the velocity spread. A relative velocity spread of 1% gives a completely stochastic time distribution of the pellets already after a few decimeters [33]. Pellet rates at the interaction region of 5 k/s and 14 k/s were chosen to reflect the range of realistic operation. Different magnitude of losses was simulated by collimation and by varying the generation frequency and stream divergence. With pellet stream conditions relevant for pellet tracking, the probability for in-stream pellet-pellet collisions should be very small, and maybe negligible already after a few decimeters below the VIC [30]. For given pellet stream conditions, the tracking performance depends on the configuration of measurement levels, time resolution and measurement efficiency. The latter was varied by introducing different camera cycle dead times. Relative velocity spreads from 1% down to 0.01% were

studied. At a spread of 0.01% the regular time distribution from the pellet generation is essentially maintained all the way down to the interaction region. At present a relative velocity spread around 0.5% is a typical best value at UPTS.

In many hadron physics studies, especially at high luminosity, it is desirable to have a smooth luminosity distribution in time. With pellet targets this could be achieved on the μs - ms scale, if there are no losses and if the relative velocity spread is small and the pellet frequency match with the vertical extension of the accelerator beam so that the same number of pellets are always in the beam. Beam region occupancies are studied for vertical beam sizes of 5 and 10 mm in these simulations and for a pellet rate of 14 k/s, the 5 mm case corresponds to one-pellet-always-in-the-beam for ideal pellet stream conditions.

4.2. Design simulations

4.2.1. Tracking procedure and simplified track reconstruction algorithm

The information about the observation of a pellet by a camera is stored as one *measurement*. The measurement contains, among other things, information about the measured pellet XZ position and the time of detection. 'Measured' means, that calculated 'true' time and position at a given measurement level is smeared using pellet and pixel size and camera cycle (see Section 2.3). The true information is also stored. Each measurement contains also information about the pellet identity - pellet index given at generation.

For the purpose of the tracking all measurements from all cameras are merged into one time-ordered measurement stream. Information about the measurement level (camera) number, where given measurement comes from, is of course preserved.

The tracking algorithm is illustrated in Figure 4.2.1. Tracking is done for each pellet detected by the upper most camera (camera 1), in the order of time of detecting. The first measurement from the first camera is picked from the measurement stream. This measurement will start a *track*. The track will store measurements from all cameras, aiming to reconstruct path, velocity and eventually position at the accelerator beam crossing of the pellet which started the track.

The mean velocity of the pellet stream is used for predicting the position of the tracked pellet at the second measurement level. The pellet will be searched for in a time window of a certain size. This size may be based on the velocity spread in the stream, and then only pellets moving with velocities differing from the mean value by, *e.g.* a certain

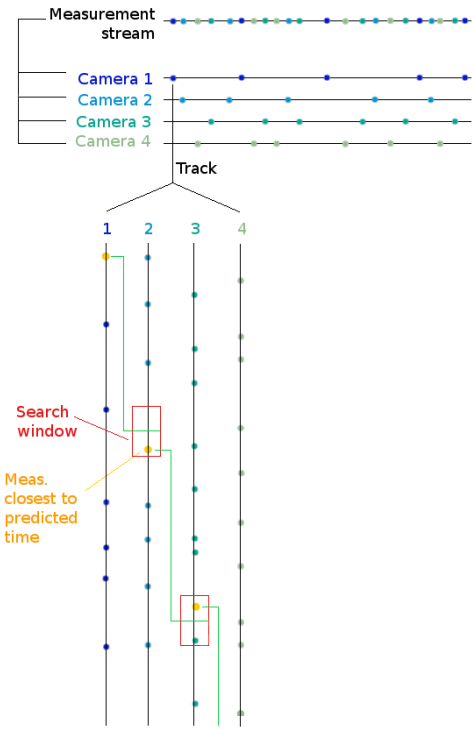

Figure 4.2.1: Illustration of the simplified tracking algorithm

number of sigmas describing the velocity spread, are accepted. Making the window smaller causes not all matching pellets to be accepted, but on the other hand making it bigger increases the probability that a not matching pellet will also be found in the time window.

Search for the pellet at the second measurement level is started, in the measurement stream, from the time of detecting the pellet at the first measurement point. All measurements found within the time window are stored in the track for further processing.

If no pellets were found in the window, the track is stopped at the current point and search for the pellet is not continued at the following measurement levels (if there exist any following measurement levels).

Among pellets found in the window, the one which is the closest to the expected time is assumed to be the matching pellet. Information about the time of detecting this pellet is used for determination of a new, more accurate, value of the pellet velocity. This velocity is then used for searching for the pellet at the third measurement level. This procedure is repeated for all measurement levels.

The tracking is repeated for all pellets detected by the upper most

camera. Result of the operation is a set of tracks, which can now be post processed to calculate information about the three dimensional pellet position at the accelerator beam crossing.

The direction of a pellet in X and Z is calculated by fitting the functions $X = f_X(Y)$ and $Z = f_Z(Y)$, where Y coordinates are given by the positions of measurement levels. X and Z coordinates are positions of the pellet measured at the measurement levels (at given Y). These functions are then used to calculate the pellet XZ position at the accelerator beam crossing (or at any desired level). Pellet velocity is also calculated by fitting. The function $t = f_t(Y)$ is fitted, where t is time of detecting the pellet at the measurement levels. This is then used to calculate the pellet time at the accelerator beam crossing. Also, one can ask about the reconstructed pellet position Y at a given time. For this, one takes the true time, when the pellet was in position Y=0, which is at the accelerator beam crossing. In a real experiment this time would be the time of a trigger occurring when there was a reaction inside the pellet. This time and function $t = f_t(Y)$ are used to reconstruct the Y position. In the fit a 1st degree polynomial (linear function) with two fitted parameters is used. The measurement uncertainties for the points in the fit are taken as sigma values of resolution distributions. The uncertainty of pellet position at the generation point (VIC) is taken as a sigma used for generation.

For the purpose of the design study, information about the tracking performance and resolution is also calculated.

4.2.2. Simulation of pellet stream and the tracking procedure

The following parameters and settings are used in the simulations presented below:

- Pellets are generated at position Y=3000 mm, where Y=0 mm is the position of the accelerator beam crossing.
- The number of initially generated pellets is 100 000. Pellets are generated with a certain frequency (see below).
- The position of the generation point is smeared with Gaussian distribution with sigma equal to 20 μm. The distribution has a cut-off at 3 sigmas. For each of X and Z directions the value is generated independently from the mentioned distribution.
- The stream divergence, measured as sigma of the pellet angular distribution, was varied in the simulations (see below). The distribution has a cut-off at 3 sigmas. For each of the X and Z directions

the value is generated independently from the mentioned distribution.

- The skimmer has a 1 mm opening diameter and is placed just above the first measurement level.
- Pellet loss due to, *e.g.*, pellet-pellet collisions, was changed between different simulations. The whole pellet loss is realized before the first measurement level and is adjusted to give the desired effective pellet rate at the measurement levels and in the beam region (see below).
- Detection related parameters were set as listed in Section 2.3, Table 2.3.1. The camera cycle, *i.e.* camera period and exposure time, was changed between different simulations (see below).
- Pellets are generated with mean velocity 70 m/s (in direction of the movement), according to a Gaussian distribution with a certain sigma (velocity spread). The distribution has a cut-off at 3 sigmas. The value of sigma was varied in the simulations (see below).
- Gravity is not included in simulating the pellet behavior nor in their tracking. (Gravity only influences significantly the time-of-passage/y-coordinate and can easily be taken into account).
- The measurement levels are located at the following Y positions:
  - First measurement level is at position Y=2300 mm, 700 mm below generation point.
  - Second measurement level is located 60 mm below the first one, at Y=2240 mm.
  - Third measurement level, is located 140 mm below the previous one, at Y=2100 mm.
  - The last, fourth, measurement level is located at Y=2040mm, 60 mm below the third one.

  All measurement levels are used for pellet identification and tracking in the Y direction. Tracking in X and Z direction is done using different measurement levels. Their order was varied in simulations, as described below. The pellet position at the VIC exit may be used as an additional point in XZ tracking.
- Half width of the search time-window at the measurement levels is a time corresponding to 2% difference from the mean velocity.
- A cut on χ^2 from fitting X and Z was set to accept only tracks for which $\chi^2 < 15$ for both X and Z.

- The X and Y dimensions of the accelerator beam region (width and height) were varied in the simulations (see below).

The following parameters were varied in the simulations:

- Generation frequency: 40 kHz, 20 kHz or 14 kHz.
- Stream divergence: 0.75 mrad (resulting in 65% loss at skimmer), 0.44 mrad (resulting in 30% loss at skimmer) and 0.075 mrad (resulting in 0% loss at skimmer).
- Pellet loss due to, *e.g.*, collisions. Two values of this parameter were used: 0.65 and 0.0. Along with loss at the skimmer, this provides an effective pellet rate at the measurement levels and in the beam region equal to, respectively, $\approx$ 5 k/s and $\approx$ 14 k/s. (For the simulated conditions, the real pellet loss due to pellet-pellet collisions between measurement levels is estimated to be well below the percent level).
- The relative velocity spread (sigma). It was set to 1%, 0.1% and 0.01% of the mean velocity.
- The camera cycle. The camera was operating with four different cycles: 12.5/10 μs (period/exposure time), 6.25/5 μs, 4/4 μs, 2/2 μs. The cycles 4/4 μs and 2/2 μs are to effectively simulate the usage of 2 cameras with shifted cycle installed at the same level and looking at the same pellet from opposite directions. 4/4 μs corresponds to the usage of two cameras with cycle 12.5/10 μs and 2/2 μs corresponds to the usage of two cameras with cycle 6.25/5 μs.
- Order of coordinates measured by the cameras. Two setups were used: XZXZ (camera 1 tracks in X direction, camera 2 tracks in Z direction, etc.) and ZXXZ.
- The usage of pellet position at generation (the VIC exit) was toggled in the track reconstruction.
- X and Y dimensions of the accelerator beam region (width and height). Two values were used: 5 mm and 10 mm.

If not stated otherwise, the example plots are for the following set of parameter settings: pellet generation frequency 40 kHz, stream divergence 0.75 mrad, random loss 65% (altogether resulting in pellet rate $\approx$ 5 k/s at measurement levels), camera cycle 2/2 μs, coordinate measurement order XZXZ, pellet position at VIC used in tracking.

4.2.3. Rejection of incorrect tracks

The presence of tracks containing measurements from incorrectly identified pellets is a big source of effective drop in tracking resolution. When fitting of the track is done with use of measurements from different pellets, it is obvious, that the fit result will be wrong and that there will be substantial difference between real and reconstructed position of the pellet. The χ^2 is checked for the X and Z fits of each track and tracks with too big χ^2 are rejected.

Figure 4.2.2 shows a comparison of χ^2 for all tracks with full information and tracks with pellet correctly identified at all measurement levels. It is clearly seen, that χ^2 for correct tracks has a clear cutoff at a certain value, while χ^2 for the rest of the tracks takes values from a huge range. This effect allows to make a cut at a certain value of χ^2. This is a very efficient tool because a proper cut does not reject any correct tracks while rejecting most of the incorrect ones at the same time.

Note, that this cut is possible only when the number of degrees of freedom of the fit is equal or greater than one. Therefore, when using a 1st order polynomial (with two parameters) and two measurement levels for each direction (for XZXZ and also ZXXZ setups), the pellet position at the VIC has to be used in the tracking, to enable this cut.

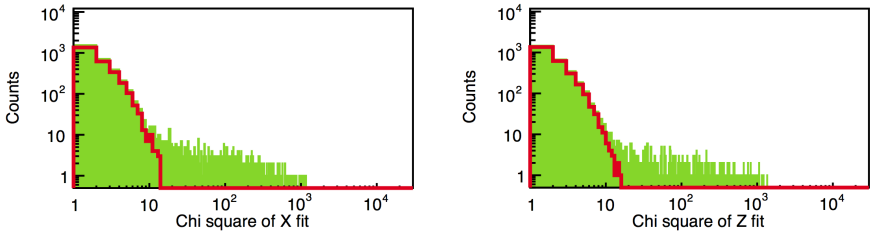

Figure 4.2.2: χ^2 of X fits (left plot) and Z fits (right plot). The solid area is for all tracks with full information and the line is for tracks with the pellet correctly identified at every measurement level

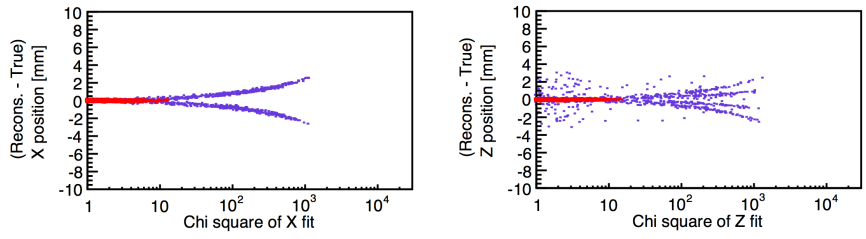

Figure 4.2.3: Correlation between χ^2 of the fit and the tracking accuracy (difference between reconstructed and true position) for X (left plot) and Z (right plot) directions. The red points indicate the tracks with the pellet correctly identified at every measurement level

Figure 4.2.3 shows a correlation between χ^2 of the fit and accuracy of the position reconstruction. The difference between the plots for X and Z directions occurs, because position of the track at the accelerator beam crossing is compared with the position of pellet which started the track (*i.e.*, was measured at first measurement level). Thus, for the XZXZ setup described here, there is only one possibility to take a wrong pellet for tracking in the X direction and it is at the third measurement level. On the other hand, since the measurement levels 2 and 4 are used to do the tracking in the Z direction, there are several possibilities of misidentification in this case: the pellet at measurement level 2 may be matching (the same as the pellet which started the track) and the pellet at measurement level 4 may be not matching; the pellet at measurement level 2 may be not matching and the pellet at measurement level 4 may be matching; both pellets may be not matching. Figure 4.2.4 shows the described cases. The most problematic is the situation, when the same pellet was used for fitting at measurement levels 2 and 4, but a different pellet started the track. In this case the track does not describe the position of the matching pellet, but cannot be rejected with the cut on χ^2.

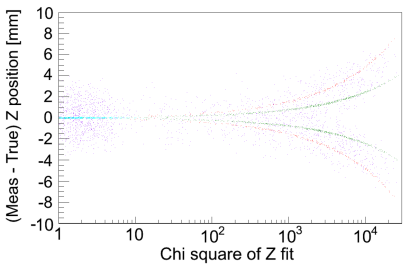

Figure 4.2.4: Correlation between χ^2 of the fit and the tracking accuracy for the Z direction with distinguished different types of misidentification. Cyan - tracks identified correctly at all measurement levels; red - tracks identified correctly at the 2nd measurement level and identified incorrectly at the 4th measurement level; green - tracks identified incorrectly at the 2nd measurement level and identified correctly at the 4th measurement level; violet - tracks identified incorrectly at the 2nd and the 4th measurement levels (plot for a different simulation case than the Figure 4.2.3)

4.2.4. Tracks quality

Initial number of tracks is by definition equal to the number of pellets detected at the first measurement level. However, the more complete tracks are required (*i.e.* with information from more measurement levels), the less tracks fulfill this condition. The cut on χ^2 also decreases the number of tracks used in analysis. Figure 4.2.5 shows the number of tracks with different quality, for the example conditions. In other

conditions the behavior is similar, with a steady decrease of the number of tracks with increased requirement on their quality.

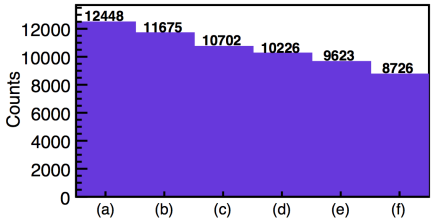

Figure 4.2.5: Number of tracks with different quality. (a) number of survived pellets at the interaction region; (b) total number of tracks; (c) tracks with information from at least two levels; (d) track with information from at least 3 levels; (e) tracks with full information (i.e. from all 4 levels); (f) tracks which passed cut on chi square

4.2.5. Performance of pellet track reconstruction

Detection case classification At each measurement level there may be a few different situations (single-layer-cases) in search for the matching pellet in the time window. They are described in Appendix C. In short, the higher the case number, the better the situation. The cases 4 and 5 are the preferred ones, indicating situations with unambiguously correct pellet identification. The case 5 is an optimal situation.

For each level all tracks are checked to determine the identification case and the number of pellets in the time window. This data is used to make Figure 4.2.6. This is made for each level. As it is expected, the higher fraction of "good" detection cases (4 and 5) occurs for lower pellet rate, shorter camera cycle, smaller velocity spread and smaller distances between the two considered measurement levels.

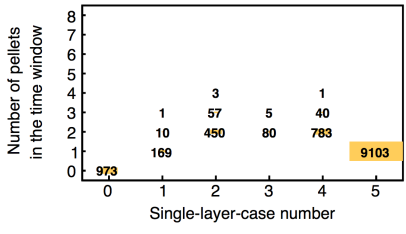

Figure 4.2.6: Study of pellet single-layer-cases at the second measurement level

Detection case transition Tracks which are in a certain single-layer-case at one measurement level might not be in the same single-layer-case at the other measurement levels. This case transition is visualized

in Figure 4.2.7. On the horizontal axis is the single-layer-case at the initial measurement level of the transition and on the vertical axis is the single-layer-case at the final measurement level. Transitions between neighboring measurement levels are used for making this kind of plot. Case '-1' at the final measurement level states the situation when the case was '0' at the initial measurement level and there is no data in this track from the final measurement level.

The general rule is that although most of the "good" cases propagate to the next level, it is also common that the pellet is not detected there because of detection inefficiency or that the velocity estimate was not accurate enough to correctly identify pellets overtaking each other. The case 5 can also change to case 4 because other pellets appear in the time window although the correct one is still correctly recognized (see Appendix C).

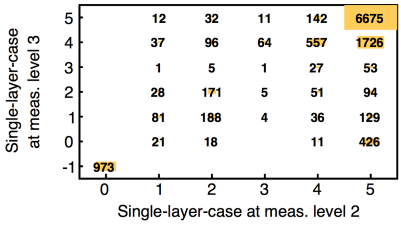

Figure 4.2.7: Detection single-layer-case transition between second and third measurement level

Probability for correct identification at the measurement levels Figure 4.2.8 shows the probability for correct pellet identification at one of the measurement levels. These plots are also derived from the single-layer-case histogram in Figure 4.2.6. The probability is calculated as a ratio of the number of counts in a 'good' case (4 or 5) to the total number of counts for a given number of pellets in the time window. *E.g.* for one pellet in the window, the probability for correct identification is a ratio between the number of pellets in case 5 and the sum of cases 1 and

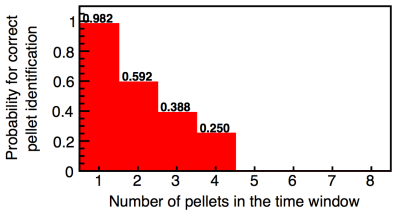

Figure 4.2.8: Probability for a correct pellet identification at the second measurement level for different number of pellets in the time window

5; probability for correct identification for 2 pellets in the window is a ratio between counts for case 4 and counts for sum of cases 1, 2, 3 and 4.

It can be seen that the probability for correct pellet identification decreases with increasing number of pellets in the time window.

It should be noted, that the presented probabilities involving high number of pellets in the time window are unreliable because of small statistics in these situations.

Single-layer-cases constituting multi-layer-cases Multi-layer-cases is a new case classification combining information from different measurement levels about the cases used so far (single-layer-cases, denoted with numbers 0..5). They are described in Appendix C.

The aim of introducing multi-layer-cases was to be able to distinguish between the best possible resolution and an effective drop of resolution caused by using incorrectly identified pellets in the track reconstruction. Resolution for multi-layer-case A will be the real resolution, when one correctly identifies pellets.

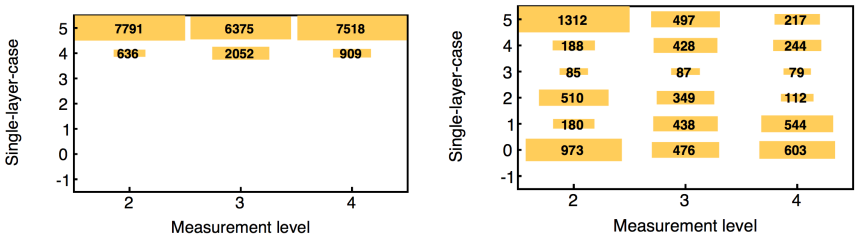

(a) Multi-layer-case A *(b) Multi-layer-case B*

Figure 4.2.9: Overview of single-layer-cases constituting tracks in multi-layer-case A and multi-layer-case B

Left plot in Figure 4.2.9 shows that the events being in multi-layer-case A belong to a certain single-layer-case for each measurement level. Right plot in this figure shows this for multi-layer-case B.

Number of pellets in time window for multi-layer-cases Left plot in Figure 4.2.10 shows the distribution of number of pellets in window among tracks of multi-layer-case A, at each measurement level. Right plot in this figure shows this distribution for case B.

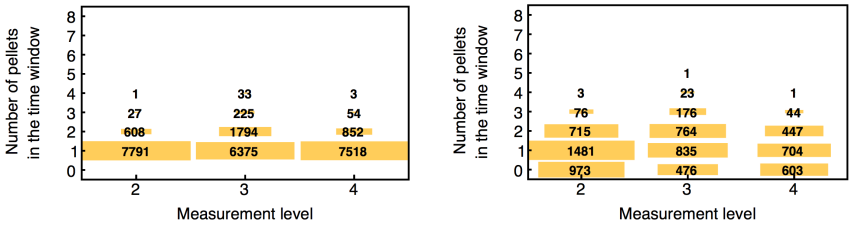

(a) Multi-layer-case A *(b) Multi-layer-case B*

Figure 4.2.10: Number of pellets in time window at different measurement levels for multi-layer-case A and B

Probability for correct identification for multi-layer-cases Using information from the previous plots one can calculate the probability for correct pellet identification when at each camera there is a certain number of pellets in the time window. This is done by dividing the value in corresponding bins in the plots for multi-layer-case A (Figure 4.2.10, left) and the sum of multi-layer-case A and B (sum of left and right plot in Figure 4.2.10). The effect is shown in Figure 4.2.11.

Similarly as with single-layer-cases, also here it is clear, that the more pellets there are in the time window, the lower is the probability for correct pellet identification.

And also here the results for high number of pellets in the window are unreliable because of a small number of events.

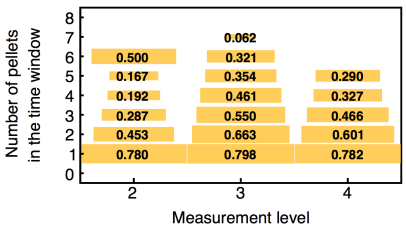

Figure 4.2.11: Probability that a pellet is correctly identified at all measurement levels (probability that the single-layer-case is A) for different number of pellets in the time window at different measurement levels

4.2.6. Tracking resolution in position and time

The tracking resolution is calculated as a difference between reconstructed and true pellet position/time. The plots in the Figure 4.2.12 show the reconstruction resolution at the interaction region for tracking in X and Z directions and the plots in Figure 4.2.13 show the resolution for the Y direction and of the time. The cut on χ^2 accepted tracks with $\chi^2 < 15$.

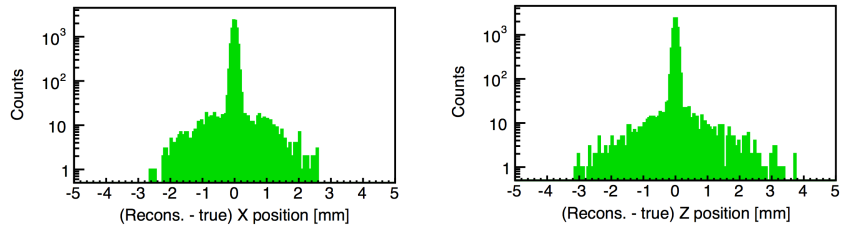

(a) X resolution, all tracks *(b) Z resolution, all tracks*

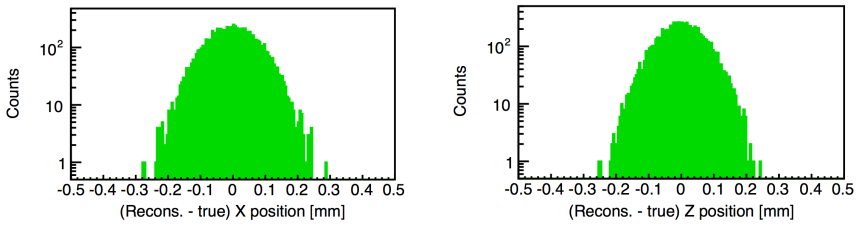

(c) X resolution, good tracks *(d) Z resolution, good tracks*

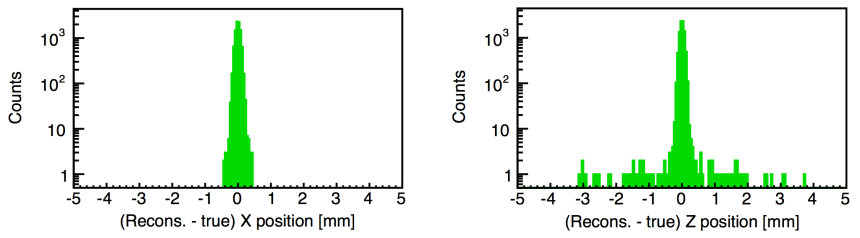

(e) X resolution, passed χ^2 cut *(f) Z resolution, passed χ^2 cut*

Figure 4.2.12: Resolution from pellet tracking in the X and Z directions, for tracks of different quality

Results for the tracking resolution at the interaction region The Tables 4.2.2 and 4.2.1 summarize the tracking resolution for different simulation parameter settings with usage of upper tracking section only. As a figure describing resolution, the sigma of distributions in Figures 4.2.12 and 4.2.13 for the case when the pellet was correctly identified at all measurement levels used in tracking, is taken. Therefore, the resolutions are the best possible, resulting from the measurement resolutions etc. They do not take into account the effective drop in resolution coming from incorrect pellet identification at the measurement levels. This effective drop would result from introduction of some events at the tails of the distributions but it would not affect the resolution essentially, *e.g.* it would not change the full width at half maximum of the distribution.

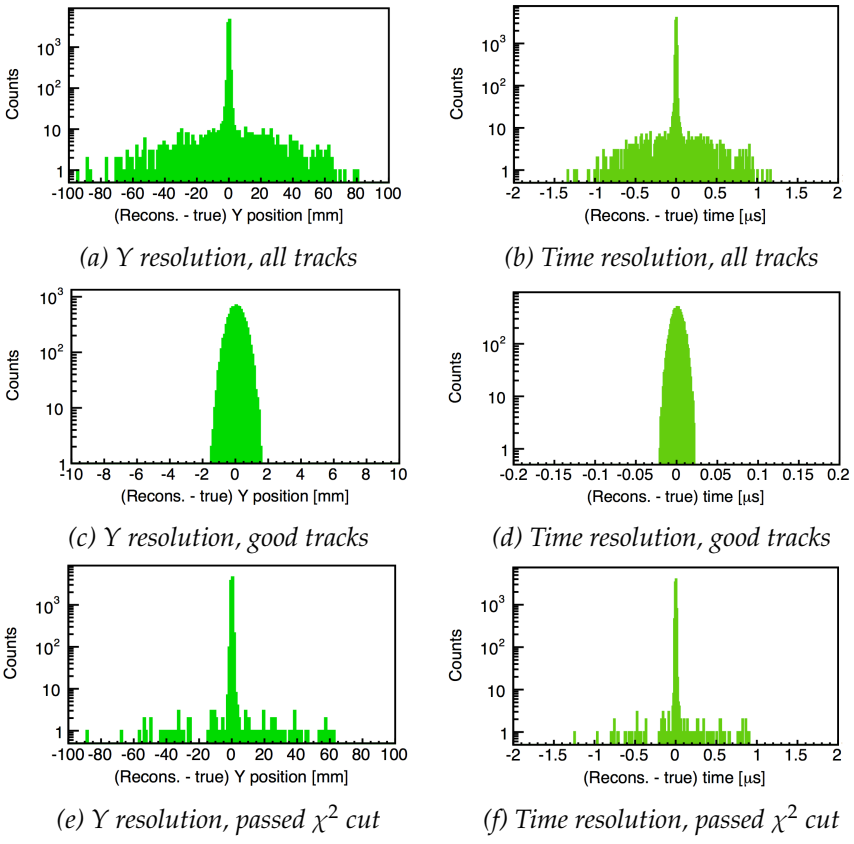

(a) Y resolution, all tracks

(b) Time resolution, all tracks

(c) Y resolution, good tracks

(d) Time resolution, good tracks

(e) Y resolution, passed χ^2 cut

(f) Time resolution, passed χ^2 cut

Figure 4.2.13: Resolution from pellet tracking in the Y direction and in time, for tracks of different quality

Table 4.2.1: Resolution σ in the X and Z at the interaction region for different measurement configurations obtained with upper tracking section

	X resolution [μm]	Z resolution [μm]
XZXZ with VIC	75	65
XZXZ without VIC	245	240
ZXXZ with VIC	70	70
ZXXZ without VIC	265	215

Table 4.2.2: Resolution σ in the Y position and time at the interaction region for different camera cycles obtained with upper tracking section

	Y resolution [mm]	Time resolution [μs]
Cycle 4/4μs	0.85	12.0
Cycle 2/2μs	0.45	6.5

Resolution with two tracking sections The tracking resolution was checked also with the presence of lower tracking section. There were three measurement levels at the lower section, separated by 60 mm and located at positions -2130 mm (tracking in Z direction), -2190 mm (tracking in X direction) and -2250 mm (tracking in Z direction).

The obtained time resolution for 4/4 μs camera cycle is 0.46 μs, what corresponds to 74 μm vertical (Y) resolution. The obtained time resolution for 2/2 μs camera cycle is 0.26 μs, what corresponds to 41 μm vertical (Y) resolution.

The X resolution obtained in simulations is 26 μm and the Z resolution is 21 μm. In reality these two values may be, however, close to the predictions from only upper section, because of the limited mechanical precision of the camera mounting.

4.2.7. Tracking performance

When talking about the *true pellets* one means simulated pellets propagating in the modeled experimental setup, corresponding to pellets in a real experiment. The term *reconstructed pellet* means a position of a pellet in a given moment, obtained based on pellet track (reconstructed by the tracking algorithm).

Beam region occupancy The model presented below allows to simulate which true and reconstructed pellets occupy the accelerator beam region at a given time.

The accelerator beam is directed along the Z axis. The beam region is defined as a solid similar to a cuboid, infinitely long along the Z axis and with certain X and Y dimensions.

Information is needed about the number of true and reconstructed pellets that were in the beam region at any moment in time, and exactly which true and reconstructed pellets these were.

The procedure for true and reconstructed pellets is the same. First, for each true and reconstructed pellet the time is calculated when the pellet entered the beam region (passing the top boundary) and the time when it left the beam region (passing the bottom boundary).

In the next step, it is checked if the true or reconstructed pellet fits within the beam region boundaries in the X direction. The true and reconstructed pellets, which fulfill this condition, are used in the further analysis. At this point it should be noted, that because the X position of true/reconstructed pellet is checked only at entrance to the beam region, the actual XY cross section of the beam region would not be a square, but rather a trapezoid, because of the pellet/track divergence (although the difference from square is very small because of very small pellet stream divergence).

All information about true and reconstructed pellets entering to or exiting from the beam region is stored together and sorted chronologically. Based on this, a new set of information is prepared: a chronological list of records containing indexes of pellets and tracks currently occupying the beam region. Each record contains also a time stamp, marking its beginning, and information about its duration. Each time the occupancy of the beam region changes, a new record is created and added to the list.

Analysis of the efficiency The described model may be used for different studies. Figure 4.2.14 shows the probability for situations with different number of true pellets and different number of reconstructed pellets in the beam region. The plot is made in the following way: Each entry to the histogram is added with a certain weight, which is the length of the period with a certain occupancy of the beam region. So initially each bin would contain total time with a certain occupancy of the beam region. Then the histogram is normalized to 1, so each bin shows the fraction of time with a given beam region occupancy.

Plots in the upper row in the Figure 4.2.15 show the probability for a certain number of true pellets in the beam region and the plots in the center row in the same figure shows the probability for a certain number of reconstructed pellets in the beam region. The two plots are compared in the plots in the bottom row. The number of true pellets in the beam region is a result of a stochastic distribution. Concerning the reconstruction, the general conclusion is that the number of pellets in the beam region is in most cases reconstructed correctly, although there is a clear tendency for underestimation of this number. It is caused mostly by the reconstruction inefficiency resulting in a smaller number of tracks than the number of pellets in the sample.

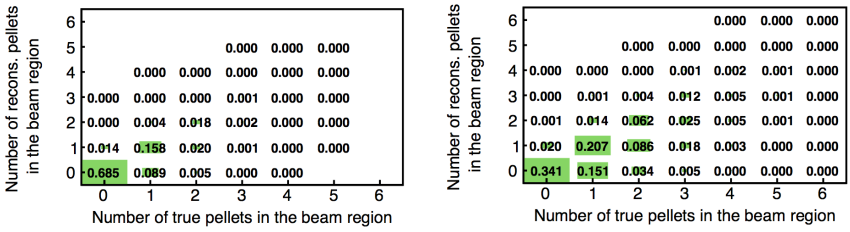

(a) Pellet rate 5 k/s *(b) Pellet rate 14 k/s*

Figure 4.2.14: Probability for situations with different number of true and reconstructed pellets in the beam region for a pellet rate of 5 k/s and 14 k/s

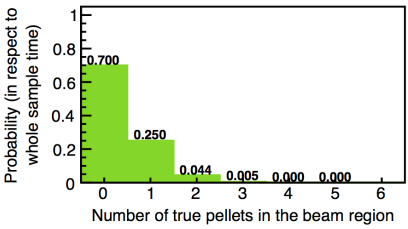

(a) Probability for a certain number of true pellets in the beam region, pellet rate 5 k/s

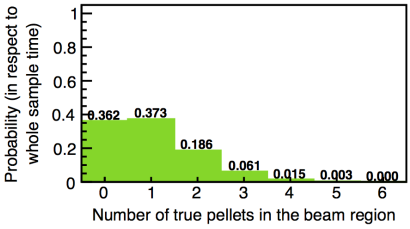

(b) Probability for a certain number of true pellets in the beam region, pellet rate 14 k/s

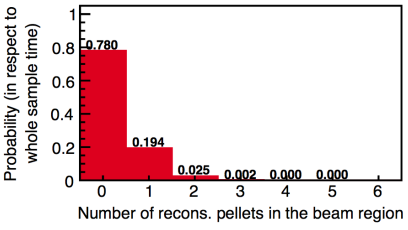

(c) Probability for a certain number of recons. pellets in the beam region, pellet rate 5 k/s

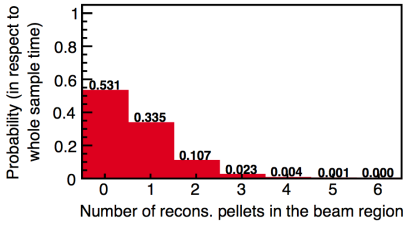

(d) Probability for a certain number of recons. pellets in the beam region, pellet rate 14 k/s

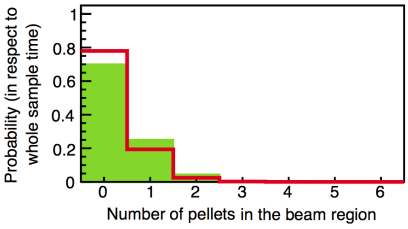

(e) Comparison, pellet rate 5 k/s

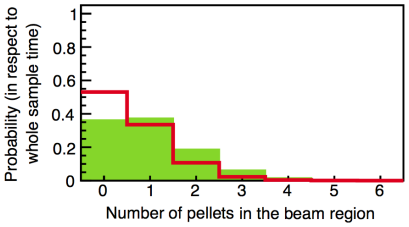

(f) Comparison, pellet rate 14 k/s

Figure 4.2.15: Probability for a certain number of true pellets in the beam region (upper), probability for a certain number of reconstructed pellets in the beam region (center), and their comparison (lower), for a pellet rate of 5 k/s (left) and 14 k/s (right)

A number of probabilities can be defined to describe performance of the tracking system:

- The probability to have the same number of true pellets as the number of reconstructed pellets and
- the probability for the same number of reconstructed pellets as a certain number of true pellets (examples in Figure 4.2.16).

- The probability for exactly one reconstructed pellet and a certain number of true pellets in the beam region and
- the probability for exactly one true pellet and a certain number of reconstructed pellets in the beam region (examples in Figure 4.2.17).

- The probability for a certain number of true pellets in the beam region, when there is exactly one reconstructed pellet in the beam region and
- the probability for a certain number of reconstructed pellets in the beam region when exactly one true pellet is in the beam region (examples in Figure 4.2.18).

- The probability for exactly one reconstructed pellet and a matching true pellet in the beam region and
- the probability for exactly one true pellet and a matching reconstructed pellet in the beam region (examples in Figure 4.2.19).

- The probability for a matching true pellet in the beam region when exactly one reconstructed pellet is in the beam region and
- the probability for a matching reconstructed pellet in the beam region when exactly one true pellet is in the beam region (examples in Figure 4.2.20).

- The probability that a matching true pellet is among true pellets in beam region when exactly one reconstructed pellet is in the beam region and
- the probability that a matching reconstructed pellet is among reconstructed pellets in the beam region when exactly one true pellet is in the beam region (examples in Figure 4.2.21).

Exact definitions of the listed probabilities can be found in Appendix C. Based on them one can compare performance of the tracking system in different conditions.

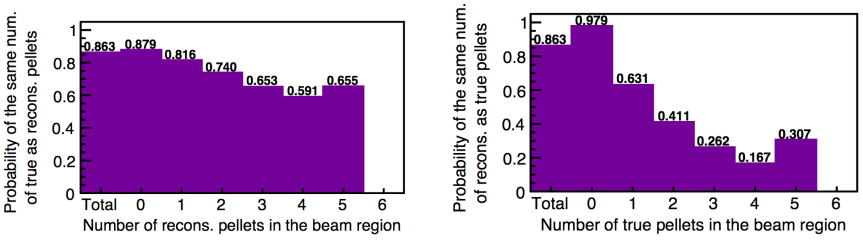

(a) The same number of true as reconstructed pellets

(b) The same number of reconstructed as true pellets

Figure 4.2.16: Examples of probabilities for the same number of true pellets as a certain number of reconstructed pellets (in respect to the total time with a certain number of recons. pellets, left) and probabilities for the same number of reconstructed pellets as a certain number of true pellets (in respect to the total time with a certain number of true pellets, right), for a pellet rate of 5 k/s

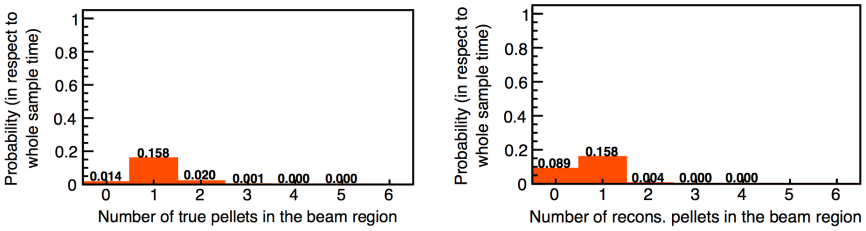

(a) Exactly one reconstructed pellet and a certain number of true pellets

(b) Exactly one true pellet and a certain number of reconstructed pellets

Figure 4.2.17: Examples of probabilities for exactly one reconstructed pellet and a certain number of true pellets in the beam region (left) and probabilities for exactly one true pellet and a certain number of reconstructed pellets in the beam region (right), for a pellet rate of 5 k/s

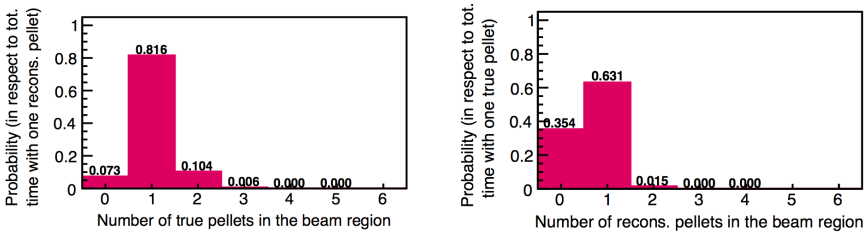

(a) A certain number of true pellets when exactly one recons. pellet

(b) A certain number of reconstructed pellets when exactly one true pellet

Figure 4.2.18: Examples of probabilities for a certain number of true pellets in the beam region when there is exactly one reconstructed pellet is in the beam region (left) and probabilities for a certain number of reconstructed pellets in the beam region when exactly one true pellet is in the beam region (right), for a pellet rate of 5 k/s

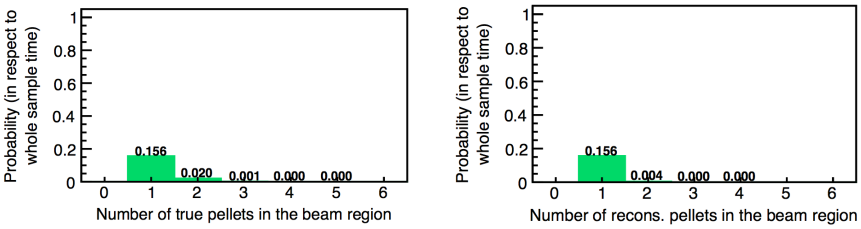

(a) Exactly one reconstructed pellet and a matching true pellet

(b) Exactly one true pellet and a matching reconstructed pellet

Figure 4.2.19: Examples of probabilities for exactly one reconstructed pellet and a matching true pellet in the beam region as a function of true pellets number (left) and probabilities for exactly one true pellet and a matching reconstructed pellet in the beam region as a function of reconstructed pellets number (right), for a pellet rate of 5 k/s

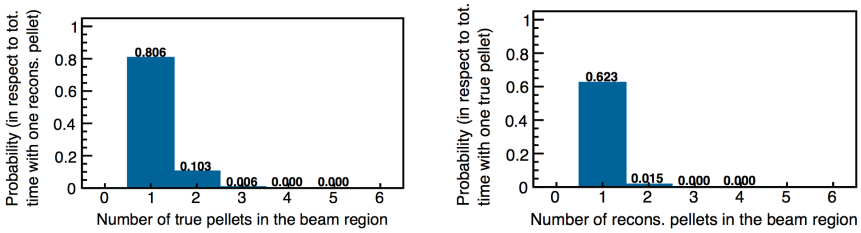

(a) Matching true pellet when exactly one reconstructed pellet

(b) Matching reconstructed pellet when exactly one true pellet

Figure 4.2.20: Examples of probabilities for a matching true pellet in the beam region when exactly one reconstructed pellet is in the beam region (left) and probabilities for a matching reconstructed pellet in the beam region when exactly one true pellet is in the beam region (right)

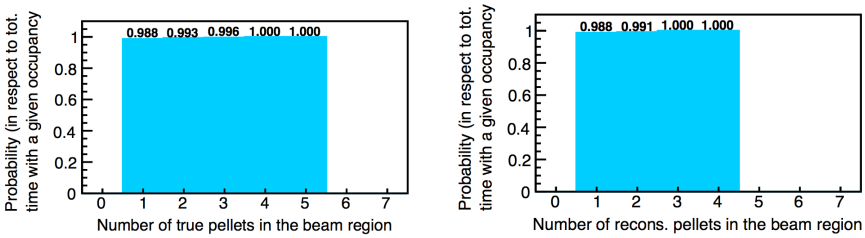

(a) Matching true pellet among true pellets in the beam when one reconstructed pellet in the beam

(b) Matching reconstructed pellet among recons. pellets in the beam when one true pellet in the beam

Figure 4.2.21: Examples of probabilities that a matching true pellet is among the true pellets in the beam region when exactly one recons. pellet is in the beam region (left) and probabilities that a matching reconstructed pellet is among recons. pellets in the beam region when exactly one true pellet is in the beam region (right), for a pellet rate of 5 k/s

Summary of the tracking performance for different simulation parameter settings

The plots in Figure 4.2.23 - 4.2.28 summarize the various probabilities describing pellet tracking performance for a fixed set of example parameters. The parameters are listed on the left side of each plot. Additionally, they are indicated in the plot according to the key in Figure 4.2.22: the three marked groups correspond to different velocity spreads, the two bar colors correspond to different beam region sizes, the four marker colors correspond to different pellet rates and the three marker shapes correspond to different camera cycle structures. The plots are based on the values listed in Appendix D.

Pellet rate 5 k/s with 40 kHz generation frequency is achieved by using 0.75 mrad stream divergence and with 65% additional loss. The pellet rate 14 kHz with the same generation frequency is achieved by having loss only at skimmer. The rate 14 k/s with 20 kHz generation frequency is obtained with 0.44 mrad stream divergence and no other loss and the rate 14 k/s with 14 kHz generation frequency is obtained with 0.075 mrad stream divergence

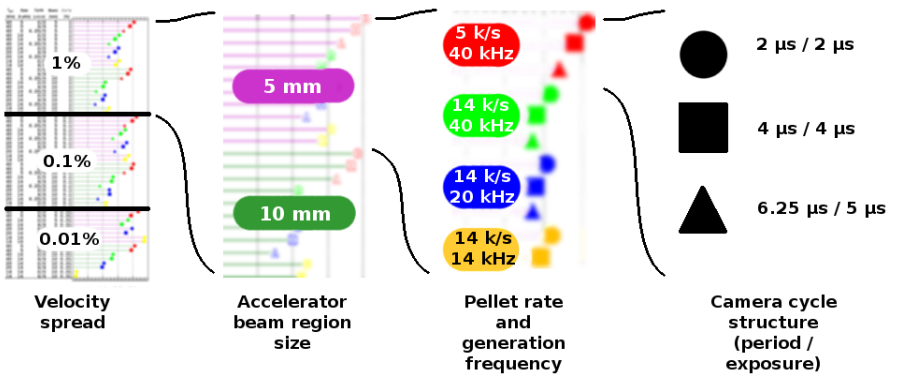

Figure 4.2.22: Key to the plots showing results of design simulations

One pellet/track in the beam region

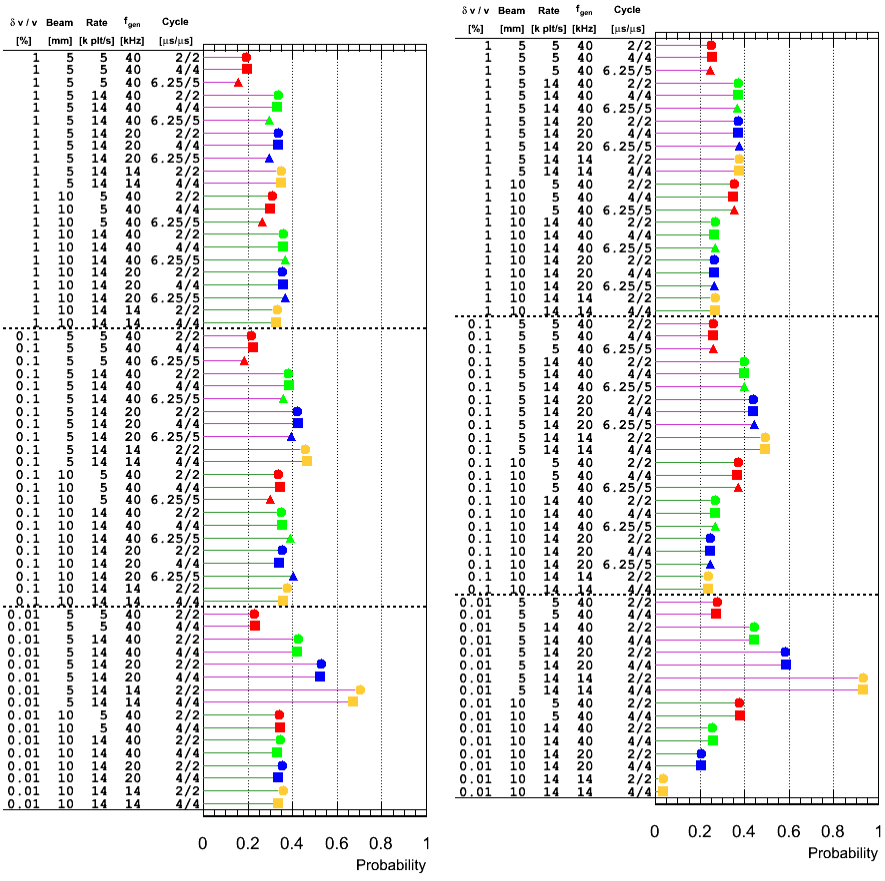

Figure 4.2.23: Probabilities of exactly one reconstructed pellet in the beam region (time fraction) - left plot, and probabilities of exactly one true pellet in the beam region (time fraction) - right plot

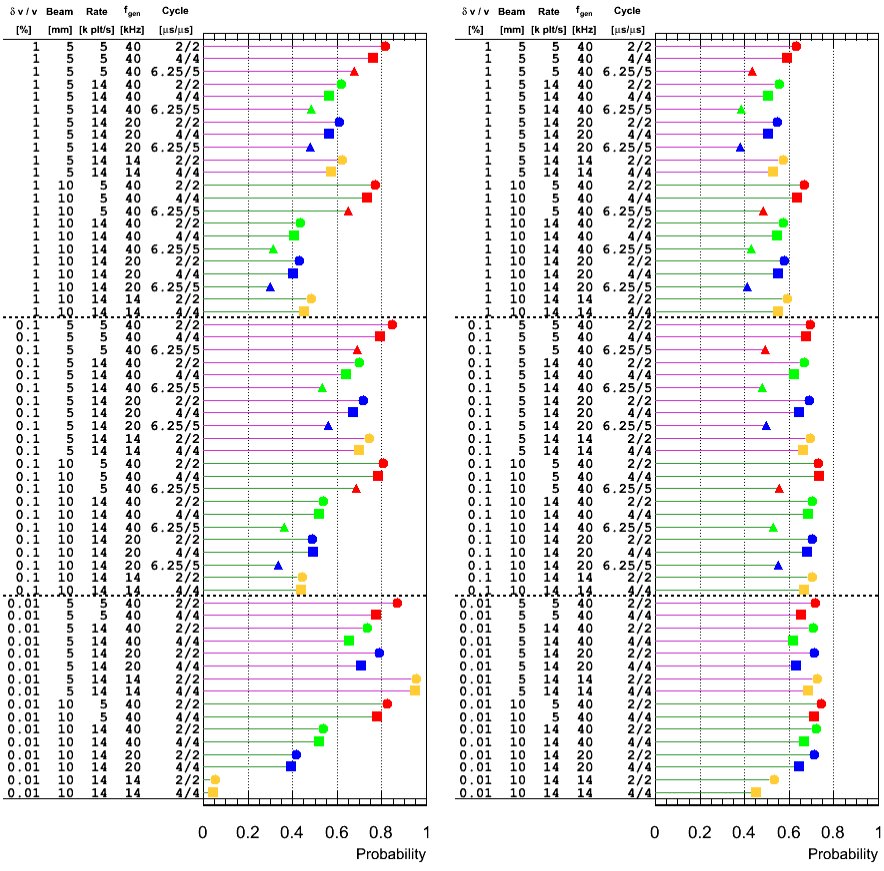

Figure 4.2.24: Probabilities of exactly one true pellet in the beam region when exactly one reconstructed pellet is in the beam region (left plot) and probabilities of exactly one reconstructed pellet in the beam region when exactly one true pellet is in the beam region (right plot)

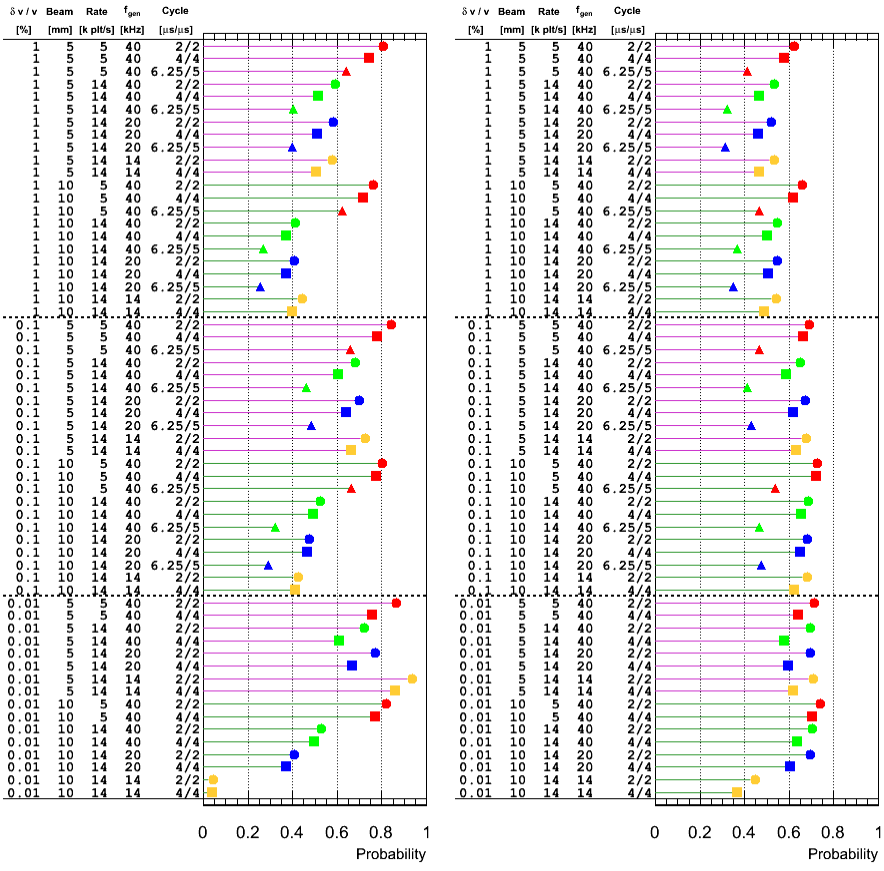

Figure 4.2.25: Probabilities of one-matching true pellet in the beam region when exactly one reconstructed pellet is in the beam region (left plot) and probabilities of one-matching reconstructed pellet in the beam region when exactly one true pellet is in the beam region (right plot)

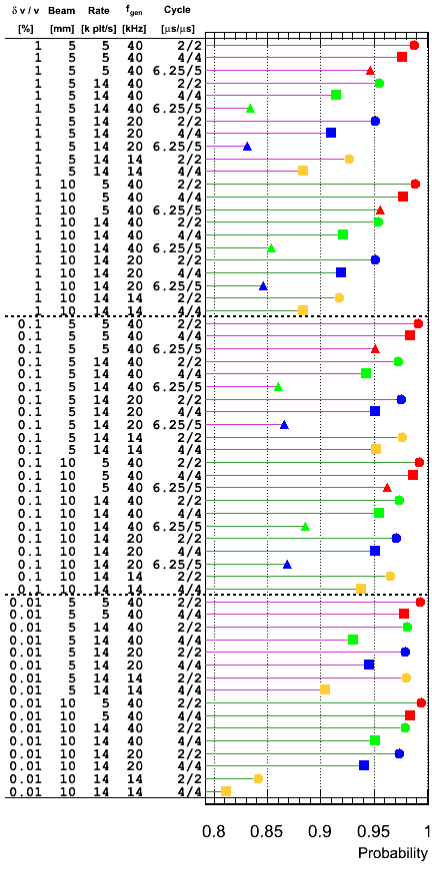

Figure 4.2.26: Probabilities that the true and reconstructed pellet are matching when there are one true pellet and one reconstructed pellet in the beam region

Zero pellets/tracks in the beam region

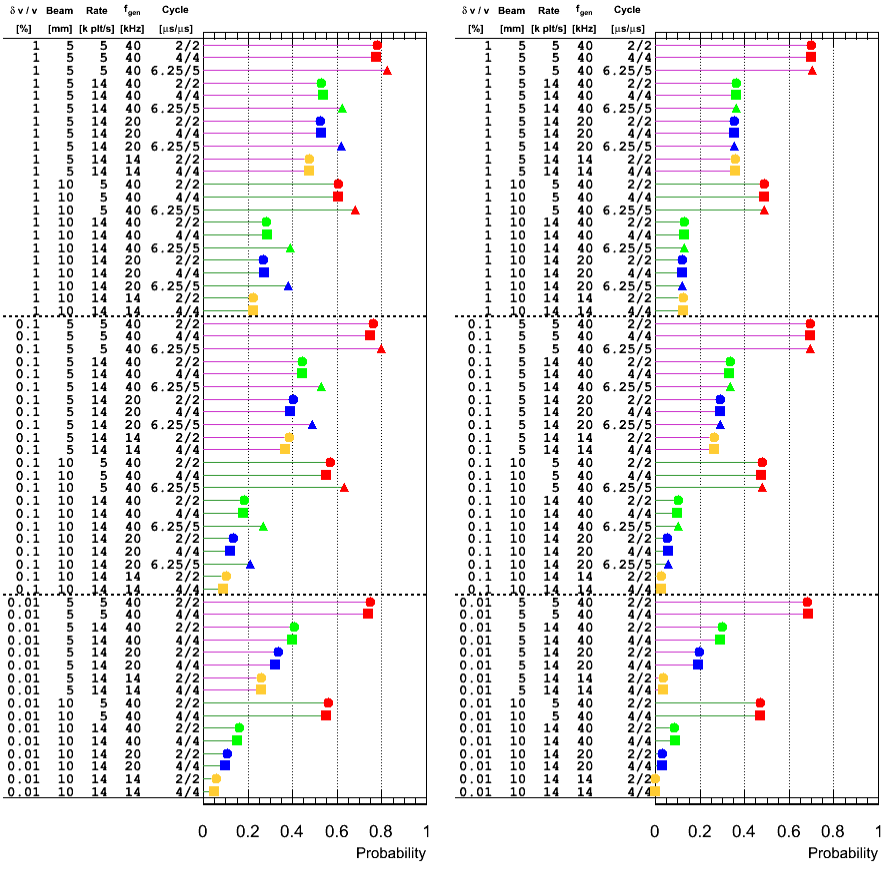

Figure 4.2.27: Probabilities of no reconstructed pellet in the beam region (time fraction) - left plot, and probabilities of no true pellet in the beam region (time fraction) - right plot

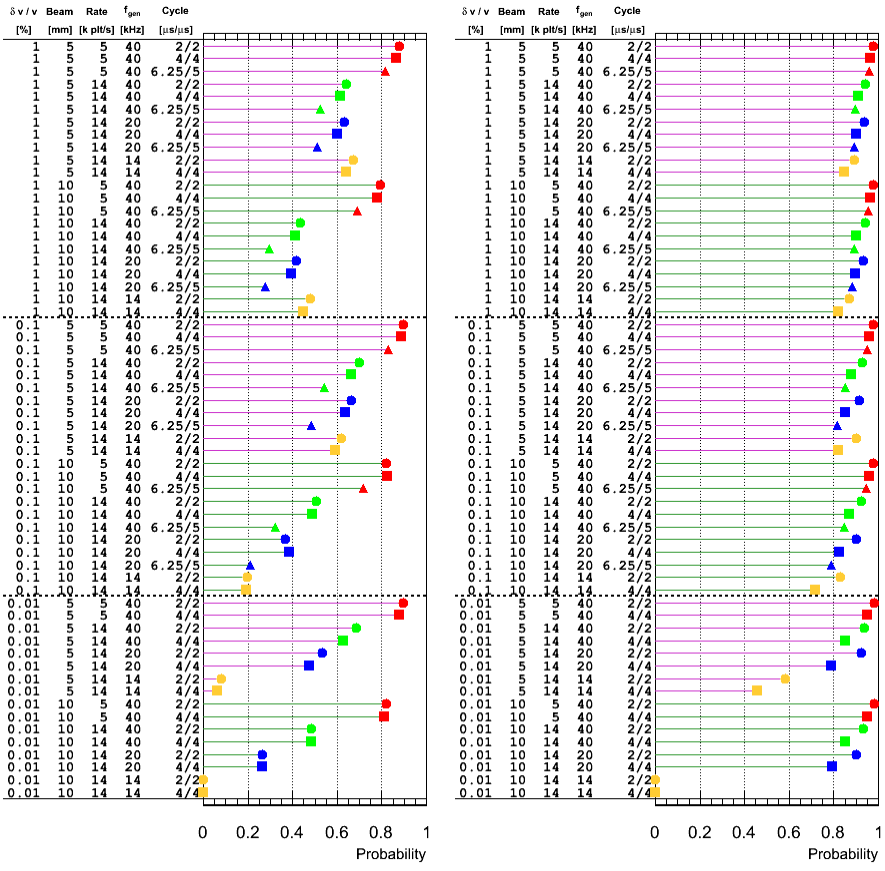

Figure 4.2.28: Probabilities of no true pellet in the beam region when no reconstructed pellet is in the beam region (left plot) and probabilities of no reconstructed pellet in the beam region when no true pellet is in the beam region (right plot)

4.2.8. Tracking performance obtained with a more advanced algorithm

A more advanced track reconstruction algorithm was developed to provide higher reconstruction efficiency. The algorithm is described in detail in Chapter 5.

The simulations for the more advanced algorithm were carried out for the standard settings for the PANDA setup, the same as simulations for the simpler algorithm. A comparison of the efficiency of the two algorithms is presented in Table 4.2.3.

The tracking efficiency is the ratio between reconstructed tracks and survived pellets. The reconstruction efficiency is the ratio of reconstructed tracks to detected pellets. The reconstruction correctness is

Table 4.2.3: Comparison of the performance of the tracking algorithms for different pellet stream and measurement conditions. The tracking efficiency is the ratio of reconstructed tracks to survived pellets. The reconstruction efficiency is the ratio of reconstructed tracks to detected pellets. The reconstruction correctness is the ratio of correct reconstructed tracks to all reconstructed tracks

Camera cycle, pellet rate	Algorithm	Tracking efficiency	Reconstruction efficiency	Reconstruction correctness
12.5/10µs, 5 k/s	Simple, 4 levels	35.9%	43.1%	90.9%
	Adv., 4 levels	25.9%	29.9%	95.7%
	Adv., 7 levels	83.8%	91.8%	97.8%
6.25/5µs, 5 k/s	Simple, 4 levels	54.3%	60.6%	94.7%
	Adv., 4 levels	70.9%	77.6%	98.5%
	Adv., 7 levels	91.6%	97.1%	99.1%
4/4µs, 5 k/s	Simple, 4 levels	70.7%	74.8%	95.0%
	Adv., 4 levels	83.1%	86.7%	98.4%
	Adv., 7 levels	92.7%	95.3%	99.2%
2/2µs, 5k/s	Simple, 4 levels	70.1%	74.9%	96.6%
	Adv., 4 levels	89.4%	94.6%	99.6%
	Adv., 7 levels	93.9%	97.1%	99.4%
12.5/10µs, 14 k/s	Simple, 4 levels	30.6%	36.9%	74.9%
	Adv., 4 levels	26.4%	30.5%	88.5%
	Adv., 7 levels	68.8%	75.4%	93.7%
6.25/5µs, 14 k/s	Simple, 4 levels	47.4%	53.2%	83.5%
	Adv., 4 levels	69.4%	76.0%	96.6%
	Adv., 7 levels	85.6%	90.7%	97.2%
4/4µs, 14 k/s	Simple, 4 levels	62.0%	65.3%	87.8%
	Adv., 4 levels	80.0%	83.5%	97.4%
	Adv., 7 levels	88.9%	91.4%	97.6%
2/2µs, 14 k/s	Simple, 4 levels	63.3%	67.5%	90.9%
	Adv., 4 levels	87.2%	91.8%	98.7%
	Adv., 7 levels	92.2%	95.4%	98.7%

the ratio of the correct reconstructed tracks to all reconstructed tracks. The number of survived pellets in the discussed cases is constant at all measurement levels and in the interaction region.

Except in the case with a camera cycle of 12.5/10µs (period/exposure), which is not suitable for tracking, the more advanced algorithm behaves very well and is much better than the simpler one. Efficiency of the more advanced algorithm ranges from 75% to 95% for the 4 level setup. In

case of a high pellet rate and detection inefficiency, the efficiency of the more advanced algorithm is approx. 1.5 times better than for the simpler one. Also, the correctness is higher and goes from 96 to over 99%.

Addition of 3 levels in the lower section (with the assumption of no pellet loss on the way) gives algorithm efficiency over 90% and correctness over 97%.

Table 4.2.4: Comparison of pellet tracking performance with two reconstruction algorithms. Results for the situation with no true/reconstructed pellet in the beam region, for 5 mm beam region size and 1% velocity spread

Camera cycle, pellet rate	Algorithm (S - simple, A - advanced; number of levels)	Probability of no recons. pellet in the beam region (time fraction)		Probability of no true pellet in the beam region when no recons. pellet is in the beam region	
		recons.	true	true	recons.
2/2 μs, 5 k/s	S 4-lev	0.780	0.700	0.878	0.979
	A 4-lev	0.726	0.700	0.938	0.973
	A 7-lev	0.715	0.700	0.983	0.999
4/4 μs, 5 k/s	S 4-lev	0.778	0.700	0.865	0.964
	A 4-lev	0.742	0.700	0.892	0.947
	A 7-lev	0.717	0.700	0.980	0.998
6.25/5 μs, 5 k/s	S 4-lev	0.826	0.700	0.818	0.960
	A 4-lev	0.778	0.700	0.858	0.951
	A 7-lev	0.710	0.700	0.978	0.997
2/2 μs, 14 k/s	S 4-lev	0.531	0.366	0.642	0.942
	A 4-lev	0.413	0.366	0.817	0.930
	A 7-lev	0.377	0.366	0.951	0.997
4/4 μs, 14 k/s	S 4-lev	0.537	0.366	0.613	0.909
	A 4-lev	0.445	0.366	0.706	0.862
	A 7-lev	0.388	0.366	0.935	0.994
6.25/5 μs, 14 k/s	S 4-lev	0.622	0.366	0.524	0.896
	A 4-lev	0.494	0.366	0.632	0.858
	A 7-lev	0.390	0.366	0.914	0.991

The tracking performance was checked with the use of the more advanced algorithm and compared with the results of the simplified algorithm. The results are shown in Tables 4.2.4 and 4.2.5. The probability of correct prediction of the number of pellets in the beam region is higher, compared to the simplified algorithm, because of the higher reconstruction efficiency. This this also means, that the probabilities of no reconstructed pellet in the beam region are lower with the new algorithm, and the probabilities of one reconstructed pellet in the beam region are higher. Higher reconstruction efficiency together with higher

Table 4.2.5: Comparison of pellet tracking performance with two reconstruction algorithms. Results for the situation with one true/reconstructed pellet in the beam region, for 5 mm beam region size and 1% velocity spread

Camera cycle, pellet rate	Algorithm (S - simple, A - advanced; number of levels)	Probability of exactly one recons. | true pellet in the beam region (time fraction)		Probability of exactly one true | recons. pellet in the beam region when exactly one recons. | true pellet is in the beam region		Probability of one-matching true | recons. pellet in the beam region when exactly one recons. | true pellet is in the beam region		Probability of correct match when there are one true and one reconstructed pellet in the beam region
2/2 μs, 5 k/s	S 4-lev	0.194	0.250	0.816	0.631	0.806	0.623	0.988
	A 4-lev	0.235	0.250	0.869	0.808	0.862	0.802	0.992
	A 7-lev	0.240	0.250	0.976	0.950	0.967	0.941	0.991
4/4 μs, 5 k/s	S 4-lev	0.195	0.250	0.764	0.590	0.746	0.576	0.976
	A 4-lev	0.221	0.250	0.750	0.663	0.726	0.642	0.968
	A 7-lev	0.239	0.250	0.973	0.942	0.958	0.928	0.985
6.25/5 μs, 5 k/s	S 4-lev	0.158	0.250	0.678	0.434	0.642	0.411	0.947
	A 4-lev	0.195	0.250	0.711	0.559	0.676	0.531	0.950
	A 7-lev	0.245	0.250	0.967	0.938	0.950	0.921	0.983
2/2 μs, 14 k/s	S 4-lev	0.335	0.375	0.619	0.557	0.591	0.531	0.955
	A 4-lev	0.367	0.375	0.766	0.760	0.744	0.737	0.971
	A 7-lev	0.373	0.375	0.948	0.948	0.926	0.926	0.976
4/4 μs, 14 k/s	S 4-lev	0.332	0.375	0.566	0.507	0.517	0.464	0.914
	A 4-lev	0.364	0.375	0.626	0.614	0.570	0.559	0.911
	A 7-lev	0.367	0.375	0.928	0.928	0.891	0.891	0.960
6.25/5 μs, 14 k/s	S 4-lev	0.293	0.375	0.483	0.384	0.403	0.320	0.834
	A 4-lev	0.352	0.375	0.556	0.531	0.481	0.460	0.866
	A 7-lev	0.377	0.375	0.904	0.908	0.862	0.865	0.953

reconstruction correctness provide also a higher probability that for a true pellet in the beam region there is a match with a reconstructed pellet.

4.3. Discussion and summary – tracking system design

The overall goal for the presented target system is to provide useful pellet position information for as many hadronic events as possible together with a smooth, in time, target thickness that allows a high luminosity. This requires not only efficient pellet detection and a well performing tracking system but also a proper combination of pellet stream and accelerator beam properties. The time structure of the pellets in the stream should be as uniform as possible and the average distance between pellets should match the vertical size of the beam so

that most of the time there is exactly one pellet in the beam region. At the presently operating pellet generators, the relative velocity spread is around 1%. This gives a completely stochastic time structure. Some improvements are expected from ongoing developments (at UPTS 0.5% has been obtained so far). Therefore relative velocity spreads from 1% down to 0.01% were studied. At a spread of 0.01% the regular time distribution from the pellet generation is essentially maintained all the way down to the interaction region if there are no losses of pellets on the way. Also different assumptions for pellet losses, 0%, 30% and 65% were introduced in the simulations.

For the discussion in this section, some reference conditions for pellet tracking operation with the following pellet stream and accelerator beam properties are defined:
– Pellet rate at the interaction region: 14 k/s;
– Pellet loss: 30%;
– Pellet velocity and relative spread: 70 m/s and 0.1%;
– Accelerator beam vertical size: 5 mm.

The reference conditions for pellet detection are based on a camera cycle of 4 μs without any inefficiency due to dead time and on a position resolution $\sigma \approx 20$ μm.

4.3.1. Number of pellets in the beam

This study focuses on investigating how the fraction of time with no pellets and with exactly one pellet in the beam region is influenced by different parameters. The reason is that for these cases a tracking system could give very clear information. The one-pellet case gives the best possibility for having useful tracking position information and that any hadronic event that would occur in a zero-pellet situation is an undesirable background.

- For the reference conditions, the probability for exactly one pellet in the beam region is 44% of the time. With no losses it is 49% and with 65% loss it is 40%. For velocity spreads of 1% and 0.01% it is 37% and 58% respectively. For the ideal case with no losses and the smallest velocity spread (0.01%), the probability for exactly one pellet in the beam region is 93%, *i.e.* almost one as expected.

- For the reference conditions, the probability for no pellets in the beam region is 29%. With no losses it is 27% and with 65% loss it is 33%. For velocity spreads of 1% and 0.01% it is 35% and 19% respectively. For the ideal case with no losses and the smallest velocity spread (0.01%), the probability for no pellets in the beam region is 3%, *i.e.* almost zero as expected.

It should be noted that for a velocity spread of 1%, the time distribution is completely stochastic and for a given (average) pellet rate in the beam region, both the probability for no pellets and the probability for exactly one pellet are independent of the size of the losses.

4.3.2. Position and time resolution from tracking

The position resolution at the interaction region in the transverse coordinates X and Z depends on the measurement resolution in the coordinates at the camera levels, while the resolution in the vertical coordinate Y depends on the time resolution of the cameras. For the studied camera cycles and measurement level configurations, the accuracy in the velocity determination dominates the Y coordinate resolution.

The tracking resolution obtained with the upper section is discussed below.

- The resolution in the X and Z directions depends directly on the position measurement resolution and on the distance between the measurement levels. A resolution $\sigma \approx 250$ μm is obtained when using information from the tracking section only. A slight improvement ($\approx 10\%$) in one of the directions *e.g.* Z, is possible by a reconfiguration of the measurement levels. This resolution is good enough for accurate consistency checks on whether a track originates from the VIC exit (situated about 700 mm above the tracking section). If this is the case, the pellet stream position at the VIC can be used as an additional point on the track fit, which substantially increases the lever arm. A position resolution $\sigma \approx 70 \mu m$ at the interaction region is then obtained.
- For the reference conditions, the resolution in the Y direction depends mainly on the accuracy in the velocity determination *i.e.* on the time resolution from the cameras and the distance between first and last level in the measurement section. The additional measurement levels in between, improve the resolution by $\approx 30\%$ and results in a resolution $\sigma \approx 0.8$ mm.
- The resolution in the time when a pellet is expected to traverse the interaction region is, similarly to the Y direction resolution, dominated by the accuracy in the velocity determination. The resolution $\sigma \approx 12$ μs for a 4 μs camera cycle ($\sigma_{cam} \approx 1.2$ μs).

The resolution in the time and Y coordinate determination scales with measurement time resolution for pellet velocity spreads above a few times 0.01%.

Usage of the lower tracking section substantially improves the tracking resolution, especially in the time and Y coordinate. The Y resolution

of ≈75 μm is predicted for 4 μs camera cycle. This value is comparable to the X and Z resolution obtained without the lower tracking section. The X and Z resolutions with the lower section, obtained from simulations are 20-25 μm. However, these values do not take into account the limited precision of the system alignment. Therefore, values comparable to predictions from only upper section are foreseen.

4.3.3. Tracking efficiency

The tracking system should provide useful *i.e.* correct tracking information for as many hadronic events as possible. To evaluate the performance one compares the position and time information for the true pellets with position and time information from the tracks that are reconstructed from the pellet measurements.

For given accelerator beam and target conditions the performance of the tracking system depends on the pellet detection system and on the tracking procedure. Both track reconstruction algorithms were used. The simplified algorithm was used in comprehensive study involving various pellet stream and detection parameters. The more advanced algorithm was used to produce exemplary results for the case with 1% velocity spread and 5 mm accelerator beam size.

Some results with the use of the simplified algorithm for the situation with low relative velocity spread (0.01%), a pellet rate of 14 k/s and vertical accelerator beam size of 5 mm can be used as an illustration. With no loss of pellets there is exactly one true pellet in the beam region about 93% of the time, while there is exactly one reconstructed pellet only in 70% of the time. With 30% pellet loss the corresponding time fractions are 58% and 52%. Most of the difference between the number of true and reconstructed pellets can be attributed to a loss of reconstructed tracks due to shortcomings of the simpler tracking procedure.

For the reference conditions, the probability that the tracking system with the simplified algorithm predicts correct number of pellets in the beam region, for no pellet in the beam region is 85% and for one pellet in the beam region 65%. The probability increases ≈5% points with a doubled time resolution (2/2 μs cycle). A detection inefficiency of 20% (*e.g.* camera cycle dead time) at each measurement level leads to a reduction of the probability of about 20%.

Similarly, for the reference conditions, the probability that the predicted number of pellets in the beam region is correct, for no reconstructed pellet in the beam region is 64% and for one reconstructed pellet in the beam region it is 67%. The probability increases a few percent units with a doubled time resolution.

For a more stochastic time distribution *i.e.* for 1% relative velocity spread, both probabilities are ≈20% lower than for 0.1% spread.

From of these studies one can deduce that for the reference conditions about 70% of the hadronic events (based on the time when pellets are in the beam region) would have correct information from the tracking system and for about 50% of the events there would be unambiguous position information.

4.3.4. Possibility for improvements

Further developments are needed both on the hardware and the software side for the final design of the whole tracking system. These are directly and indirectly connected to the work on simulations. Physical effects like pellet loss due to in stream collisions and gravity could be implemented in more detail. The pellet detection process including optical effects and the two opposite camera operation is not simulated in detail.

There are design developments of the hardware setup foreseen, both fine-tuning on the details of the measurement level configuration and the design of a lower tracking section at the dump.

For the development of alignment procedures for hardware, both within measurement sections and global relative to the accelerator beam, simulations are needed. Development of the procedure of merging pellet tracking information with the data produced in pellet-beam interactions needs simulations.

Simulation

Pellet loss between measurement levels For simplicity and to make the interpretation of the results easier, pellets are now lost only before the first measurement level. The number of pellets at all measurement levels remains constant. In the future studies the tracking efficiency with pellet loss between levels should be checked. The expected total loss at the skimmer and between the measurement levels will be similar to the one used in the study. Assuming the same total pellet loss as in the study, the efficiency of the system should be comparable.

The effect of gravity The gravity is currently not used in the pellet generation and tracking. The effect of gravity in the X and Z directions is small, of the order of ≈5 μm at the distance from the generation point to the interaction region. On the other hand, the effect of gravity in the Y direction is considerable, of the order of ≈70 μs, which corresponds to a distance of ≈5 mm.

Shifted camera cycle In the current study a short camera cycle without dead time is used to effectively simulate the usage of two cameras with shifted cycles. It simulates in the first order the properties of the shifted cycle setup. However, additional studies may be needed to model the behavior of such a setup in more detail.

Setup

The layer configuration within a tracking section The tracking efficiency might increase with a shorter distance between some of the layers. Whether this is possible from a technical point of view has to be investigated.

Lower tracking section The lower tracking section will improve the resolution and can also be used for tuning and monitoring of the tracking performance. The details of its design have to be studied further. The size of the pellet stream is a complication in this region. It is about 6 mm in diameter, which requires a larger depth of field of the camera optics and a wider laser beam.

Chapter 5

Pellet track processing

To make use of the pellet tracking information, it has to be included in the analysis chain of the hadronic events. In this chapter a scheme for such inclusion is discussed. The pellet information has to be provided with highest possible efficiency also in the case of detection inefficiencies and pellet losses. For this purpose an advanced tracking algorithm to be used together with the event analysis has been prepared and is described in this chapter. The expected algorithm performance is also presented.

5.1. Processing of the pellet tracking information

A typical rate of event collected at a hadron physics experiment, taking WASA-at-COSY as an example, is about 20 000 events/s. The mean time between events is then 50 μs and the time of one event (time needed to collect signals from the particle detectors) is within 1 μs. Each recorded event is approx. 5 kB in size. Given the event rate, the resulting data flow is then 100 MB/s. Each event is stored as one data bunch contains full collected information about a hadronic event.

In the pellet tracking, an event means passage of the pellet through the beam region. Information about the event will be collected by approx. 16 cameras in total, located at two measurement sections – approx. 2 m above and 2 m below the interaction region. Because of the time needed for pellet to travel the distance between the measurement sections and the interaction region, the relevant information from the pellet tracking detectors is collected during about 100 ms. For a pellet rate 15 k/s and 16 cameras, there will be 240 000 subevents (processed camera pictures) recorded each second. Given the data rate and the subevent size of about 128 bytes, the data flow will be of the order of 2 MB/s. This also means that the 16 subevents for a given event will be scattered among 24 000 subevents recorded during the 100 ms period.

The difference in time scales of the two systems is shown in Figure 5.1.1. The hadronic data and pellet data differ in the size of data flow (100 MB/s compared to 2 MB/s). The structure of the data is also different – events are stored as single bunches in case of hadronic data and scattered as subevents among subevents of other events, in case of pellet data. Moreover, the pellet data recorded at any given moment has no direct relation to the hadronic data recorded at this time. It is therefore practical to handle the pellet tracking information separately.

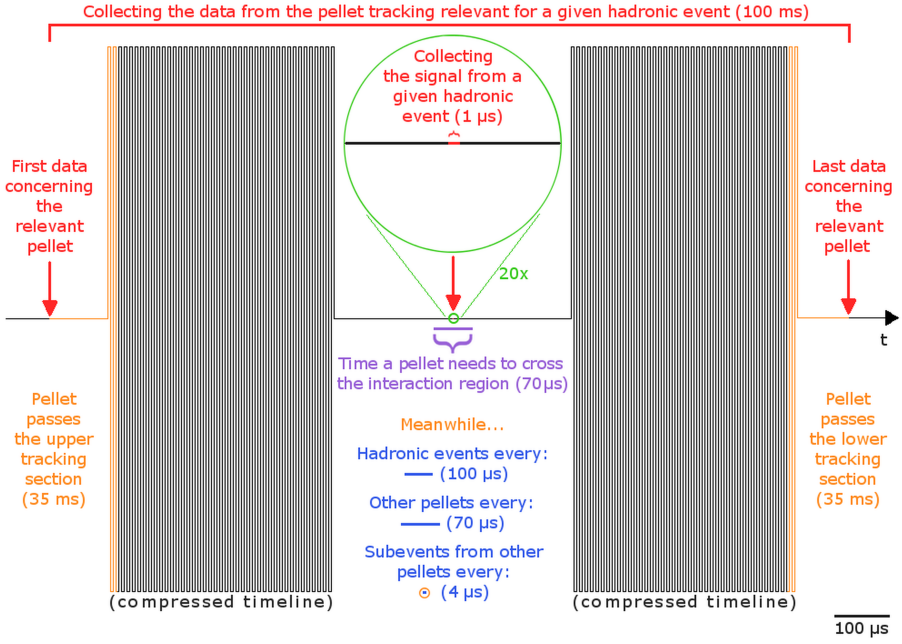

Figure 5.1.1: Illustration of the difference in time scales in which the hadronic DAQ and the pellet tracking operate

5.1.1. Data acquisition

A prerequisite for the usage of the pellet tracking system information is the provision of a common time frame for the PTR and the DAQ of the particle detector systems. The measurement information of the pellets and the hadronic events must have time stamps from a common clock. This information is written for each hadronic event together with a unique number of this event and should also be written for each pellet measurement detected by every single camera.

The information from pellet tracking will at this stage be a stream of pellet measurements. Each of these measurements has to contain at least the following information:

- time (from the common clock),
- measured position,
- an identifier of the measurement level and the camera, and
- a unique identifier of the measurement.

5.1.2. Track reconstruction

The information from pellet tracking will have to be processed to reconstruct pellet tracks. The data can be processed in two ways: online and offline.

The online analysis will allow for checking pellet stream parameters during the data taking and keeping the performance optimal. This includes pellet rate, pellet stream direction, divergence and shape of the stream. It will allow optimal positioning of the stream inside the pipes and scattering chamber. It will also be possible to check the mean number of pellets in the beam region. The online analysis will require a fast reconstruction algorithm. Such algorithm was proposed in Section 4.2.

In the offline analysis it will be most important to have the pellet information for the highest possible fraction of hadronic events. This will require very efficient track reconstruction algorithm, able do deal well with detection inefficiencies and pellet loss. Such a tracking algorithm has been developed and is described in Section 5.2.

5.1.3. Event classification

The tracking system will provide a set of pellet tracks. For each of these tracks it is possible to calculate a time when the pellet is expected to enter and exit the beam region. Based on this a record of beam region occupancy can be prepared (see Section 4.2.7) with information about the number of pellets expected to be in the beam region at any moment together with identifiers of these pellets.

During analysis of the hadronic events, the time of each event can be compared to this occupancy record, providing the number of pellets which were in the beam region when the event occurred. This will allow a **classification of each hadronic event** if it occurred when there was:

- **no pellet** in the beam region;
- **one pellet** in the beam region;
- **more than one pellet** in the beam region.

The events which occurred when the tracking system indicates lack of pellets in the beam region, can be classified as background events. They originate from rest-gas or from other sources of background. These events can be used in two ways:

- they can be rejected from the analysis of the "good" event sample and
- they can be analyzed separately providing a background sample for subtraction in the final kinematic distributions.

The events which occurred when the tracking system indicates one pellet in the beam region can be accepted and used as "good" events in the analysis. Also, in general, the events which occurred when there was more than one pellet in the beam region can be used in the analysis. It should then be checked, whether the information from the pellet tracking can be used for building tracks of particles from this event (see the next section).

As it will be discussed in Chapter 6, the presence of pellet in the beam region does not assure that the event occurred in the pellet. It may also come from interaction with the rest-gas. This is the reason why the distributions from background events will be useful in subtracting the background from the data sample. However, in situation with pellet in the beam region, it is typically 5-10 times more probable that the event indeed comes from the pellet.

There is a difference in reliability of beam occupancy information, depending on whether the reconstructed tracks are based only on information from the upper section or on information from both sections. If the pellet was detected in both sections, one can be sure, that it was present in the beam region. However, if the information from the lower section is missing, it could mean, that the pellet was lost somewhere between the two sections. It can be lost before or after passing the interaction region. Thus, the event classification mentioned earlier (0, 1 or more than one pellets) only gives the general idea, and it will be up to the user of the analysis framework to choose conditions for keeping and rejecting the events. The system will provide information about minimum and maximum number of pellets expected in the beam region, based on the presence of information from the lower section in the tracks. The user will be able to make conditions on these values. The situations when minimum = maximum = 0 and minimum = maximum = 1 can be used as reference data sets, and the other combinations can be assigned to the group of "good" or "bad" events, depending on the obtained results.

5.1.4. Usage of pellet position information together with Micro Vertex Detector tracks

When the pellet tracking system indicates that a pellet (or more pellets) is present in the beam region at the time of hadronic event, one can use the time of this event to calculate the pellet XYZ position in the moment when the interaction took place. This position can be used in the event analysis.

There are two possibilities determining how the pellet position information should be used:

- the pellet position is the expected origin of tracks recorded by other detectors and the pellet position could be used as an additional point in the tracks; or
- the pellet position gives the expected position of the primary interaction but the reconstructed particle tracks originate from a secondary vertex. In this case the pellet position is not used in fitting the tracks, but is used as the origin of the reconstructed primary particle path. From the secondary vertex, determined from particles tracks, the direction of movement and decay distance of the primary particle can be directly determined.

The Micro Vertex Detector (MVD) [3] is a detector in the PANDA setup which is designed to reconstruct interaction vertices with an accuracy around 100 μm in X, Y and Z (see Figure 1.3.3). The vertex position from this detector is thus of similar accuracy as the pellet position from pellet tracking and these pieces of information can be used together. The MVD has its optimal resolution within Z = +/- 3 mm around the nominal interaction point, which well covers the pellet stream region (see Appendix B for the coordinate system definition).

If, during the particle tracks reconstruction procedure, the pellet position from the tracking is in agreement with the interaction vertex given by MVD, the pellet position can be used as additional point in the particle track, improving the accuracy. The information from pellet tracking would be especially useful for tracks with polar angles below 15 degrees, for which the MVD resolution deteriorates drastically.

If the pellet position is not in agreement with the information from MVD, this could mean, than the pellet position indicates the primary vertex. In this case, a vector could be determined between the pellet position and the secondary vertex given by MVD.

The situation with more than one pellet in the beam region in a time of hadronic interaction is less favorable because of the resulting ambiguity. However, with two pellets in the beam region, it may be still reasonable to use information about their positions as a hypotheses and checking which one fits better to the event information measured in other ways (mainly MVD).

5.2. Advanced pellet track reconstruction algorithm

5.2.1. Motivation and guidelines

The simplified tracking algorithm, described in Section 4.2 allows for checking many properties of the designed tracking system. However, for the analysis of experimental data there is a need for a more advanced algorithm, that provides a very high efficiency track reconstruction, also in situations of detection inefficiency.

In the simpler algorithm, the first level plays a special role - it is the starting point for a track. If a pellet is not detected here, the track will be missing. Also, a continuity of the track is required – a pellet has to be detected at all consecutive levels. This also is a source of reconstruction inefficiency in the case of detection inefficiency. Moreover, all decisions to be taken, such as which measurement should be chosen as the next point in the track, are taken on the fly. The structure of the algorithm makes it impossible to improve its parameters without introducing confusion and pile-up complications.

Because of these reasons, a more advanced algorithm has been designed for offline analysis, based on the following guidelines:

- No measurement level plays a special role. All measurement levels are of the same importance.
- All possibilities of detection inefficiencies are dealt with to reconstruct a track whenever it is possible - *i.e.* when the total number of levels in the track is sufficient to reconstruct the pellet velocity and direction, regardless of possible missing measurements.
- All the information is approached in a holistic manner. All decisions are taken when all information is present. The decision about a track is taking into account also other tracks.
- The basic idea and rules of the algorithm have to be simple and transparent. Preferably, the algorithm should be able to operate in a set of separate and independent steps where the following step is run after the previous step has been processed for the whole sample.

5.2.2. Idea of operation

The more advanced tracking procedure consists of two conceptual phases. The first phase consists in finding all possible measurement combinations. In the second phase are the correct tracks chosen among these combinations.

Phase I - finding all possible measurement combinations

Finding all possible measurement pairs between two measurement levels

As a *measurement* one understands the single act of obtaining information at a given level, which is assumed to originate from a passing pellet.

Measurements from two different levels can come from the same pellet, if the time between them corresponds to the time of flight between these two levels. Because of the velocity spread in the stream, the time of flight distribution of the pellets is smeared. Thus, one can define a time window, corresponding to time of flight of pellets with velocity in a certain range. All measurements from two different measurement levels, for which the time of flight is within this window, are saved as measurement pairs, possibly coming from the same pellet. The width of the time window is given by the velocity spread in the stream, accepting pairs of measurements originating from pellets traveling with velocity in a certain range. Making the window bigger increases the probability that the matching pellet is in the window, but also increases the number of incorrect pairs. A window of $\pm 2\sigma_v$ appears to be a reasonable choice. If required, the ranges of the time window are calculated taking into account the effect of gravity.

The pairs of measurements will be used in the next step for building track candidates (measurement combinations).

The simplest situation is when the pellet is detected at all measurement levels. Then, the only interesting pairs are between two subsequent levels. However, the presence of detection inefficiency (and pellet loss) forces us to consider situations, when the pellet was not detected at some of the measurement levels. In case of detection inefficiency, the pellet could be missed at a given level, but appear at the following ones. Because of this, one has to consider all possible combinations of measurement levels.

The search for measurement pairs and different versions of detection inefficiency are illustrated in Figures 5.2.1 and 5.2.2.

Pellet loss may occur between measurement levels. Because of this one have to take into account the possibility that a measurement at a certain level is the last measurement of a given pellet. To achieve this, while making a list of measurement pairs between two levels, for each measurement from a given level there is also a special, dummy pair produced, which does not contain the information about the second measurement. During the step of building the tracks it will be an indication that the track should end there.

When a pellet is detected in a window at a given level, this does not necessarily has to be the correct pellet. It is possible that it was

not detected and only other pellets were detected within the window. Because of this, the possibility that the pellet was not detected at a given level is checked even if there are other pellets within a window at this level.

When a pellet is not detected in several consecutive measurement levels, there is a high probability, that it was lost. At the same time, pairs between distant measurement levels require a big time window, which is filled with many incorrect combinations, which would have to be processed. To optimize the algorithm for such situations, one can define a maximum size of a gap between measurement levels (maximum number of omitted levels between the two given ones).

Merging the pairs into combinations

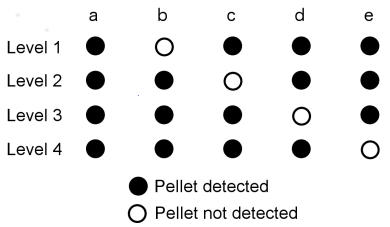

Figure 5.2.1: Different possibilities of detection efficiency (a-e) checked by the tracking algorithm. Example for 4 measurement levels with pellet information missing at maximum at one level. All combinations have to be checked to ensure that the track is reconstructed even in the case of detection inefficiencies

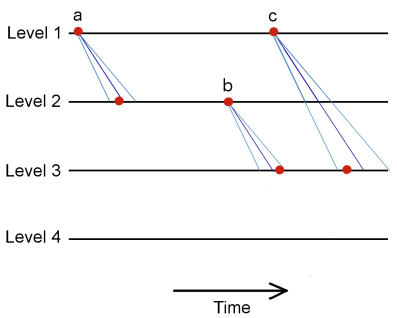

Figure 5.2.2: Examples of searching for measurement pairs. Pellets are searched for within a time window corresponding to a pellet velocity $v_{mean} + / - 2\sigma_v$. The dark blue line corresponds to the mean velocity in the stream, and the light blue lines correspond to the boundary velocities. Examples of a measurement pair between first level and the following level (a), measurement pair between second level and the following level (b) and a measurement pair with one level gap (c)

The measurement combinations (full pellet tracks) are built by merging the measurement pairs. At the beginning of the procedure, the first measurement pair is taken from the container of found pairs. The identifier of the first measurement in the pair is saved as the first measurement for a new track, and the identifier of the second measurement in the pair is checked. Then, the container is searched to find all measurement pairs with the first measurement the same as the second measurement in the initial pair. Usually, many such complementary pairs are found. In this case the first of the found pairs is followed, to find following complementary pairs. This process of going deeper into the branches and following the first one is repeated until the found pair indicates the end of the track (*i.e.* a dummy measurement used for taking into account a possibility of pellet loss or marking that we went past the last measurement level). In such case, the track is saved and the procedure goes to the next measurement pair found at a given branching level and tries to follow it. When all pairs at a given branching level are processed (and resulting tracks saved), the procedure moves to the next found pair at the lower branching level. This way all possible matching combinations of measurement pairs are found and merged into tracks.

Phase II - choosing correct tracks

In the first phase, two kinds of undesirable combinations are produced:

- Incorrect combinations, *i.e.* combinations containing measurements for different pellets.
- Redundant correct combinations *i.e.* combinations containing measurements for only one pellet, but existing in many versions – with measurements from a different number of levels and different combinations of them.

Removing incorrect combinations

A set of measurements for the same pellet gives consistent information about its velocity and direction. Inconsistency of this information is an indication, that the measurements come from different pellets. Two methods are used do distinguish such events: (1) a calculation of combination consistency and (2) evaluation of the quality of the fitted track. The first method is much faster, while the second one is more precise and also it is a byproduct of the necessary step of fitting the track. The two steps are executed one after the other.

1) Calculation of consistency

In a measurement pair, the time difference between two measurements is within the assumed time window. Since the size of the time

window is based on a fixed velocity range, then the position in the window for a given pair is an indication of a velocity between these two levels. Position *-1* in the window (minimum allowed time difference) corresponds to the high velocity bound (*e.g.* $v_{mean} + 2\sigma_v$) and position *+1* in the window (maximum allowed time difference) corresponds to the low velocity bound (*e.g.* $v_{mean} - 2\sigma_v$).

If all measurement pairs used for building a track come from the same pellet, then their position in the window should be similar. On the other hand, the positions in the window for tracks built from pairs containing different pellets can show a significant deviation. This idea is illustrated in Figure 5.2.3.

The time measurement resolution introduces some deviations for measurements of the same pellet. However, for the time resolutions intended to be used in the tracking, these deviations are still much smaller than in the case of different pellets.

The deviation *Dev* is calculated according to the formula

$$Dev = \frac{\sum \left(\frac{\delta_i - \delta_{mean}}{\sigma_i} \right)^2}{n_{pairs} - 1}, \tag{5.2.1}$$

based on the position in a window of a given pair δ_i (ranging from -1 to 1), number of pairs n_{pairs} and a mean position in window for all pairs calculated as $\delta_{mean} = \frac{\sum \delta_i \frac{1}{\sigma_i^2}}{\sum \frac{1}{\sigma_i^2}}$, with $\sigma_i = \sqrt{\sigma_{i,first}^2 + \sigma_{i,second}^2}$ as the total uncertainty of measurements at the two levels from the pair $\sigma_{i,first}$, $\sigma_{i,second}$.

In an analogous manner one calculates the deviation for the X and Z directions. In these cases, the pellet direction is used. The pellet direction dir_x is calculated as a difference in pellet position at the two levels x_{second}, x_{first}, divided by the distance between the levels $d_{first,second}$:

$$dir_x = \frac{x_{second} - x_{first}}{d_{first,second}}.$$

The deviation for Z is calculated analogously.

The values of deviation in T, X and Z are executed in sequence and a cut is made after each of them. Thus, the values of a deviation for a given direction are calculated only if the track passed the cut for the previous one.

The value for the cuts is based on simulations. This method allows to remove a high fraction of incorrect combinations (80-95%).

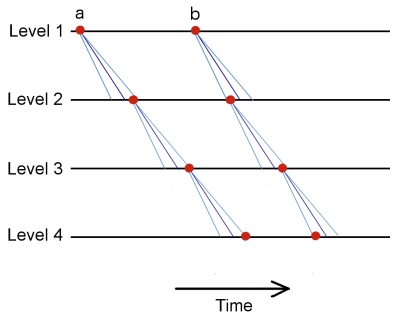

Figure 5.2.3: Example of the simple track consistency check, based on pellet positions in the time window. When the track contains measurements for the same pellet, the pellet position in the time window is similar for all measurement pairs (a). When the track contains measurements for different pellets, the pellet position in the time window may be very different for different measurement pairs (b)

2) Fitting the tracks and checking their quality

The fits for T, X and Z are done using linear functions. For X and Z this is sufficient even in the presence of gravity. For T, the function can be easily replaced with parabola to take gravity into account.

The functions fitted are the following: $T = f_T(Y)$, $X = f_X(Y)$ and $Z = f_Z(Y)$. Y is the position of the measurement levels and it is assumed to be exact. The uncertainties in the T, X and Z measurements are based on the measurement resolution at given levels.

In the case of T, measurements from all available levels are used for fitting. In the case of X and Z, one uses measurements from levels which participate in the tracking in a given direction. Additionally, the position of the pellet generation point (VIC exit) is always used in fitting X and Z. The uncertainty of this position is based on previous studies.

The χ^2 parameter is calculated for each fitted track. A reduced chi-squared is then calculated:

$$\chi^2_{red} = \frac{\chi^2}{n_{dof}},$$

where n_{dof} is the number of degrees of freedom for the current track (number of levels in the track minus the number of parameters of the fitted function).

By making a cut at a certain value of χ^2_{red} one can remove many incorrect tracks preserving almost all the correct ones. The value for the cut is determined by simulations. The fits and cuts are made in sequence and fitting for a given direction is made only if the track passed the cut for previous direction.

Since the VIC position is used in the fit, the cut removes pellets which do not originate from there, *i.e.* scattered pellets. Even though a scattered pellet could make a valid track, it is highly unlikely that this pellet would reach the interaction region.

Removing redundant correct combinations

After the previous phase, the majority of incorrect tracks is removed. Now the main task is to deal with multiple tracks for one pellet. The removing of redundant tracks is done in two stages.

1) Evaluating the quality of the tracks

Each track gets assigned a number describing its quality. It was chosen to rank the track quality by the number of measurements in the track. The more measurements in the track the higher is its quality. This method works sufficiently well.

2) Rating the tracks

The common ground where one can compare quality of different tracks is a measurement contributing to these tracks. During the reconstruction each measurement is normally assigned to a number of tracks. In the described procedure one wants to find the best track containing a given measurement.

To do this, all tracks containing a given measurement are checked. The one with the highest quality wins and gets "one point" in respect to this measurement. This procedure is done for all measurements and every track becomes ranked with respect to all measurements it contains.

After this procedure, one has tracks with different rating. The best tracks are these with the rating equal to the number of measurements in the track (in the ideal case). When one pellet results in tracks containing different number of measurements, the track with the highest quality is chosen. The method is illustrated in Figure 5.2.4.

The final selection of tracks is made by applying a *threshold on the track rating* and on the *maximum rating deficiency*. The rating deficiency states the difference between number of measurements in the track and the track rating. With rating deficiency equal to 0, the track was the best one at all levels present in the track (see Figure 5.2.4). With rating deficiency equal to 1 the track has a rating equal to the number of levels in the track minus 1. This means that while the track was the best track from the perspective of (normally) a few constituent measurements, it was not the best track from the perspective of one of them. Such situation is unfavorable and can occur when an incorrect track passes the rejection procedures and competes with correct tracks in the track

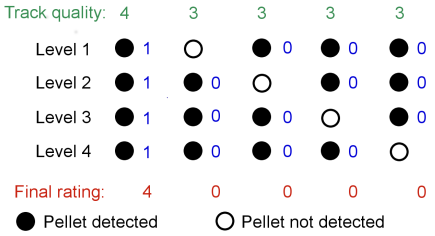

Figure 5.2.4: Rating of the tracks to remove redundant correct tracks for the same pellet. In the first step the tracks get assigned a number describing their quality. The number is equal to the number of measurements in the track (green). Then the tracks are judged in respect to the measurements. The best track for a given measurement is looked for. (All filled dots for a given level correspond to the same measurement). The best track for a given measurement gets one point with respect to this level (this measurement), and the other tracks get zero points (blue). The rating of each track is then summed up (red). The highest rating is given to the track with the highest number of measurements

rating and happens to win in a comparison. This effect often makes it reasonable to allow for some rating deficiency threshold, to not reject correct tracks with happened to lose at some point the competition with an incorrect track. On the other hand, a higher threshold on the rating deficiency increases the number of incorrect tracks which pass the selection.

5.2.3. Example results

Some results of the track reconstruction efficiency and correctness were presented in Section 4.2.8 in comparison to the results of the simpler algorithm. Presented here are the results obtained for different algorithm settings, listed in Table 5.2.1. The results in Table 5.2.2 show the difference in reconstruction efficiency and correctness for different values of maximum rating deficiency, obtained for a set of pellet conditions described in Section 4.2.2.

The tracking efficiency is the ratio of reconstructed tracks to survived pellets. The reconstruction efficiency is the ratio of reconstructed tracks to detected pellets. The reconstruction correctness is the ratio of the correct reconstructed tracks to all reconstructed tracks. The number of survived pellets in the discussed cases is constant at all measurement levels and in the interaction region. All pellet loss is realized before all measurement levels. Pellets are lost at the skimmer (for the pellet rate of 14 k/s it is the only source of pellet loss) and due to an additional random loss at the generation (for 5 k/s). The number of detected pellets is the average of the number of detected pellets from all levels used in tracking. Pellet was detected if it was at least partially visible during

the camera exposure time and the amount of collected light was above the threshold value. The number of reconstructed tracks is the number of tracks left after the aforementioned selection process.

In the case of 4 levels only the results with deficiency equal to 0 are presented, because a change of this value has almost no effect on the results. For the 7 levels case, the increase of the maximum deficiency increases the algorithm efficiency because more tracks are accepted. It also decreases the algorithm correctness because the fraction of incorrect tracks becomes higher. While using the algorithm in the hadronic reactions analysis, it will be possible to choose the settings to obtain the optimal algorithm behavior.

Table 5.2.1: Parameters of simulations and settings of the pellet tracking algorithm

Number of measurement levels	varied (4 and 7)
Maximum gap between levels with a measured pellet	2
Half size of the time window	2 velocity sigmas
Rating threshold for tracks	3
Maximum rating deficiency	varied (0, 1 and 2)

Table 5.2.2: Performance of the tracking algorithm for different pellet stream and measurement conditions. The tracking efficiency is the ratio of reconstructed tracks to survived pellets. The reconstruction efficiency is the ratio of reconstructed tracks to detected pellets. The reconstruction correctness is the ratio of correct reconstructed tracks to all reconstructed tracks

Camera cycle, pellet rate	Algorithm settings	Tracking efficiency	Recons. efficiency	Recons. correctness
12.5/10 μs, 5 k/s	4 levels, Rating thr. 0	25.9%	29.9%	95.7%
	7 levels, Rating thr. 0	83.8%	91.8%	97.8%
	7 levels, Rating thr. 1	88.7%	97.2%	95.8%
	7 levels, Rating thr. 2	94.7%	100.1%	99.9%
6.25/5 μs, 5 k/s	4 levels, Rating thr. 0	70.9%	77.6%	98.5%
	7 levels, Rating thr. 0	91.6%	97.1%	99.1%
	7 levels, Rating thr. 1	94.2%	99.8%	98.0%
	7 levels, Rating thr. 2	94.7%	100.5%	97.6%
4/4μs, 5 k/s	4 levels, Rating thr. 0	83.1%	86.7%	98.4%
	7 levels, Rating thr. 0	92.7%	95.3%	99.2%
	7 levels, Rating thr. 1	94.7%	97.4%	98.3%
	7 levels, Rating thr. 2	94.9%	97.6%	98.2%
2/2 μs, 5k/s	4 levels, Rating thr. 0	89.4%	94.6%	99.6%
	7 levels, Rating thr. 0	93.9%	97.1%	99.4%
	7 levels, Rating thr. 1	95.2%	98.4%	98.9%
	7 levels, Rating thr. 2	95.3%	98.6%	98.8%
12.5/10 μs, 14 k/s	4 levels, Rating thr. 0	26.4%	30.5%	88.5%
	7 levels, Rating thr. 0	68.8%	75.4%	93.7%
	7 levels, Rating thr. 1	77.9%	85.4%	89.9%
	7 levels, Rating thr. 2	86.0%	94.2%	86.0%
6.25/5 μs, 14 k/s	4 levels, Rating thr. 0	69.4%	76.0%	96.6%
	7 levels, Rating thr. 0	85.6%	90.7%	97.2%
	7 levels, Rating thr. 1	91.5%	97.0%	95.0%
	7 levels, Rating thr. 2	93.6%	99.2%	94.1%
4/4 μs, 14 k/s	4 levels, Rating thr. 0	80.0%	83.5%	97.4%
	7 levels, Rating thr. 0	88.9%	91.4%	97.6%
	7 levels, Rating thr. 1	93.6%	96.3%	95.8%
	7 levels, Rating thr. 2	94.4%	97.2%	95.5%
2/2 μs, 14 k/s	4 levels, Rating thr. 0	87.2%	91.8%	98.7%
	7 levels, Rating thr. 0	92.2%	95.4%	98.7%
	7 levels, Rating thr. 1	95.3%	98.5%	97.5%
	7 levels, Rating thr. 2	95.5%	98.7%	97.5%

5.3. Summary – pellet track processing

- Essential pellet tracking data will be stored during the experiment with time stamps synchronized with the common experimental clock.
- The tracks will be reconstructed online, with a fast algorithm, to provide monitoring and tuning capabilities, as well as offline, with high performance algorithm, for the purpose of hadronic data analysis.
- The information from pellet tracking about the number of pellets in the beam region during the interaction will be used in the data analysis. The hadronic events will undergo classification based on the pellet tracking information. Events from different classes could be then handled separately.
- The information about pellet position can be used together with MVD information. This will allow separating primary and secondary interaction vertices. Pellet tracking information will also provide additional point for fitting of charged particle tracks curved in the magnetic field of the solenoid.
- A pellet track reconstruction algorithm has been developed that will provide high tracking performance even in demanding conditions. For high pellet rate (14 k/s), long camera cycle (6.25 μs), high detection inefficiency (20%) and using only upper detection section, tracks will be reconstructed for 70% of pellets and the reconstruction correctness will be 97%. In the simulations for more favorable conditions, with pellet rate 5 k/s, 2 μs camera cycle, no detection inefficiency and using both measurement sections, tracks for 94% of pellets are reconstructed and the reconstruction efficiency is 99.5%. The results show that the pellet tracking system will provide information about the interaction point for the majority of hadronic events (70-95%).

Chapter 6

Studies on implementation of pellet tracking in hadron physics experiments based on usage of a Long Range TDC at WASA

This chapter describes the usage of information obtained from an external system synchronized with the DAQ of the WASA experiment – similarly to how a pellet tracking system would operate. It has been used to provide a classification of the analyzed hadronic events as coming from pellets or being due to non-pellet background. The results clearly show that such classification is possible and that the synchronizing of the systems work well.

6.1. An alternative method of rejecting events not coming from the nominal interaction point

One of the advantages given by the pellet tracking is the suppression of events not coming from pellets, but from background – from the rest-gas or from other non-pellet sources. This functionality can be demonstrated by using an alternative system based on long-range TDCs.

It is known from previous studies, that pellets are present in the beam region only for some fraction of time. Events from rest-gas, on the other hand, happen continuously. However, it is more probable that when a pellet is in the beam region, the recorded event originates from a pellet. Bearing this in mind, one can exploit an alternative method of checking when pellets are in the beam region, based on the instantaneous event

rate of interactions, since there are more interactions when a pellet passes through the beam.

This method only works when pellets are in the beam for a fraction of the time. It is not possible to distinguish the source of the interaction when a pellet is in the beam region – this is a matter of probability. For this reason one can only reject events from the rest-gas when there was no pellet in the beam region.

The method, described in detail in the following sections, has also been proven to favor events occurring close to the nominal interaction point. This property is favorable for a separation between "good" events and non-pellet background.

The method is based on an external system being used in a different (longer) time scale than the regular DAQ. Since this also is true for the full scale pellet tracking system, the method gives an experience in working with such system. This includes the hardware part of the project, as well as the data processing and using the information in the analysis of hadronic reactions.

6.2. Analysis of example reaction

The reaction $pp \to pp\pi^0 \to pp\gamma\gamma$ was used to show the differences in the analyzed data, resulting from the presence of non-pellet background. When events do not come from the nominal interaction point, are the reconstructed theta (polar) angles of the particles reconstructed incorrectly. This occurs, because the interaction point is assumed to be in (0,0,0) position – the nominal interaction point. As a result of a sometimes incorrect assumption, various kinematic properties may be violated in the analysis results.

6.2.1. The WASA detector setup

The 4π WASA detector setup is divided into two main parts: Forward Detector (FD) and Central Detector (CD). A schematic view of the WASA setup is shown if Figure 6.2.1. Coordinates are according to the definition in Appendix B.

The Forward Detector is designed mainly for detection and identification of scattered projectiles and recoil particles such as protons, deuterons and He nuclei in π and η production reactions. The scattering angle (theta) coverage of the FD is $3°$- $17°$.

The Central Detector surrounds the interaction region and is used mainly for detection and identification of decay products from π^0 and η mesons: electrons, neutrons and charged pions. Angular acceptance of the CD in the polar angle is $20°$- $169°$.

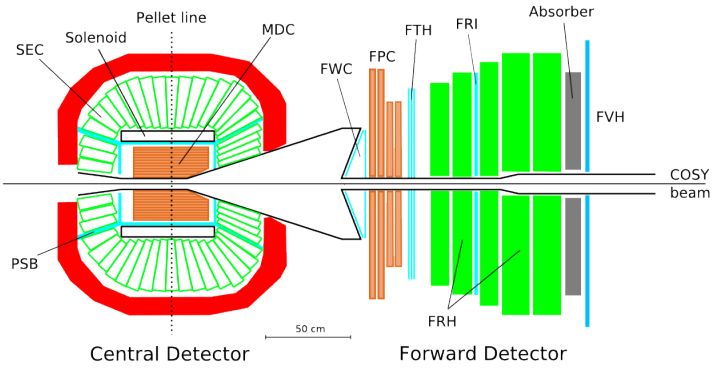

Figure 6.2.1: Schematic view of the WASA detector setup. The meaning of the abbreviations is given in the text below

The Forward Detector consists of the following parts:

- Forward Window Counters (FWC),
- Forward Proportional Chambers (FPC),
- Forward Trigger Hodoscope (FTH),
- Forward Range Hodoscope (FRH),
- Forward Range Interleaving detector (FRI),
- Forward Veto Hodoscope (FVH).

The focus is put on the Forward Range Hodoscope. This is because the energy deposits in different layers of FRH are used in particle identification with E/dE method. The FRH consist of 5 layers, each built from 24 elements (see Figure 6.2.2). The maximum energy deposit for protons in each of the first 3 layers is 105 MeV, and for last two (thicker) layers 130 MeV.

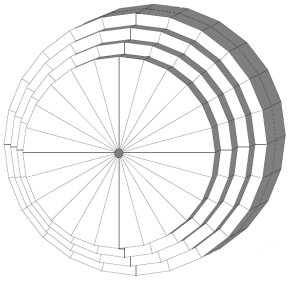

Figure 6.2.2: Schematic view of the Forward Range Hodoscope. FRH consists of 5 layers, each of them is built of 24 elements

The FPC is the main detector responsible for track direction determination and the other detectors are used to select events during the data taking. They also provide information for the track reconstruction.

The Forward Detector provides scattering angle resolution of 0.2°and the energy resolution for stopping particles is ≈3%.

The Central Detector consists of the following parts:

- Mini Drift Chamber (MDC),
- Superconducting solenoid,
- Plastic Scintillator Barrel (PSB),
- Scintillating Electromagnetic Calorimeter (SEC).

In the analysis, focus is put on the calorimeter (SEC) which records photons. The position of the SEC crystals is used to reconstruct the angles of the emitted photons. The PSB detector is only sensitive to charged particles and is used to discriminate between neutral and charged particle tracks.

The scattering angle resolution of the calorimeter is ≈5°(FWHM) and energy resolution for photons is ≈8°(FWHM).

A comprehensive description of the WASA detector setup can be found in Reference [10].

6.2.2. Experimental data

Information about the data The analyzed experimental data come from the August-September 2012 $pp \to pp\pi^0$ beamtime. During this measurement 16 minutes were devoted to collect data in special conditions, enabling the analysis described here. The data were collected in synchronization with information from Long Range TDC (see Section 6.5.1). This allowed to combine the information about the analyzed hadronic interaction with information about the conditions in the beam region when the interactions occurred. The kinetic energy of the proton beam was 0.44985 GeV.

Triggers Particles coming from the reactions are recorded in separate detector parts. The trigger is a certain coincidence condition between those different parts. The information from a given event is saved to the disk if the condition of a trigger is fulfilled. This enables to reject at the early stage most of the events obviously uninteresting for the current measurement. This is especially important taking into account limited speed of the data acquisition system (DAQ).

The experimental triggers important for the described analysis were:

- **TR0** - requiring at least one charged particle track in the forward detector with a veto on Forward Veto Hodoscope. A track is here defined as a match of modules in phi angle between FTH, FWC and FRH. The trigger 0 was prescaled with a factor of 24. The prescaling is done due to limited speed of writing the data.
- **TR17** - a coincidence between the forward and central part of the Plastic Scintillator (at least one module above threshold in each of these detector parts). The trigger was prescaled 500 times.
- **TR21** - a coincidence between the first layer of the Forward Range Hodoscope and a central part of the Plastic Scintillator (at least one module above threshold in each of these detector parts). The trigger was prescaled 500 times.

6.2.3. Monte Carlo events

Monte Carlo simulations were used to provide an aid in the data analysis. The source of simulated events is the Pluto generator [34]. It simulates interactions between a given beam and target particles at a given kinetic energy. Reaction and decay channels can be chosen. Events generated by Pluto are distributed according to phase-space. A phase-space approximation is sufficient for the purpose of the presented studies.

Figure 6.2.3 show angular distribution of protons and photons from the $pp \to pp\pi^0 \to pp\gamma\gamma$ reaction. The acceptance ranges of WASA Forward and Central detectors are indicated.

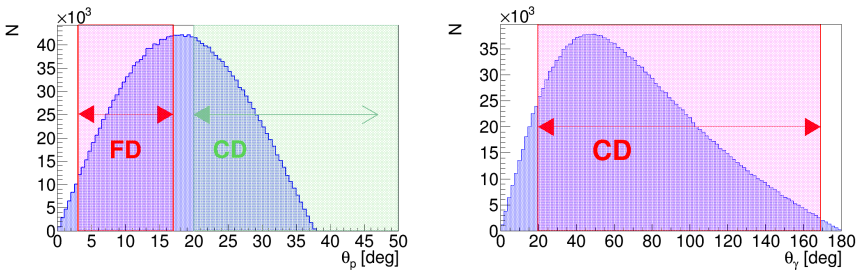

(a) Protons *(b) Photons*

Figure 6.2.3: Simulated polar angles (theta) of protons and photons. The acceptance ranges of WASA are indicated (FD - Forward Detector, CD - Central Detector)

The generated events are further processed by the WASA Monte Carlo (WMC) software, which reproduces detector response of WASA. WMC simulations take into account detector acceptance, resolution

and various interactions and physical effects taking place during the measurement. It is based on GEANT3 framework [35].

6.2.4. Fine tuning of energy calibration in the experimental data

The energies of particles recorded by Forward Detector and Central Detector (in the experimental data) were fine tuned to obtain agreement with Monte Carlo. Because the main part of the analysis will be based on comparing the results obtained when photons are recorded at different theta angles (see Section 6.3.2), the same division was used during the fine tuning. The high and low energy photons are grouped into three angular ranges: 0 - 40 degrees, 40 - 107 degrees, 107 - 180 degrees. The aim of the calibration was to obtain agreement in positions of missing mass and invariant mass peaks (see Section 6.2.5).

Central Detector The recorded photon energies are multiplied by a factor that takes into account energy leakage from calorimeter crystals. The required correction was the highest for the forward part, where the crystals are shorter and there is a high amount of structural material:

- 1.2 for theta 20 - 40 degrees;
- 1.035 for theta 40 - 107 degrees;
- 1.025 for theta 107 - 180 degrees.

Forward Detector The calibration constants for each element of first two FRH layers were adjusted to allow for better agreement between measured and simulated energy deposits in each element. Also, additional correction was applied for FRH1 and FRH2 to take into account that a proton depositing a certain amount of energy in one of FRH layers produces different amount of light, depending on whether the proton stopped in this layer or punched through it. The adjustments improved the agreement between experimental data and WMC in the plots for the nine photon angle combinations.

6.2.5. Selection of $pp \to pp\pi^0 \to pp\gamma\gamma$ events

Reconstruction of events coming from the desired reaction and separating them from the background was the first step of the analysis. A schematic view of the particles coming from the reaction is shown in Figure 6.2.4. Events with two protons recorded in the forward detector and two photons recorded in the central detector are taken into account in the analysis.

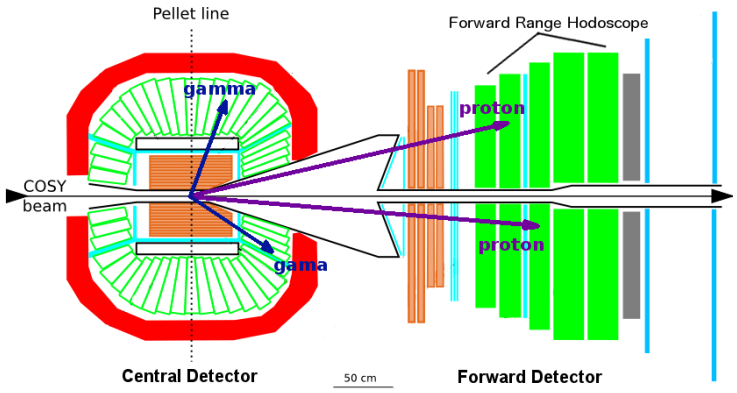

Figure 6.2.4: Particles coming from the analyzed $pp \to pp\pi^0 \to pp\gamma\gamma$ reaction

Selection criteria

A number of criteria were used to select the events coming from the desired reaction.

Selection of the trigger Only events which fired the trigger 0 were accepted.

Condition on the number of tracks The following condition has been taken in the analysis:

$$CD\text{-}N == 2 \text{ and } FD\text{-}C == 2 \text{ and } CD\text{-}C == 0,$$

(CD – central detector, FD – forward detector, C – charged particle track, N – neutral particle track).

Only in about 25% of the cases are both protons from the reaction present in the FD. However, it was not possible to use protons going to the CD in the analysis. Because of their high kinetic energy there was no information from MDC or the information was incorrect for virtually all these protons (also in the WMC). In addition, there are many CD-C tracks in the experimental data, coming from other reactions. In this situation, accepting only neutral particle tracks provided efficient rejection of the background. The presented analysis relies therefore only on cases when both protons are in the FD.

Two neutral clusters are searched for in the central detector. However, sometimes one photon may produce more than one cluster. One may consider taking into account these events, and search for the pair, which would reproduce the most correct value of π^0 mass. This happens only in about 10% of cases, and these cases reduce the invariant mass resolution. They were therefore skipped in the analysis.

Thresholds on the detectors Following thresholds on the forward part detectors were used:

- ≈0.2 MeV for FWC detectors,
- ≈0.3 MeV for FTH detectors,
- 3 - 4 MeV for FRH detectors,
- 0.4 MeV for FVH detector.

For each FD-C it was first checked, if the energy deposit in all layers of FWC and FTH is above threshold. This was a necessary condition for the track to be accepted. Then, the stopping plane was determined. Tracks which stopped in one of the FRH layers were accepted. In addition, the energy deposit in the FVH must be always below the threshold. This condition is used, because only a few events in WMC reach the FVH, and there were substantially more of these events in the experimental data.

The threshold on the minimum energy for a cluster member in the calorimeter was 2 MeV and the minimum energy for a cluster was set to 10 MeV.

Angular cut in the central detector The minimum theta angle in the central detector was set to 27°to limit the edge effects (*e.g.* energy leaks) from first layer of the crystals.

Selected tracks

The plots in Figure 6.2.5 - 6.2.10 show a comparison of several properties of selected FD and CD tracks between the experimental data and the Wasa Monte Carlo (WMC) for events originating from the nominal interaction region (0, 0, 0). Table 6.2.1 shows relative number of tracks recorded in different FRH layers.

Forward detector

Table 6.2.1: Percentage of protons recorded in each FRH layer, relative to the number of protons recorded in the first FRH layer

	Exp. data	WMC
FRH1	100%	100%
FRH2	38%	34%
FRH3	8%	4%
FRH4	0.8%	0.03%
FRH5	0.3%	0.003%

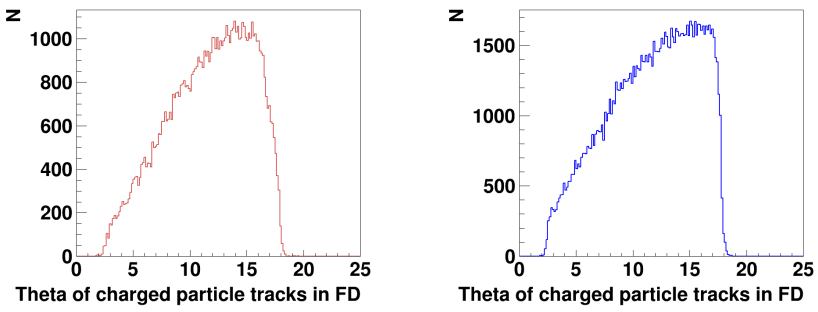

(a) Experimental data *(b) WMC simulations*

Figure 6.2.5: Theta angle of charged particles tracks detected in the Forward Detector

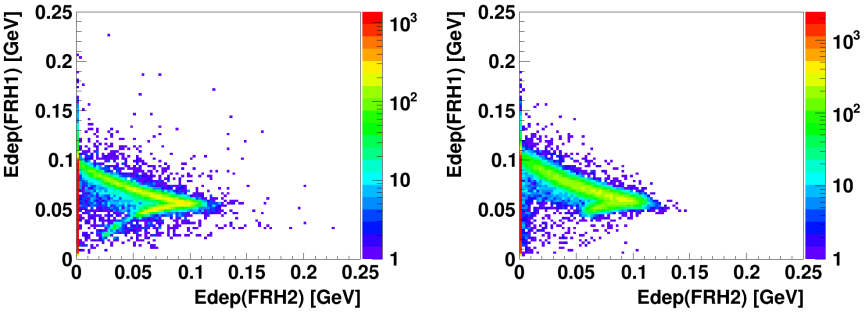

(a) Experimental data *(b) WMC simulations*

Figure 6.2.6: Energy deposit in FRH1 vs energy deposit in FRH2

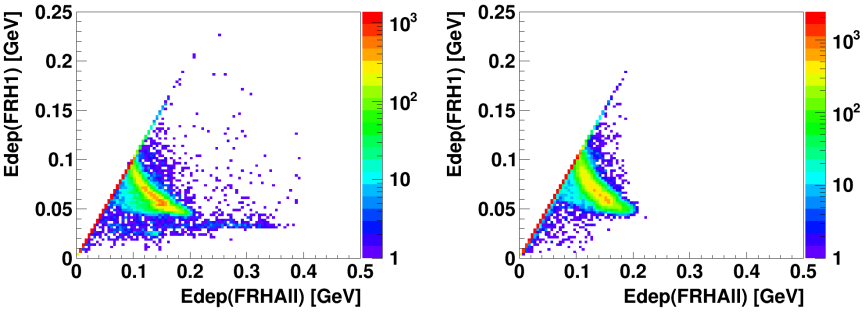

(a) Experimental data *(b) WMC simulations*

Figure 6.2.7: Energy deposit in FRH1 vs energy deposit in all FRH layers

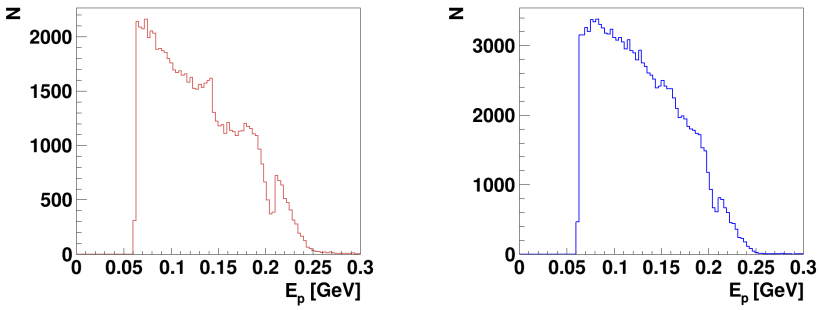

(a) Experimental data *(b) WMC simulations*

Figure 6.2.8: Reconstructed kinetic energy of protons recorded in the Forward Detector

Central detector

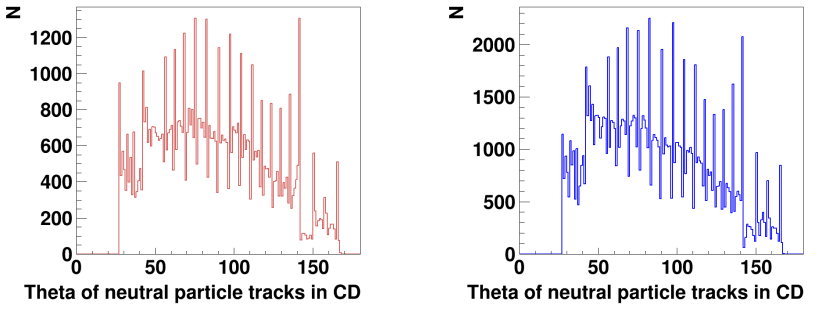

(a) Experimental data *(b) WMC simulations*

Figure 6.2.9: Theta angle of neutral particles tracks detected in the Central Detector

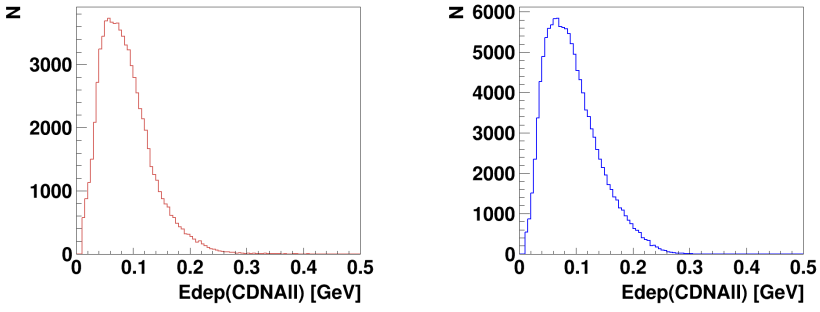

(a) Experimental data *(b) WMC simulations*

Figure 6.2.10: Energy deposited by neutral particles in the Central Detector

Invariant and missing mass of π^0

The measured information about the photons is their directions (angles θ_{γ_1}, θ_{γ_2} and φ_{γ_1}, φ_{γ_2}) and energies E_{γ_1}, E_{γ_2}. The measured information about the protons is their directions (angles θ_{p_1}, θ_{p_2} and φ_{p_1}, φ_{p_2}) and energy deposits in each FRH layer. Kinetic energies of the protons E_{kin,p_1}, E_{kin,p_2} are reconstructed from these deposits with E/dE technique using an automated procedure based on information from Monte Carlo simulations. The beam kinetic energy $E_{kin,beam}$ is known. m_p is a proton mass.

Invariant mass of two photons $m_{\gamma\gamma}$ is calculated according to the formula[1]:

$$m_{\gamma\gamma} = \sqrt{\left(E_{\gamma_1} + E_{\gamma_2}\right)^2 - \left\|\mathbf{p}_{\gamma_1} + \mathbf{p}_{\gamma_2}\right\|^2}, \tag{6.2.1}$$

where $\mathbf{p}_{\gamma_i} = \left[E_{\gamma_i} \sin\theta_{\gamma_i} \cos\varphi_{\gamma_i},\ E_{\gamma_i} \sin\theta_{\gamma_i} \sin\varphi_{\gamma_i},\ E_{\gamma_i} \cos\theta_{\gamma_i}\right],\ i = 1,\ 2.$

Missing mass of two protons mm_{pp} is calculated according to the formula:

$$mm_{pp} = \sqrt{\left[E_{kin,beam} - \left(E_{kin,p_1} + E_{kin,p_2}\right)\right]^2 - \left\|\mathbf{p_{beam}} - \left(\mathbf{p_{p_1}} + \mathbf{p_{p_2}}\right)\right\|^2}, \tag{6.2.2}$$

where

$\mathbf{p_{beam}} = \left[0, 0, \sqrt{E_{kin,beam}^2 + 2m_p E_{kin,beam}}\right]$ and

$\mathbf{p_{p_i}} = \left[p_{p_i} \sin\theta_{p_i} \cos\varphi_{p_i},\ p_{p_i} \sin\theta_{p_i} \sin\varphi_{p_i},\ p_{p_i} \cos\theta_{p_i}\right],\ i = 1,\ 2.$

$p_{p_i} = \sqrt{E_{kin,p_i}^2 + 2m_p E_{kin,p_i}},\ i = 1,\ 2.$

The invariant mass plots for the experimental data and WMC are shown in Figure 6.2.11. The plots of missing mass are shown in Figure 6.2.12. Figure 6.2.13 shows the correlation of the missing and invariant mass. Small discrepancies exist between the experimental and simulated results. Invariant mass distribution for the experimental data is slightly broader in the low mass part. Also there is an excess of events with masses below 20 MeV. A shoulder in the high mass part of the missing mass distribution is much more pronounced in the experimental data. The sources of the discrepancies are effects not reproduced in the simulation procedures: possible misidentified events from other reaction, events pile-up and reaction of accelerator beam halo with pipe walls.

[1]The formulas are presented in natural units, assuming the speed of light equal to 1.

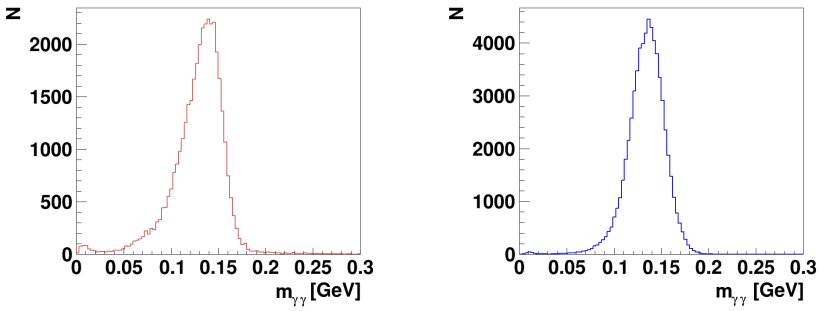

(a) Experimental data *(b) WMC simulations*

Figure 6.2.11: Invariant mass of two photons

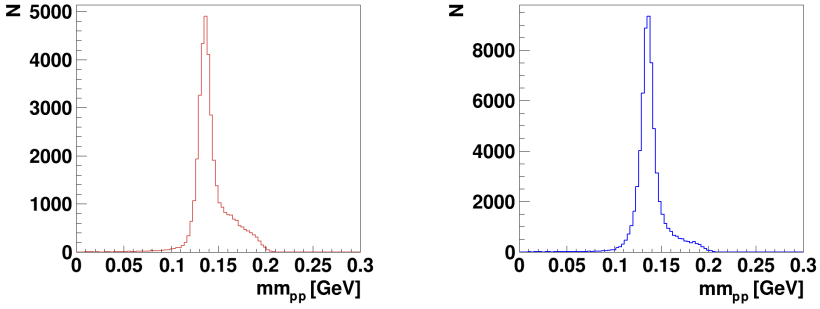

(a) Experimental data *(b) WMC simulations*

Figure 6.2.12: Missing mass of two protons

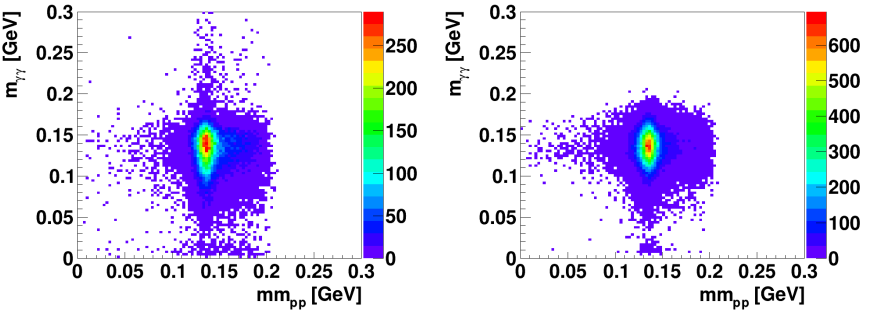

(a) Experimental data *(b) WMC simulations*

Figure 6.2.13: Missing mass of two protons (horizontal axis) and invariant mass of two photons (vertical axis)

6.2.6. Test reaction acceptance

A simulation study was made to check how the acceptance of the test reaction depends on the position of the interaction vertex. For this study, 75% of the events were generated at the intersection of the pellet stream and accelerator beam and 25% were generated along the accelerator beam (see Section 6.3).

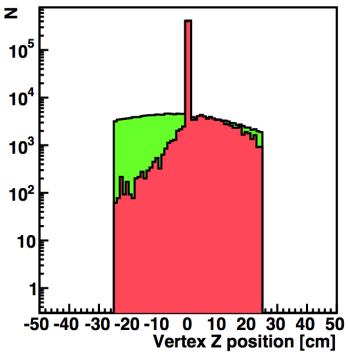

Figure 6.2.14: Distributions of generated (green) and reconstructed (red) events of the test reaction along the accelerator beam (z axis). The distribution of the reconstructed events is normalized to have matching number of events in the nominal interaction point

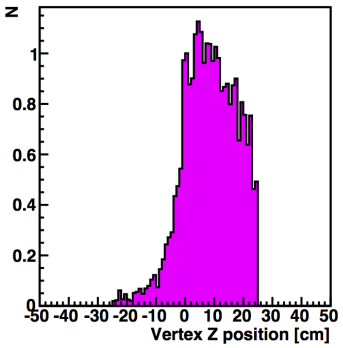

Figure 6.2.15: Acceptance relative to the acceptance in the nominal interaction point

For each position along the accelerator beam, the number of reconstructed events was divided by the number of events generated at this position. The distribution was then normalized to the height of the peak in the experimental data. The result is shown in Figure 6.2.14. To check the acceptance along the beam in respect to the acceptance in the nominal vertex, the distribution for accepted events was divided by the distribution for generated events. The result is shown in Figure 6.2.15.

The study shows that the test reaction is less sensitive to the upstream rest-gas than to the downstream rest gas.

6.3. Simulations of the influence of rest-gas events

6.3.1. Simulation parameters

The settings of the Wasa Monte Carlo influencing the interaction vertex position are listed in Table 6.3.1. The parameters are based on previous studies. The shape of the rest gas distribution is in agreement with vacuum calculations, see *e.g.* Reference [36].

Table 6.3.1: Parameters of the vertex in WMC simulations

Pellet stream	density distribution	rectangular
	sigma	1.1 mm
Accelerator beam	density distribution	Gaussian
	sigma	2.1 mm
Rest-gas	density distribution in XY	Gaussian
	sigma in XY	8 mm
	density distribution in Z	Gaussian
	upstream-downstream asymmetry in Z	0.36 (upstream)
	sigma in Z upstream	200 mm
	range in Z upstream	250 mm
	sigma in Z downstream	300 mm
	range in Z downstream	250 mm
	generated contribution	**varied (0%, 25%, 50%, 75%)**

The simulations were carried out for four values of the generated rest-gas contribution: 0%, 25%, 50% and 75%. Because of the decreasing acceptance away from the nominal interaction point, the fraction of rest-gas events among the reconstructed events is smaller and equals to 10% for 25% generated contribution, 23% for 50% generated contribution and 48% for 75% generated contribution. The reconstructed rest gas contributions are used as parameters in the further studies.

6.3.2. Investigated properties

A method was developed, based on the reconstructed theta angles of photons, to distinguish the events coming from the rest-gas.

The plots in Figure 6.3.1 show how the theta angles of the two photons are correlated. The angle of the higher energetic photon of

the pair is on the horizontal axis, and the angle of the lower energetic photon is on the vertical axis.

One can make separate Missing Mass / Invariant Mass plots for different ranges of the theta angle. Three ranges were chosen:

- A: 0-40 degrees
- B: 40-107 degrees
- C: 107-180 degrees

Figures 6.3.2 and 6.3.3 show the MM/IM plots for the different angular classes for the experimental data and WMC, respectively. Table 6.3.2 provides a handy visualization of the location of the classes with a given designation at the 3x3 plot sets.

The division into angular classes is the basis of the analysis method. If an event does not come from the nominal vertex point (0, 0, 0), the assumption of the track origin is incorrect and the reconstructed theta angle is incorrect. The classes AA and CC were chosen for the further studies since for these classes the influence of the rest-gas on the shape and position of missing mass and invariant mass distributions is the most visible.

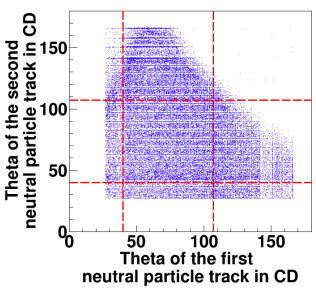

(a) WMC for 0% rest-gas contribution

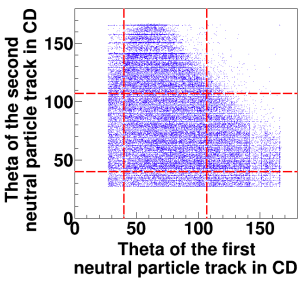

(b) WMC for 23% rest-gas contribution

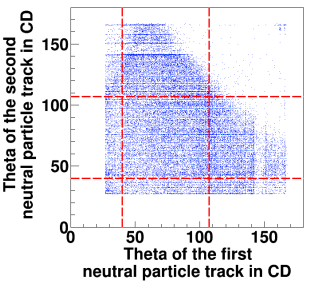

(c) Experimental data

Figure 6.3.1: Theta angle of low energy photon (first photon) versus theta angle of high energy photon (second photon) in an event

Table 6.3.2: Visual representation of angular classes used in the analysis. The first of the letters is the angle of high energy photon, and the second of the letters is the angle of the low energy photon. The angle ranges are the following: A: 0-40 degrees, B: 40-107 degrees and C: 107-180 degrees

AC	BC	CC
AB	BB	CB
AA	BA	CA

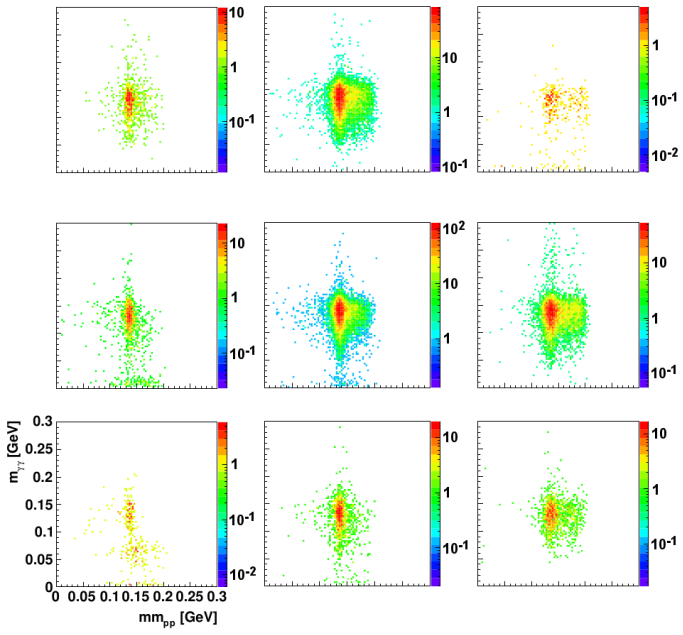

Figure 6.3.2: Missing mass of two protons (horizontal axis) and invariant mass of two photons (vertical axis) for different angular classes – experimental data

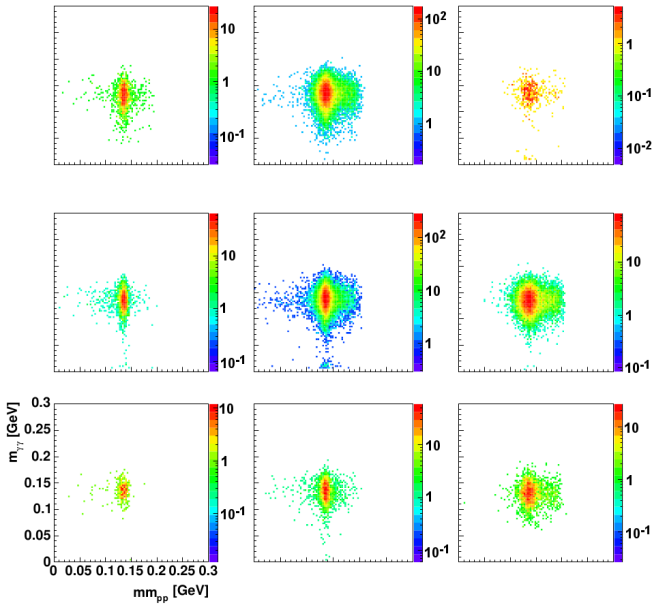

(a) 0% rest-gas contribution

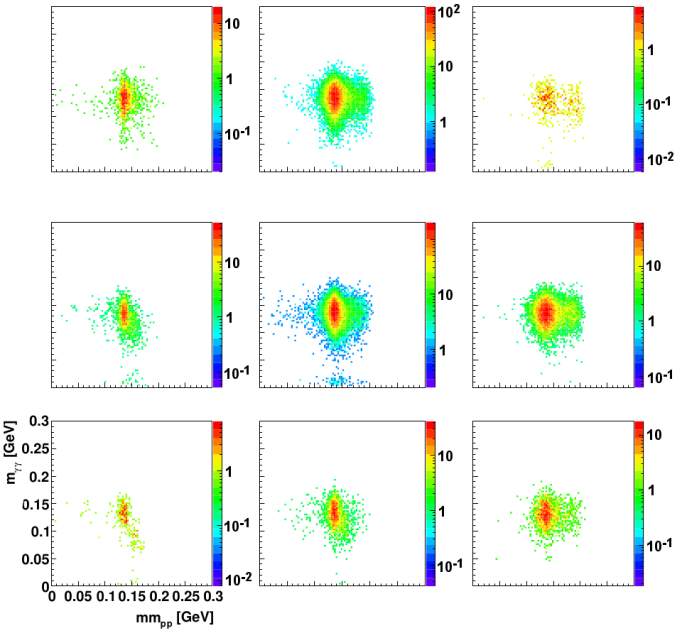

(b) 23% rest-gas contribution

Figure 6.3.3: Missing mass of two protons and invariant mass of two photons for different angular classes – WMC simulations

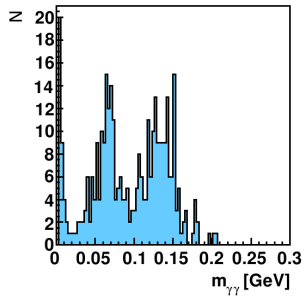

(a) Invariant mass, exp. data

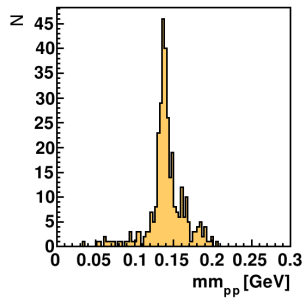

(b) Missing mass, exp. data

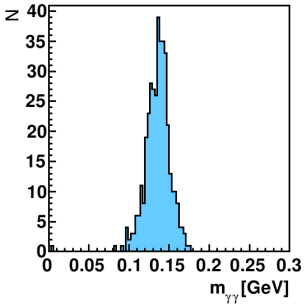

(c) Invariant mass, 0 % rest-gas WMC

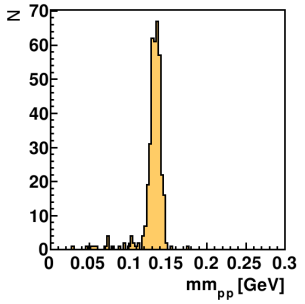

(d) Missing mass, 0 % rest-gas WMC

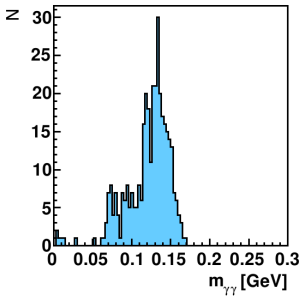

(e) Invariant mass, 23% rest-gas WMC

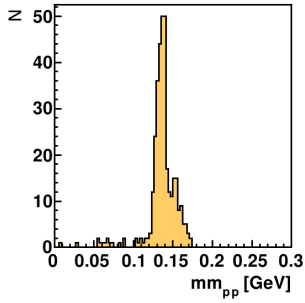

(f) Missing mass, 23% rest-gas WMC

Figure 6.3.4: Invariant mass of two photons and missing mass of two protons for the class AA for the experimental data and WMC with different rest-gas contributions

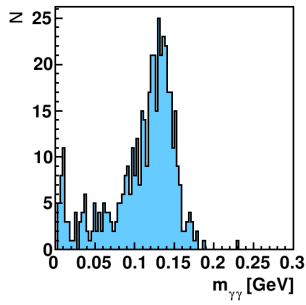

(a) Invariant mass, exp. data

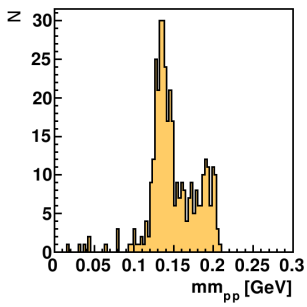

(b) Missing mass, exp. data

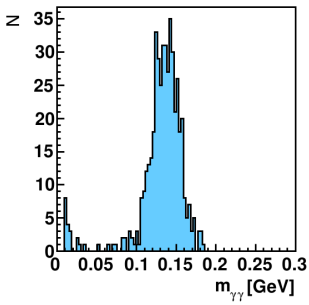

(c) Invariant mass, 0 % rest-gas WMC

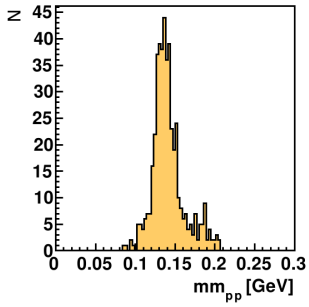

(d) Missing mass, 0 % rest-gas WMC

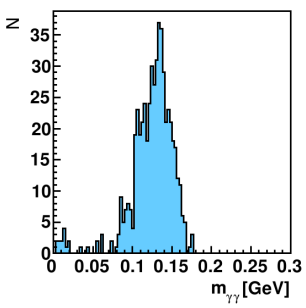

(e) Invariant mass, 23% rest-gas WMC

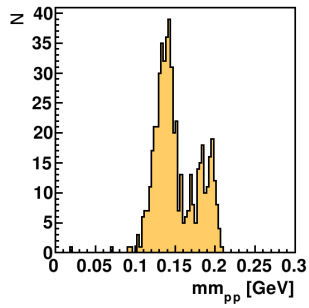

(f) Missing mass, 23% rest-gas WMC

Figure 6.3.5: Invariant mass of two photons and missing mass of two protons for the class CC for the experimental data and WMC with different rest-gas contributions

6.3.3. Differences between the experimental data and WMC

Separate plots of different properties were made for events in each angular class. The plots show missing mass, invariant mass, missing vs. invariant mass and also energy and theta and phi angles of high and low energy protons and photons. The plots for experimental data

and WMC are mostly in agreement and most of the structures in the plots are explained by the presence of events from rest-gas. However, some discrepancies exist in some variables, which cannot be explained by presence of the rest-gas. The differences are described below.

Invariant Mass: The differences in the invariant mass distributions are described below.

- Comparison of the experimental data to 0% rest-gas WMC:
  - Distinct structures for IM smaller than π^0 mass visible especially for angles AA, CC, AB and BA in the data. Some smaller differences are visible also for other angular classes.
- Comparison of the experimental data to 23% rest-gas WMC:
  - Similar differences as for 0% rest-gas WMC.

Figure 6.3.6 shows plots for example angular classes (AA and CC).

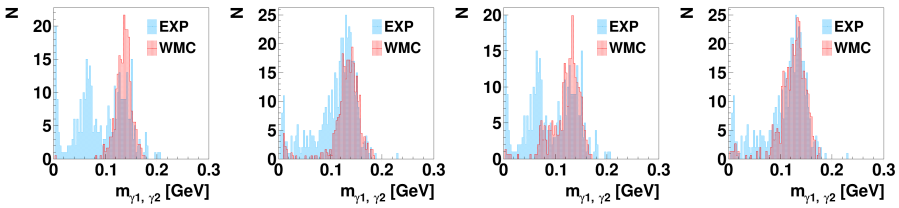

(a) Class AA and 0% r-g *(b) Class CC and 0% r-g* *(c) Class AA and 23% r-g* *(d) Class CC and 23% r-g*

Figure 6.3.6: Invariant mass distributions for the experimental data and WMC for different simulated rest-gas contributions and for different angular classes

Missing Mass: The differences in the missing mass distributions are described below.

- Comparison of the experimental data to 0% rest-gas WMC:
  - Additional structures neighboring the π^0 peak in the direction of higher mass present in the experimental data. These structures are visible especially for classes AA, CC and also for AC, BC, CB and CA (in some cases the WMC also have such structures, but they are more pronounced in the experimental data). Structures of this kind are also present at other angles, but there the difference between the experimental data and WMC is less distinct.

- Comparison of the experimental data to 23% rest-gas WMC:
  - The plots for the classes AA, CC and AC for the experimental data start to agree with WMC. The differences for other classes stay the same as for 0% rest-gas WMC.

Figure 6.3.7 shows plots for example angular classes (AA and CC).

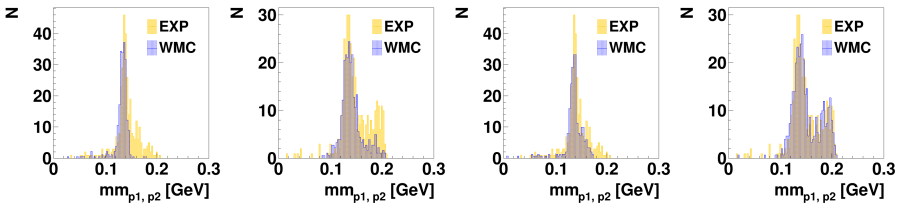

(a) Class AA and 0% r-g *(b) Class CC and 0% r-g* *(c) Class AA and 23% r-g* *(d) Class CC and 23% r-g*

Figure 6.3.7: Missing mass distributions for the experimental data and WMC for different simulated rest-gas contributions and for different angular classes

High Energy Photon Energy: The differences in the high energy photon energy distributions are described below.

- Comparison of the experimental data to 0% rest-gas WMC:
  - Structures in the direction of lower energy visible very clearly for the classes AA and AB in the data. They are also visible for the class BA. Tails in the direction of high and low energies are visible in the class CC. Also, a difference in distribution shape is observed for the class AC.
- Comparison of the experimental data to 23% rest-gas WMC:
  - Similar differences as for 0% rest-gas WMC.

Figure 6.3.8 shows plots for example angular classes (AA and CC).

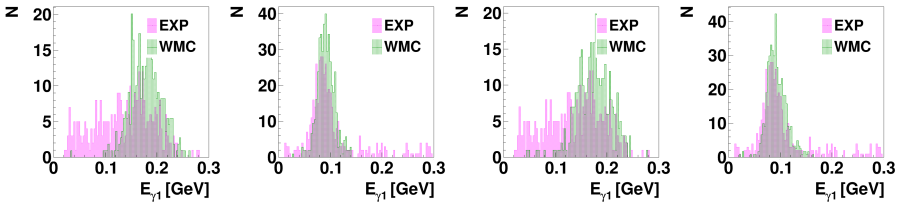

(a) Class AA and 0% r-g *(b) Class CC and 0% r-g* *(c) Class AA and 23% r-g* *(d) Class CC and 23% r-g*

Figure 6.3.8: High energy photon energy distributions for the experimental data and WMC for different simulated rest-gas contributions and for different angular classes

Low Energy Photon Energy: The differences in the low energy photon energy distributions are described below.

- Comparison of the experimental data to 0% rest-gas WMC:
  - Very distinct peak in the direction on low energies in classes AA and AB visible in the experimental data. In the class CC a small but clear additional peak is observed for lower energies, and a tail of single events is observed for higher energies.
- Comparison of the experimental data to 23% rest-gas WMC:
  - The distributions for the WMC change their shape slightly, becoming more similar to the experimental data, but the structures in classes AA, AB and CC are still clearly visible in the experimental data.

Figure 6.3.9 shows plots for example angular classes (AA and CC).

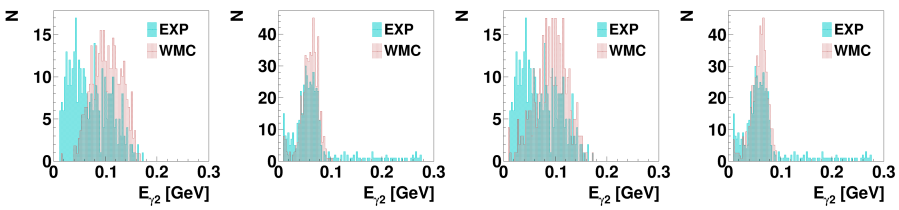

(a) Class AA and 0% r-g *(b) Class CC and 0% r-g* *(c) Class AA and 23% r-g* *(d) Class CC and 23% r-g*

Figure 6.3.9: Low energy photon energy distributions for the experimental data and WMC for different simulated rest-gas contributions and for different angular classes

High Energy Proton Energy: The differences in the high energy proton energy distributions are described below.

- Comparison of the experimental data to 0% rest-gas WMC:
  - Distinct tail in the direction of higher energy visible for the classes AA and AB in the experimental data (especially pronounced for the class AA).
  - The distribution for class CC is broader in the experimental data
  - An additional peak at ≈220 MeV, visible also in the experimental data for some classes, is higher in WMC for classes BC, BB and CA.
- Comparison of the experimental data to 23% rest-gas WMC:
  - The peak for class CC gets broader in WMC and is almost in agreement with the experimental data.
  - Additional structures appear in class AA in the direction of higher energy from the peak, but they are still much shorter and smaller than in the experimental data.
  - The difference of the small peak at 220 MeV stays the same as for 0% rest-gas.

Figure 6.3.10 shows plots for example angular classes (AA and CC).

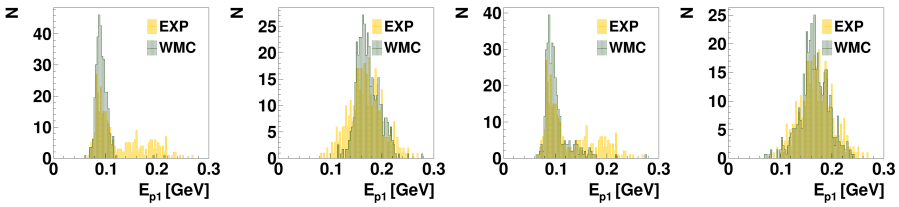

(a) Class AA and 0% r-g *(b) Class CC and 0% r-g* *(c) Class AA and 23% r-g* *(d) Class CC and 23% r-g*

Figure 6.3.10: High energy proton energy distributions for the experimental data and WMC for different simulated rest-gas contributions and for different angular classes

Low Energy Proton Energy: The differences in the low energy proton energy distributions are described below.

- Comparison of the experimental data to 0% rest-gas WMC:
  - Additional structures (tails) in the direction of higher energy from the peak, visible in classes AA and AB in the experimental data.
  - In the class CC, there are more events in the experimental data than in WMC in the low energy part of the distribution.

- Comparison of the experimental data to 23% rest-gas WMC:
  - The additional structures in classes AA and AB in the experimental data are still not explained by the WMC.
  - In the class CC, now there are more events in the experimental data than in WMC in the high energy part of the distribution.

Figure 6.3.11 shows plots for example angular classes (AA and CC).

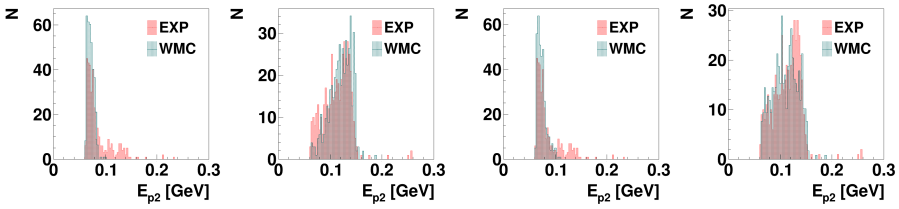

(a) Class AA and 0% r-g *(b) Class CC and 0% r-g* *(c) Class AA and 23% r-g* *(d) Class CC and 23% r-g*

Figure 6.3.11: Low energy proton energy distributions for the experimental data and WMC for different simulated rest-gas contributions and for different angular classes

High Energy Photon Theta: The differences in the high energy photon theta angle distributions are described below.

- Comparison of the experimental data to 0% rest-gas WMC:
  - Excess of the experimental data events in range $\approx 27 - 30$ degrees, observed for the classes AA, AB and AC.
  - Deficiency of the experimental data events in range $\approx 37 - 40$ degrees, observed for the class AA.
  - Additional peak in the range $\approx 160 - 170$ degrees, observed in the class CC in the experimental data.
- Comparison of the experimental data to 23% rest-gas WMC:
  - The described differences stay the same.

Figure 6.3.12 shows plots for example angular classes (AA and CC).

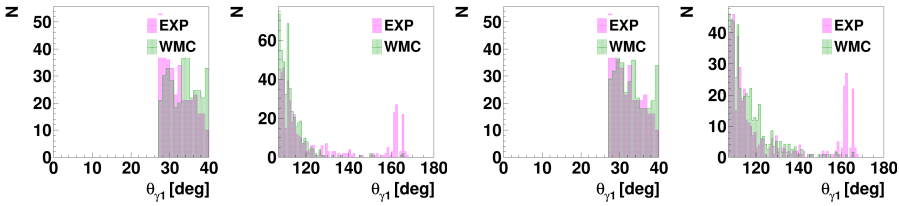

(a) Class AA and 0% r-g *(b) Class CC and 0% r-g* *(c) Class AA and 23% r-g* *(d) Class CC and 23% r-g*

Figure 6.3.12: High energy photon theta angle distributions for the experimental data and WMC for different simulated rest-gas contributions and for different angular classes

Low Energy Photon Theta: The differences in the low energy photon theta angle distributions are described below.

- Comparison of the experimental data to 0% rest-gas WMC:
  - Additional peak in the range $\approx 160 - 170$ degrees, observed in the class CC in the experimental data.
  - Excess of the experimental data events in range $\approx 27 - 28$ degrees, observed especially for the class AA, but also slightly for the classes BA and CA
  - Excess of the experimental data events in range $\approx 42 - 46$ degrees, observed for the class AB
- Comparison of the experimental data to 23% rest-gas WMC:
  - The described differences stay the same.

Figure 6.3.13 shows plots for example angular classes (AA and CC).

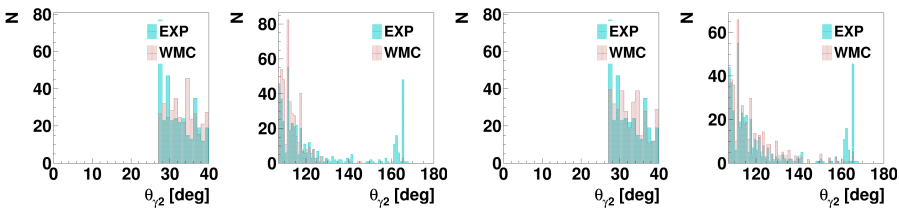

(a) Class AA and 0% r-g *(b) Class CC and 0% r-g* *(c) Class AA and 23% r-g* *(d) Class CC and 23% r-g*

Figure 6.3.13: Low energy photon theta angle distributions for the experimental data and WMC for different simulated rest-gas contributions and for different angular classes

High Energy Proton Theta: The differences in the high energy proton theta angle distributions are described below.

- Comparison of the experimental data to 0% rest-gas WMC:
  - The distribution is skewed towards lower angles for the class AA and towards higher angles for classes CC and CB in the experimental data.
- Comparison of the experimental data to 23% rest-gas WMC:
  - The difference in the distribution for the class CC is even clearer. Other classes do not change clearly.

Figure 6.3.14 shows plots for example angular classes (AA and CC).

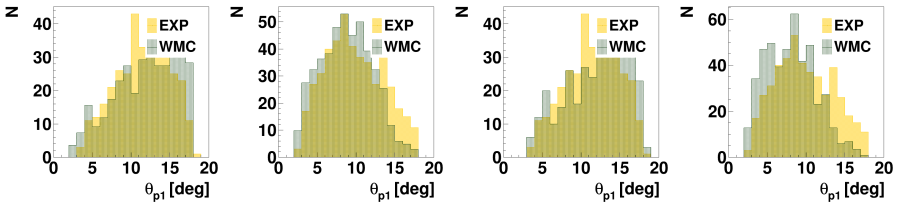

(a) Class AA and 0% r-g *(b) Class CC and 0% r-g* *(c) Class AA and 23% r-g* *(d) Class CC and 23% r-g*

Figure 6.3.14: High energy proton theta angle distributions for the experimental data and WMC for different simulated rest-gas contributions and for different angular classes

Low Energy Proton Theta: The differences in the low energy proton theta angle distributions are described below.

- Comparison of the experimental data to 0% rest-gas WMC:
  - For the case CC in the experimental data, the distribution has additional peaks around 5 and 17 degrees.
- Comparison of the experimental data to 23% rest-gas WMC:
  - For the class CC, the distributions become to agree in the low angle part, but the peak in the experimental data in the higher angle part is still not explained by the WMC.

Figure 6.3.15 shows plots for example angular classes (AA and CC).

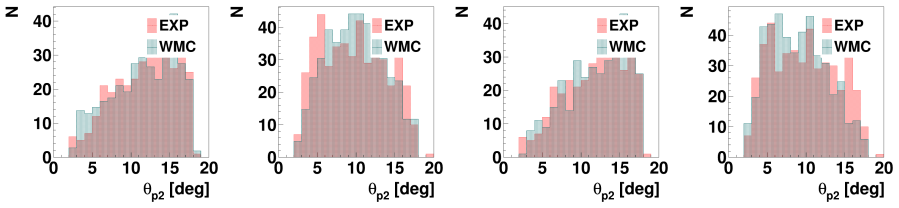

(a) Class AA and 0% r-g *(b) Class CC and 0% r-g* *(c) Class AA and 23% r-g* *(d) Class CC and 23% r-g*

Figure 6.3.15: Low energy proton theta angle distributions for the experimental data and WMC for different simulated rest-gas contributions and for different angular classes

Gamma and Proton Phi: No clear difference between the experimental data and WMC is observed.

A cut was made to select only events from the region in which the discrepancy between the experimental data and WMC is the biggest. Events coming from classes AA, AB and BA, with $\gamma\gamma$ invariant mass less than 80 MeV were selected. This allowed to check different properties of the problematic events. However, it was found, that those events have the same distribution as the rest of events. The following distributions were checked:

- Energy deposits in Forward Detector: (1) energy deposited in FRH2 versus energy deposited in FRH1 and (2) energy deposited in all FRH layers versus energy deposited in FRH1, separately for high and low energy protons.
- Kinetic energy versus theta angle, separately for high and low energy protons.
- Time differences: (1) time difference between charged particle tracks, (2) time difference between neutral particle tracks and (3) time difference between mean charged particle tracks time and mean neutral particle tracks time.
- Opening angle between the neutral clusters

Taking into account the experimental conditions and kinematical considerations it can be concluded that the background events not reproduced by the rest gas contribution most probably come from the interactions of accelerator beam halo with beam pipe walls as well as from event pile-ups.

6.4. Elastic triggers

6.4.1. Trigger conditions

Two triggers in WASA are called elastic triggers. The conditions of these triggers are designed to make them especially sensitive to the events from the elastic scattering.

The triggers are numbered as trigger 17 and trigger 21. The trigger 17 requires a correlation between the forward part of the Plastic Scintillator Barrel (PSF) and the central part of the Barrel (PSC). The trigger 21 requires a correlation between the first layer of the Forward Range Hodoscope (FRH1) and the central part of the Plastic Scintillator Barrel (PSC) (Figure 6.4.1).

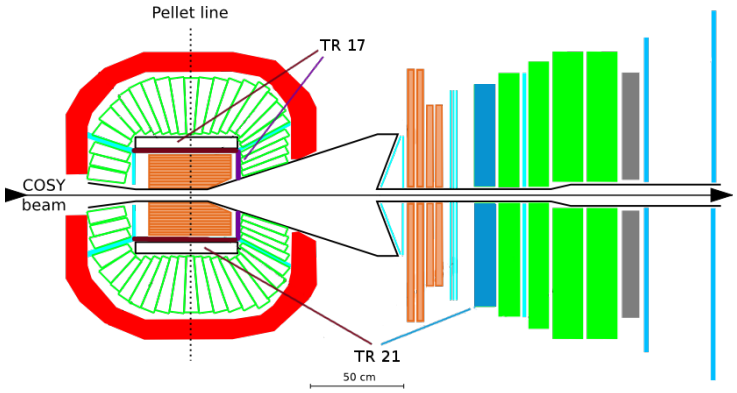

Figure 6.4.1: Detectors used in the condition of the elastic triggers

All these detector parts are sensitive to charged particles and their location makes the triggers sensitive to particles with opening angle close to 90°, thus making them simple and functional conditions selecting elastic scattering events (assuming that the particles originated from the nominal interaction point).

6.4.2. Elastic triggers acceptance

A simulation study was made to check the fraction of elastic scattering events accepted by the elastic triggers, depending on the position of the interaction point.

Conditions reproducing the TR17 and TR21 were implemented in the analysis. For each position along the accelerator beam, the number of events accepted by the trigger was divided by the number of events generated at this position. Then the distribution was normalized to the height of the peak in the experimental data. The result is shown in Figure 6.4.2. To check the acceptance along the beam in respect to the

acceptance in the nominal vertex, the distribution for accepted events was divided by the distribution for generated events. The result is shown in Figure 6.4.3.

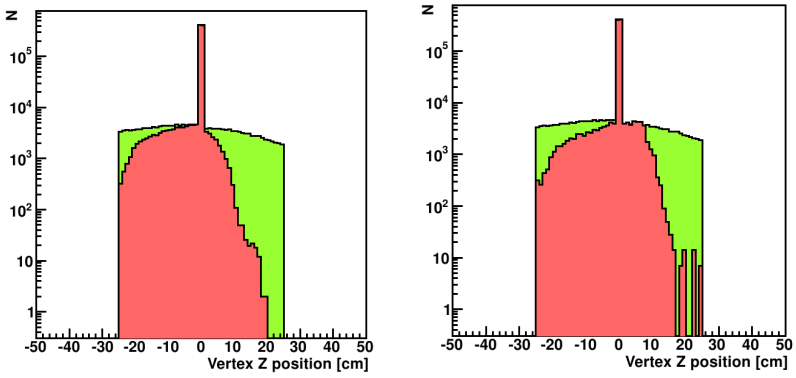

(a) Trigger 17 *(b) Trigger 21*

Figure 6.4.2: Distributions of generated (green) and reconstructed (red) elastic scattering events. The distribution of the reconstructed events is normalized to have matching number of events in the nominal interaction point

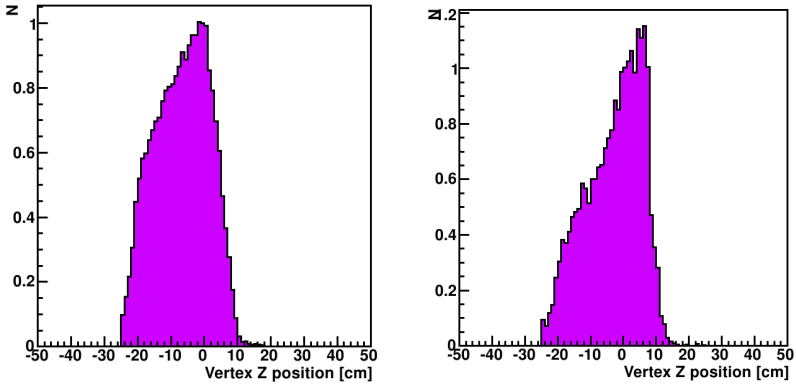

(a) Trigger 17 *(b) Trigger 21*

Figure 6.4.3: Acceptance of the elastic scattering events by the elastic triggers, relative to the acceptance in the nominal interaction point

It can be seen that the acceptance of the elastic triggers is the highest close to the nominal interaction region. It is also visible that the elastic triggers are less sensitive to the downstream rest-gas than to the upstream rest gas. As it was shown it the Section 6.2.6, the acceptance

of the test reaction decreases quicker in the opposite direction. This makes the probability to simultaneously record a test reaction event and an elastic trigger event to be the highest close the nominal interaction region. It makes the rate of elastic triggers a relatively good tool for separating events from nominal interaction region from events which occur in different places along the accelerator beam.

In the further analysis only the trigger 17 is used, because the maximum acceptance of the TR21 is not at the pellet stream position, but is shifted downstream. The TR17 also provides higher event rate.

6.5. Long Range TDC spectra

6.5.1. The Long Range TDC

A TDC (Time to Digital Converter) is a device which records the time of an input signal in a digital format. The so-called Long Range TDC is a kind of TDC able to record signals over a long time scale. For the experimental data being used, the LR TDC continuously saved the time of events during almost 1000 s with resolution of about 0.1 ns.

In this experiment the LR TDC was recording the times of two elastic triggers. All trigger signals were taken into account, independently on any prescaling present in the regular experimental DAQ.

The LR TDC was operated in synchronization with the regular experimental DAQ so that the times of WASA events (events stored by the regular DAQ) and times of the elastic triggers were recorded by the LR TDC in the same time frame. Also, the unique identification number of each WASA event was stored by the LR TDC readout system together with the TDC time. These features allow to check what was the situation in the beam (based on the LR TDC spectra) in the moment when a given WASA event took place.

Figure 6.5.1 shows a spectrum of the TR17. The plot shows the number of events recorded in time bins of 25 μs duration. The structures visible in the spectrum correspond to passage of pellets through the beam, which takes about 70 μs. The structures are also in agreement with a pellet rate of 5 – 10 k/s, as given by the Photo Multiplier Tube pellet counter installed at WASA. The results agree also with previous studies that have shown that the probability of no pellet in a 5 mm high interaction region is 71% for a pellet rate 5 k/s, 51% for a pellet rate 10 k/s and 32% for a pellet rate 15 k/s, corresponding to stochastic distribution [30].

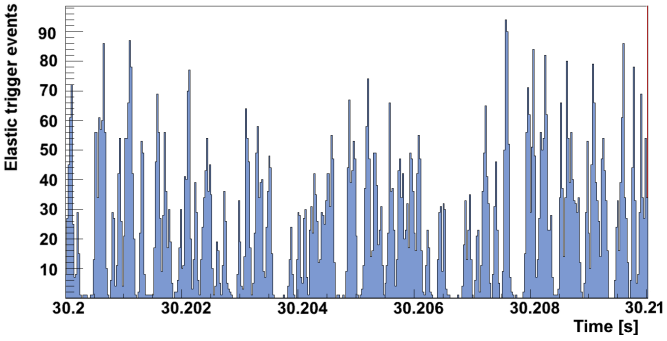

Figure 6.5.1: Example plot of the experimental LR TDC spectrum

6.5.2. Simulations of LR TDC spectra

A procedure of simulating the LR TDC operation was developed in order to understand the spectra.

Simulation procedure description

Basis

Beam shape

The accelerator beam is assumed to have elliptic XY cross-section with X and Y dimensions and density described by a two-dimensional Gaussian function. The parameters in each direction are the sigma and a cutoff value and the function is normalized to 1. The cutoff value tells the radius outside which the function is set to 0. The beam is along Z axis. The density of the beam is a primary parameter to calculate the probability of pellet-beam interaction.

Pellet size

The pellet size is neglected and pellets are treated as points. This is justified since a pellet is much smaller than the accelerator beam diameter.

Pellet path inside the beam

A vertical path of pellets through the beam is assumed due to the small pellet stream divergence (≈1 mrad).

Time binning

The procedure is based on a time binning and it is simulated how many interactions each pellet had during its passage through the beam in time bins.

Probability of interaction

The average number of interactions with a pellet during the time bin $n_{int,bin}$, is based on the beam density $\rho_{beam,bin}$ at the path passed during

this time bin and on an empirical scaling parameter s:

$$n_{int,bin} = \rho_{beam,bin} \cdot s.$$

The value of the scaling parameter is determined based on the required average event rate. The parameter combines various physical properties and effects: target thickness, number of particles in the beam, cross section for the interaction, detector acceptance, etc. The beam density is the average density in a section of the beam corresponding to the pellet position during a given time bin.

Definition of pellet being inside the beam

The beam may have a large diameter, but its density far from the center may be very small. For this reason, an additional value of the beam size is used for counting the number of pellets in the beam, which may be equal or smaller than the cutoff value of the beam density distribution.

Simulations procedure

Events from pellets

The procedure of simulations is the following:

- The pellet X position at the beam center is calculated and used as X coordinate of the pellet path inside the beam.
- Y coordinates of positions of pellet entering and leaving the beam are calculated based on the shape of the beam boundaries and the pellet X position. The time when pellet enters and leaves the beam is also calculated.
- The time, counted continuously from the beginning of the sample, is divided into bins of a given size. It is checked within which bins the pellet passage inside the beam took place.
- Pellet Y position for the boundaries of the time bins is calculated.
- Calculation of the mean beam density in the path passed by the pellet inside each time bin is done.
- This information together with the scaling parameter gives the average number of events.
- Events which occurred in a given time bin are generated according to Poisson distribution.
- This procedure is repeated for each pellet so the time bins contain the number of events summed from all pellets.

Events from background

For each time bin events from background are also simulated. The average number of these events during one time bin is calculated based on a given signal/background ratio.

Results

Table 6.5.1 lists the values of the most important parameters.

The beam density profile is shown in Figure 6.5.2. Figure 6.5.3 shows example event rate spectra and number of pellets in the beam for the simulated conditions. From this, one can judge that the pellet rate in the experimental sample (see Figure 6.5.1) is ≈8 k/s. Figure 6.5.4 shows the correlation between the number of events and the number of pellets in the beam at a certain time. Although it is not possible to unambiguously tell the number of pellets based on the event rate, the plots allow to select a range for which the probability for a certain beam occupancy is the highest.

Table 6.5.1: Parameters for the pellet – accelerator beam interaction simulations

Beam density	distribution	Gaussian
	center X	0.0 mm
	sigma X	2.1 mm
	range X	from -4.2 mm to 4.2 mm
	center Y	0.0 mm
	sigma Y	2.1 mm
	range Y	from -4.2 mm to 4.2 mm
Radius for determination of the number of pellets in the beam region	in X	2.5 mm
	in Y	2.5 mm
Time bin size		25 μm
Pellet generation frequency		64 kHz
Distance from VIC to the interaction region		2680 mm
Skimmer	position	700 mm below VIC
	diameter	1 mm
	pellet stream divergence	0.75 mrad
	loss at skimmer	65%
Additional pellet loss		82% or 64% (varied)
Effective pellet rate		4 k/s or 8 k/s (depending on the additional pellet loss)
Fraction of events from the background		0%
Event rate		950 k/s

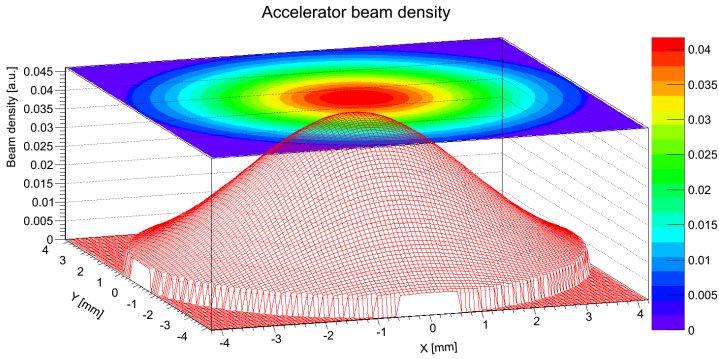

Figure 6.5.2: Accelerator beam density profile (in XY plane)

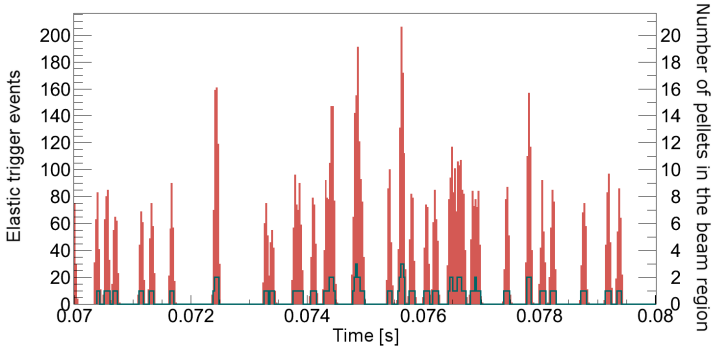

(a) Pellet rate 4 k/s

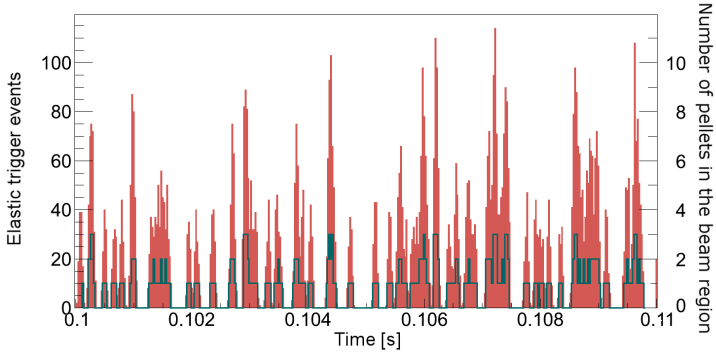

(b) Pellet rate 8 k/s

Figure 6.5.3: Simulations of time spectra of pellet-beam interactions for pellet rates 4 k/s and 8 k/s during 0.01 s. The superimposed dark green line indicates the number of pellets present in the beam region at given moment

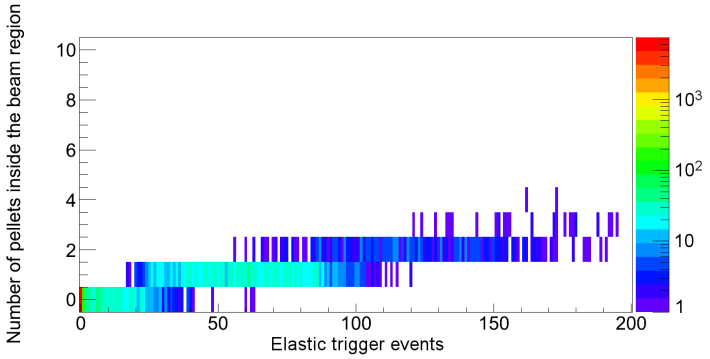

(a) Pellet rate 4 k/s

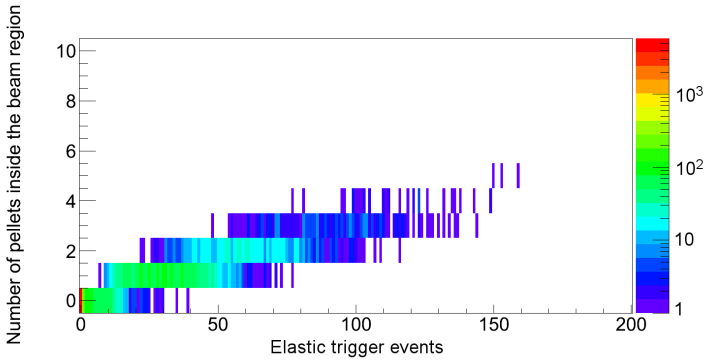

(b) Pellet rate 8 k/s

Figure 6.5.4: Correlation between the number of events in one time bin and number of pellets in the beam region at this time

6.6. Event classification of the experimental data

6.6.1. Classification method

The aim of this study is to separate the analyzed hadronic events between the events coming from pellets and events coming from non-pellet background. The classification will be based on the instantaneous rate of elastic trigger at the time of a given hadronic event.

For each WASA event the number of LR TDC events in corresponding time bin is checked. Based on this the WASA events are assigned to one of two *LR TDC classes*. They correspond to a certain number of LR TDC events in a 25 μs time bin. The following values provide the clearest event separation:

- **Non-pellet class** (N-P-class): 0 – 20 LR TDC events,
- **Pellet class** (P-class): 21 or more LR TDC events.

The mentioned ranges are, however, used only at the beginning of the accelerator cycle.

One accelerator cycle has a period of 60 s, and for 50 s the beam is present. During this 50 s interval, the event rate drops approx. two times, due to the decrease of the beam intensity. A correction for this effect is applied by adjusting the ranges of each pellet class. For example, at the moment when the beam appears, the non-pellet class corresponds to the range 0-20 LR TDC events, and after 50 seconds it corresponds to the range 0-10 LR TDC events. The pellet class is adjusted correspondingly.

An example LR TDC spectrum with the classification applied is shown in Figure 6.6.1 below.

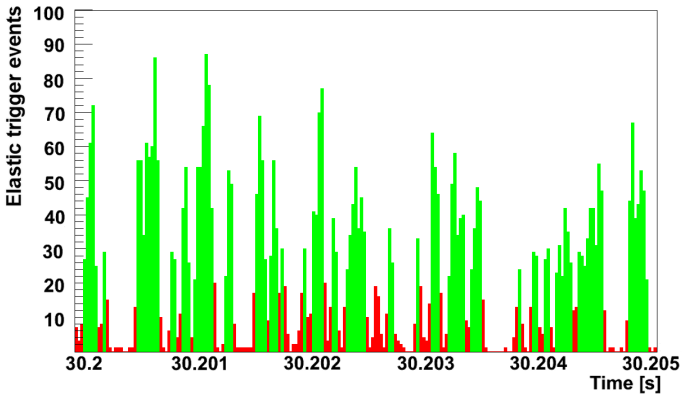

Figure 6.6.1: Example of a LR TDC spectrum with classification of pellet and non-pellet periods. Green - pellet expected in the beam region, red - no pellet expected in the beam region

6.6.2. Results of the LR TDC "tracking"

Figure 6.6.2 shows a comparison between missing and invariant masses in the experimental data for the two classes. Plots in Figure 6.6.3 and 6.6.4 show a comparison between the experimental data and WMC. The whole experimental data sample is compared to WMC with 23% reconstructed (50% generated) rest-gas contribution. The non-pellet class in the experimental data is compared to WMC with 48% reconstructed (75% generated) rest-gas. That the contribution of the generated rest-gas is smaller than 100% is reasonable since it is possible that a pellet was in the beam region even if the LR TDC rate was small. The pellet class in the experimental data is compared to WMC with 10% reconstructed (25% generated) rest-gas contribution. This value was chosen, because for the estimated pellet rate during the experimental run (≈8 k/s), is

a pellet in the beam region approx. 50% of the time. Assuming 50% contribution of events coming from rest-gas, half of them, *i.e.* 25%, took place when a pellet was in the beam region.

Two angular classes, AA and CC, were chosen because these classes give the highest possibility to distinguish between rest-gas and pellet events (see Section 6.3.2). The plots were normalized to obtain the same number of entries as in the angular class BB.

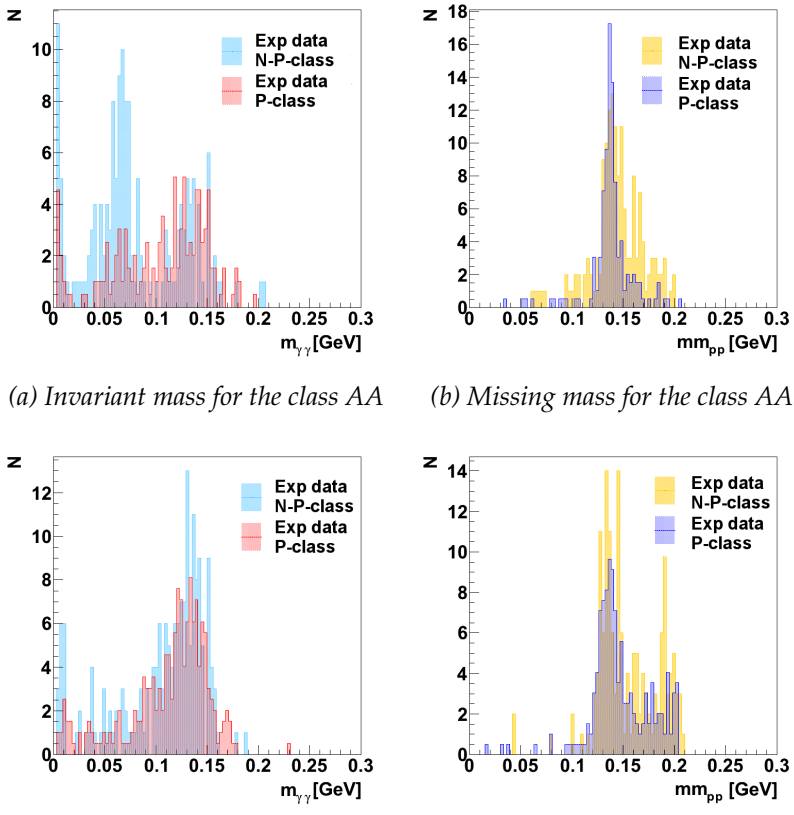

(a) Invariant mass for the class AA *(b) Missing mass for the class AA*

(c) Invariant mass for the class CC *(d) Missing mass for the class CC*

Figure 6.6.2: Effect of event classification in angular class AA and CC (see Section 6.3.2) in the experimental data for the invariant mass of two photons (left) and missing mass of two protons (right)

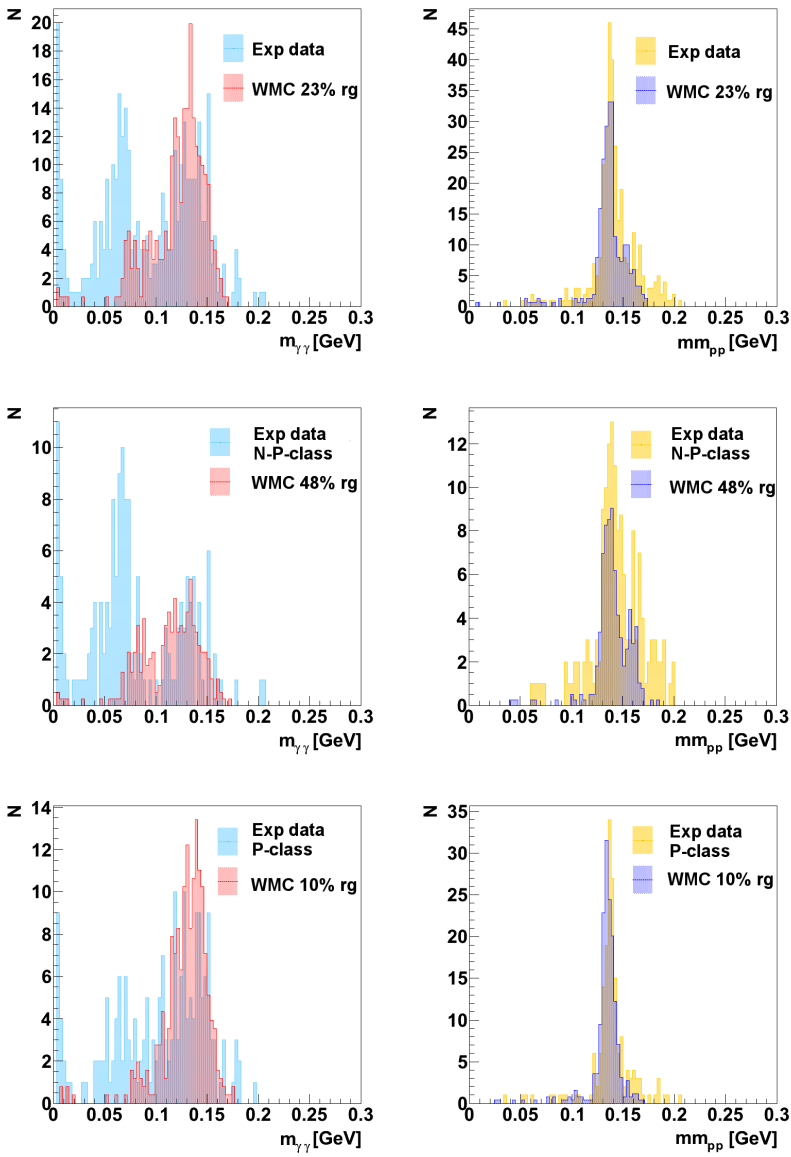

Figure 6.6.3: Effect of event classification in angular class AA. Invariant mass (left column) and missing mass (right column). Different experimental data classes are compared with simulations with different rest-gas contribution

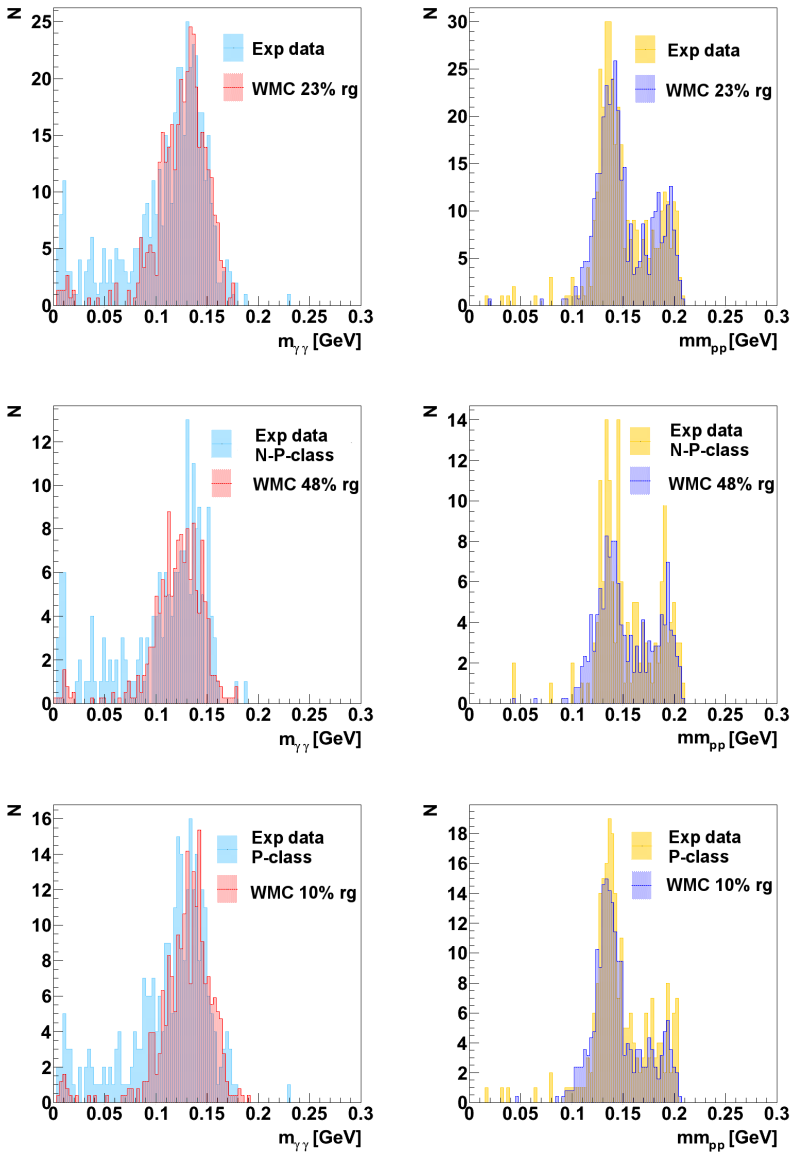

Figure 6.6.4: Effect of event classification in angular class CC. Invariant mass (left column) and missing mass (right column). Different experimental data classes are compared with simulations with different rest-gas contribution

The non-pellet LR TDC class is expected to mainly contain the events from non-pellet background, and the pellet LR TDC class is expected to mainly contain good pellet events which occurred in the nominal interaction region. The most clear difference between the data for the two classes is observed in the MM plots for the angular class AA.

For the non-pellet class, the peak at a position of π^0 mass is relatively small, compared to additional peaks at ≈70 MeV and 10 MeV. On the other hand, for the pellet class, the peak at π^0 mass is clearly the highest one, and the additional peaks are reduced.

Differences between the non-pellet and pellet classes are also visible in IM plots for the angular class AA, where the peak corresponding to π^0 mass is much broader for the non-pellet class, compared to the pellet class.

The differences between the two classes in the experimental data are clear. The separation is also visible when comparing the two classes to WMC simulations with suitable rest-gas contributions. The pellet class is in good agreement with low rest-gas WMC and the high rest-gas simulations reproduce the rest-gas contribution in the non-pellet class. Additional structures not reproduced in simulations are also visible in this class for the angular class AA: the peaks at 10 MeV and 70 MeV. They most probably come from the interactions of accelerator beam halo with beam pipe walls as well as from event pile-ups.

6.7. Summary – implementation of pellet tracking

One of the advantages offered by the pellet tracking system is the possibility to reject events which did not occur in the nominal interaction region. At WASA, this feature could be tested by using information about instantaneous rate of the hadronic events by analyzing the rate of an "elastic" trigger.

An increased elastic trigger rate indicates that there was a pellet in the interaction region. Knowing that the probability of an interaction with a pellet is much higher than the probability of interaction with the rest-gas, there is high probability that events recorded at that time originated in a pellet.

On the other hand, when an event was recorded when the elastic trigger rate was small, the event most probably did not come from a pellet.

The study shows that the mentioned method is indeed able to provide a distinction between pellet and non-pellet events.

The results are only quantitative due to the small statistics. Although the evaluation does not provide a sharp distinction between the two classes of events, the possibility of distinguishing the events is evident.

Besides showing the possibility of separating pellet-events and non-pellet events at WASA, the study demonstrates the feasibility of analysis of the hadronic events data together with the data from another system that similarly to the pellet tracking is operating in much longer time scale.

Chapter 7

Summary, conclusions and outlook

This chapter gives a summary and conclusions of the results presented in Chapters 2 – 6. An outlook for further studies is presented.

7.1. Summary and conclusions

Pellet detection conditions

Pellet detection conditions were studied at the UPTS (Uppsala Pellet Test Station) to find the best possible conditions to be used in the pellet tracking system. Various illumination options were checked, including use of different lasers and different illumination angles, in respect to the camera. Lasers providing a light beam of size 50 μm x 16 mm at the pellet stream position were chosen. For illumination with one laser, the angle 135 degrees with respect to the camera was chosen as the best of all checked – it was shown that pellets provide three times better refraction than reflection of light. Cameras with optics f = 50 mm, providing field of view of 40 μm x 20 mm x 5 mm (DOF, depth-of-field) at the working distance were chosen. Also, optics f=25 mm, offering field of view of 80 μm x 40 mm x 10 mm (DOF) were tested and found suitable for usage in lower tracking section. The cameras were successfully operated with a cycle of 12.5 μs period and 10 μs exposure times (shortest cycle allowing for stable operation). Spatial detection resolution was approx. 40 μm for 50 mm optics and 80 μm for 25 mm optics. The detection conditions provide detection efficiency >90% (camera dead time not taken into consideration).

Conclusions The detection efficiency together with the obtained time and position resolutions are sufficient for the purpose of pellet tracking.

Pellet stream The pellet stream parameters were investigated. Measurements at single levels as well as correlations between measurements at different levels were carried out. Values of various pellet stream parameters were measured. The pellet stream divergence was found to be approx. 0.7-1 mrad. The mean pellet velocity is 70-80 m/s and the relative velocity spread in the stream is approx. 0.5-1% (σ_v/v).
Conclusions The pellet stream parameters are suitable for pellet tracking and the obtained values are used in the simulations for development of the tracking system.

Design simulations

The studies of pellet detection conditions and pellet stream parameter provided the necessary input for development of simulation software reproducing experiments with pellets. This software was then used for making design simulations for the pellet tracking system for PANDA. Realistic pellet stream and detection conditions from UPTS experiments and physical constraints from PANDA were used. The simulations aimed to obtain predicted efficiency and resolution of the tracking system. For this purpose, two versions of track reconstruction algorithm were developed: a fast algorithm, quickly reconstructing pellet tracks, enabling first approach to the data analysis and possible to be used in online analysis, and an advanced algorithm, providing very high efficiency of pellet track reconstruction required in the final analysis.
Conclusions The study showed that it is possible to have correct information from pellet tracking for 80-90% of pellets, assuming realistic pellet stream and detection conditions. This means that 80-90% of "good" events (originating from pellets), will have information about vertex position from the tracking, and most of the background events will be rejected. The pellet position resolution from the tracking is predicted to be <100 μm (sigma) in all directions, giving high precision information for particle tracks fitting.

Pellet track processing

After reconstruction of the pellet tracks, the information from the tracking will be used in the data analysis. The number of pellets in the beam region at a time of hadronic event will be known, along with position of these pellets.
Conclusions The information from pellet tracking can be used in background events rejection and to provide the vertex position in particle the track fitting.

Usage of Long Range TDC information in data analysis

The ideal situation would be to test the pellet tracking system operation at a working particle detector system. Such tests were not possible, however, it was possible to conduct another kind of study, giving valuable input as concerns the studies on the pellet tracking system.

One information given by the tracking system is the number of pellets in the beam region at a given moment. This enables rejection of events which occurred when the system predicts no pellets in the beam region. These events can be assumed to be a background not originating in the nominal interaction region.

This kind of event rejection, based on Long Range TDC information, was studied at WASA. The LR TDC was recording times of WASA elastic trigger signals, and a classification procedure was used based on the instantaneous trigger rate. This was based on the fact, that the presence of pellet in the beam region causes an increase of the instantaneous trigger rate.

LR TDC data was collected in synchronization with the normal experimental DAQ. A common time stamp and event number was written in both systems. This allowed analyzing separately events collected in "pellet" and "non-pellet" time periods. The results of this study clearly show that it is possible to perform such kind of event classification.
Conclusions The improvement of the quality of analyzed data by rejecting events not coming from the nominal interaction region was shown. Moreover, the work with Long Range TDC data gave an experience in working with another system operated in synchronization with normal experimental DAQ. (The LR TDC information was used in time scale similar to real pellet tracking, which is much longer, ca. 1000x, than for the normal DAQ).

7.2. Outlook

Pellet detection conditions

A very important step for the improvement of pellet detection conditions is the implementation of a shifted cycle camera operation. This means installing two cameras at each level, mounted opposite to each other. The cycle of the cameras will be shifted approx. half of the period. This will eliminate the inefficiency caused by the camera dead time, because at any moment at least one camera will be in the exposure time, ready to detect pellets. This mode of operation will also improve the time resolution 3-4 times. This will be possible by checking which camera observed the pellet and in which cycle. To make operation in this mode possible it is necessary to conduct experiments and develop a reliable method of using the information from two cameras.

Another important step is to investigate a possibility of using faster

cameras for pellet detection. These cameras, with a cycle two times faster than in the currently operated ones, are now commercially available. Usage of these cameras would improve resolution in vertical direction and time. This would be especially important for pellets detected only in the upper tracking section.

Usage of more powerful lasers is also planned. This will improve the illumination conditions which are especially important in the lower section, where a wide illumination angle is necessary. More powerful lasers will also reduce the necessity of precise focusing.

A very important task is to design and produce mechanical mounting system offering rigid construction and possibility of precise and stable adjustments. It should hold together the cameras and lasers allowing for their adjustments, and then the full holder can be mounted at the measurement level without loss of the alignment.

A crucial step in development of the pellet tracking is building of a new dedicated readout system, based on FPGA electronics. Such a system, being currently tested, will replace the frame grabber connected to PC computer, being used so far. The FPGA readout will provide a speed necessary to process images from many cameras and save information about pellets position and time.

Tracking system design

In the current simulations all pellet loss takes place before first measurement level and the number of survived pellets is constant at all measurement levels and in the interaction region. Even if additional losses are expected to be small, a study should be done to check performance of the system with pellet loss along all the way.

Also the effect of gravity is currently neglected in simulations of pellet behavior and track reconstruction. The tracking procedure should be checked with the presence of gravity.

The camera shifted cycle operation is now simulated simply, by using a shorter camera cycle without any dead time. For further studies it would be important to operate the simulations reproducing usage of doubled cameras operating with shifted cycle.

Interfacing the tracking system with data acquisition system and integration of pellet tracking information with data analysis chain

It will be necessary to develop a low-level integration between the tracking system and experimental DAQ. This will require development of suitable firmware for FPGA electronics of the DAQ. Also the format and structure of the pellet tracking information written in the data stream needs to be developed. An implementation of the pellet tracking information into the PANDA data analysis software needs to be done.

Chapter 8

Summary in English

The subject of the thesis is the development of a target device allowing an increase of the quality of the data in accelerator based hadron physics experiments studying fundamental properties of matter.

Introduction to the scientific field

The elementary particles from which all visible matter is built are *leptons* and *quarks*. The most known lepton is the *electron*. It is also the lightest of the charged leptons, which also includes the *muon* and the *tauon*. Of these, only the electron is stable. The other two decay within a small fraction of a second after their creation in high energy interactions. Each of the charged leptons has its neutral lepton partner, a *neutrino* – there exist the electron neutrino, the muon neutrino and the tauon neutrino. The quarks are another group of charged elementary particles. The two lightest of them are called *up* and *down*. The nucleons – protons and neutrons – forming atomic nuclei, are composed of these quarks. The other four quarks are called *charm*, *strange*, *top* and *bottom*. Particles composed of these quarks can be created in collisions of highly energetic particles. Each of the mentioned leptons and quarks exist as "normal" particles and as anti-particles.

Quarks do not exist separately but only bound into *hadrons*. *Baryons* are hadrons consisting of three constituent quarks. The most commonly known baryons are protons and neutrons. Hadrons consisting of a quark and an antiquark are called *mesons*. Examples of them are *pions* and *eta* mesons. Many different baryons and mesons exist. Studying them is a subject of hadron physics. The proton is the only stable hadron. Neutrons are stable only inside of atomic nuclei.

All interactions taking place in nature can be reduced to four fundamental interactions: *gravitational*, *electromagnetic*, *strong* and *weak*. The interactions are mediated by force carriers. Exchange of these force car-

rier particles is observed on macroscopic scale as interactions between elements of a system. The force carriers, or *gauge bosons*, are the third group of elementary particles. The electromagnetic interaction is mediated by *photons* and the weak interaction is mediated by three bosons: W^+, W^- and Z^0. The strong force is carried by *gluons*. The existence of a force carrier for gravity (*graviton*) is still a subject for searches. While the gravitational and electromagnetic interactions act over potentially infinite distance, the strong and weak nuclear interactions act only on the subatomic scale.

The strong force keeps the quarks bound into hadrons. By analogy to charge in the electromagnetic interaction, the strong interaction is also said to involve a certain charge. In this case, there are three different variants of charge. By analogy to optics these charge variants are called with the names of the primary colors: red, green and blue. Similarly to normal charge being positive or negative, also in addition to positive red, green and blue charges, there exist negative anti-charges (anti-colors): anti-red, anti-green and anti-blue. Only color neutral objects can be observed which means that the colors of quarks in a hadron have to add up to what in the optics analogy would give a white color (*e.g.* red-green-blue or color-anticolor). It should be also noted, that a given color is not an intrinsic property of quarks. The colors are constantly changing by emission and absorption of gluons. In this way the strong interaction is mediated.

The strong interaction displays two peculiar properties: *color confinement* and *asymptotic freedom*. The asymptotic freedom means, that for small distances between quarks, smaller than the size of a nucleon, the interaction becomes very weak and quarks and gluons behave like non-interacting. To put it in other words, the *coupling constant* of the interactions becomes very weak. The color confinement means, that for bigger distances between quarks, the interaction between them becomes stronger (the coupling constant increases) which in turn leads to that isolated quarks cannot be observed. This is very different from the case of the electromagnetic interaction, where the force between the charges diminishes while taking the charges apart, allowing *e.g.* for the negatively charged electrons in the atom to be unbound from the positively charged nucleus. In the case of the strong force, the separation of quarks to bigger distances requires more and more energy. At some point this energy is big enough to create quark-antiquark pairs that form new hadrons with the quarks originally being separated.

A theory called *Quantum Chromo Dynamics* (QCD) has been developed to describe the properties of strong interaction. It is a part of a set of theories called the *Standard Model* of particle physics, summarizing our current knowledge about the particles and interactions present in the universe. Foundations for QCD have been laid 50 or so years

ago and application of the theory is being constantly developed and improved ever since.

In the high energy regime, which corresponds to small distances between quarks and thus a weak coupling constant, the description of the strong force is easier because it is possible to use a *perturbative approach*. In this approach, the complicated system is described in terms of a simpler system with an addition of a small disturbance (perturbation).

More problematic is the QCD in the low energy regime implying a strong coupling constant. In these conditions it is not possible to use the perturbative approach. This region is still the least known and new measurements are especially needed.

Physics with the PANDA experiment

A valuable input to understanding of the properties of hadrons and the strong interaction will be given by the new PANDA experiment which will be located at the GSI research center in Darmstadt, Germany. PANDA will be operated at the HESR accelerator (High Energy Storage Ring) providing anti-proton beams with momenta of 1.5 – 15 GeV/c. The target material will be mainly hydrogen (protons) but it will be also possible to use heavier gases. HESR is equipped with electron and stochastic cooling of the beam, which gives very well defined beam energy and allows measuring the masses and widths of hadronic resonances with accuracies of 50 – 100 keV. One of the advantages of colliding antiprotons with protons is that it makes possible formation of states of all quantum numbers. $\bar{p}p$ collisions will allow for hadron spectroscopy of charmonium, D mesons and strange and charmed baryons. Also, it will be possible to search for glueballs (particles consisting solely of gluons) and hybrids (consisting of quark, antiquark and excited glue). These states are allowed by QCD, but their existence has not been confirmed experimentally. At PANDA it will be possible to search for gluonic hadrons with masses above 2.5 GeV/c^2, where the density of conventional quark-antiquark states becomes smaller. Also a study of non-perturbative QCD dynamics will be possible in baryon-antibaryon interactions. Collisions of antiprotons with heavier nuclei will allow for study of $\Lambda\Lambda$ hypernuclei and hadrons in the nuclear medium.

Targets

Main target material in the PANDA experiment will be hydrogen. Usage of this element implies the requirement of having a cryogenic target since frozen hydrogen is the only solution providing high density of the target, good vacuum conditions and lack of any structural material

in the interaction region. Cryogenic hydrogen target exists in two variants: cluster jet target and pellet target. Clusters have various sizes (below 1 μm), contain 10^5 atoms on average and are produced as a spray. Pellets have uniform size (in the range 10 – 30 μm, depending on conditions), contain 10^{14} – 10^{15} atoms and are produced at a constant pace. Studies described in the thesis revolve around the latter kind of target.

The pellets (and the clusters) have to be generated at a certain distance (2 – 3 m) above the interaction region because it is surrounded with various particle detectors. They travel towards there inside a thin pipe. Below the interaction region the next pipe leads pellets to the dump, where they are collected. Because of its angular divergence, the pellet stream, although very narrow at the generation point, has a few millimeters diameter at the interaction region. The accelerator beam region also has a few millimeters diameter. Because of this, even though single pellets are very small, the possible region from which the interaction may come extends to a few millimeters in each direction. Unfortunately in practice even this is not the case, because the interaction may come also from various kinds of background material. The source of a background can be *e.g.* a rest-gas resulting from evaporation of pellets and constantly present in the chambers or it can be interactions of accelerator beam halo with the pipe walls.

Pellet tracking

A method is being developed to exploit the possibilities given by the sub-millimeter target size offered by pellets. It will enable the knowledge of position of pellets at the time of interaction with a resolution of approx. 100 μm in each direction. This will not only help reducing the background by knowing which hadronic events took place at the time when no pellet was present in the beam region but it will also provide additional information about the good (non-background) events. By knowing the interaction point with this high resolution it will be possible to more precisely reconstruct trajectories of charged particles bending in the magnetic field. Thanks to this, their momenta will be measured more precisely, thus further improving the quality of the hadronic data analysis results.

Furthermore, in some cases the only particles produced during the collision are unstable neutral particles, which then decay at a distance from a fraction of millimeter to a few millimeters. The decay point of this particle (secondary *interaction vertex*) can be reconstructed from tracks of resulting charged particles, but the knowledge of the pellet position may be the only way of reconstructing the primary interaction vertex.

Because of the design of the particle detector system, the pellet stream pipe can be accessed only below the generation point and above the dump. Measurement sections will be installed at these two regions to allow recording the two-dimensional positions and times of the passing pellets at a few levels in each section. The time of detecting a pellet will be based on the same clock which gives time stamps to the events measured by the particle detectors. This way it will be possible to use the pellet information in the hadronic data analysis. Then, in the offline analysis, pellets will be identified and their tracks will be reconstructed based on the measurements. Having the tracks reconstructed, the number of pellets in the beam region and their position during a hadronic interaction can easily be retrieved.

Detection of pellets will be done optically. They will be illuminated with laser diodes and detected with fast line-scan CCD cameras (*i.e.* CCD cameras with only one line of pixels).

Problems studied and discussed in the thesis

To develop a pellet tracking system and optimize values of its parameters, extensive research and development is needed, involving experimental tests and measurements, hardware development, experimental data analysis, simulations and preparing of procedures for data processing. Optimal illumination conditions have to be found. Cameras have to be tested from the optical point of view as well as concerning their electronic properties. A way of mounting the cameras and lasers rigidly and with possibility of adjustments has to be designed. Readout system, hardware as well as software, has to be created to allow fast processing of the big amount of data from the cameras, extracting pellet features and saving them. Procedures of pellet track reconstruction have to be developed. The methods of using the pellet information in hadronic data analysis have to be designed.

Pellet detection conditions Development of the pellet tracking is being done at the Uppsala Pellet Test Station (UPTS). This is a standalone pellet target device, independent of any accelerator or detector setup, which enables convenient experiments with pellets and tests of the pellet tracking prototypes. The prerequisite for development of pellet tracking system is a study of pellet detection conditions. Various illumination conditions were checked and optimized, concerning different models of lasers, different optics, different illumination angle and number of lasers. Also different models of cameras were checked, with different optics and operated with different cycle structure. Means of processing the image from the cameras to obtain information about detected pellets were investigated.

Pellet stream Parameters of the pellet stream were also measured. The measurements were done at single fixed levels and in correlation between different measurement levels. Distributions of pellet stream density, pellet stream shape and divergence were measured. Also, measurements of pellet velocity, velocity spread and a source of the velocity spread were carried out.

Tracking system design The knowledge about pellet detection conditions and pellet stream behavior has been used to develop Monte Carlo procedures simulating experiments with pellets at UPTS. In the next stage, simulations of pellet tracking performance expected ad PANDA were carried out based on realistic pellet stream and detection parameters from UPTS measurements and constraints from the PANDA setup. Performance and resolution of the tracking was checked for various parameters of pellet stream and pellet detection. A procedure of pellet track reconstruction was developed for the purpose of the study. It could also be used in the data analysis when full scale pellet tracking system is operated at a particle detector system.

Pellet tracks processing Hadronic data acquisition and pellet tracking work in completely different time scales. The full information about one hadronic event is mostly collected within one microsecond and the typical time between subsequent hadronic events of interest is 10–100 microseconds. On the other hand, the time needed for the pellet tracking system to collect information relevant for one hadronic event is approx. 100 milliseconds and the information comes as a dozen or so subevents (processed camera pictures), which are mixed with many thousands of subevents for other pellets recorded within this time. Also, the pellet tracking information recorded at a given moment is not relevant to any hadronic event recorded near this time. The total amount of pellet data which needs to be handled is two orders of magnitude smaller than the amount of hadronic data. Taking into account the differences in nature of the two systems, it is necessary to develop a dedicated pellet data acquisition enabling efficient usage of pellet tracking information in the hadronic data analysis. Also, track reconstruction procedures have to be included in the data analysis framework. In a next step procedures will be needed to use the pellet tracks in the classification of hadronic events. It will be checked if any pellet was expected to be in the interaction region at the time of given event and if it maybe was more than one pellet. The tracking system information will be used together with the PANDA micro vertex detector and other tracking detectors. In this way it will be possible to distinguish between primary and secondary vertices and also to have

access to an additional point in fitted particle tracks. Guidelines for the inclusion of pellet tracking system information in the data taking and analysis chain have been prepared. Also, an advanced algorithm of pellet track reconstruction has been developed. This algorithm is very robust, flexible and provides very high reconstruction efficiency even in case of substantial pellet detection inefficiencies.

Studies on implementation of pellet tracking Important parts of the development of the pellet tracking are tests of system operation in a real hadron physics experiment. Now before such opportunity is possible at PANDA site, some test of principle measurements at WASA were done. One piece of information given by the pellet tracking is the number of pellets in the interaction region at a certain time. Possibility of obtaining and making use of this information was checked at WASA in an alternative way - by using a stand-alone Long Range TDC, recording times of elastic scattering events. Based on the instantaneous event rate and the knowledge that presence of pellet in the beam region increases this rate, an event classification method was developed and the hadronic data were analyzed separately for "pellet" and "non-pellet" case. The study clearly showed that one can distinguish between the two event classes and this test provided an experience on using two different systems synchronized with each other – the normal experiment DAQ and another system, in this case the Long Range TDC, which works with a much longer time scale – similar to the pellet tracking system.

Chapter 9

Summary in Swedish - Svensk sammanfattning

Abstrakt

Ett system för optisk spårning av frysta mikrosfärer av väte (pelletar) har utvecklats för användning i det kommande hadronfysikexperimentet PANDA vid FAIR, Darmstadt i Tyskland. Kunskapen om positionen för växelverkan som fås med hjälp av detta system kommer att förbättra möjligheten att diskriminera mot bakgrund, att öka precisionen i partikelspårsrekonstruktionen och kommer också att hjälpa till att skilja mellan primära och sekundära växelverkanspunkter.

Undersökningar av pelletdetektionsmöjligheter och pelletströmmens egenskaper har gjorts vid Uppsala Pellet Test Station vid The Svedberglaboratoriet. Olika belysnings och detektionsvillkor har testats och optimerats. Den erhållna kunskapen har använts för att utveckla en Monte-Carlo procedur för att kunna simulera de olika experimenten med pelletar. Därefter genomfördes simuleringar av förväntade pelletspårningsprestanda för PANDA uppställningen. Prestanda och upplösning av spårningen kontrollerades för olika pelletsström och detektionsförhållanden. Två procedurer för spårrekonstruktion utvecklades för studien – en snabbare och en med högsta möjliga effektivitet. Den kommer att kunna användas i dataanalysen när fullskalig pelletspårning används ihop med ett partikeldetektorsystem. Studien gjordes för två fall, dels för en spårningssektion (placerad just under pelletgeneratorn) och dels med ytterligare en sektion (placerad just ovanför pelletdumpen). Studien visade att positionsupplösningen som förväntas från spårningssystemet är bättre än 100 μm (sigma) i varje riktning och att växelverkanspunkten kan rekonstrueras för 70-95% av de hadroniska händelserna, för lämpliga pelletströms- och detektionsvillkor.

Användningen av pelletspårningsinformationen i analysen av hadroniska händelsedata diskuterades m.a.p. datainsamling, m.a.p. partikelspårsrekonstruktion ihop med PANDA's mikrovertexdetektor och m.a.p. klassificering av händelser. Det gjordes testmätningar med WASA-uppställningen vid FZJ, Jülich i Tyskland för att se hur informationen om antalet pelletar i acceleratorstrålområdet kan användas i experimentets dataanalys. Den momentana frekvensen av elastiska spridningshändelser användes för en grov klassificering av händelsers ursprung såsom varande antingen från en pellet eller från någon källa till bakgrund. Studien visade klart att man kan skilja de båda klasserna åt. Studien gav också erfarenhet av hur man kan använda två synkroniserade datasystem – experimentets datainsamlingssystem och ett annat system som arbetar med en mycket längre tidsskala – liknande pelletspårningssystemets.

Denna avhandling handlar om utveckling av en strålmålsenhet som ökar kvaliteten på data i acceleratorbaserade hadronfysikexperiment som syftar till studier av materiens grundläggande egenskaper.

Introduktion till det vetenskapliga fältet

De elementarpartiklarna som all synlig materia är uppbyggd av är leptoner och kvarkar. Den mest kända leptonen är elektronen. Det är också den lättaste av de laddade leptonerna, som även omfattar myonen och tauonen. Bara elektronen är stabil av dessa. De andra två sönderfaller inom en bråkdel av en sekund efter att de skapats. De laddade leptonerna har sin neutrala leptonpartner, en neutrino – det finns en elektronneutrino, myonneutrino och tauneutrino. Kvarkarna är en annan grupp av laddade elementarpartiklar. De två lättaste av dem kallas "upp" och "ner". Nukleonerna – protoner och neutroner – som bildar atomkärnor, består av dessa kvarkar. De andra fyra kvarkarna kallas "charm", "sär", "topp" och "botten". Partiklar som består av dessa kvarkar kan skapas i kollisioner av högenergiska partiklar. Alla de nämnda leptonerna och kvarkarna finns som "normala" partiklar och antipartiklar.

Kvarkar finns inte som fria partiklar utan endast bundna i hadroner. Baryoner är hadroner som består av tre kvarkar. De mest kända baryonerna är protoner och neutroner. Hadroner som består av två kvarkar kallas mesoner. Två exempel på dem är pioner och etamesoner. Det finns många olika typer av baryoner och mesoner. Studierna av dessa är föremål för hadronfysiken. Protonen är den enda stabila hadronen. Neutronen är stabil endast när den är bunden i en atomkärna.

All växelverkan som sker i naturen härrör från fyra grundläggande krafter: gravitationen, den elektromagnetiska, den starka och den svaga kärnkraften. Krafterna förmedlas också av partiklar och utbytet av dessa kraftbärarpartiklar observeras på makroskopisk skala som växelverkningar mellan elementen i ett system. Dessa kraftbärare eller bosoner, är den tredje gruppen av elementarpartiklar. Elektromagnetisk växelverkan förmedlas av fotoner och den svaga växelverkan förmedlas av tre bosoner: W^+, W^- och Z^0. Den starka kraften bärs av gluoner. Man söker fortfarande efter förekomsten av en kraftbärare för gravitation (gravitonen). Medan gravitationen och den elektromagnetiska kraften verkar över, i princip, oändliga avstånd, verkar den starka och svaga kärnkraften bara på subatomär nivå.

Den starka kärnkraften håller kvarkarna bundna i hadronerna. Analogt med laddning i elektromagnetisk växelverkan, involverar också stark växelverkan viss laddning. I detta fall finns det tre olika varianter av laddning. Analogt till optik brukar dessa varianter av laddning benämnas med de primära färgerna: röd, grön och blå. På samma sätt som elektrisk laddning är positiv eller negativ, så finns det utöver de

positiva laddningarna röd, grön och blå, också negativa laddningar (antifärger): anti-röd, anti-grön och anti-blå. Endast färgneutrala objekt kan observeras vilket innebär att färgerna av kvarkar i en hadron måste kombineras ihop till vad i analogi med optiken skulle ge en vit färg (t.ex. röd-grön-blå eller färg-antifärg). Det bör också noteras att en viss färg inte är en inneboende egenskap hos kvarkarna. Färgerna förändras ständigt genom emission och absorption av gluoner. På detta sätt förmedlas den starka växelverkan.

Stark växelverkan uppvisar två utmärkande egenskaper: färginneslutning och asymptotisk frihet. Asymptotisk frihet innebär att för mycket små avstånd mellan kvarkar, mindre än storleken av en nukleon, blir växelverkan mycket svag och kvarkar och gluoner beter sig som om de vore helt fria. För att uttrycka det med andra ord, blir kopplingskonstanten för växelverkan mycket svag. Färginneslutningen innebär, att för större avstånd mellan kvarkarna, så blir växelverkan mellan dem kraftigare (kopplingskonstanten blir starkare) vilket i sin tur leder till att isolerade kvarkar inte kan observeras. Detta beteende skiljer sig från elektromagnetisk växelverkan, där kraften mellan laddningarna minskar samtidigt som laddningarna dras isär, vilket möjliggör att de negativt laddade elektronerna i atomen kan vara obundna från den positivt laddade atomkärnan. I fallet med den starka växelverkan kräver separationen av kvarkarna till större avstånd mer och mer energi. Efter hand blir denna energi tillräckligt stor för att skapa ett nytt kvark-antikvark par som bildar nya hadroner med kvarkarna som ursprungligen separerades.

En teori som kallas kvantkromodynamik (Quantum Chromo Dynamic, QCD) har utvecklats för att beskriva alla egenskaperna hos stark växelverkan. Den är en del av den så kallade Standardmodellen för partikelfysiken, som sammanfattar vår nuvarande kunskap om partiklar och växelverkan i universum. Grunden till QCD lades för 50 år sedan och sedan dess har förståelsen av QCD stegvis utvecklats och förbättrats.

Växelverkan vid hög energi innebär små avstånd mellan kvarkarna och därmed en svag kopplingskonstant. I detta fall är beskrivningen av den starka kraften lättare eftersom det är möjligt att använda störningsberäkning. Det innebär att det komplicerade systemet beskrivs i form av ett enklare system med tillägg av små störningar.

Mer problematiskt är att använda QCD vid låg energi eftersom det innebär en stark kopplingskonstant. Under dessa förhållanden är det inte möjligt att använda störningsberäkning. Området är fortfarande det minst kända och nya mätresultat behövs kontinuerligt för ökad förståelse och kontroll av teoretiska modeller.

Fysik med PANDA experiment

Värdefull information för förståelsen av hadronernas grundläggande byggstenar och stark växelverkan kommer att fås från den nya experimentuppställningen PANDA vid forskningscentret GSI i Darmstadt, Tyskland. PANDA kommer att placeras vid HESR acceleratorn (en högenergilagringsring) som tillhandahåller strålar av anti-protoner med rörelsemängd 1,5-15 GeV/c. Som strålmål kommer man främst att använda väte, det vill säga protoner, men det blir också möjligt att använda tyngre gaser. HESR är utrustad med elektronkylning och stokastisk kylning av strålen, vilket ger mycket väl definierad energi och gör det möjligt att mäta massa och bredder av hadroniska resonanser med en hög noggrannhet (av 50 — 100 keV). En av fördelarna med att kollidera antiprotoner med protoner är att det möjliggör bildande av nya tillstånd med alla kvanttal. $\bar{p}p$ kollisioner kommer tex att möjliggöra spektroskopi av charmonium, D-mesoner och baryoner med särtals och charmkvarkar. Det blir också möjligt att söka efter gluonbollar (partiklar som skulle bestå av enbart gluoner) och hybrider (bestående av kvark, anti-kvark och exciterade gluoner). Dessa tillstånd borde kunna finnas enligt QCD, men deras existens har inte bekräftats experimentellt. Vid PANDA kommer det vara möjligt att söka efter gluoniska hadroner med en massa över 2,5 GeV/c^2, där tätheten av konventionella kvark-antikvark tillstånd blir mindre. En studie av lågenergi QCD-dynamik blir också möjlig i baryon-antibaryon växelverkningar. Kollisioner av antiprotoner med tyngre kärnor möjliggör studiet av $\Lambda\Lambda$ hyperkärnor och hadroner i det nukleära mediet.

Strålmål

Strålmålsmaterialet i de flesta PANDA-experimenten kommer att vara väte. Det krävs nedkylt eller fryst väte eftersom det är den enda möjligheten att samtidigt ha hög densitet, bra vakuum förhållanden och ett minimum av andra material i växelverkansområdet. Nedkylt väte som strålmål finns i två varianter: kluster jet och pelletar. Klustren kan ha olika storlekar (under 1 μm) och innehåller cirka 10^5 atomer och produceras som en gasstråle. Pelletarna har enhetlig storlek (i området 10-30 μm, beroende på förhållanden) och innehåller 10^{14}–10^{15} atomer och produceras i en konstant takt. Studierna som behandlas i avhandlingen gäller den senare typen av strålmål.

Pelletarna (och klustren) skapas på ett visst avstånd (2-3 m) ovanför växelverkansområdet eftersom detta omges av en mängd olika partikeldetektorer. Strålmålen leds in till växelverkansområdet genom ett tunt vakuumrör och därefter ut genom nästa rör ner till en dump. Pelletstrålen är initialt mycket smal men på grund av sin divergens är dess diame-

ter några millimeter vid växelverkansområdet. Acceleratorstrålen har också några millimeters diameter. Även om enstaka pelletar är mycket små, blir alltså det möjliga området för växelverkan ett par millimeter i varje riktning. I praktiken är det ännu större, eftersom reaktionen också kan ske i olika typer av bakgrundsmaterial. Källan till bakgrund kan t.ex. vara gas från avdunstning av pelletar eller växelverkningar mellan acceleratorstrålens halo och acceleratorrörets väggar.

Pelletspårning

Nu utvecklas en teknik att spåra pelletar för att utnyttja den möjlighet som erbjuds, nämligen att verkligen ha sub-millimeters strålmålstorlek. Tekniken gör det möjligt att veta positionen för pelletarna vid tiden för växelverkan med en upplösning på ca 0.1 mm i varje riktning. Detta kommer inte bara att hjälpa till att diskriminera mot bakgrund, genom att veta vilka händelser som inträffade vid en tid då ingen pellet var närvarande i strålregionen, utan det kommer också att ge ytterligare information om de önskvärda händelserna (icke-bakgrund). Genom att känna växelverkanspunkten med denna upplösning kommer det att vara möjligt att mer exakt rekonstruera de laddade partiklarnas krökta banor i magnetfältet. Tack vare detta kommer deras rörelsemängder att kunna mätas mer exakt och därmed ytterligare förbättra kvaliteten på analysresultaten. I vissa fall är de enda partiklarna som produceras under kollisionen instabila neutrala partiklar, som sönderfaller efter en sträcka på en bråkdel av millimeter upp till ett par millimeter. Sönderfallspunkten för en sådan partikel (sekundärt vertex) kan rekonstrueras från spår av laddade sönderfallsprodukter, men kunskapen om pelletposition kan vara det enda sättet att rekonstruera den primära växelverkanspunkten.

Detektorns konstruktion tillåter bara direkt åtkomst till pelletströmmens vakuumrör just under genereringspunkten och just över dumpen. Sektioner för mätning av tvådimensionella positioner och tider för passerande pelletar kommer att installeras i dessa två områden med några nivåer i varje område. Tiden för mätning av en pellet baseras på samma klocka som ger tidsstämplar för händelserna som mäts av partikeldetektorerna. På detta sätt kommer det vara möjligt att använda pelletinformation i dataanalysen. I pelletdataanalysen, kommer pelletarna att identifieras och deras spår kommer att rekonstrueras utifrån mätningarna. Med de rekonstruerade spåren, kan antalet pelletar i strålregionen och deras position vid en hadronisk växelverkan enkelt beräknas.

Detektionen av pelletarna sker optiskt. De belyses med diodlasrar och identifieras med snabba linje-scanningskameror (CCD kameror med endast en rad av pixlar).

Problem som studeras och diskuteras i avhandlingen

För att utveckla ett system för spårning av pelletar och optimera värdena för dess parametrar, behövs omfattande forskning och utveckling, som omfattar experimentella tester och mätningar, hårdvaruutveckling, experimentell dataanalys, simuleringar och utarbetandet av förfaranden för databehandling. Optimala belysningsvillkor måste hittas. Kameror måste testas optiskt och med avseende på elektroniska egenskaper. Stabil montering av kameror och lasrar med möjlighet till noggranna justeringar måste utformas. Utläsningssystem, hårdvara, samt programvara, måste skapas för att möjliggöra snabb bearbetning av den stora mängden data som kommer från kamerorna och extraktion av relevant pelletinformation. Procedurer för rekonstruktion av pelletspår och användandet av informationen i analysen av de hadroniska händelserna måste utvecklas.

Pelletdetektionsvillkor Utvecklingen av pelletspårning görs vid Uppsala PelletTestStation (UPTS). Detta är en fristående pelletstrålmålenhet, oberoende av accelerator eller detektoruppställning, vilket smidigt möjliggör experiment med pelletar och tester av prototyper. En förutsättning för utveckling av pelletspårning är studier av pelletdetektionsmöjligheter. Olika belysningsvillkor har undersökts och optimerats vad gäller olika modeller av lasrar, optik, infallsvinklar och antal lasrar. Olika modeller av kameror har också testats, med olika optik och exponeringscykler. Flera sätt att bearbeta bildinformationen från kamerorna för att upptäcka pelletar har studerats.

Pelletströmsparametrar Pelletströmmens egenskaper har studerats och olika parametrar har uppmätts. Mätningar gjordes på individuella nivåer och korrelation mellan två olika nivåer. Fördelningar av pelletströmsdensitet, pelletströmsform och divergens mättes. Dessutom genomfördes mätningar av pellethastighet, hastighetsspridning och studier av källor till spridningen.

Utformning av spårningssystemet Den erhållna kunskapen om pelletdetektion och pelletströmmens beteende har använts för att utveckla en Monte-Carlo procedur för att simulera de olika experimenten med pelletar vid UPTS. Därefter genomfördes simuleringar av förväntade spårningsprestanda vid PANDA baserat på realistiska pelletströms- och detektionsparametrar från UPTS. Prestanda och upplösning av spårningen kontrollerades för olika pelletsström och detektionsförhållanden. En procedur för spårrekonstruktion utvecklades för studien. Den kommer att kunna användas i dataanalysen när fullskalig pelletspårning används ihop med ett partikeldetektorsystem.

Pelletspårbearbetning Datainsamlingen för reaktionsstudier och för pelletspårning omfattar helt olika tidsskalor. Fullständig information om en reaktion samlas normalt in inom en mikrosekund och den typiska tiden mellan dessa är 10-100 mikrosekunder. Den tid som behövs för pelletspårsystemet att samla in information som är relevant för dessa reaktioner är ca: 100 millisekunder och kommer som ett tiotal delhändelser (kamera"bilder") ihopblandade med många tusentals delhändelser från andra pelletar som också registreras inom denna tid. Den totala mängden av pelletdata som måste hanteras är två tiopotenser gånger mindre än mängden för reaktionshändelsen. Med beaktande av skillnaderna mellan de två systemen, måste ett dedicerat datainsamlingssystem utvecklas som sparar informationen från pelletmätdata för senare användning i rekonstruktionen av reaktionsprodukterna. Här används denna information för klassificering av de hadroniska händelserna. Det kontrolleras hur många pelletar var i växelverkansområdet vid tiden för en given. Pelletspårningssystemet kommer att användas ihop med PANDA's mikrovertexdetektor och andra partikelspårdetektorer. På detta sätt kommer det vara möjligt att skilja mellan primära och sekundära vertex och även att ha tillgång till en extra punkt för anpassningen av laddade partikelspår. Riktlinjer för inkluderandet av pelletinformationen i datatagningen och analyskedjan har uppställts. En algoritm för pelletspårrekonstruktion har utvecklats. Denna är mycket robust, flexibel och ger mycket hög effektivitet även vid betydande detektionsineffektivitet.

Implementering av pelletspårning En viktig del i utvecklingen av pelletspårning är systemtester i ett riktigt hadronfysikexperiment. Eftersom detta ännu inte är möjligt vid PANDA, så har en del tester av principen gjorts vid WASA, som är ett pågående experiment vid FZJ i Jülich, Tyskland. En information som fås genom pelletspårning är antalet pelletar i växelverkansområdet. Möjligheten att erhålla och använda sådan information har kontrollerats vid WASA på ett alternativt sätt – med hjälp av en fristående tids-till-digitalomvandare (TDC) med stort tidsfönster som registrerar elastiska spridningshändelser. Baserat på den momentana händelsefrekvensen och kunskapen om att närvaro av pelletar i strålregionen ökar denna frekvens så har en metod för att klassificera händelser utvecklats och reaktionsdata har analyserats separat för "pellet" och "icke-pellet" fallen. Studien visade tydligt att man kan skilja mellan de två händelseklasserna och testen gav erfarenhet av hur man kan använda två olika, men synkroniserade system -– det normala experimentdatainsamlingssystemet DAQ och ett annat system, i detta fall en TDC, som arbetar med en mycket längre tidsskala - liknande pelletspårningssystemets.

Chapter 10

Summary in Polish - Polskie podsumowanie

Abstrakt

Wykonane zostały prace nad rozwojem systemu pozwalającego na optyczne śledzenie zamarzniętych wodorowych mikrokulek (pelletów). System przeznaczony jest do zastosowania w planowanym eksperymencie z dziedziny fizyki hadronowej, PANDA (FAIR, Darmstadt, Niemcy). Wiedza o położeniu punktu interakcji, uzyskana dzięki temu systemowi, poprawi redukcję tła, precyzję rekonstrukcji torów cząstek, a także pomoże w rozróżnianiu pierwotnych i wtórnych wierzchołków interakcji.

Na Uppsalskiej Stacji Pelletowej (Uppsala Pellet Test Station) umieszczonej w Laboratorium The Svedberga, przeprowadzone zostały badania warunków detekcji pelletów i parametrów strumienia pelletowego. Różne warunki oświetlenia oraz detekcji pelletów zostały sprawdzone i zoptymalizowane. Uzyskana wiedza została użyta do stworzenia procedur Monte Carlo symulujących eksperymenty z pelletami. W następnym kroku przeprowadzone zostały symulacje śledzenia pelletów biorące pod uwagę więzy narzucone przez konstrukcję systemu PANDA. Wydajność systemu sprawdzona została dla różnych warunków strumienia pelletowego i detekcji pelletów. Stworzone zostały dwie procedury rekonstrukcji torów pelletowych – procedura szybka i procedura wysokoefektywna. Badania przeprowadzone zostały dla jednej sekcji śledzącej (bezpośrednio poniżej generatora pelletów) oraz dla dwóch sekcji (druga bezpośrednio nad miejscem zbierania pelletów) i pokazały, że rozdzielczość systemu śledzenia może być lepsza niż 100 μm (sigma) w każdym z kierunków oraz że punkt interakcji będzie zrekonstruowany dla 70-95% zdarzeń hadronowych, dla odpowiednich warunków strumienia pelletów i warunków detekcji.

Użycie informacji ze śledzenia pelletów w analizie danych hadronowych zostało przedyskutowane uwzględniając proces zbierania danych, rekonstrukcję torów cząstek we współpracy z mikrodetektorem wierzchołków systemu PANDA, klasyfikację zdarzeń hadronowych oraz sposób traktowania różnych klas zdarzeń. Pomiary testowe z użyciem detektora WASA (FZJ, Jülich, Niemcy) zostały dokonane w celu sprawdzenia jak informacja o liczbie pelletów w obszarze wiązki może zostać użyta w analizie danych hadronowych. Chwilowe częstotliwości "elastycznych" triggerów systemu WASA zostały użyte w celu klasyfikacji zdarzeń hadronowych jako pochodzących z interakcji wiązka-pellet lub wiązka-tło. Badania wykazały iż możliwe jest rozróżnienie między tymi dwoma klasami zdarzeń. Uzyskano również doświadczenie w używaniu dwóch różnych systemów zsynchronizowanych ze sobą – eksperymentalnego systemu zbierania danych oraz innego systemu, działającego w znacznie dłuższej skali czasowej – podobnie do systemu śledzenia pelletów.

Tematem niniejszej pracy doktorskiej jest rozwój urządzenia tarczy pozwalający na zwiększenie jakości danych w eksperymentach fizyki hadronowej bazujących na użyciu akceleratorów cząstek, używanych w badaniach fundamentalnych własności materii.

Wprowadzenie do dziedziny naukowej

Cząstkami elementarnymi z których zbudowana jest cała widzialna materia są *leptony* i *kwarki*. Najbardziej znanym leptonem jest *elektron*. Jest to też najlżejszy z leptonów obdarzonych ładunkiem, do których zaliczają się również *mion* oraz *tauon*. Jedynie elektron jest cząstką trwałą. Pozostałe dwa rozpadają się w ciągu niewielkiego ułamka sekundy po ich utworzeniu (w wysokoenergetycznym oddziaływaniu). Każdy z naładowanych leptonów posiada swojego neutralnego leptonowego partnera, *neutrino* – istnieje neutrino elektronowe, neutrino mionowe oraz neutrino tauonowe. Kwarki są następną grupą naładowanych cząstek elementarnych. Dwa najlżejsze z nich nazwane zostały kwarkami *górnym* oraz *dolnym*. Nukleony – protony i neutrony – tworzące jądra atomowe, zbudowane są z tych kwarków. Pozostałe cztery kwarki noszą nazwy: *powabny*, *dziwny*, *wysoki* i *niski*. Cząstki zbudowane z tych kwarków mogą być tworzone w zderzeniach wysokoenergetycznych cząstek. Każdy ze wspomnianych leptonów i kwarków istnieje jako "normalna" cząstka oraz jako antycząstka.

Kwarki nie istnieją oddzielnie lecz jedynie związane w *hadrony*. Np. *bariony* są hadronami zbudowanymi z trzech kwarków. Najbardziej znanymi barionami są protony i neutrony. Hadrony zbudowane z dwóch kwarków noszą nazwę *mezonów*. Ich przykładami są *piony* i mezony *eta*. Istnieje wiele różnych barionów i mezonów. Badanie ich jest przedmiotem fizyki jądrowej i wysokich energii. Proton jest jedynym stabilnym hadronem. Neutrony są stabilne jedynie wewnątrz jąder atomowych.

Wszystkie oddziaływania zachodzące w przyrodzie mogą zostać sprowadzone do czterech oddziaływań fundamentalnych: *grawitacyjnego*, *elektromagnetycznego*, *silnego* oraz *słabego*. Oddziaływania przenoszone są przez cząstki – nośniki oddziaływań. Wymiana tych cząstek jest w skali makroskopowej obserwowana jako oddziaływanie między elementami układu. Nośniki oddziaływania, lub inaczej *bozony cechowania*, są trzecią grupą cząstek elementarnych. Oddziaływanie elektromagnetyczne przenoszone jest przez *fotony*, zaś oddziaływanie słabe przez trzy bozony: W^+, W^- oraz Z^0. Oddziaływanie silne przenoszone jest przez *gluony*. Istnienie nośników oddziaływania grawitacyjnego (*grawitonów*) jest ciągle przedmiotem badań. Podczas gdy oddziaływania grawitacyjne i elektromagnetyczne działają na potencjalnie nieskoń-

czone odległości, silne i słabe oddziaływania jądrowe działają jedynie w skali subatomowej.

Oddziaływanie silne utrzymuje kwarki związane w hadrony. Przez analogię do ładunku w oddziaływaniu elektromagnetycznym mówi się, że oddziaływanie silne również związane jest z istnieniem pewnego ładunku. W tym przypadku istnieją jednak trzy warianty ładunku. Przez analogię do optyki te warianty koloru noszą nazwy barw podstawowych: czerwonej, zielonej oraz niebieskiej. Analogicznie do normalnego ładunku mogącego mieć znak pozytywny lub negatywny, również w przypadku ładunków kolorowych oprócz czerwonego, zielonego i niebieskiego istnieją negatywne antyładunki (antykolory): anty-czerwony, anty-zielony i anty-niebieski. Jedynie obiekty o neutralnym kolorze mogą być obserwowane, co oznacza, że kolory kwarków w hadronach muszą zsumować się do tego, co w optyce dałoby barwę białą (np. czerwony-zielony-niebieski lub kolor-antykolor). Należy również zaznaczyć, że dany kolor nie jest wewnętrzną cechą kwarków – kolory zmieniają się ciągle poprzez emisję i absorpcję gluonów. W ten właśnie sposób następuje przenoszenie oddziaływania silnego.

Oddziaływanie silne odznacza się dwoma ciekawymi właściwościami: *uwięzieniem koloru* i *swobodą asymptotyczną*. Swoboda asymptotyczna oznacza, że dla małych odległości między kwarkami, mniejszych niż rozmiary nukleonu, oddziaływanie staje się bardzo słabe i kwarki oraz gluony zachowują się jak nieoddziałujące. Innymi słowy, *stała sprzężenia* tego oddziaływania staje się bardzo słaba. Uwięzienie koloru oznacza, iż wraz ze zwiększaniem się odległości między kwarkami, oddziaływanie między nimi staje się silniejsze (silniejsza stała sprzężenia) co z kolei prowadzi do tego, że oddzielne kwarki nie mogą być obserwowane. Różni się to bardzo od przypadku oddziaływania elektromagnetycznego, gdzie siła pomiędzy ładunkami zanika przy ich oddalaniu, pozwalając np. aby ujemnie naładowane elektrony w atomie zostały oddzielone od dodatnio naładowanego jądra. W przypadku oddziaływania silnego, oddalanie kwarków na większe dystanse wymaga coraz więcej energii. W pewnym momencie ta energia jest wystarczająco duża do powstania pary kwark-antykwark, które tworzą nowe hadrony z kwarkami początkowo rozdzielanymi.

Teoria zwana *chromodynamiką kwantową* (ang. QCD - Quantum Chromo Dynamics) została stworzona do opisu wszystkich własności oddziaływania silnego. Teoria ta jest częścią zestawu teorii zwanego *Modelem Standardowym* fizyki cząstek elementarnych, podsumowującego aktualną wiedzę na temat cząstek i oddziaływań obecnych we wszechświecie. Podwaliny pod QCD położone zostały ok. 50 lat temu; od tego czasu teoria jest ciągle rozwijana i ulepszana.

W obszarze wysokich energii, odpowiadającym małym odległo-

ściom między kwarkami, a przez to słabej stałej sprzężenia, opis oddziaływania silnego jest łatwiejszy ponieważ możliwy jest do zastosowania tzw. *rachunek zaburzeń*. W tym podejściu skomplikowany układ opisywany jest poprzez prostszy układ z dodatkiem niewielkiego zaburzenia. Bardziej problematyczny jest niskoenergetyczny obszar QCD, w którym stała sprzężenia jest silna. W tych warunkach niemożliwe jest zastosowanie rachunku zaburzeń. Ten obszar jest ciągle najmniej zbadany i nowe pomiary są szczególnie potrzebne.

Fizyka z eksperymentem PANDA

Wartościowy wkład w zrozumienie własności hadronów i oddziaływania silnego będzie pochodził z nowego eksperymentu PANDA, który będzie mieścił się w centrum badawczym GSI w Darmstadt (Niemcy). PANDA będzie działała na akceleratorze HESR (ang. High Energy Storage Ring – wysokoenergetyczny pierścień akumulacyjny), dostarczającym wiązkę antyprotonów o pędzie 1.5 – 15 GeV/c. Materiałem tarczy będzie głównie wodór; możliwe będzie również użycie cięższych gazów. HESR wyposażony jest w chłodzenie elektronowe i stochastyczne wiązki, co zapewnia bardzo dobre określenie energii wiązki i pozwala mierzyć masy i szerokości rezonansów hadronowych z dokładnością 50 – 100 keV. Jedną z zalet zderzeń antyprotonów z protonami jest to, iż umożliwia to tworzenia stanów wszystkich liczb kwantowych. Zderzenia $\bar{p}p$ pozwolą na spektroskopię hadronową czarmonium, mezonów D oraz dziwnych i powabnych barionów. Będą możliwe również poszukiwania kul gluonowych (cząstek składających się jedynie z gluonów) oraz hybryd (składających się z kwarka, antykwarka i gluonu). Stany te są dozwolone przez QCD, ale ich istnienie nie zostało potwierdzone eksperymentalnie. PANDA umożliwi poszukiwania gluonowych hadronów o masach powyżej 2.5 GeV/c^2, gdzie gęstość konwencjonalnych stanów kwark-antykwark jest mniejsza. Również studia dynamiki niezaburzeniowego obszaru QCD będą możliwe w zderzeniach barionów z antybarionami. Zderzenia antyprotonów z cięższymi jądrami pozwolą na badanie hiperjąder $\Lambda\Lambda$ oraz hadronów w ośrodku jądrowym.

Tarcze

Głównym materiałem tarczy w eksperymencie PANDA będzie wodór. Użycie tego pierwiastka wiąże się z koniecznością zastosowania tarczy kriogenicznej – zamarznięty wodór jest jedynym rozwiązaniem zapewniającym wysoką gęstość tarczy, dobre warunki próżniowe oraz brak jakiegokolwiek materiału strukturalnego w obszarze oddziaływania. Kriogeniczna tarcza wodorowa istnieje w dwóch odmianach: jako

tarcza klastrowa oraz tarcza pelletowa. Klastry posiadają zróżnicowany rozmiar (poniżej 1 μm), zawierają ok. 10^5 atomów i są produkowane jako spray. Pellety posiadają jednorodny rozmiar (25 – 40 μm, zależnie od warunków), zawierają 10^{14} – 10^{15} atomów i są produkowane ze stabilną częstotliwością. Badania opisane w tej pracy dotyczą tego drugiego typu tarczy.

Pellety (oraz klastry) muszą być generowane w pewnej odległości (2 – 3 m) ponad obszarem interakcji, ponieważ jest on otoczony różnorodnymi detektorami cząstek. Pellety podróżują do obszaru interakcji wewnątrz cienkiej rury. Poniżej tego obszaru następna rura wiedzie pellety do miejsca, gdzie są zbierane. Ze względu na swoją rozbieżność kątową, strumień pelletów, mimo iż bardzo wąski w punkcie generacji, ma kilka milimetrów średnicy w obszarze interakcji. Wiązka akceleratora również posiada kilkumilimetrową średnicę. Z powodu tego, pomimo że pojedynczy pellet jest bardzo mały, możliwy obszar z którego może pochodzić oddziaływanie zwiększa się do kilku milimetrów w każdym kierunku. W praktyce niestety nawet taka sytuacja nie ma miejsca, ponieważ oddziaływanie mogło pochodzić również z różnego rodzaju tła. Źródłem tła może być np. gaz resztkowy pochodzący z parowania pelletów i obecny ciągle w komorach, lub też oddziaływanie halo wiązki akceleratora ze ścianami rur.

Śledzenie pelletów

Rozwijana jest metoda, która pozwoli wykorzystać możliwości dawane przez tarczę o submilimetrowych rozmiarach, oferowaną przez pellety. Metoda ta pozwoli znać pozycję pelletów w czasie interakcji z rozdzielczością ok. 100 μm w każdym kierunku. Pomoże to nie tylko zredukować tło poprzez wiedzę które zdarzenia hadronowe zostały zarejestrowane w czasie gdy żaden pellet nie był obecny w obszarze wiązki. Dostarczy ona również dodatkowych informacji o dobrych (nie pochodzących z tła) zdarzeniach. Znając z wysoką rozdzielczością położenie punktu interakcji będzie możliwa dokładniejsza rekonstrukcja torów naładowanych cząstek zakrzywianych w polu magnetycznym. Dzięki temu ich pędy będą mierzone precyzyjniej, zwiększając tym samym jeszcze bardziej jakość wyników analizy danych hadronowych.

Ponadto, w niektórych przypadkach jedynymi cząstkami produkowanymi podczas zderzenia są niestabilne cząstki neutralne, które później rozpadają się na odległości od ułamka milimetra do kilku milimetrów. Punkt rozpadu takiej cząstki (*wtórny wierzchołek interakcji*) może zostać zrekonstruowany z torów powstałych cząstek naładowanych, jednak wiedza o położeniu pelletu jest jedynym sposobem rekonstrukcji pierwotnego wierzchołka interakcji.

Ze względu na to jak układ detektorów cząstek jest zaprojektowany,

dostęp do strumienia pelletowego możliwy jest jedynie poniżej miejsca ich generacji oraz ponad miejscem ich zbierania. W tych miejscach zainstalowane zostaną sekcje pomiarowe pozwalające rejestrować dwuwymiarowe pozycje oraz czasy przejścia pelletów na kilku poziomach w każdej sekcji. Czas rejestracji pelletu będzie oparty na tym samym zegarze, który dostarcza znaczników czasu zdarzeniom mierzonym przez detektory cząstek. W ten sposób możliwe będzie użycie informacji pelletowej w analizie danych hadronowych. Następnie, w analizie offline, pellety będą identyfikowane a ich tory będą rekonstruowane w oparciu o pomiary. Mając zrekonstruowane tory, liczba pelletów oraz ich pozycja podczas zdarzenia hadronowego mogą być łatwo odtworzone.

Detekcja pelletów dokonywana będzie optycznie. Pellety będą oświetlane diodami laserowymi i rejestrowane za pomocą szybkich liniowych kamer CCD (zawierających jedynie jedną linię pikseli).

Zagadnienia dyskutowane w niniejszej pracy

By opracować system śledzenia pelletów oraz zoptymalizować jego parametry, potrzebne są rozległe prace badawczo-rozwojowe, zawierające w sobie eksperymentalne testy i pomiary, rozwój sprzętu, analizę danych eksperymentalnych, symulacje oraz przygotowanie procedur przetwarzania danych. Znalezione muszą zostać optymalne warunki oświetleniowe. Kamery muszą być przetestowane z optycznego punktu widzenia jak również biorąc pod uwagę ich własności elektroniczne. Zaprojektowany musi zostać sposób sztywnego montowania kamer i laserów z możliwością ich wygodnego ustawiania. System zbierania danych musi zostać stworzony, zarówno pod względem sprzętu jak i oprogramowania, by pozwolić na szybkie przetwarzanie dużych ilości danych z kamer, wyodrębnianie informacji o pelletach oraz zapisywanie ich. Rozwinięte muszą zostać procedury rekonstrukcji torów pelletowych. Zaprojektowane muszą być także metody wykorzystywania informacji pelletowej w analizie danych hadronowych.

Warunki detekcji pelletów Rozwój systemu śledzenia pelletów ma miejsce na Uppsalskiej Stacji Pelletowej (ang. UPTS – Uppsala Pellet Test Station). Jest to samodzielne urządzenie tarczy pelletowej, niezależne od jakiegokolwiek akceleratora czy detektora cząstek, co pozwala na wygodne eksperymenty z pelletami oraz testy prototypów systemu śledzenia pelletów. Wymogiem wstępnym do rozwoju systemu śledzenia pelletów jest zbadanie warunków detekcji pelletów. Rozmaite warunki oświetleniowe zostały sprawdzone i zoptymalizowane, biorąc pod uwagę różne modele laserów, różną optykę, różny kąt oświetlenia oraz liczbę laserów. Sprawdzone zostały również różne modele kamer,

wyposażone w różną optykę i działające z cyklem o różnej strukturze. Sposoby obróbki obrazu z kamer w celu uzyskania informacji o wykrytych pelletach zostały zbadane.

Parametry strumienia pelletowego Parametry strumienia pelletowego zostały również zmierzone. Pomiary dokonywane były na pojedynczych ustalonych poziomach pomiarowych jak również w korelacji między różnymi poziomami pomiarowymi. Zmierzone zostały rozkłady gęstości strumienia pelletowego jak również jego kształt oraz rozbieżność. Ponadto, przeprowadzone zostały pomiary prędkości pelletów oraz rozrzutu prędkości i jego przyczyn. Wiedza o warunkach detekcji pelletów i o zachowaniu strumienia pelletowego została wykorzystana do stworzenia procedur Monte Carlo symulujących eksperymenty z pelletami przeprowadzane na UPTS.

Projekt systemu śledzenia Symulacje wydajności systemu śledzenia pelletów spodziewanej w eksperymencie PANDA zostały przeprowadzone w oparciu o realistyczne parametry strumienia pelletowego i detekcji oparte na pomiarach z UPTS oraz o więzy wynikające z budowy detektora PANDA. Różne parametry strumienia pelletowego oraz detekcji pelletów zostały sprawdzone. Procedura rekonstrukcji torów pelletów została stworzona na użytek badań. Będzie ją można użyć również w analizie danych online, gdy pełnoskalowy system śledzenia będzie funkcjonował przy układzie detektorów cząstek.

Badania nad implementacją systemu śledzenia pelletów Akwizycja danych hadronowych i śledzenie pelletów działają w zupełnie innej skali czasowej. Pełna informacja o zderzeniu hadronowym jest zbierana zazwyczaj w ciągu mikrosekundy, zaś typowy czas między kolejnymi interesującymi zdarzeniami hadronowymi wynosi 10-100 mikrosekund. Z drugiej strony, czas potrzebny systemowi śledzenia pelletów na zebranie informacji mających znaczenie dla jednego zdarzenia hadronowego wynosi około 100 milisekund a informacja ma postać kilkunastu podzdarzeń (opracowanych obrazów z kamer), zmieszanych z wieloma tysiącami podzdarzeń dla innych pelletów zarejestrowanych w tym czasie. Ponadto, informacja ze śledzenia pelletów zarejestrowana w danym czasie nie ma związku z żadnym zdarzeniem hadronowym zachodzącym w pobliżu tego czasu. Całkowita ilość danych pelletowych która musi zostać obsłużona jest dwa rzędy wielkości mniejsza od ilości danych hadronowych. Biorąc pod uwagę różnice w naturze wspomnianych dwóch systemów, niezbędne jest rozwinięcie dedykowanego systemu zbierania danych pelletowych umożliwiającego efektywne użycie informacji ze śledzenia pelletów w analizie danych

hadronowych. Ponadto, procedury rekonstrukcji torów muszą zostać włączone w skład oprogramowania do analizy danych. W następnym kroku potrzebne będą procedury pozwalające użyć tory pelletów w klasyfikacji zdarzeń hadronowych. Sprawdzane będzie, czy jakiś pellet znajdował się w obszarze interakcji w czasie danego zdarzenia i czy może było ich tam więcej niż jeden. Informacja z systemu śledzenia używana będzie wspólnie z informacją z mikro detektora wierzchołków interakcji i z innych detektorów śledzących. W ten sposób możliwe będzie rozróżnienie między pierwotnymi i wtórnymi wierzchołkami interakcji, jak również posiadanie dodatkowego punktu przy dopasowywaniu torów cząstek. Wytyczne na temat włączenia informacji z systemu śledzenia pelletów w łańcuch zbierania i analizy danych zostały przygotowane. Ponadto, stworzony został bardziej zaawansowany algorytm rekonstrukcji torów pelletowych. Algorytm ten jest bardzo odporny i elastyczny i zapewnia bardzo wysoką efektywność rekonstrukcji nawet w przypadku znacznej nieefektywności detekcji.

Ważną częścią prac nad śledzeniem pelletów są testy systemu funkcjonującego przy działającym eksperymencie fizyki hadronowej. Zanim będzie to możliwe na detektorze PANDA, pomiary testowe zostały dokonane na detektorze WASA. Jedną z informacji dawanych przez śledzenie pelletów jest liczba pelletów w obszarze oddziaływania. Możliwość uzyskania i zrobienia użytku z takiej informacji została sprawdzona używając samodzielnego długookresowego TDC (ang Long Range Time-to-Digital Converter, długookresowy konwerter czasu na postać cyfrową), zapisującego czasy zdarzeń rozpraszania elastycznego. Znając chwilową częstotliwość tych zdarzeń i wiedząc, że obecność pelletu w obszarze wiązki zwiększa tę częstotliwość, stworzono metodę klasyfikacji zdarzeń hadronowych, co umożliwiło zanalizowane tych zdarzeń osobno dla klasy “pelletowej” i “niepelletowej”. Badania jasno pokazały iż możliwe jest rozróżnienie między tymi dwoma klasami zdarzeń, a przeprowadzony test dostarczył doświadczenia w używaniu dwóch różnych systemów zsynchronizowanych ze sobą – głównego systemu akwizycji danych oraz drugiego systemu, w tym przypadku długookresowego TDC, pracującego w znacznie dłuższej skali czasowej – podobnej do tej w jakiej będzie pracował system śledzenia pelletów.

Appendix A

List of acronyms

Facilities and experiments:

COSY	COoler SYnchrotron (Accelerator at FZJ)
FAIR	Facility for Antiproton and Ion Research (Accelerator facility at Darmstadt)
FZJ	Forschungszentrum Jülich - Research Center Juelich, Germany
GSI	Gesellschaft für Schwerionenforschung (Centre for Heavy Ion Research)
HESR	High-Energy Storage Ring (Accelerator at FAIR)
IKP	Institut für Kernphysik (Institute for Nuclear Physics (FZJ))
PANDA	Anti-Proton ANnihilation at DArmstadt (particle detector system at FAIR)
TSL	The Svedberg Laboratoriet, Uppsala
UPTS	Uppsala Pellet Test Station (at TSL)
WASA	Wide Angle Shower Apparatus (particle detector system, now at FZJ)

Detectors in the PANDA setup:

DIRC	Detector of Internally Reflected Cherenkov light
GEM	Gas Electron Multiplier
MVD	Micro Vertex Detector
RICH	Ring Imaging CHerenkov detector
STT	Straw Tube Tracker

Detectors in the WASA setup:

FPC	Forward Proportional Chambers
FRH	Forward Range Hodoscope
FTH	Forward Trigger Hodoscope
FVH	Forward Veto Hodoscope
FWC	Forward Window Counters
PSB	Plastic Scintillator Barrel
SEC	Scintillating Electromagnetic Calorimeter

Pellet tracking related terms:

CCD	Charge Coupled Device - a kind of sensor widely used in cameras
DC	Droplet Chamber
DOF	Depth-of-field
LS	Line Scan - a kind of CCD cameras containing only one line of pixels
PTR	Pellet Tracking (system)
SNF	Name of a series a structured light lasers (being used in the tracking system)
SM2	A type of camera (being used in the tracking system, AViiVA SM2)
VIC	Vacuum Injection Capillary

Other:

DAQ	Data Acquisition (System)
FPGA	Field Programmable Gate Array - a kind of integrated circuits designed to be configured after manufacturing
FW	Full Width
FWHM	Full Width at Half Maximum
LR TDC	Long Range TDC
MC	Monte Carlo
PC	Personal Computer

QCD	Quantum Chromo Dynamics
QDC	Charge-to-Digital Converter
TDC	Time-to-Digital Converter
TOF	Time of Flight
WMC	Wasa Monte Carlo

Appendix B

Most important definitions

A number of terms have been defined for the purpose of the described studies. The definitions are listed below.

Pellet track (also, in a proper context: track) – A set of information describing the pellet trajectory. The pellet track is constructed by fitting a function (first or second degree polynomial) to the measured pellet positions and times obtained at the measurement levels. The pellet track allows to obtain pellet position at any moment. All tracks contain fits of pellet time. Also the position on one of transverse directions is present. The presence of information for the second direction depends if the track contains information from at least 2 levels participating in tracking in a given direction.

True pellet – true presence of pellet at a given position at a given moment. In the described studies this term is used mainly while speaking of simulated pellets, and "true" means the simulated values.

Reconstructed pellet (abbrev.: recons. pellet) – presence of a pellet at a given position at a given time, indicated by the tracking system, based on reconstructed pellet track.

Correct pellet track (also, in a proper context: correct track) – pellet track constructed based on measurements of one pellet.

Incorrect pellet track (also, in a proper context: incorrect track) – pellet track constructed based on measurements of different pellets.

Matching pellet / matching track – when a pellet and pellet track are compared to each other in some way, they are called matching, when

the track has been created based on measurements of the same pellet which is then used in the comparison.

Pellet track reconstruction efficiency (also, in a proper context: track reconstruction efficiency, reconstruction efficiency) – ratio of reconstructed tracks to detected pellets.

Pellet track reconstruction correctness (also, in a proper context: track reconstruction correctness, reconstruction correctness) – ratio of the correct reconstructed tracks to all reconstructed tracks.

Pellet tracking efficiency (also, in a proper context: tracking efficiency) – ratio of reconstructed tracks to survived pellets.

Performance – the term is used in a general meaning to tell how well various aspects connected to the pellet tracking behave.

Particle track (also, in a proper context: track) – trajectory of elementary particle resulting from the pellet - accelerator beam interaction, reconstructed based on the information from the particle detector system.

Nominal interaction point – nominal point of intersection of the accelerator beam and pellet stream axes; the origin of the coordinate system in the WASA and PANDA setups (position 0,0,0).

Coordinate system – The coordinate system at PANDA and WASA is a right handed system with z axis in the direction of the accelerator beam and y axis going upwards (Figure B.1). The z axis is the accelerator beam axis and the y axis is the pellet/cluster stream axis. The origin of the system is in the nominal interaction point.

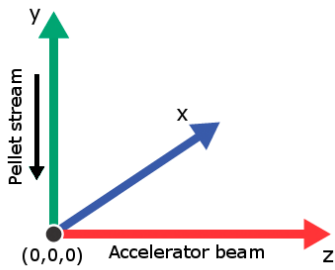

Figure B.1: Coordinate system at PANDA and WASA

Appendix C

Cases classification in a search for pellets

Single-layer-cases At each measurement point there may be a few different situations (cases) in the search for the correct pellet in the time window:

- Case 0 – No pellets were found in the time window
- Case 1 – some pellets were found in the window, but the correct one was not among them
- Case 2 – some pellets were found, the correct one was one of them, but it was not the closest to the expected time
- Case 3 – some pellets were found, the correct one was one of them and was the closest to the expected time, but was not the only closest one (more pellets were detected in the same exposure)
- Case 4 – some pellets were found and the correct one was (alone) the closest to the expected time
- Case 5 – the correct pellet was the only pellet found in the window

It is possible to increase efficiency of pellet identification by separating correct pellets from case 3. This may be done by checking the geometrical overlap of the pellet transverse positions at different measurement points.

Multi-layer-cases Multi-layer-cases is a new case classification combining information from different measurement points about the cases used so far (single-layer-cases, denoted with numbers 0..5). There are two such multi-layer-cases:

- Multi-layer-case A – The pellet was correctly identified at all existing measurement points. Strictly: the case (single-layer-case) at all measurement points was always 4 or 5.
- Multi-layer-case B – The pellet was not identified correctly at least one of the measurement points. Strictly: at one or more measurement points the case was 0, 1, 2 or 3.

Since case 3 contains also correctly recognized pellets, it is possible that multi-layer-case B may contain also pellets correctly recognized at all measurement points.

A number of probabilities were defined to describe performance of the tracking system:

The probability to have **the same number of true pellets as the number of reconstructed pellets** is calculated by dividing the probability for a situation with a certain number of reconstructed pellets and the same number of true pellets, by the probability for the situation with this number of reconstructed pellets. The probability for **the same number of reconstructed pellets as a certain number of true pellets** is calculated analogously.

The probability for **exactly one reconstructed pellet and a certain number of true pellets** in the beam region shows the probability for a certain beam region occupancy (*i.e.* time with this occupancy divided by the total time of the sample). The probability for **exactly one true pellet and a certain number of reconstructed pellets in the beam region** is analogous.

The probability for **a certain number of true pellets in the beam region, when there is exactly one reconstructed pellet in the beam region**, is calculated by dividing the probability for exactly one reconstructed pellet and a certain number of true pellets in the beam region, described above (Figure 4.2.17), by the probability for exactly one reconstructed pellet in the beam region. The probability for **a certain number of reconstructed pellets in the beam region when exactly one true pellet is in the beam region** is calculated analogously.

Probability for **exactly one reconstructed pellet and a matching true pellet in the beam region** is defined as the time with this occupancy divided by the total time of the sample. The match of the pellet is checked by comparing indexes of pellets in the beam region with index of the pellet track. Exactly one reconstructed pellet in the beam region is required to make this comparison, but on the other hand, there may

be one or more true pellets in the beam region. In this case it is checked if the matching one is among them. The probability for **exactly one true pellet and a matching reconstructed pellet in the beam region** is calculated analogically.

Probability for a **matching true pellet in the beam region when exactly one reconstructed pellet is in the beam region** is calculated by dividing the probability for exactly one reconstructed pellet and a matching true pellet in the beam region, mentioned above (Figure 4.2.19), by the probability for exactly one reconstructed pellet in the beam region. The probability for a **matching reconstructed pellet in the beam region when exactly one true pellet is in the beam region** is analogous.

Probability that a **matching true pellet is among true pellets in beam region when exactly one reconstructed pellet is in the beam region** is calculated by dividing the probability for the case with exactly one reconstructed pellet and a matching true pellet in the beam region, by the probability for exactly one reconstructed pellet and a certain number of true pellets in the beam region. The probability that a **matching reconstructed pellet is among reconstructed pellets in the beam region when exactly one true pellet is in the beam region** is analogous.

Appendix D

Detailed results of tracking system design simulations

Tables D.1 – D.12 summarize, for different simulation conditions, several probabilities describing pellet tracking performance with zero and one true/reconstructed pellet in the beam region.

Pellet rate 5 k/s with 40 kHz generation frequency is achieved by using 0.75 mrad stream divergence and with 65% additional loss. The pellet rate 14 kHz with the same generation frequency is achieved by having only loss at skimmer. The rate 14 k/s with 20 kHz generation frequency is obtained with 0.44 mrad stream divergence and no other loss and the rate 14 k/s with 14 kHz generation frequency is obtained with 0.075 mrad stream divergence.

Table D.1: Summary of pellet tracking performance with no true/reconstructed pellet in the beam region, for 5 mm beam region size and 1% velocity spread

	Probability of no recons. | true pellet in the beam region (time fraction)		Probability of no true | recons. pellet in the beam region when no recons. | true pellet is in the beam region	
Cycle 2/2μs f_{gen} : 40kHz, $Loss$: 87.5% Pellet rate 5 k/s	0.780	0.700	0.878	0.979
Cycle 4/4μs f_{gen} : 40kHz, $Loss$: 87.5% Pellet rate 5 k/s	0.778	0.700	0.865	0.964
Cycle 6.25/5μs f_{gen} : 40kHz, $Loss$: 87.5% Pellet rate 5 k/s	0.826	0.700	0.818	0.960
Cycle 2/2μs f_{gen} : 40kHz, $Loss$: 65% Pellet rate 14 k/s	0.531	0.366	0.642	0.942
Cycle 4/4μs f_{gen} : 40kHz, $Loss$: 65% Pellet rate 14 k/s	0.537	0.366	0.613	0.909
Cycle 6.25/5μs f_{gen} : 40kHz, $Loss$: 65% Pellet rate 14 k/s	0.622	0.366	0.524	0.896
Cycle 2/2μs f_{gen} : 20kHz, $Loss$: 30% Pellet rate 14 k/s	0.523	0.353	0.633	0.939
Cycle 4/4μs f_{gen} : 20kHz, $Loss$: 30% Pellet rate 14 k/s	0.528	0.353	0.602	0.902
Cycle 6.25/5μs f_{gen} : 20kHz, $Loss$: 30% Pellet rate 14 k/s	0.616	0.353	0.509	0.892
Cycle 2/2μs f_{gen} : 14kHz, $Loss$: 0% Pellet rate 14 k/s	0.475	0.358	0.673	0.892
Cycle 4/4μs f_{gen} : 14kHz, $Loss$: 0% Pellet rate 14 k/s	0.474	0.358	0.639	0.846

Table D.2: Summary of pellet tracking performance with one true/reconstructed pellet in the beam region, for 5 mm beam region size and 1% velocity spread

	Probability of exactly one recons. | true pellet in the beam region (time fraction)		Probability of exactly one true | recons. pellet in the beam region when exactly one recons. | true pellet is in the beam region		Probability of one-matching true | recons. pellet in the beam region when exactly one recons. | true pellet is in the beam region		Probability of correct match when there are one true and one reconstructed pellet in the beam region
Cycle 2/2μs f_{gen} : 40kHz, $Loss$: 87.5% Pellet rate 5 k/s	0.194	0.250	0.816	0.631	0.806	0.623	0.988
Cycle 4/4μs f_{gen} : 40kHz, $Loss$: 87.5% Pellet rate 5 k/s	0.195	0.250	0.764	0.590	0.746	0.576	0.976
Cycle 6.25/5μs f_{gen} : 40kHz, $Loss$: 87.5% Pellet rate 5 k/s	0.158	0.250	0.678	0.434	0.642	0.411	0.947
Cycle 2/2μs f_{gen} : 40kHz, $Loss$: 65% Pellet rate 14 k/s	0.335	0.375	0.619	0.557	0.591	0.531	0.955
Cycle 4/4μs f_{gen} : 40kHz, $Loss$: 65% Pellet rate 14 k/s	0.332	0.375	0.566	0.507	0.517	0.464	0.914
Cycle 6.25/5μs f_{gen} : 40kHz, $Loss$: 65% Pellet rate 14 k/s	0.293	0.375	0.483	0.384	0.403	0.320	0.834
Cycle 2/2μs f_{gen} : 20kHz, $Loss$: 30% Pellet rate 14 k/s	0.336	0.375	0.611	0.549	0.581	0.522	0.951
Cycle 4/4μs f_{gen} : 20kHz, $Loss$: 30% Pellet rate 14 k/s	0.336	0.375	0.563	0.507	0.513	0.462	0.910
Cycle 6.25/5μs f_{gen} : 20kHz, $Loss$: 30% Pellet rate 14 k/s	0.295	0.375	0.481	0.379	0.400	0.315	0.831
Cycle 2/2μs f_{gen} : 14kHz, $Loss$: 0% Pellet rate 14 k/s	0.349	0.378	0.623	0.576	0.577	0.533	0.927
Cycle 4/4μs f_{gen} : 14kHz, $Loss$: 0% Pellet rate 14 k/s	0.349	0.378	0.572	0.528	0.505	0.467	0.883

Table D.3: Summary of pellet tracking performance with no true/reconstructed pellet in the beam region, for 10 mm beam region size and 1% velocity spread

	Probability of no recons. | true pellet in the beam region (time fraction)		Probability of no true | recons. pellet in the beam region when no recons. | true pellet is in the beam region	
Cycle 2/2μs f_{gen} : 40kHz, $Loss$: 87.5% Pellet rate 5 k/s	0.605	0.493	0.791	0.980
Cycle 4/4μs f_{gen} : 40kHz, $Loss$: 87.5% Pellet rate 5 k/s	0.607	0.493	0.779	0.965
Cycle 6.25/5μs f_{gen} : 40kHz, $Loss$: 87.5% Pellet rate 5 k/s	0.680	0.493	0.688	0.957
Cycle 2/2μs f_{gen} : 40kHz, $Loss$: 65% Pellet rate 14 k/s	0.282	0.131	0.436	0.946
Cycle 4/4μs f_{gen} : 40kHz, $Loss$: 65% Pellet rate 14 k/s	0.287	0.131	0.411	0.900
Cycle 6.25/5μs f_{gen} : 40kHz, $Loss$: 65% Pellet rate 14 k/s	0.391	0.131	0.297	0.899
Cycle 2/2μs f_{gen} : 20kHz, $Loss$: 30% Pellet rate 14 k/s	0.269	0.120	0.417	0.934
Cycle 4/4μs f_{gen} : 20kHz, $Loss$: 30% Pellet rate 14 k/s	0.273	0.120	0.393	0.898
Cycle 6.25/5μs f_{gen} : 20kHz, $Loss$: 30% Pellet rate 14 k/s	0.380	0.120	0.277	0.883
Cycle 2/2μs f_{gen} : 14kHz, $Loss$: 0% Pellet rate 14 k/s	0.223	0.123	0.481	0.869
Cycle 4/4μs f_{gen} : 14kHz, $Loss$: 0% Pellet rate 14 k/s	0.224	0.123	0.450	0.819

Table D.4: Summary of pellet tracking performance with one true/reconstructed pellet in the beam region, for 10 mm beam region size and 1% velocity spread

	Probability of exactly one recons. | true pellet in the beam region (time fraction)		Probability of exactly one true | recons. pellet in the beam region when exactly one recons. | true pellet is in the beam region		Probability of one-matching true | recons. pellet in the beam region when exactly one recons. | true pellet is in the beam region		Probability of correct match when there are one true and one reconstructed pellet in the beam region
Cycle 2/2μs f_{gen} : 40kHz, *Loss* : 87.5% Pellet rate 5 k/s	0.307	0.350	0.772	0.668	0.763	0.660	0.988
Cycle 4/4μs f_{gen} : 40kHz, *Loss* : 87.5% Pellet rate 5 k/s	0.301	0.350	0.734	0.635	0.717	0.620	0.977
Cycle 6.25/5μs f_{gen} : 40kHz, *Loss* : 87.5% Pellet rate 5 k/s	0.264	0.350	0.652	0.486	0.624	0.464	0.956
Cycle 2/2μs f_{gen} : 40kHz, *Loss* : 65% Pellet rate 14 k/s	0.357	0.274	0.433	0.575	0.413	0.549	0.954
Cycle 4/4μs f_{gen} : 40kHz, *Loss* : 65% Pellet rate 14 k/s	0.358	0.274	0.405	0.545	0.373	0.502	0.921
Cycle 6.25/5μs f_{gen} : 40kHz, *Loss* : 65% Pellet rate 14 k/s	0.365	0.274	0.315	0.428	0.269	0.366	0.854
Cycle 2/2μs f_{gen} : 20kHz, *Loss* : 30% Pellet rate 14 k/s	0.354	0.264	0.430	0.576	0.409	0.548	0.951
Cycle 4/4μs f_{gen} : 20kHz, *Loss* : 30% Pellet rate 14 k/s	0.360	0.264	0.403	0.549	0.370	0.505	0.919
Cycle 6.25/5μs f_{gen} : 20kHz, *Loss* : 30% Pellet rate 14 k/s	0.365	0.264	0.299	0.414	0.253	0.350	0.846
Cycle 2/2μs f_{gen} : 14kHz, *Loss* : 0% Pellet rate 14 k/s	0.331	0.270	0.483	0.591	0.443	0.542	0.917
Cycle 4/4μs f_{gen} : 14kHz, *Loss* : 0% Pellet rate 14 k/s	0.329	0.270	0.452	0.552	0.399	0.487	0.883

Table D.5: Summary of pellet tracking performance with no true/reconstructed pellet in the beam region, for 5 mm beam region size and 0.1% velocity spread

	Probability of no recons. | true pellet in the beam region (time fraction)		Probability of no true | recons. pellet in the beam region when no recons. | true pellet is in the beam region	
Cycle 2/2μs f_{gen} : 40kHz, $Loss$: 87.5% Pellet rate 5 k/s	0.760	0.700	0.895	0.977
Cycle 4/4μs f_{gen} : 40kHz, $Loss$: 87.5% Pellet rate 5 k/s	0.751	0.700	0.889	0.958
Cycle 6.25/5μs f_{gen} : 40kHz, $Loss$: 87.5% Pellet rate 5 k/s	0.799	0.700	0.827	0.948
Cycle 2/2μs f_{gen} : 40kHz, $Loss$: 65% Pellet rate 14 k/s	0.445	0.334	0.699	0.931
Cycle 4/4μs f_{gen} : 40kHz, $Loss$: 65% Pellet rate 14 k/s	0.442	0.334	0.662	0.880
Cycle 6.25/5μs f_{gen} : 40kHz, $Loss$: 65% Pellet rate 14 k/s	0.528	0.334	0.544	0.854
Cycle 2/2μs f_{gen} : 20kHz, $Loss$: 30% Pellet rate 14 k/s	0.404	0.292	0.662	0.916
Cycle 4/4μs f_{gen} : 20kHz, $Loss$: 30% Pellet rate 14 k/s	0.390	0.292	0.636	0.851
Cycle 6.25/5μs f_{gen} : 20kHz, $Loss$: 30% Pellet rate 14 k/s	0.488	0.2920	0.485	0.815
Cycle 2/2μs f_{gen} : 14kHz, $Loss$: 0% Pellet rate 14 k/s	0.386	0.266	0.619	0.900
Cycle 4/4μs f_{gen} : 14kHz, $Loss$: 0% Pellet rate 14 k/s	0.368	0.266	0.592	0.818

Table D.6: Summary of pellet tracking performance with one true/reconstructed pellet in the beam region, for 5 mm beam region size and 0.1% velocity spread

	Probability of exactly one recons. | true pellet in the beam region (time fraction)		Probability of exactly one true | recons. pellet in the beam region when exactly one recons. | true pellet is in the beam region		Probability of one-matching true | recons. pellet in the beam region when exactly one recons. | true pellet is in the beam region		Probability of correct match when there are one true and one reconstructed pellet in the beam region
Cycle 2/2μs f_{gen} : 40kHz, *Loss* : 87.5% Pellet rate 5 k/s	0.214	0.265	0.848	0.696	0.841	0.690	0.992
Cycle 4/4μs f_{gen} : 40kHz, *Loss* : 87.5% Pellet rate 5 k/s	0.222	0.265	0.791	0.676	0.779	0.665	0.984
Cycle 6.25/5μs f_{gen} : 40kHz, *Loss* : 87.5% Pellet rate 5 k/s	0.183	0.265	0.693	0.492	0.659	0.468	0.951
Cycle 2/2μs f_{gen} : 40kHz, *Loss* : 65% Pellet rate 14 k/s	0.383	0.400	0.701	0.670	0.682	0.652	0.972
Cycle 4/4μs f_{gen} : 40kHz, *Loss* : 65% Pellet rate 14 k/s	0.386	0.400	0.643	0.626	0.606	0.587	0.943
Cycle 6.25/5μs f_{gen} : 40kHz, *Loss* : 65% Pellet rate 14 k/s	0.357	0.400	0.535	0.479	0.460	0.412	0.860
Cycle 2/2μs f_{gen} : 20kHz, *Loss* : 30% Pellet rate 14 k/s	0.422	0.442	0.716	0.689	0.699	0.672	0.975
Cycle 4/4μs f_{gen} : 20kHz, *Loss* : 30% Pellet rate 14 k/s	0.423	0.442	0.673	0.648	0.641	0.616	0.952
Cycle 6.25/5μs f_{gen} : 20kHz, *Loss* : 30% Pellet rate 14 k/s	0.392	0.442	0.558	0.495	0.483	0.429	0.866
Cycle 2/2μs f_{gen} : 14kHz, *Loss* : 0% Pellet rate 14 k/s	0.459	0.492	0.744	0.694	0.727	0.678	0.977
Cycle 4/4μs f_{gen} : 14kHz, *Loss* : 0% Pellet rate 14 k/s	0.466	0.492	0.699	0.663	0.666	0.631	0.952

Table D.7: Summary of pellet tracking performance with no true/reconstructed pellet in the beam region, for 10 mm beam region size and 0.1% velocity spread

	Probability of no recons. | true pellet in the beam region (time fraction)		Probability of no true | recons. pellet in the beam region when no recons. | true pellet is in the beam region	
Cycle 2/2μs f_{gen} : 40kHz, $Loss$: 87.5% Pellet rate 5 k/s	0.569	0.480	0.821	0.979
Cycle 4/4μs f_{gen} : 40kHz, $Loss$: 87.5% Pellet rate 5 k/s	0.553	0.480	0.826	0.960
Cycle 6.25/5μs f_{gen} : 40kHz, $Loss$: 87.5% Pellet rate 5 k/s	0.634	0.480	0.716	0.950
Cycle 2/2μs f_{gen} : 40kHz, $Loss$: 65% Pellet rate 14 k/s	0.184	0.100	0.511	0.931
Cycle 4/4μs f_{gen} : 40kHz, $Loss$: 65% Pellet rate 14 k/s	0.177	0.100	0.486	0.869
Cycle 6.25/5μs f_{gen} : 40kHz, $Loss$: 65% Pellet rate 14 k/s	0.268	0.100	0.321	0.851
Cycle 2/2μs f_{gen} : 20kHz, $Loss$: 30% Pellet rate 14 k/s	0.135	0.056	0.367	0.901
Cycle 4/4μs f_{gen} : 20kHz, $Loss$: 30% Pellet rate 14 k/s	0.122	0.056	0.384	0.823
Cycle 6.25/5μs f_{gen} : 20kHz, $Loss$: 30% Pellet rate 14 k/s	0.211	0.056	0.209	0.787
Cycle 2/2μs f_{gen} : 14kHz, $Loss$: 0% Pellet rate 14 k/s	0.102	0.024	0.198	0.829
Cycle 4/4μs f_{gen} : 14kHz, $Loss$: 0% Pellet rate 14 k/s	0.090	0.024	0.193	0.715

Table D.8: Summary of pellet tracking performance with one true/reconstructed pellet in the beam region, for 10 mm beam region size and 0.1% velocity spread

	Probability of exactly one recons. | true pellet in the beam region (time fraction)		Probability of exactly one true | recons. pellet in the beam region when exactly one recons. | true pellet is in the beam region		Probability of one-matching true | recons. pellet in the beam region when exactly one recons. | true pellet is in the beam region		Probability of correct match when there are one true and one reconstructed pellet in the beam region
Cycle 2/2μs f_{gen} : 40kHz, *Loss* : 87.5% Pellet rate 5 k/s	0.334	0.375	0.809	0.731	0.803	0.726	0.993
Cycle 4/4μs f_{gen} : 40kHz, *Loss* : 87.5% Pellet rate 5 k/s	0.345	0.375	0.785	0.734	0.775	0.724	0.986
Cycle 6.25/5μs f_{gen} : 40kHz, *Loss* : 87.5% Pellet rate 5 k/s	0.301	0.375	0.688	0.557	0.662	0.536	0.962
Cycle 2/2μs f_{gen} : 40kHz, *Loss* : 65% Pellet rate 14 k/s	0.351	0.270	0.537	0.706	0.523	0.688	0.974
Cycle 4/4μs f_{gen} : 40kHz, *Loss* : 65% Pellet rate 14 k/s	0.353	0.270	0.518	0.685	0.495	0.654	0.955
Cycle 6.25/5μs f_{gen} : 40kHz, *Loss* : 65% Pellet rate 14 k/s	0.388	0.270	0.363	0.529	0.321	0.468	0.885
Cycle 2/2μs f_{gen} : 20kHz, *Loss* : 30% Pellet rate 14 k/s	0.353	0.245	0.488	0.702	0.474	0.682	0.971
Cycle 4/4μs f_{gen} : 20kHz, *Loss* : 30% Pellet rate 14 k/s	0.339	0.245	0.491	0.683	0.468	0.650	0.951
Cycle 6.25/5μs f_{gen} : 20kHz, *Loss* : 30% Pellet rate 14 k/s	0.403	0.245	0.335	0.549	0.291	0.477	0.868
Cycle 2/2μs f_{gen} : 14kHz, *Loss* : 0% Pellet rate 14 k/s	0.377	0.235	0.441	0.706	0.426	0.681	0.965
Cycle 4/4μs f_{gen} : 14kHz, *Loss* : 0% Pellet rate 14 k/s	0.358	0.235	0.438	0.666	0.411	0.625	0.938

Table D.9: Summary of pellet tracking performance with no true/reconstructed pellet in the beam region, for 5 mm beam region size and 0.01% velocity spread

	Probability of no recons. | true pellet in the beam region (time fraction)		Probability of no true | recons. pellet in the beam region when no recons. | true pellet is in the beam region	
Cycle 2/2μs f_{gen} : 40kHz, *Loss* : 87.5% Pellet rate 5 k/s	0.748	0.688	0.896	0.980
Cycle 4/4μs f_{gen} : 40kHz, *Loss* : 87.5% Pellet rate 5 k/s	0.740	0.688	0.878	0.949
Cycle 2/2μs f_{gen} : 40kHz, *Loss* : 65% Pellet rate 14 k/s	0.408	0.295	0.684	0.936
Cycle 4/4μs f_{gen} : 40kHz, *Loss* : 65% Pellet rate 14 k/s	0.397	0.295	0.625	0.849
Cycle 2/2μs f_{gen} : 20kHz, *Loss* : 30% Pellet rate 14 k/s	0.337	0.195	0.532	0.922
Cycle 4/4μs f_{gen} : 20kHz, *Loss* : 30% Pellet rate 14 k/s	0.323	0.195	0.475	0.790
Cycle 2/2μs f_{gen} : 14kHz, *Loss* : 0% Pellet rate 14 k/s	0.259	0.035	0.078	0.584
Cycle 4/4μs f_{gen} : 14kHz, *Loss* : 0% Pellet rate 14 k/s	0.260	0.035	0.060	0.455

Table D.10: Summary of pellet tracking performance with one true/reconstructed pellet in the beam region, for 5 mm beam region size and 0.01% velocity spread

	Probability of exactly one recons. | true pellet in the beam region (time fraction)		Probability of exactly one true | recons. pellet in the beam region when exactly one recons. | true pellet is in the beam region		Probability of one-matching true | recons. pellet in the beam region when exactly one recons. | true pellet is in the beam region		Probability of correct match when there are one true and one recon-structed pellet in the beam region
Cycle 2/2μs f_{gen} : 40kHz, *Loss* : 87.5% Pellet rate 5 k/s	0.228	0.282	0.870	0.716	0.864	0.711	0.994
Cycle 4/4μs f_{gen} : 40kHz, *Loss* : 87.5% Pellet rate 5 k/s	0.232	0.282	0.776	0.656	0.759	0.641	0.978
Cycle 2/2μs f_{gen} : 40kHz, *Loss* : 65% Pellet rate 14 k/s	0.425	0.440	0.737	0.706	0.723	0.693	0.981
Cycle 4/4μs f_{gen} : 40kHz, *Loss* : 65% Pellet rate 14 k/s	0.420	0.440	0.656	0.619	0.611	0.576	0.931
Cycle 2/2μs f_{gen} : 20kHz, *Loss* : 30% Pellet rate 14 k/s	0.527	0.584	0.787	0.711	0.771	0.697	0.979
Cycle 4/4μs f_{gen} : 20kHz, *Loss* : 30% Pellet rate 14 k/s	0.523	0.584	0.706	0.631	0.668	0.597	0.946
Cycle 2/2μs f_{gen} : 14kHz, *Loss* : 0% Pellet rate 14 k/s	0.706	0.931	0.956	0.725	0.937	0.710	0.980
Cycle 4/4μs f_{gen} : 14kHz, *Loss* : 0% Pellet rate 14 k/s	0.671	0.931	0.952	0.686	0.861	0.620	0.904

Table D.11: Summary of pellet tracking performance with no true/reconstructed pellet in the beam region, for 10 mm beam region size and 0.01% velocity spread

	Probability of no recons. | true pellet in the beam region (time fraction)		Probability of no true | recons. pellet in the beam region when no recons. | true pellet is in the beam region	
Cycle 2/2μs f_{gen} : 40kHz, $Loss$: 87.5% Pellet rate 5 k/s	0.562	0.471	0.822	0.979
Cycle 4/4μs f_{gen} : 40kHz, $Loss$: 87.5% Pellet rate 5 k/s	0.549	0.471	0.811	0.949
Cycle 2/2μs f_{gen} : 40kHz, $Loss$: 65% Pellet rate 14 k/s	0.159	0.088	0.484	0.939
Cycle 4/4μs f_{gen} : 40kHz, $Loss$: 65% Pellet rate 14 k/s	0.153	0.088	0.484	0.851
Cycle 2/2μs f_{gen} : 20kHz, $Loss$: 30% Pellet rate 14 k/s	0.105	0.032	0.265	0.900
Cycle 4/4μs f_{gen} : 20kHz, $Loss$: 30% Pellet rate 14 k/s	0.096	0.032	0.262	0.792
Cycle 2/2μs f_{gen} : 14kHz, $Loss$: 0% Pellet rate 14 k/s	0.059	0.000	0.000	0.000
Cycle 4/4μs f_{gen} : 14kHz, $Loss$: 0% Pellet rate 14 k/s	0.049	0.000	0.000	0.000

Table D.12: Summary of pellet tracking performance with one true/reconstructed pellet in the beam region, for 10 mm beam region size and 0.01% velocity spread

	Probability of exactly one recons. | true pellet in the beam region (time fraction)		Probability of exactly one true | recons. pellet in the beam region when exactly one recons. | true pellet is in the beam region		Probability of one-matching true | recons. pellet in the beam region when exactly one recons. | true pellet is in the beam region		Probability of correct match when there are one true and one recon-structed pellet in the beam region
Cycle 2/2μs f_{gen} : 40kHz, *Loss* : 87.5% Pellet rate 5 k/s	0.339	0.382	0.827	0.743	0.822	0.739	0.994
Cycle 4/4μs f_{gen} : 40kHz, *Loss* : 87.5% Pellet rate 5 k/s	0.347	0.382	0.782	0.714	0.770	0.703	0.984
Cycle 2/2μs f_{gen} : 40kHz, *Loss* : 65% Pellet rate 14 k/s	0.344	0.262	0.538	0.721	0.527	0.706	0.980
Cycle 4/4μs f_{gen} : 40kHz, *Loss* : 65% Pellet rate 14 k/s	0.333	0.262	0.521	0.670	0.496	0.637	0.951
Cycle 2/2μs f_{gen} : 20kHz, *Loss* : 30% Pellet rate 14 k/s	0.354	0.207	0.417	0.712	0.406	0.693	0.974
Cycle 4/4μs f_{gen} : 20kHz, *Loss* : 30% Pellet rate 14 k/s	0.337	0.207	0.396	0.645	0.373	0.607	0.941
Cycle 2/2μs f_{gen} : 14kHz, *Loss* : 0% Pellet rate 14 k/s	0.359	0.034	0.051	0.535	0.043	0.450	0.841
Cycle 4/4μs f_{gen} : 14kHz, *Loss* : 0% Pellet rate 14 k/s	0.338	0.034	0.046	0.453	0.038	0.368	0.812

Acknowledgments

I would like to express my gratitude to the people whose presence and help made this thesis possible and made the past 4 years such a wonderful and enriching time.

First of all I would like to thank Hans Calén and Zbigniew Rudy – two great man who were directly taking care of my work and working with whom shaped the time of my studies.

Hans, thank You for a wise guidance through the research and for always having a plan. For knowing answers to all my questions and for always having time to answer them. For reminding me to "take it easy", "take my time" and for saying "thank you" each time I did some little piece. For checking everything thoroughly and for very helpful corrections.

Zbigniew, thank You for always having my back, for all the support from You, for all the formal and administrative struggles and making an environment where i could focus only on what was essential. Thank You for the countless hours of interesting and developing discussions and for scrupulously checking everything I do. Thank You for the emails at 3 AM and for the sparkling water i could always find in Your room.

Tord Johansson, thank You for taking care of the formal stuff at UU, so I could do my research in comfortable conditions. Thank You for the corrections to the thesis. And for keeping together this group of great people called the Nuclear Physics division.

Kjell Fransson, thank You for introducing me to the work. For passing me Your analysis programs and teaching how to use them. Thank You for sharing Your experience and all the discussions.

Marek Jacewicz, thank You for passing me the pellet simulations program, introducing me to it and for being a wise advisor and emergency hotline. And thank You for all the discussions with a tea about new gadgets and updates about the fun stuff You were working on.

Paweł Marciniewski and Józef Złomańczuk, thank You for the fun time during lunches and making Polish the language I used the most at UU. Józek, thank You for all the jokes and stories from Your life, as

well as for the discussions about data analysis. Paweł, thank You for explaining the me so many interesting things and patiently teaching me about electronics.

Wojtek Krzemień, thank You for being a wise Papa Smurf when I needed help from experienced programmer and data analyst. Thank You for interesting scientific discussions and casual information-synchronization sessions.

Volker Hejny and Peter Wüstner, thank You for preparing the Long Range TDC and taking the data for my tests. Volker, thank You for preparing the decoding procedures.

Magnus Wolke, thank You for the help with LR TDC and for providing answers to my questions about WASA. And thank You for radiating Your always optimistic attitude everywhere You are.

Paweł Moskal, thank You very much for creating the possibility of this project, taking care of its good conditions and for all the assistance.

I would like to cordially thank all other people whose help, kindness, participation in moments of fun or smiling faces on a corridor were so much important.

I also would like to thank from the bottom of my heart all my great friends who were always there for me. And above all, I would like to express a special gratitude to my Mom, the most wonderful mom in the world.

We acknowledge support by the Foundation for Polish Science - MPD program, co-financed by the European Union within the European Regional Development Fund.

References

[1] *Physics Performance Report for PANDA: Strong Interaction Studies with Antiprotons*, W. Erni *et al.*, PANDA Collaboration, *http://arxiv.org/abs/0903.3905v1* (2009)

[2] *Technical Design Report for the PANDA Internal Targets*, PANDA Collaboration, *http://www.fair-center.eu/for-users/publications/experiment-collaboration-publications.html* (2012)

[3] *Technical Design Report for the PANDA Micro Vertex Detector*, PANDA Collaboration, arXiv:1207.6581v2 [physics.ins-det]

[4] C. Ekstrom, *Internal targets for storage rings*, Nucl. Phys. A **626** (1997) 405C

[5] B. Trostell, *Vacuum injection of hydrogen micro-sphere beams*, Nucl. Instr. and Meth. A **362** (1995) 41

[6] C. Ekström, *et al.*, *Hydrogen pellet targets for circulating particle beams*, Nucl. Instr. and Meth. A **371** (1996) 572

[7] Ö. Nordhage *et al.*, *On the behavior of micro-spheres in a hydrogen pellet target*, Nucl. Instr. and Meth. A **546** (2005) 391

[8] H. Dombrowski, *et al.*, *The Muenster cluster target for internal storage ring experiments*, Nucl. Instrum. Meth. A **386** (1997) 228

[9] Chr. Bargholtz, *et al.*, *The WASA detector facility at CELSIUS*, Nucl. Instr. and Meth. A **594** (2008) 339

[10] WASA-at-COSY Collaboration: H.-H. Adam *et al.*, *arXiv:nucl-ex/0411038* (2004)

[11] P. Adlarson *et al.* (WASA-at-COSY Collaboration), *Exclusive Measurement of the eta* $\rightarrow \pi^+\pi^-\gamma$ *Decay*, Physics Letters B **707** (2012) 243

[12] P. Adlarson *et al.* (WASA-at-COSY Collaboration), *Abashian-Booth-Crowe resonance structure in the double pionic fusion to* ^4He, Physical Review C **86** (2012) 032201

[13] P. Adlarson *et al.* (WASA-at-COSY Collaboration), *Isospin Decomposition of the Basic Double-Pionic Fusion in the Region of the ABC Effect*, Physics Letters B **721** (2013) 229

[14] P. Adlarson *et al.* (WASA-at-COSY Collaboration), *Search for the eta-mesic ^{4}He with WASA-at-COSY detector*, Physical Review C **87** (2013) 035204

[15] P. Adlarson *et al.* (WASA-at-COSY Collaboration), *Investigation of the $dd \to {}^3He n\pi^0$ reaction with WASA-at-COSY*, Physical Review C **88** (2013) 014004

[16] P. Adlarson *et al.* (WASA-at-COSY Collaboration), *Search for a dark photon in the $\pi^0 \to e^+e^-\gamma$ decay*, Physics Letters B **726** (2013) 187

[17] P. Adlarson *et al.* (WASA-at-COSY Collaboration), *Measurement of the $pn \to pp\pi^0\pi^-$ reaction in search for the recently observed resonance structure in $d\pi^0\pi^0$ and $d\pi^+\pi^-$ systems*, Phys. Rev. C **88** no. 5 (2013) 055208 [arXiv:1306.5130 [nucl-ex]]

[18] P. Adlarson *et al.* (WASA-at-COSY Collaboration), *Cross section ratio and angular distributions of the reaction p + d -> 3He + eta at 48.8 MeV and 59.8 MeV excess energy*, Eur. Phys. J. A **50** (2014) 100 [arXiv:1402.3469 [nucl-ex]]

[19] P. Adlarson *et al.* (WASA-at-COSY Collaboration), *Evidence for a New Resonance from Polarized Neutron-Proton Scattering*, Phys. Rev. Lett. **112** (2014) 202311 [arXiv:1402.6844 [nucl-ex]]

[20] P. Adlarson *et al.* (WASA-at-COSY Collaboration), *Neutron-Proton Scattering in the Context of the d*(2380) Resonance*, Phys. Rev. C **90** (2014) 035204 [arXiv:1408.4928 [nucl-ex]]

[21] *Tracked pellets – a way to improve the efficiency of charmonium studies* Ö. Nordhage *et al.*, Nucl. Instr. and Meth. A **568** (2006) 561 [arXiv:physics/0701088v1 [physics.ins-det]]

[22] K.A. Olive *et al.* (Particle Data Group), Chin. Phys. C **38** 090001 (2014)

[23] H. Calén *et al.*, Forschungszentrum Jülich IKP Annual Report, (2011), *http://www.fz-juelich.de/ikp/EN/Aktuelles/ar2011.html*

[24] A. Pyszniak *et al.*, Forschungszentrum Jülich IKP Annual Report, (2011), *http://www.fz-juelich.de/ikp/EN/Aktuelles/ar2011.html*

[25] A. Pyszniak *et al.*, Forschungszentrum Jülich IKP Annual Report, (2012), *http://www.fz-juelich.de/ikp/EN/Aktuelles/ar2012.html*

[26] A. Pyszniak, *et al., A pellet tracking system for hadron physics experiments*, EPJ Web of Conferences **66**, 11031 (2014)

[27] A. Pyszniak, *et al., A pellet tracking system for PANDA experiment*, Hyperfine Interact **229** (2014) 159 [DOI:10.1007/s10751-014-1052-5]

[28] A. Pyszniak *et al.*, Forschungszentrum Jülich IKP Annual Report, (2013), *http://www.fz-juelich.de/ikp/EN/Aktuelles/ar2013.html*

[29] 13th International Workshop on Meson Production, Properties and Interaction; Cracow, Poland, 2014 (*http://meson.if.uj.edu.pl*); proceedings to appear in EPJ Web of Conferences

[30] *Simulations for design of a pellet tracking system for PANDA and WASA*, Marek Jacewicz, January 2011, Project report, *www.physics.uu.se/np/panda/pub/*

[31] *Pellet tracking simulations software*, Marek Jacewicz, January 2011, Project report, *www.physics.uu.se/np/panda/pub/*

[32] *Design ideas for pellet tracking systems for PANDA and WASA*, Hans Calén, Kjell Fransson, Elin Hellbeck and Carl-Johan Fridén, December 2009, Milestone report for EC FP7 Hadron Physics2 WP19 , *www.physics.uu.se/np/panda/pub/*

[33] *Simulation studies for a pellet tracking system*, Pascal Scheffels, December 2010, Erasmus work, *www.physics.uu.se/np/panda/pub/*

[34] I. Frohlich *et al.*, "Pluto: A Monte Carlo Simulation Tool for Hadronic Physics," PoS ACAT **2007** (2007) 076 [arXiv:0708.2382 [nucl-ex]].

[35] *GEANT - Detector Description and Simulation Tool*, CERN Program Library Long Writeup W5013, 1993

[36] *Vacuum Calculations For Hydrogen Pellet Targets at WASA and PANDA*, Johan Löfgren, April 2014, Project report, *http://urn.kb.se/resolve?urn=urn:nbn:se:uu:diva-222973*